Government of **Western Australia**
Department of **Mines and Petroleum**

RECORD 2011/25

CAPRICORN OROGEN SEISMIC AND MAGNETOTELLURIC (MT) WORKSHOP 2011: EXTENDED ABSTRACTS

Edited by SP Johnson, AM Thorne, and IM Tyler

ROYALTIES FOR REGIONS
EXPLORATION INCENTIVE SCHEME

Australian Government
Geoscience Australia

AuScope

ANSIR NATIONAL RESEARCH FACILITY FOR EARTH SOUNDING

THE UNIVERSITY of ADELAIDE

Geological Survey of Western Australia

Government of **Western Australia**
Department of **Mines and Petroleum**

Record 2011/25

CAPRICORN OROGEN SEISMIC AND MAGNETOTELLURIC (MT) WORKSHOP 2011: EXTENDED ABSTRACTS

Edited by
SP Johnson, AM Thorne, and IM Tyler

ROYALTIES FOR REGIONS
EXPLORATION INCENTIVE SCHEME

Australian Government
Geoscience Australia

AuScope

ANSIR NATIONAL RESEARCH FACILITY FOR EARTH SOUNDING

THE UNIVERSITY of ADELAIDE

Geological Survey of Western Australia

MINISTER FOR MINES AND PETROLEUM
Hon. Norman Moore MLC

DIRECTOR GENERAL, DEPARTMENT OF MINES AND PETROLEUM
Richard Sellers

EXECUTIVE DIRECTOR, GEOLOGICAL SURVEY OF WESTERN AUSTRALIA
Rick Rogerson

REFERENCE
The recommended reference for this publication is:
Johnson, SP, Thorne, AM and Tyler, IM (eds) 2011, Capricorn Orogen seismic and magnetotelluric (MT) workshop 2011: extended abstracts: Geological Survey of Western Australia, Record 2011/25, 120p.

National Library of Australia Card Number and ISBN 978-1-74168-419-3

Published 2011 by Geological Survey of Western Australia
This Record is published in digital format (PDF) and is available online at <www.dmp.wa.gov.au/GSWApublications>.

Further details of geological publications and maps produced by the Geological Survey of Western Australia are available from:
Information Centre
Department of Mines and Petroleum
100 Plain Street
EAST PERTH WESTERN AUSTRALIA 6004
Telephone: +61 8 9222 3459 Facsimile: +61 8 9222 3444
www.dmp.wa.gov.au/GSWApublications

Contents

Plates

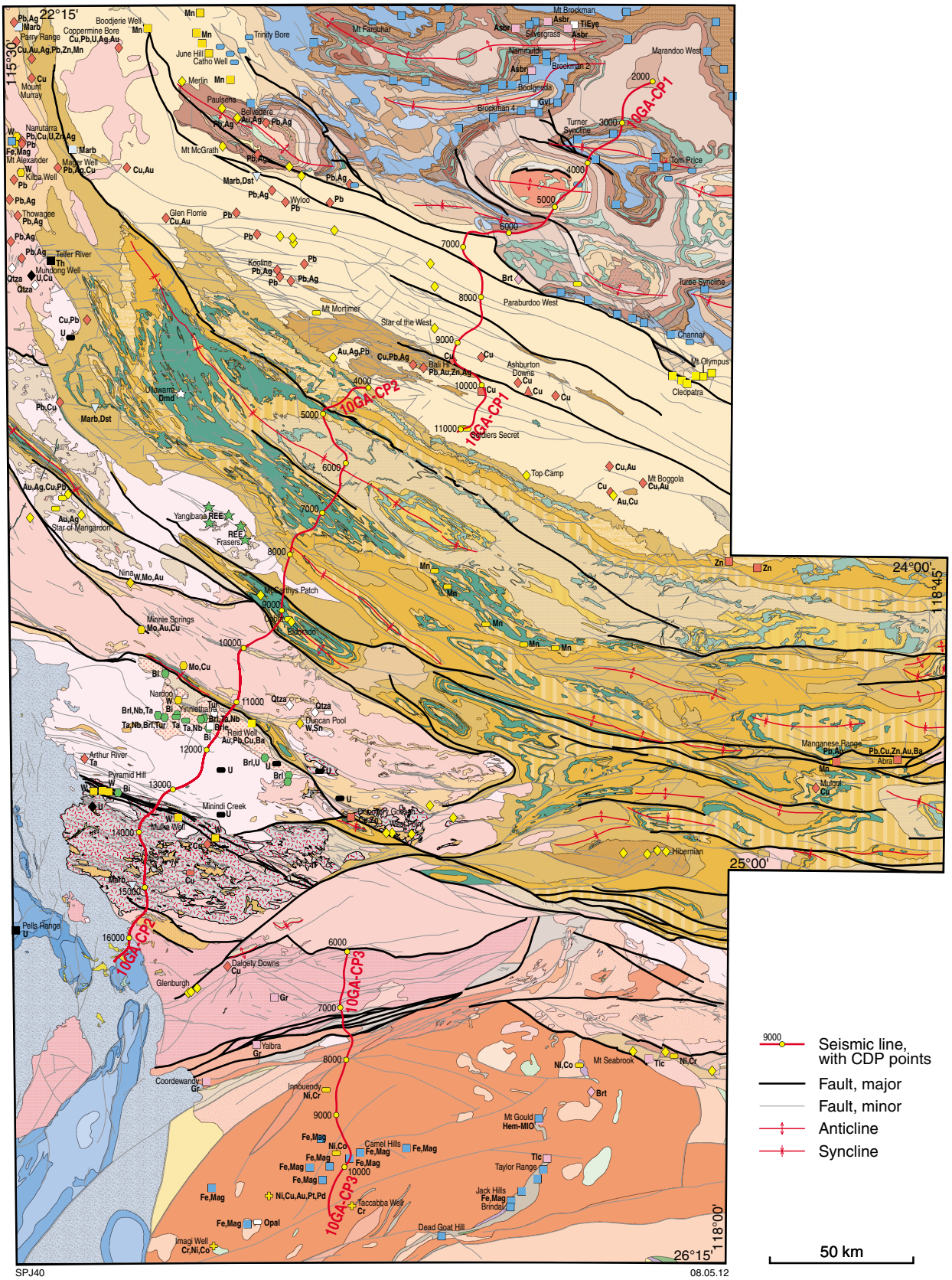

Frontispiece 1. **Geological map of the western Capricorn Orogen, showing the location of the Capricorn Orogen seismic lines 10GA–CP1, 10GA–CP2, and 10GA–CP3**

PILBARA CRATON

Unassigned Proterozoic units

Metadolerite; massive to schistose
Dolerite dyke, sill, or plug; fine- to medium-grained dolerite and gabbro

Bresnahan Group

Cherrybooka Conglomerate and Kunderong Sandstone

1680–1620 Ma Mangaroon Orogeny

Mount Minnie Group

Brodagee Sandstone, Wabco Shale, and Warramboo Sandstone

Capricorn Group

Bywash and Mooline Formations

1820–1770 Ma Capricorn Orogeny

Wyloo Group, upper

Mount McGrath Formation, Duck Creek Dolomite, and Ashburton Formation

2215–2145 Ma Ophthalmian Orogeny

Wyloo Group, lower

Beasley River Quartzite, Cheela Springs Basalt and Wooly Dolomite

Turee Creek Group

Kungarra, Koolbye and Kazput Formations

Hammersley Group

Boolgeeda Iron Formation
Woongarra Rhyolite
Weeli Wolli Formation
Brockman Iron Formation
Mount McRae Shale and Mount Sylvia Formation
Wittenoom Formation
Marra Mamba Iron Formation

Fortescue Group

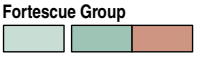

Layered mafic sills
Dolerite dyke or sill
Basalt; metamorphosed

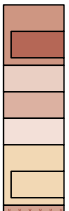

Jeerinah Formation
Pillowed and massive basaltic flows
Bunjinah Formation
Pyradie Formation
Boongal Formation
Hardey Formation
Basaltic flows and volcaniclastic rock; metamorphosed
Mount Roe Basalt
Felsic volcanic rock; metamorphosed
Quartzofeldspathic sandstone, conglomerate, mudstone, and siltstone
Bellary Formation

Undivided sedimentary units

Sedimentary rock, undivided

Unassigned granitic units

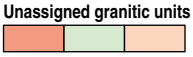

Foliated, gneissic, or migmatitic granitoid rocks
Basaltic and andesitic flows, and associated volcaniclastic rocks; metamorphosed
Metawandy Granite

GASCOYNE PROVINCE

Nadarra Formation
Pindilya Formation
Nanutarra Formation

Byro Group

Bulgadoo Shale, Cundlego Formation, Quinnanie Shale, and Wandagee Formation
Coyrie Formation and Mallens Sandstone

Wyloo Group

Fine- to coarse-grained sandstone, siltstone, minor granule to pebble conglomerate
Callytharra Formation

Lyons Group

Diamictite, sandstone and siltstone (locally calcareous), shale, and boulder beds and lags

Unassigned units

Dolerite dykes, sills, or plugs
Quartz vein or pod;

c. 570 Ma Mulka Tectonic Event

Mundine Well Dolerite Suite

1030–955 Ma Edmundian Orogeny

Thirty Three Supersuite

Leucocratic granite and metagranite, and pegmatite
Errabiddy Sandstone

Gifford Creek Carbonatite Complex

Ferroan carbonatite; sills and dykes of Fe-carbonate
Hematite–magnetite veins
Kulkatharra Dolerite

Collier Group

Ilgarari Formation
Backdoor Formation and Calyie Formation

1385–1200 Ma Mutherbukin Tectonic Event

Narimbunna Dolerite

Edmund Group

Discovery, Devil Creek, Ullawarra and Coodardoo Formations
Kiangi Creek Formation and Muntharra Formation
Gooragoora Formation, Blue Billy Formation and Cheyne Springs Formation
Yilgatherra Formation and Irregully Formation
Mount Augustus Sandstone

1680–1620 Ma Mangaroon Orogeny

Unassigned units

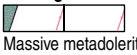

Massive metadolerite and foliated amphibolite
Metadolerite

Durlacher Supersuite

Granite and minor gabbro

Pooranoo Metamorphics

Pelitic and psammitic schist, quartz metasandstone, feldspathic metasandstone and metaconglomerate, and phyllite
Mount James Subgroup
Coor-de-wandy Formation:

1820–1770 Ma Capricorn Orogeny

Moorarie Supersuite

Undivided; granite and minor gabbro
Gooche Gneiss
Massive, subophitic metagabbro

Leake Spring Metamorphics

Pelitic and psammitic schist

Bertibubba Supersuite

Granite and metagranitic rocks

2005–1950 Ma Glenburgh Orogeny

Unassigned units

Amphibolite
Plagioclase–actinolite–tremolite gneiss
Fine- to medium-grained ultramafic schist

Camel Hills Metamorphics

Pelite, calc-silicate rock

Dalgaringa Supersuite

Metagranite and granitic gneiss

Moogie Metamorphics

Psammitic and peliti schist

Halfway Gneiss

Interlayered leucocratic and mesocratic granitic gneiss

YILGARN CRATON

Padbury Group

Undivided; sandstone, siltstone, mudstone, banded iron-formation, granular iron-formation, conglomerate, and dolostone
Millidie Creek Formation
Wilthorpe Formation
Labouchere Formation

2005–1950 Ma Glenburgh Orogeny

Bryah Group

Narracoota Formation
Trillbar Complex

Unassigned granitic units

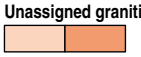

Granitic rocks, undivided
Granitic gneiss with greenstone enclaves

Unassigned greenstone units

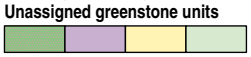

Amphibolite
Ultramafic rock, undivided
Felsic volcanic rock, undivided
Mafic volcanic rocks with minor mafic and ultramafic intrusive rocks

Unassigned sedimentary units

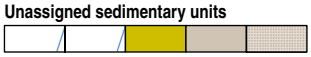

Calc-silicate gneiss
Banded iron-formation and ferruginous banded chert
Meta banded iron-formation
Quartzite, quartz–mica schist, pelite, amphibolite, meta-ultramafic rocks
Foliated quartzite

Unassigned igneous units

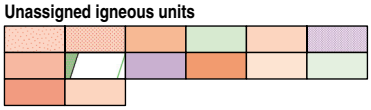

Leucocratic granitic gneiss
Granite gneiss
Foliated metagranitic rocks
Mafic rock, undivided
Granitic rocks, undivided
Fine- to medium-grained ultramafic rock
Granitic gneiss
Foliated biotite metamonzogranite
Gneiss, undivided
Amphibolite
Ultramafic rock, undivided
Granitic gneiss and granitic rocks
Felsic and mafic granulite, undivided
Interlayered meta-ultramafic and metamafic rocks

Rocky Bore Granite
Warrigal Gneiss

SPJ41

08.05.12

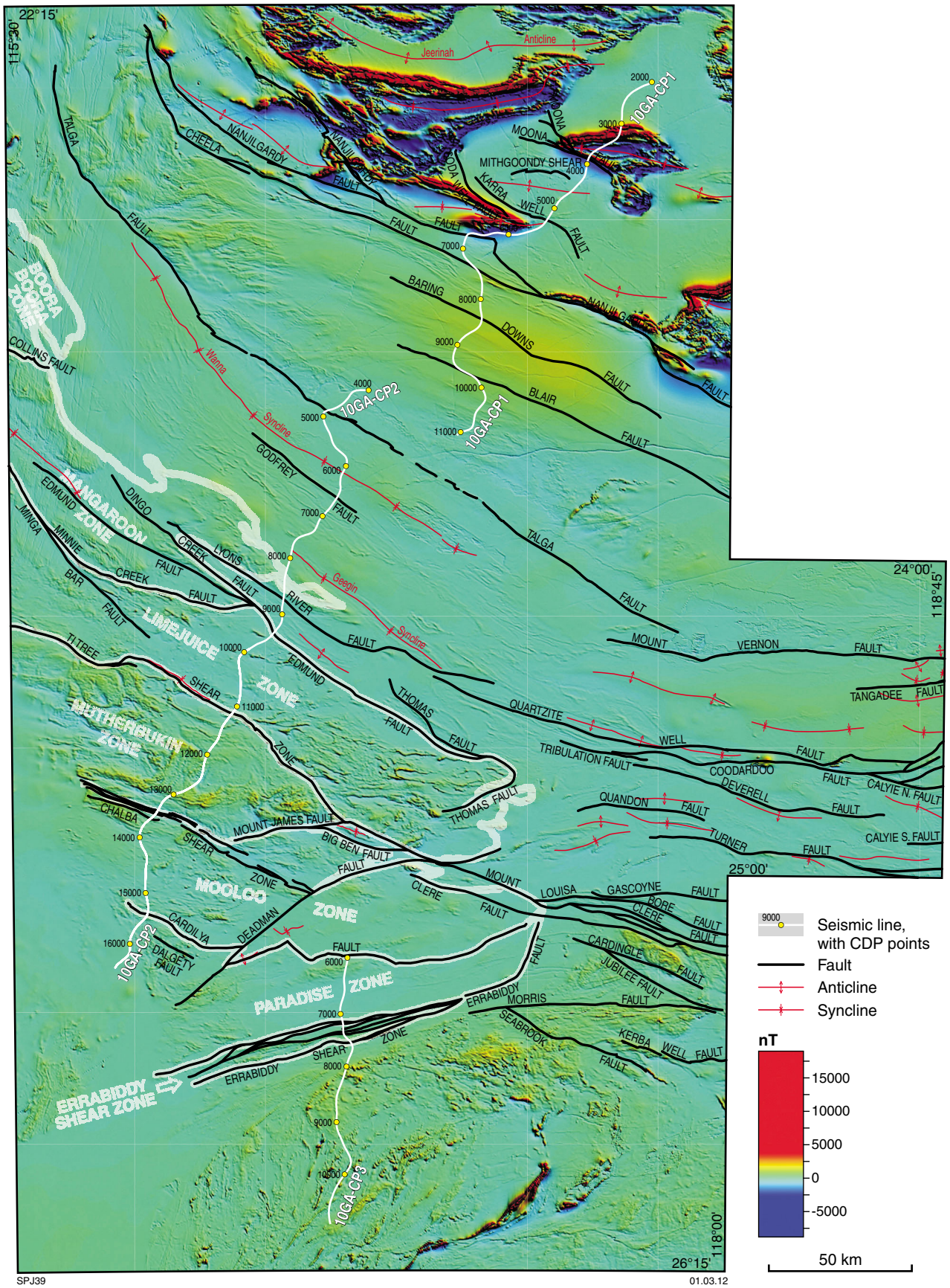

Frontispiece 2. Regional 300–500 m line-spaced TMI aeromagnetic data

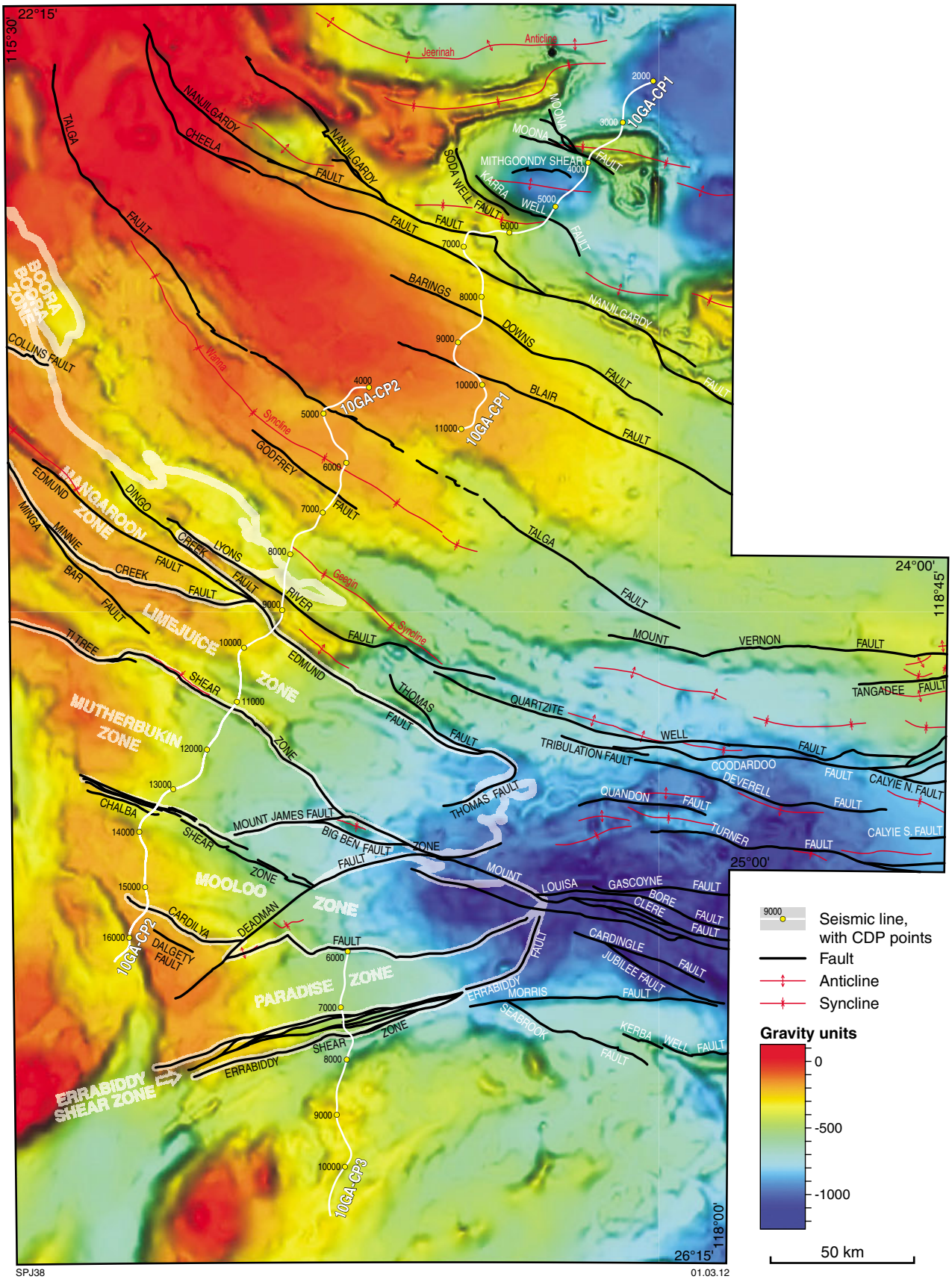

Frontispiece 3. Regional 2.5 km bouguer anomaly gravity data

The Capricorn seismic survey: experimental design, acquisition, and processing

by

BLN Kennett[1], IM Tyler, J Maher[2], J Holzschuh[2], T Fomin[2], and RD Costelloe[2]

Introduction

Following the establishment of the AuScope infrastructure initiative in 2007, a call for proposals was made for transect components, particularly seismic reflection profiling. Ian Tyler (Geological Survey of Western Australia) and Peter Cawood (University of Western Australia, now University of St Andrews) had already developed a comprehensive plan for reflection transects across Western Australia, and they selected a line crossing the Capricorn Orogen for submission to the AuScope call. The proposal received excellent reviews and was selected for AuScope support. Detailed planning was therefore undertaken to establish a practical line of survey.

The objective was to start in the Pilbara Craton, cross the Fortescue, Hamersley, Turee Creek, Ashburton, Edmund and Collier Basins, and the Gascoyne Province, and finish in the northern part of the Yilgarn Craton. This was rather more than could be supported by AuScope alone; fortunately, the Western Australian Goverment's 'Exploration Incentive Scheme' enabled the Geological Survey of Western Australia (GSWA) to join as an equal partner in the reflection survey. AuScope also provided additional support for a detailed magnetotelluric survey to be run along the line of the reflection profiles.

The nature of the terrain and availability of access meant that it would not be possible to have a single continuous survey line. However, by exploiting roads and minor tracks, it was possible to identify three segments that were logistically feasible, and which allowed along-strike connection of geological structures (see Frontispiece 1; Plate 1). The length of reflection profiling over the three segments was 581 km; although some sharp bends were required by the nature of the available access, these were confined to a small part of the total survey.

[1] Research School of Earth Sciences, The Australian National University, Canberra ACT 2000

[2] Mineral and Natural Hazards Division, Geoscience Australia, GPO Box 378, Canberra ACT 2601

Background to the transect

The following summary of the Capricorn Orogen's geological history is modified from Cawood and Tyler (2004), Sheppard et al. (2010), and Johnson et al. (2010, 2011). The Capricorn Orogen records the operation of one or more Paleoproterozoic Wilson cycles. These cycles involved the late Archean and early Paleoproterozoic rifting and break-up of two late Archean continents to form continental margin assemblages on what are now the southern margin of the Pilbara Craton and the northern margin of the Yilgarn Craton. These margins were juxtaposed, overlain by foreland basin sequences, and deformed — together with accreted exotic continental and ?oceanic fragments, and arc sequences — during the subsequent subduction and closure of an intervening ocean or oceans. The cycles culminated in mid to late Paleoproterozoic collision and suturing to form the amalgamated West Australian Craton. The Capricorn Orogen is more 'complete' than any other within the Australian Precambrian, and is unique in having distinctly different, opposing, continental fragments exposed along both the northern and southern orogen margins, together with the exposure of upper- to mid-crustal rock units within the orogen itself. As such, this orogen provides an important insight into Paleoproterozoic collisional processes.

The Capricorn Orogen consists of the Paleoproterozoic plutonic igneous rocks and medium- to high-grade metamorphic rocks of the 2550–1620 Ma Gascoyne Province; a series of Paleoproterozoic volcano-sedimentary and sedimentary basins, including the 2200–1805 Ma Ashburton Basin, the c. 1805 Ma Blair Basin, the 2150–1840 Ma Yerrida Basin, the 2020–1900 Ma Bryah and Padbury Basins, and the 1840–1800 Ma Earaheedy Basin; and the deformed margins of the Pilbara and Yilgarn Cratons. The Narryer Terrane, located along the northwestern margin of the Yilgarn Craton, includes early Archean granitic gneisses (3650–3300 Ma) that contain older lenses and fragments of c. 3730 Ma anorthosite, and mafic to ultramafic rocks; metasedimentary rocks from this region contain detrital zircons as old as c. 4400 Ma. The Pilbara Craton and

overlying Hamersley Basin contain some of the earliest records of life on Earth, and are a source of major hematite iron ore deposits.

The orogen underwent major tectonothermal events during the 2215–2145 Ma Ophthalmian Orogeny, the 2005–1950 Ma Glenburgh Orogeny, the 1820–1770 Ma Capricorn Orogeny, and the 1680–1620 Ma Mangaroon Orogeny. The Mesoproterozoic Edmund and Collier Basins are exposed across significant areas of the central part of the orogen, and reactivation within the orogen has produced extensive deformation of these basins during the Mesoproterozoic Mutherbukin Tectonic Event (1385–1200 Ma), and the Neoproterozoic Edmundian Orogeny (1030–955 Ma) and c. 570 Ma Mulka Tectonic Event.

The Errabiddy Shear Zone separates early to late Archean rocks of the Narryer Terrane (northwestern Yilgarn Craton) from the latest Archean to Paleoproterozoic rocks of the Glenburgh Terrane (Gascoyne Province). The Narryer Terrane underwent reworking in part during the Glenburgh and Capricorn Orogenies, and the southern margin of the Capricorn Orogen is defined by the southern limit of this reworking. The northern margin of the Capricorn Orogen comprises the Paleoproterozoic Ashburton, Blair, Mount Minnie, and Bresnahan Basins. Deformation of this region during the Ophthalmian and Capricorn orogenic events formed a number of fold belts; the northern limit of the Ophthalmia Fold Belt marks the northern limit of the orogen.

Thus, the present transect across the Capricorn Orogen and bounding margins of the Yilgarn and Pilbara Cratons passes through a world-class example of Precambrian continental assembly and reworking.

The major objectives of the transect were to:

1. image the crust and upper mantle structure along the survey lines, passing through the Fortescue, Hamersley, and Turee Creek Basins of the Pilbara Craton, the Gascoyne Province, and the northern margin of the Yilgarn Craton
2. establish the subsurface extent of Archean crust beneath the Capricorn Orogen, and identify whether the Pilbara and Yilgarn Cratons are in direct contact, or whether they are separated by one of more Proterozoic crustal elements
3. determine the nature and character of basement to the Proterozoic basins flanking the Yilgarn and Pilbara Cratons (e.g. the Ashburton, Yerrida, and Earaheedy Basins)
4. link surface units and structures (e.g. the Errabiddy Shear Zone) — including their age, geochemical signature, and, in the case of structures, their movement history — with their deep geophysical character, in order to better understand the geological evolution of the orogen
5. understand the processes driving the Proterozoic assembly of the West Australian Craton, and the subsequent processes of repeated crustal reworking within a long-lived orogen
6. identify structures cutting through the crust to the mantle, which may have acted as pathways for fluid flow to mineral systems, including the world-class hematite iron ore deposits of the Hamersley Basin, copper–lead mineralization at Abra, and orogenic lode-gold mineralization at Mount Olympus on the Pilbara Craton margin.

Acquisition of the seismic reflection data

AuScope and GSWA collaborated with Geoscience Australia in the acquisition and processing of the reflection survey, with Terrex Seismic contracted to collect the data in the field. Due to wet conditions in central Australia at the time, the seismic crew became available somewhat earlier than anticipated, and the survey was carried out in April and May 2010.

Acquisition of the reflection seismic survey commenced on 11 April 2010, at the north end of the 10GA–CP1 line. The first base camp was on Rocklea Station; the survey headed initially in a southwesterly direction, and afterwards in a more southerly direction. Conditions at the southern end of the line were found to be too difficult for seismic acquisition, and the line was terminated about 4 km short of the original target.

Following the completion of 10GA–CP1, there was a significant remobilization to start at the northern end of the 10GA–CP2 line. The first base camp on 10GA–CP2 was located on the Wanna Station access road, approximately 19 km north of the Cobra – Mount Augustus Road. The northern part of this line exploited station tracks that allowed access into the rugged Minnierra Range. The reflection profiling then continued south along the Cobra – Dairy Creek Road.

The 10GA–CP3 line started at the junction of the Dalgety Downs – Landor Road and the Erong Road, following the Erong Road south to end at the junction with the Beringarra–Byro Road. The crew then shifted from the end of the 10GA–CP3 line to the east, to the start of the 10GA–YU1 line of the Youanmi Survey, approximately 8 km west of Beringarra Homestead. The survey was completed on 20 May 2010.

Seismic processing was carried out at Geoscience Australia, with preliminary migrated sections made available for interpretation workshops held in Perth, in March and June 2011.

The location of the line segments, superimposed on a gravity image of the area, is displayed in Frontispieces 2 and 3. The seismic acquisition parameters for the survey are shown in Table 1.

The seismic data were collected using 300 live channels spread over 12 km, with the source array located at the centre of the spread. The maximum offset receiver groups were 6 km from the source. The seismic data were recorded using a Sercel 428XL recording system in SEG-D de-multiplexed format. The recording system

cross-correlated each of the three recorded sweeps for each vibration point (VP) with its respective reference sweep, and then stacked the cross-correlated sweeps, creating a single, 20 s record for each VP that was then written to a LTO2V tape. The average survey production rate was of 182 VPs, or 14.9 km, per day.

Table 1. Acquisition parameters used for the Capricorn seismic survey

Source type	3 IVI Hemi-60 vibrators
Source array	15 m pad-to-pad, 15 m moveup
Sweep length	3 x 12 s
Sweep frequency	6–64 Hz, 12–96 Hz, 8–72 Hz
Vibration Point (VP) interval	80 m
Received group	12 geophones @ 3.3 m spacing
Group interval	40 m
Number of recorded channels	300
Fold (nominal)	75
Record length	20 x @ 2 ms

Processing of the seismic reflection data

The reflection seismic data from the Capricorn seismic survey were processed by the Seismic Acquisition and Processing team of the Onshore Energy and Minerals Division at Geoscience Australia, using Disco/Focus processing software on a Red Hat Enterprise Linux Sun Fire X4600 M2 server.

The following sequence was used to process seismic reflection data for lines 10GA–CP1, 10GA–CP2, and 10GA–CP3:

- SEG-D to Disco format conversion, resample to 4 ms
- Quality control displays
- Crooked line geometry definition (CDP interval 20 m)
- Inner trace edits
- Common midpoint sort
- Gain recovery (spherical divergence)
- Spectral equalization (1000 ms AGC gate)
- Application of floating datum residual refraction statics
- Application of automatic residual statics
- Velocity analysis
- Normal moveout
- Band pass filter
- Offset regularization and dip moveout (DMO) correction
- Velocity analysis
- Common midpoint stack
- Migration
- Signal coherency enhancement (digistack and fkpower)
- Application of mean datum statics, datum 200 m (AHD), replacement velocity 5900 m/s
- Trace amplitude scaling for display

A reduced processing stream was used in the field to produce field stacks to control and monitor data quality whilst the survey was in progress. As the transect was linear, with some changes of geometry, it was processed using algorithms based on an assumption of 2D geometry. This 2D assumption has implications for the processing and interpretation of the resulting processed data; these implications are explained in the description of the key processing steps.

Crooked line geometry definition

As the seismic line followed the available access routes, none of the three segments were straight. 10GA–CP1 had strong changes in direction, and the northern end of 10GA–CP2 also had sharp bends around topographic ridges. Therefore, the processing was based around the definition of a section line (Common Depth Point, or CDP, line) that smooths out variations in the line.

The data was binned into common midpoint gathers based on a calculated CDP line, and then processed using the CDP method. The CDP line is a curve of best fit through the midpoints between sources and receivers, which optimizes the fold of the data and minimizes the subsurface area of reflections contributing to each nominal CDP. Each trace (source–receiver pair) is allocated to the CDP bin nearest to its midpoint. The CDP bins were defined to be 20 m along the line. The effects of bin size, and of midpoint scatter within the bin, are most critical at shallow depths. Where the line has sharp bends, there is likely to be smearing and poor resolution of shallow data. The effect of bends on deeper data can also be significant, depending on the relative directions of the seismic line, and the dip of the structures to be imaged.

The CDP line was processed as if it was straight, ignoring the effects of changing azimuth along the line. This simplification of the processing to 2D geometry, applied at the start of the processing sequence, is reasonable for large sections of the line that are relatively straight, although it later becomes impossible to correctly migrate reflections, and therefore to correctly image reflectors at significant bends in the line.

Refraction statics

Variations in surface elevation, weathering layer depth, and weathering layer velocity can produce significant time delays in land seismic data. Variations over distances shorter than the spread length can degrade the stack, with the reflections no longer aligning across the traces to be stacked. Variations over distances longer than a spread length will not significantly affect the stack quality, but can introduce spurious long wavelength structures in the stacked reflections; static corrections are applied in the processing stream to remove these effects. For the Capricorn reflection seismic processing, static corrections were calculated by picking first-break refracted arrivals from shot records, and then creating a near-surface refractor model of the weathering layer. The refraction static corrections were applied in two stages using a floating datum. An intermediate step of automatic residual static corrections produced fine tuning of the corrections.

The final static corrections were calculated relative to a datum of 200 m (AHD), using a replacement velocity of 5900 m/s.

The process of picking first breaks for each shot is time consuming. Although automatic methods of picking are used, each set of first breaks needs to be checked and these frequently require editing. Also, the quality of the first-break waveforms depends on the nature of the geology, both at the source and at the receiver arrays. In some parts of the line, a significant proportion of the first break picks were discarded due to poor signal-to-noise ratios. The number of picks for each shot in the model can vary along the lines, and as a result, the number of layers to be modelled must be specifically selected. Once the first breaks for the line have been picked and edited and the number of layers to be modelled is selected, the refractor model can be calculated. A one or two layer model can usually provide a suitable solution to the effects of weathering. For the Capricorn line, a single layer model was selected to best represent weathering over the entire transect.

Spectral equalization

Spectral equalization is a process used to sharpen the reflection wavelet and to suppress low-frequency energy, primarily ground-roll energy, which is surface wave energy generated by the vibrators. The frequency spectrum of the data is flattened over a specified frequency range and within a specified time gate, thereby reducing the high energy, low frequency surface-wave noise relative to the higher frequency energy of the reflections. Therefore, the resulting data has better resolution, particularly in the shallow part of the section (0–2 s two-way travel time (TWT)). The selection of an appropriate frequency range and time gate is based on selective testing and on spectral analysis of the data.

Normal moveout correction

The normal moveout (NMO) correction removes time variations across CDP gathers, by adjusting for time delays caused by progressively increasing offset between source and receivers. The NMO correction is applied as a stacking velocity that best aligns the reflections in the CDP gather. Two different techniques were used to calculate the stacking velocities: velocity scans and constant velocity stacks. Both techniques result in a velocity field varying in time and space (along the line), which maximizes the stack response of the data. Velocity analysis requires interactive selection of optimal stack responses, and is one of the most time consuming processes in the processing sequence. Velocity analysis is usually made on spectral equalized CDP gathers after automatic residual statics, and also after dip moveout corrections are applied. Analyses can also be iterated where required, and areas of complex geology or poor stacking quality may require more closely spaced velocity analyses. The velocity boxes annotated onto the seismic sections are the final velocities picked from the dip moveout gathers, with all corrections applied except for the mean refraction statics; that is, the velocities are applied prior to moving the data to its final datum.

Dip moveout correction

The dip moveout (DMO) correction, also known as partial pre-stack migration, adjusts the NMO correction based on the increase in stacking velocity encountered as the structural dip increases, and has the effect of correcting the NMO to account for different dips occurring along the line. The process effectively moves reflection energy between traces within and between CDP gathers based on the apparent dip of the reflectors, creating a new set of DMO-corrected CDP gathers. After DMO, intersecting dipping and flat reflections will correctly stack with the same stacking velocity. DMO is a computationally intensive processing step.

Common midpoint stack

The common midpoint stack is simply the summing of traces in a CDP gather to produce a single trace at the CDP location. The traces in the gather are aligned by the NMO and DMO processes, with the aim of an optimal sum. In principle, stacking the data can improve the signal-to-noise ratio of the data by $\sqrt{n}$, where n is the number of traces summed (the fold). A nominal fold of 75 resulted from the acquisition geometry for the Capricorn seismic survey.

Post-stack time migration

Migration is the final processing step, and involves moving dipping reflections to their most likely lateral positions based on an assumed velocity distribution. Reflections that appear to be dipping on the stack section will be moved up-dip and shortened after migration. Diffraction hyperbolas resulting from discontinuities, such as the termination of reflectors at faults, and which are visible on the stack section, should collapse into a small region after migration. Note that areas with poor signal-to-noise ratios, and those with sharp bends in the line, can produce artefacts in the data that will not migrate successfully. The main parameters to be selected when performing migration are the velocity field, and the dip ranges to process. The velocity field used usually consists of a percentage of the stacking velocity. Tests are run with different percentages and the optimum migration velocity selected. If migrated correctly, the final time section should have dipping reflections in the correct spatial location. A migration velocity function of 70–85% of the stacking velocities was applied to the Capricorn seismic data. The Omega-X (frequency–space) migration algorithm is a finite difference approximation to the monochromatic wave equation (Yilmaz, 2001), used to migrate data for lines 10GA–CP1 and 10GA–CP2. The time–space Kirchhoff migration algorithm (Stolt and Benson, 1986) was used to migrate data for the 10GA–CP3 line. The effect of migration on the stacked data is illustrated in Figure 1, which shows stacked and migrated images for part of the Capricorn Orogen. Coherency filters were applied to the data to enhance reflections for the final display images.

Conclusions

Reflection profiling has provided very clear images along the Capricorn Orogen seismic lines, identifying many

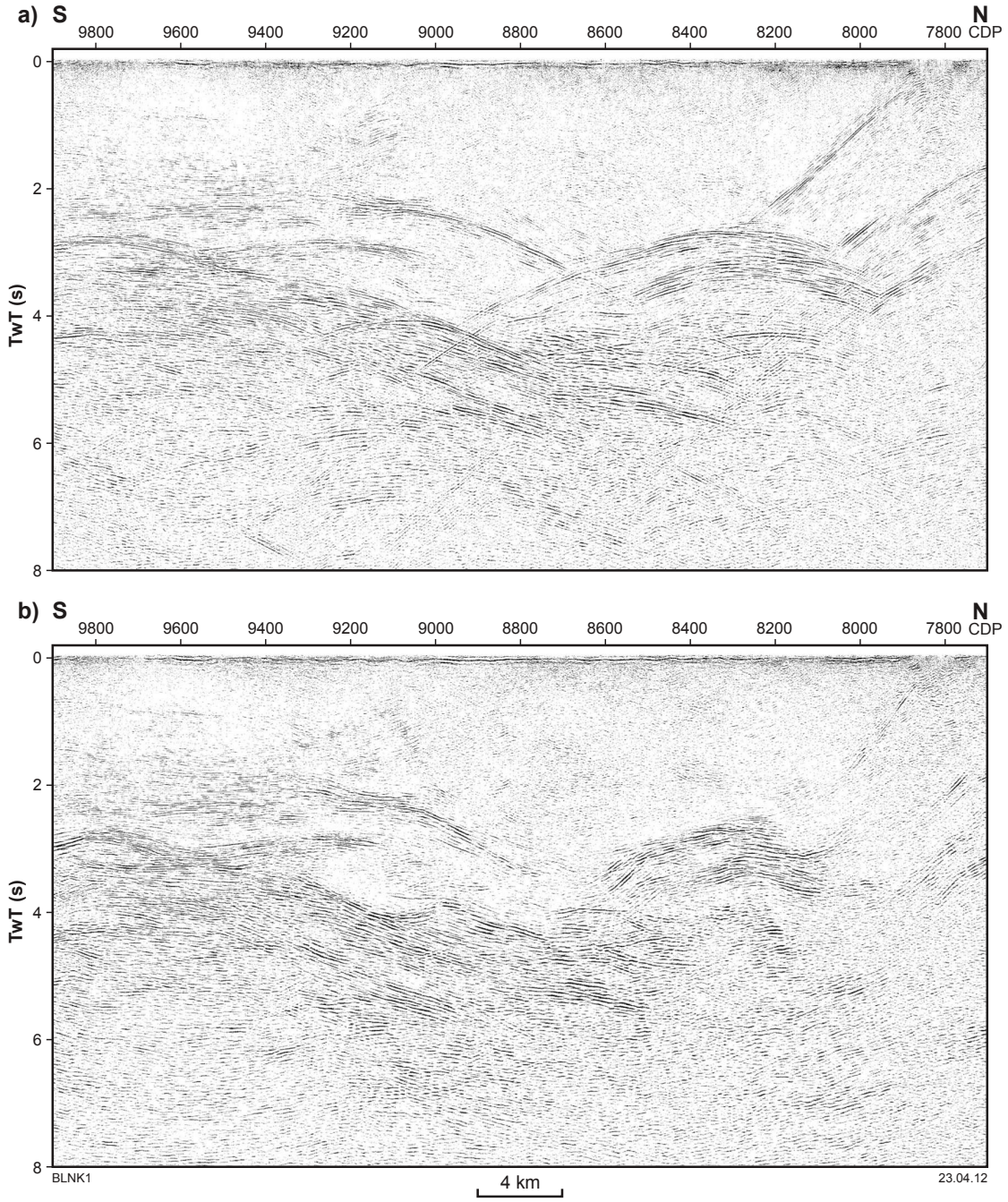

Figure 1. a) fragment of the final stack section for seismic transect 10GA–CP1 of the Capricorn seismic survey; b) final migrated section for the same part of the line, showing how the migration process collapses diffraction energy and moves dipping reflections to the correct location. CDP equal 20 m; V:H=1 for a crustal velocity of 6000 m/s.

dramatic structures that extend right through the crust. As most of the geological targets can be recognized and tracked to depth, the transect provides valuable information to help elucidate the evolution of the orogen.

Unfortunately, in the Hamersley region, the transect geometry imposed by the available access meant that the resolution of near-surface structures was diminished at the edges of some major geological contrasts. The base of the crust varies significantly, changing from a shallow but variable Mohorovičić ('Moho') character visible beneath the Pilbara Craton, to a deep, indistinct crust–mantle boundary beneath the southern part of the Capricorn Orogen, and passing into a shallower Moho once the northern edge of the Yilgarn Craton is reached (at the southern end of line 10GA–CP3).

Acknowledgements

The success of this survey is the result of hard work by many people, and we would like to acknowledge assistance from AuScope headquarters (R Haydon and T Down), and contributions from the seismic contractors, Terrex Seismic, and those individuals involved in the interpretation workshops.

References

Cawood, PA and Tyler, IM 2004, Assembling and reactivating the Proterozoic Capricorn Orogen: lithotectonic elements, orogenesis and significance: Precambrian Research, v. 128, p. 201–218.

Johnson, SP, Sheppard, S, Rasmussen, B, Wingate, MTD, Kirkland, CL, Muhling, JR, Fletcher, IR and Belousova, E 2010, The Glenburgh Orogeny as a record of Paleoproterozoic continent–continent collision: Geological Survey of Western Australia, Record 2010/5, 54p.

Johnson, SP, Sheppard, S, Thorne, AM, Rasmussen, B, Fletcher, IR, Wingate, MTD and Cutten, HN 2011, The role of the 1280–1250 Ma Mutherbukin Tectonic Event in shaping the crustal architecture and mineralization history of the Capricorn Orogen, *in* GSWA 2011 extended abstracts: promoting the prospectivity of Western Australia: Geological Survey of Western Australia, Record 2011/2, p. 1–3.

Sheppard, S, Bodorkos, S, Johnson, SP, Wingate, MTD and Kirkland, CL 2010, The Paleoproterozoic Capricorn Orogeny: intracontinental reworking not continent–continent collision: Geological Survey of Western Australia, Report 108, 33p.

Stolt, RH and Benson, AK 1986, Seismic migration: theory and practice: Geophysical Press Ltd, London, UK, 382p.

Yilmaz, O 2001, Seismic data analysis: processing, inversion, and interpretation of seismic data (2nd edition): Society of Exploration Geophysicists, Tulsa, Oklahoma, USA, 2027p.

Geology of the northern Capricorn Orogen

by

AM Thorne, SP Johnson, IM Tyler, HN Cutten, and O Blay

Introduction

Seismic transects 10GA–CP1, 10GA–CP2, and 10GA–CP3 are located in the western part of the Capricorn Orogen, a major zone of Proterozoic sedimentation, deformation, metamorphism, and magmatism lying between the Archean Yilgarn and Pilbara Cratons (Gee, 1979; Cawood and Tyler, 2004; Plate 1; Frontispieces 1–3). The orogen includes metamorphic and igneous rocks of the Gascoyne Province, and a number of low-grade metasedimentary and metavolcanic basins, including the late Paleoproterozoic to Mesoproterozoic Edmund and Collier Basins. It also includes the deformed margins of the Yilgarn and Pilbara Cratons. The northern transect, 10GA–CP1, crosses granite–greenstones of the Pilbara Craton and an overlying supracrustal succession that begins within the Archean Fortescue Basin and ends within the Paleoproterozoic Blair Basin (Plate 1; Frontispiece 1). Transect 10GA–CP2 starts in the Edmund and Collier Basins, and extends southwards across Paleoproterozoic to Neoproterozoic rocks of the Mangaroon, Limejuice, Mutherbukin, Mooloo, and Paradise Zones of the Gascoyne Province. The southern transect, 10GA–CP3, begins in the Paradise Zone of the Gascoyne Province, crosses the Errabiddy Shear Zone, and ends in the Archean Narryer Terrane of the Yilgarn Craton.

The seismic transects across the Capricorn Orogen provide an important opportunity to gain insight into the deep crustal structure and geological evolution of a Proterozoic orogenic belt and its associated Archean cratons (Kennett et al., 2011). Early interpretations of the Capricorn Orogen — e.g. Horwitz and Smith (1978), and Gee (1979) — favoured an intracratonic setting. These were followed by plate tectonic models in which Proterozoic orogeny was driven by collision between the hitherto unrelated Pilbara and Yilgarn Cratons (Muhling, 1988; Tyler and Thorne, 1990; Evans et al., 2003). More recent work has highlighted the complexity of the Capricorn Orogen, which has now been shown to record seven major orogenic events: the 2215–2145 Ma Ophthalmian Orogeny, the 2005–1950 Ma Glenburgh Orogeny, the 1820–1770 Ma Capricorn Orogeny, the 1680–1620 Ma Mangaroon Orogeny, the 1385–1200 Ma Mutherbukin Tectonic Event, the 1030–950 Ma Edmundian Orogeny (Occhipinti et al., 2001, 2004; Rasmussen et al., 2005; Sheppard et al., 2005, 2007, 2010a,b; Johnson et al., 2009, 2010, 2011a,b), and the c. 570 Ma Mulka Tectonic Event (Sheppard et al., 2010a; Johnson et al., 2011a). The oldest of these, the 2215–2145 Ma Ophthalmian Orogeny, is now believed to be the result of a collision between the Pilbara Craton and the Glenburgh Terrane of the Gascoyne Province (Occhipinti et al., 2004; Sheppard et al., 2004; Johnson et al., 2010, 2011b). It was followed by collision between the combined Pilbara Craton – Glenburgh Terrane and the Yilgarn Craton, an event that resulted in the 2005–1950 Ma Glenburgh Orogeny (Occhipinti et al., 2004; Sheppard et al., 2004; Johnson et al., 2010, 2011b). Subsequent orogenic events, including the 1820–1770 Ma Capricorn Orogeny, which was formerly thought to record the main Pilbara–Yilgarn collision (Tyler and Thorne, 1990; Evans et al., 2003), have since been shown to result from intracratonic reworking within the orogen (Sheppard et al., 2005, 2007, 2010a,b; Johnson et al., 2009).

Geological setting of seismic line 10GA–CP1

Seismic line 10GA–CP1 extends across the northern margin of the Capricorn Orogen, from the northern limb of the Turner Syncline, through the Rocklea Dome and southern Hardey Syncline, before crossing the Nanjilgardy Fault system into the Ashburton Basin to the south (Plate 1; Frontispiece 1). In doing so, it crosses greater than one billion years of geological history, ranging from the Archean Pilbara Craton granite–greenstone basement, to the overlying Archean to Paleoproterozoic supracrustal succession consisting of, in ascending order, the Fortescue, Hamersley, Turee Creek, Wyloo, and Capricorn Groups (Fig. 1). The Wyloo Group is generally discussed in terms of lower and upper divisions, based on the presence of a significant unconformity in the middle of the succession, representing a hiatus of up to 200 million years.

During the late Archean and Paleoproterozoic, the northern part of the orogen evolved from a rifted margin to a passive margin, before being converted to an active margin, and subsequently into a series of foreland

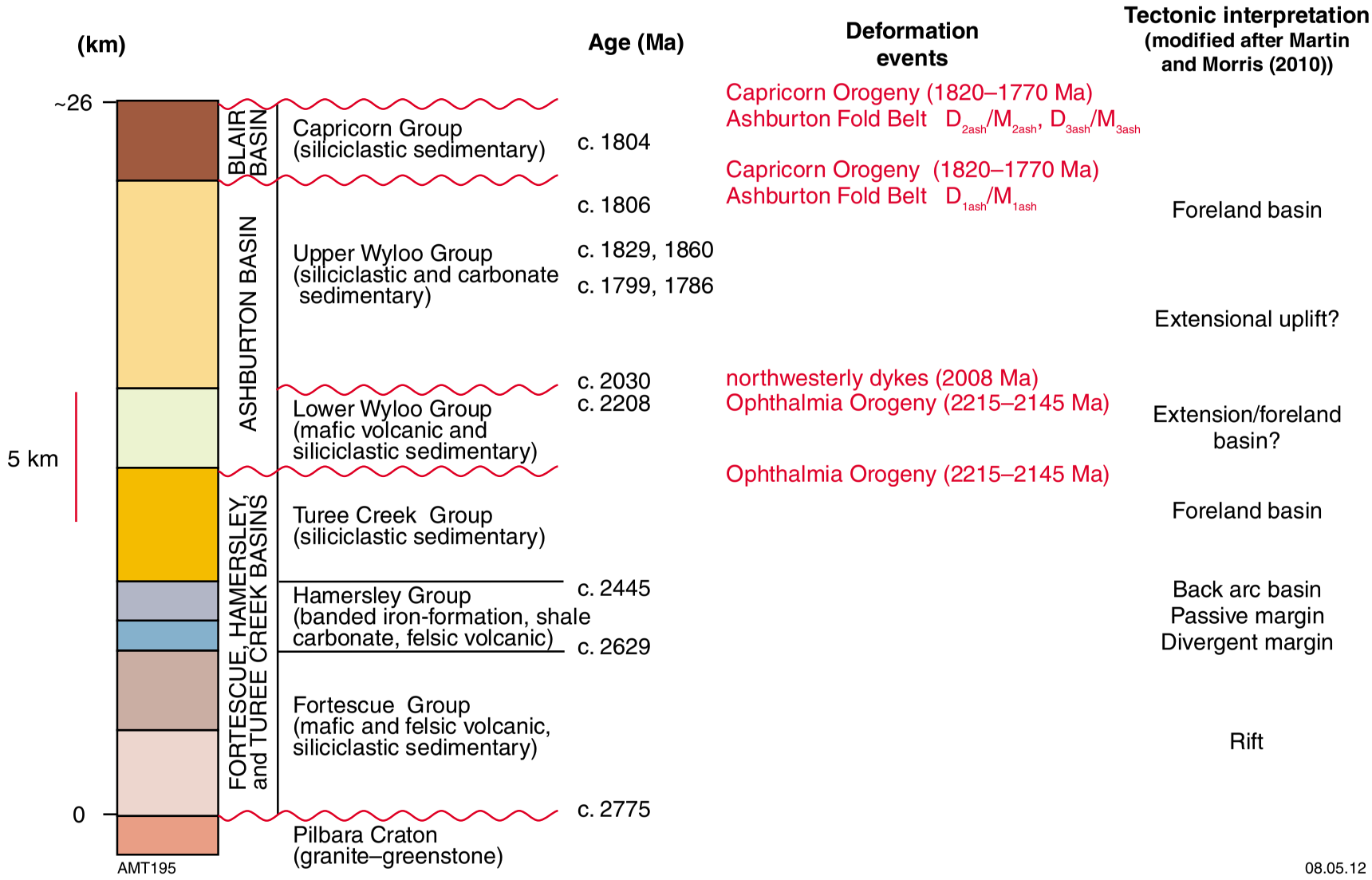

Figure 1. Generalized stratigraphy and deformation history of the northern Capricorn Orogen. The tectonic interpretation is modified after Martin and Morris (2010). Geochronology sources are cited in the text.

basins (Blake and Barley, 1992; Martin et al., 2000; Trendall et al., 2004; Martin and Morris, 2010). As part of this evolution, basement and supracrustal rocks were subject to two major orogenic events, the 2215–2145 Ma Ophthalmian Orogeny (Rasmussen et al., 2005) and the 1820–1770 Ma Capricorn Orogeny (Sheppard et al., 2010a,b).

Pilbara Craton basement

Within the northern Capricorn Orogen, Pilbara Craton granite–greenstone basement rocks are exposed in the Wyloo, Rocklea, and Milli Milli Domes, and in the Sylvania Inlier (Frontispiece 1; Plate 1). Greenstones are dominated by low-grade metamorphosed mafic volcanic and siliclastic sedimentary rocks. Granitic rocks are mostly biotite monzogranite and minor pegmatite, and are locally intruded by pre- Fortescue Group metadolerite dykes. The minimum age of the granite–greenstones is fixed by the c. 2775 Ma age of the overlying basal Fortescue Group (Trendall et al., 2004). Their maximum age is unknown, although comparison with similar granite–greenstone assemblages in the northern Pilbara Craton (Hickman and Van Kranendonk, 2008) suggests they probably formed between 3800–2830 Ma.

Fortescue Group: Pilbara Craton rifting

Granite–greenstone rocks are unconformably overlain by mixed volcano-sedimentary rocks of the Fortescue Group, formed during protracted rifting of the Pilbara Craton between c. 2775 and c. 2630 Ma (Blake, 1993, 2001; Thorne and Trendall, 2001; Blake et al., 2004; Trendall et al., 2004). In the northwestern and northeastern Pilbara, Fortescue Group sedimentation and volcanism was controlled by a northeast-trending extensional fault system (Blake, 2001), whereas in the southern Pilbara, Thorne and Trendall (2001) argued that the fault system was principally oriented east-southeast. It is also likely that during much of the early to middle rifting stages, these areas were separated from each other by topographic highs, such as the Yule–Sylvania high. These architectural controls created separate sub-basins (Blake, 1984; Thorne and Trendall, 2001), in which the local Fortescue Group stratigraphies have a broadly similar framework, but are each quite different in detail.

In the South Pilbara Sub-basin (Thorne and Trendall, 2001), the Fortescue Group is up to 6.5 km thick, and is subdivided, in ascending order, into seven formations, which are grouped into four major tectono-stratigraphic units (Fig. 2). From the base upwards, Unit 1 comprises the Bellary Formation and Mount Roe Basalt; Unit 2 comprises the Hardey Formation; Unit 3 comprises the Boongal, Pyradie, and Bunjinah Formations; and Unit 4 is the Jeerinah Formation. Thick mafic to ultramafic sills intrude much of the succession above the Mount Roe Basalt.

The Bellary Formation is a localized, 0.4 km thick, lacustrine or shallow-marine unit at the base of the Fortescue Group. It is conformably overlain by the 0 – 1.4 km thick Mount Roe Basalt that consists largely of subaerial basaltic lavas and subaqueous volcaniclastic rocks. These are unconformably overlain by the Hardey Formation, which is up to 1.8 km thick, and consists of a wide range of sedimentary and mafic and felsic volcanic rocks, laid down in a continental to shallow-marine setting. The middle to upper parts of the Fortescue Group conformably overly the Hardey Formation, and form a 3 km thick succession of subaqueous basaltic to komatiitic lavas and volcaniclastic rocks (the Boongal, Pyradie, and Bunjinah Formations). The Jeerinah Formation, the uppermost unit within the Fortescue Group, is up to 1.8 km thick, and consists of argillaceous sedimentary rocks interbedded with significant amounts of basaltic lava and volcaniclastic deposits.

The origin of the four major tectono-stratigraphic units of the Fortescue Group are interpreted as the result of deposition in an extensional tectonic setting. Units 1 and 2 were deposited in isolated fault-bounded sub-basins between c. 2775 and c. 2745 Ma (Trendall et al., 2004), under largely subaerial conditions. The separate sub-basins coalesced during the time of Unit 3 (2745–2715 Ma), when regional subsidence, accentuated by further normal faulting and tilting in the south, resulted in a change to coastal and deeper-shelf volcanism and sedimentation. Further subsidence during the time of Unit 4 (2715–2630 Ma) resulted in a major marine transgression and the establishment of deeper marine-shelf conditions over the entire Fortescue Basin. During this evolution, growth faulting appears to have had a major effect on Fortescue Group stratigraphy, with a marked increase in thickness and paleo- water depth being recorded when traced from north to south across the main faults that cut the sub-basin. Similarly, the thickness and frequency of intrusive sills in the Fortescue Group increases in a southward direction across the sub-basin fault system.

Hamersley Group: passive- to active-margin sedimentation and igneous activity

The 2.5 – 3.0 km thick Hamersley Group conformably overlies the Fortescue Group, and was deposited between c. 2630 and c. 2450 Ma, when the southern Pilbara evolved from a rifted to a passive continental margin and finally to an active margin (Morris and Horwitz, 1983; Blake and Barley, 1992; Thorne and Trendall, 2001; Trendall et al., 2004, Martin and Morris, 2010). Hamersley Group rocks reflect this largely deeper-marine distal setting, and are dominated by banded iron-formation (BIF), shale, chert, and fine-grained carbonate. Thin spherule layers, interpreted as resedimented impact debris, have also been recorded (Simonson and Hassler, 1997). Average (compacted) depositional rates for BIF, carbonate, and shale were 180 m per million years, 12 m per million years, and 5 m per million years, respectively (Trendall et al., 2004).

Seven major lithostratigraphic units are recognized within the Hamersley Group (Fig. 3). In ascending order, these are the Marra Mamba Iron Formation, Wittenoom Formation, Mount Sylvia Formation, Mount McRae Shale,

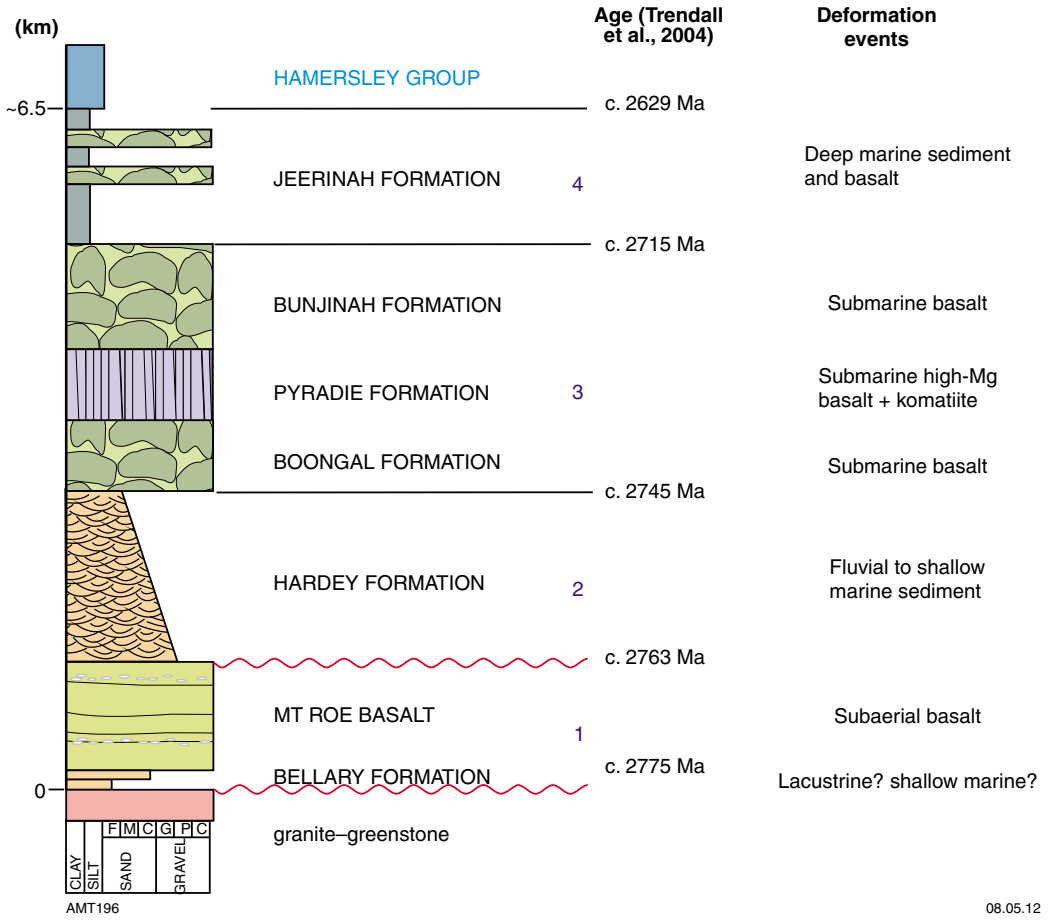

Figure 2. Stratigraphy of the Fortescue Group, showing tectono-stratigraphic units 1–4 and associated depositional environments. Major erosion surfaces are shown in red.

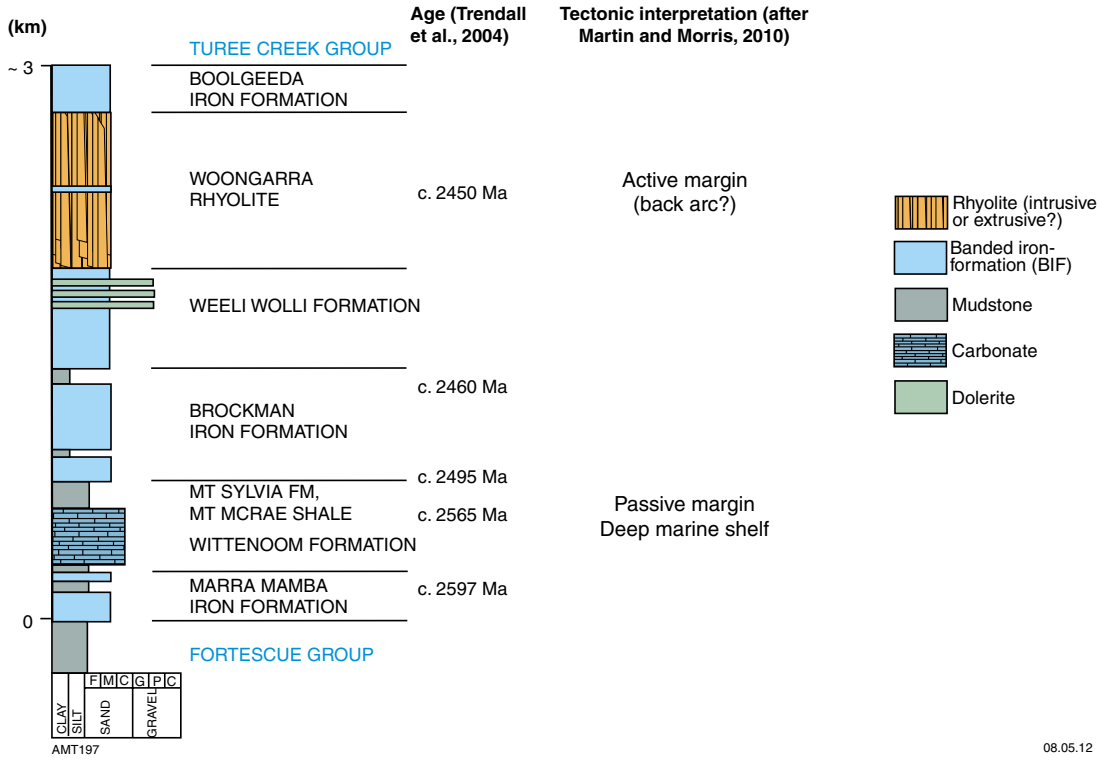

Figure 3. Stratigraphy of the Hamersley Group, showing the distribution of the principal rock types and interpreted tectonic setting.

Brockman Iron Formation, Weeli Wolli Formation, and Boolgeeda Iron Formation (Trendall and Blockley, 1970; Trendall, 1990; Simonson et al., 1993; Trendall et al., 2004). The status of the ~400 m thick Woongarra Rhyolite, which occurs below the Boolgeeda Iron Formation, is controversial. Trendall (1995) favoured an intrusive origin for this unit, whereas Doyle et al. (2001) suggested that it is has both intrusive and extrusive components. Significant thicknesses of mafic intrusive rocks are interlayered within the Weeli Wolli Formation; however, it is not known if these are coeval with the Woongarra Rhyolite.

Turee Creek Group and lower Wyloo Group: foreland basin sedimentation and volcanism during the Ophthalmian Orogeny

Deposition of the uppermost Hamersley Group (Boolgeeda Iron Formation), plus the overlying Turee Creek and lower Wyloo Groups, took place during the early foreland-basin stage of the 2215–2145 Ma Ophthalmian Orogeny, when the Pilbara Craton collided with a continent to the south (Blake and Barley, 1992; Martin et al., 2000; Rasmussen et al., 2005). Recent evidence suggests that this southern continent was the Glenburgh Terrane of the Gascoyne Province (Occhipinti et al., 2004; Sheppard et al., 2004, 2010a; Martin and Morris, 2010; Johnson et al., 2010, 2011b). An alternative view was put forward by Krapež and McNaughton (1999), who considered the post- Turee Creek Group history in terms of two megasequences that record the opening and closure of an Atlantic-type ocean.

Along the southern Pilbara margin, the Turee Creek and lower Wyloo Groups have a maximum thickness of about 4 km and 3 km, respectively, and are separated by a significant angular unconformity (Fig. 4). This unconformity, together with another occuring within the upper Turee Creek Group, are interpreted to reflect the northward propagation of the Ophthalmia fold-and-thrust belt into the foreland basin (Martin and Morris, 2010). The maximum age of the Turee Creek Group – lower Wyloo Group stratigraphy is c. 2450 Ma, the age of the Woongarra Rhyolite, clasts of which are present in the Boolgeeda Iron Formation (Martin, 1999). The minimum age is c. 2210 Ma, the age of the Cheela Springs Basalt and the dolerite sills that intrude the upper Turee Creek Group (Martin et al., 1998; Müller et al., 2005; Martin and Morris, 2010). A c. 2030 Ma age for the Wooly Dolomite (Müller et al., 2005), usually considered to be the uppermost unit of the lower Wyloo Group (Thorne and Seymour, 1991), instead suggests that this unit was deposited in the interval between lower and upper Wyloo Group deposition.

The Turee Creek Group is subdivided, in ascending order, into the Kungarra, Koolbye, and Kazput Formations (Thorne and Tyler, 1996). Much of the Kungarra Formation is dominated by deep-marine mudstones and turbidite sandstones, interbedded with minor dolostone. A prominent glacigene diamictite, the Meteorite Bore Member (Trendall, 1976), outcrops in the upper part of the formation. Fluvial to shallow-marine sandstones of the Koolbye Formation overlie the Kungarra Formation, and are themselves overlain by deltaic and shallow-marine sandstones, siltstones, and dolostones belonging to the Kazput Formation.

Fluvial to shallow-marine sandstones and conglomerates belonging to the ~300 m thick Beasley River Quartzite (lower Wyloo Group) unconformably overly the Kazput Formation, and are conformably overlain by the ~2.5 km thick Cheela Springs Basalt. Martin and Morris (2010) argue convincingly that these continental tholeiite lavas are coeval with c. 2210 Ma dolerite sills that intrude the underlying Turee Creek Group. Throughout most of the southern Pilbara, the Cheela Springs Basalt is unconformably overlain by the upper Wyloo Group. An exception to this occurs on the Wyloo Dome, where the basalts are conformably overlain by the Wooly Dolomite, a 300 m thick succession of high- and low-energy shelf carbonates.

Upper Wyloo and Capricorn Groups: foreland-basin sedimentation and volcanism during the Capricorn Orogeny

Turee Creek and lower Wyloo Group rocks were deformed during the 2215–2145 Ma Ophthalmian Orogeny (Rasmussen et al., 2005), overlain locally by the c. 2030 Ma Wooly Dolomite, and then intruded by c. 2010 Ma northwest-trending dolerite dykes (Müller et al., 2005). Both the Ophthalmian folds and the c. 2010 Ma dykes were then truncated by the unconformity at the base of the upper Wyloo Group.

The upper Wyloo Group (Fig. 5) has an estimated thickness of about 7.5 km, and comprises, in ascending order, the Mount McGrath Formation, Duck Creek Dolomite, and Asburton Formation (Thorne and Seymour, 1991). A ~120 m thick, mixed mafic and felsic volcanic unit, the June Hill Volcanics, overlies the Duck Creek Dolomite north of the Wyloo Dome. The Ashburton Formation is unconformably overlain by siliciclastic, carbonate, and felsic volcanic rocks of the Capricorn Group, deposited following the early deformation stage (D_{1ash} — Ashburton Fold Belt) of the 1820–1770 Ma Capricorn Orogeny.

The age of the upper Wyloo Group is still poorly constrained. Evans et al. (2003) obtained an age of c. 1800 Ma for the June Hill Volcanics, whereas a tuffaceous unit in the overlying Ashburton Formation has been dated at c. 1829 Ma (Sircombe, 2003). The apparent contradiction in these ages, coupled with the c. 1804 Ma age of felsic volcanic rocks in the Capricorn Group (Hall et al., 2001) has led Evans et al. (2003) to suggest that deposition of the upper part of the upper Wyloo Group and of the Capricorn Group were strongly diachronous due to oblique basin closure during the Capricorn Orogeny.

The ~1.2 km thick Mount McGrath Formation comprises ferruginous conglomerate and sandstone, quartz sandstone, mudstone, and locally developed carbonate. Coarse-grained siliciclastic detritus was laid down on gravelly, braided deltas that fringed the northeastem margin of

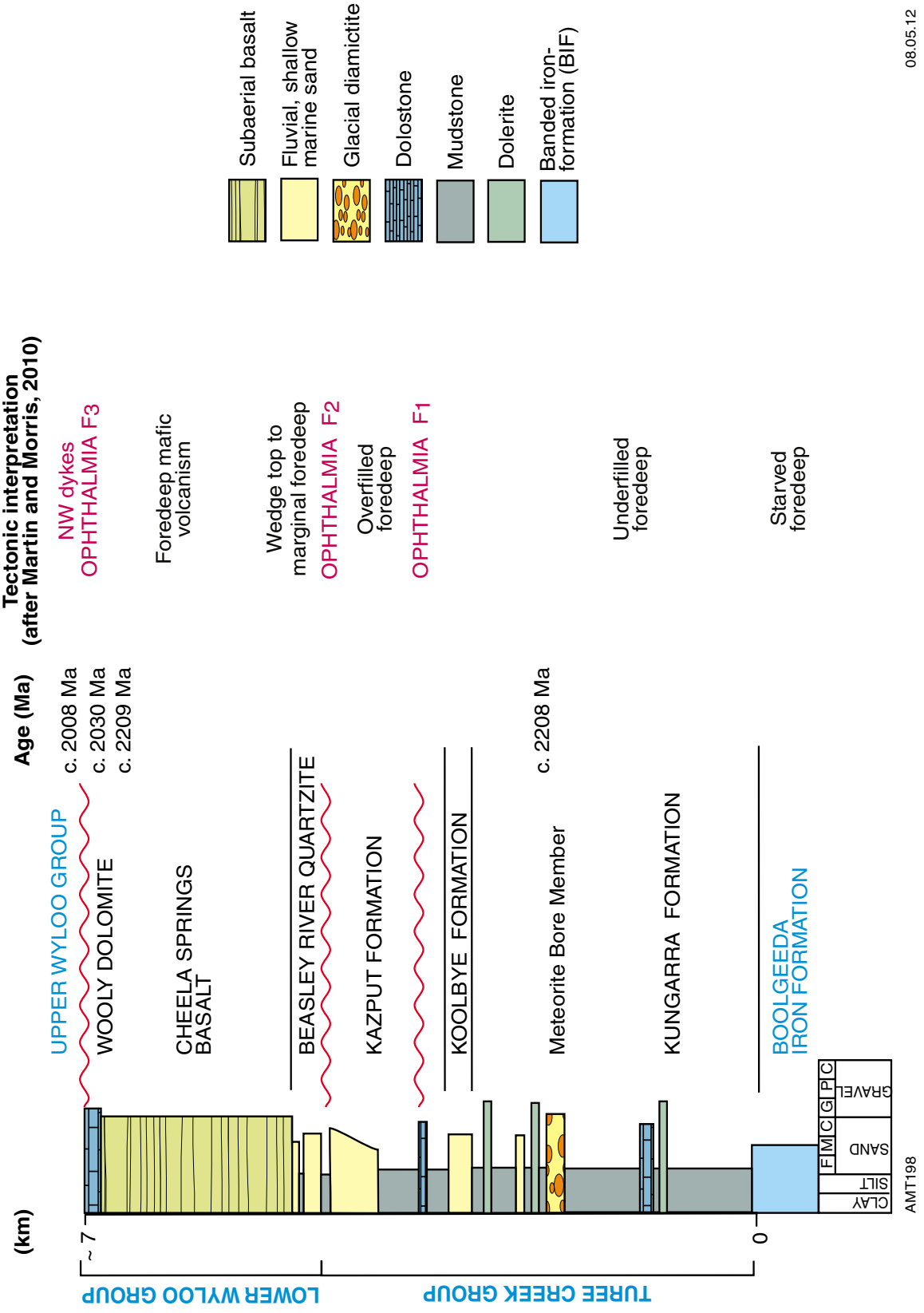

Figure 4. Stratigraphy of the Turee Creek Group and lower Wyloo Group, showing the distribution of the principal rock types, major deformation events, and interpreted tectonic settings. The sources for the geochronology are discussed in the text.

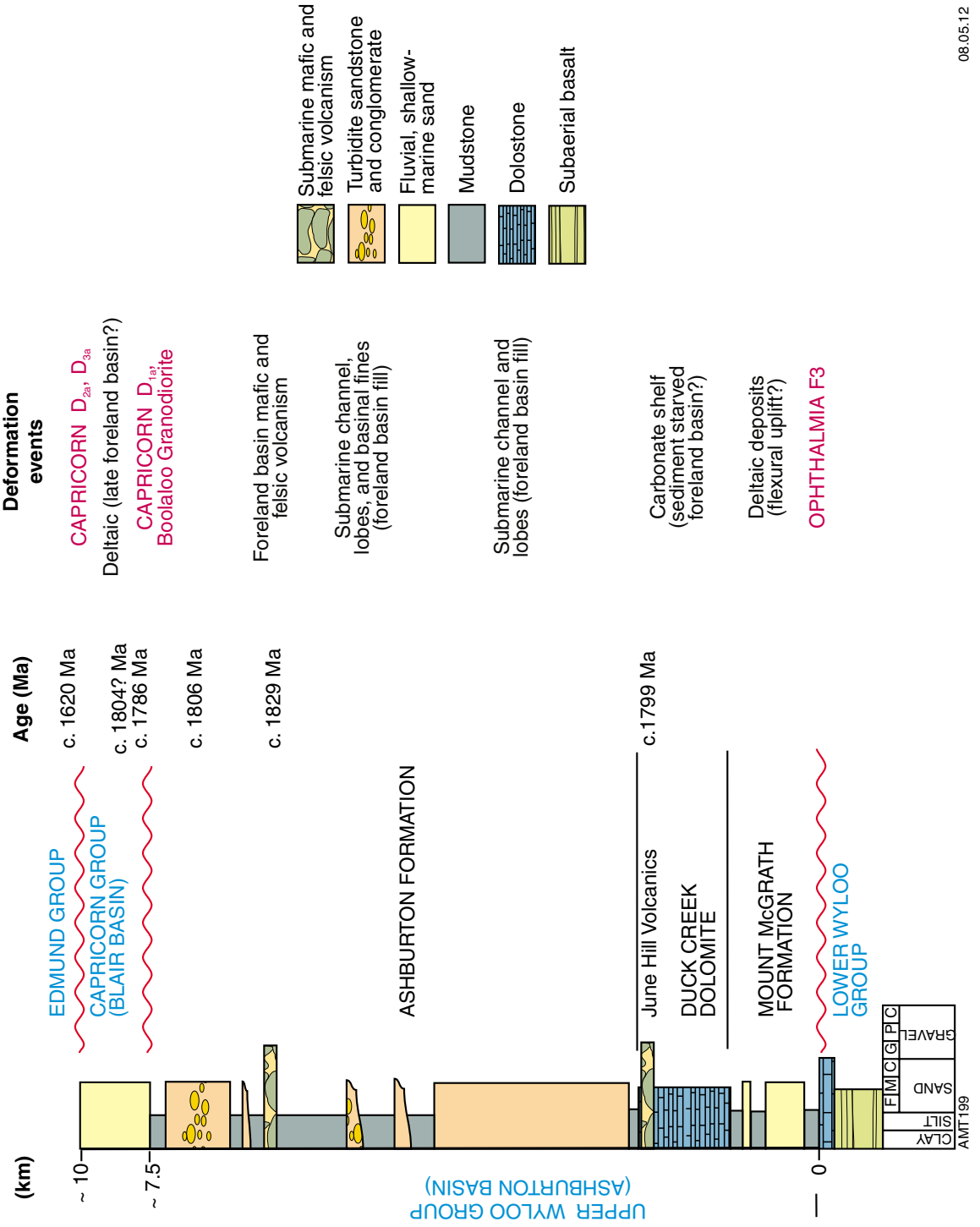

Figure 5. Stratigraphy of the upper Wyloo Group, showing the distribution of the principal rock types, major deformation events, and interpreted tectonic settings. The sources for the geochronology are discussed in the text.

the Ashburton Basin. Mud, silt, and carbonate were deposited in open shelf waters further to the south and west. Maximum development of the deltaic complex occured during deposition of the lower Mount McGrath Formation. The middle and upper parts of the formation record a gradual waning of siliciclastic supply; this was accompanied by a deepening of shelf waters throughout the basin (Thorne and Seymour, 1991).

Carbonate rocks of the ~1.0 km thick Duck Creek Dolomite conformably overly the Mount McGrath Formation, and are dominated by stromatolitic inner-shelf facies and thin-bedded or conglomeratic outer-shelf and slope facies. Deposition of the lower Duck Creek Dolomite took place in a relatively deep-water, shelf, slope, and basin environment that existed along the northeastern margin of the Ashburton Basin. To the north and east, a belt of shallow, marine, inner-shelf carbonate deposition fringed the low-relief Pilbara Craton. The carbonate shelf underwent one major episode of progradation during the deposition of the middle Duck Creek Dolomite. The upper parts of the formation were laid down in a gradually deepening basin, which received increasing amounts of fine-grained siliciclastic detritus (Thorne and Seymour, 1991).

The Ashburton Formation has an estimated thickness of about 5 km, and conformably overlies the Duck Creek Dolomite, except in the northwestern part of the Ashburton Basin, where it is disconformable upon the June Hill Volcanics. Principal rock types are: mudstone; thin- to thick-bedded sandstone; conglomerate; BIF and chert; and local mafic and felsic volcanic rock. These deposits were laid down in a deep marine basin, with most sediment being derived from a Paleoproterozoic granitic source to the southeast, south of the exposed southern Pilbara margin (Thorne and Seymour, 1991; Sircombe, 2002).

The tectonic setting of the upper Wyloo Group is thought to be a foreland basin associated with the onset of the 1820–1770 Ma Capricorn Orogeny (Tyler and Thorne, 1990; Thorne and Seymour, 1991, Evans et al., 2003), although Martin and Morris (2010) suggest that the setting may have been extensional in its early stages.

Ophthalmia and Ashburton Fold Belts

The southern Pilbara margin was deformed during two Paleoproterozoic orogenic events related to the assembly and subsequent tectonic reworking of the West Australian Craton. The earliest of these, the 2215–2145 Ma Ophthalmian Orogeny (Rasmussen et al., 2005), formed the Ophthalmia Fold Belt and reflects collision of the southern Pilbara Craton with the Glenburgh Terrane of the Gascoyne Province (Occhipinti et al., 2004; Sheppard et al., 2004, 2010a; Martin and Morris, 2010; Johnson et al., 2010, 2011b). Subsequent crustal reworking during the 1820–1770 Ma Capricorn Orogeny created the Ashburton Fold Belt (Thorne and Seymour, 1991; Sheppard et al., 2010a,b).

Ophthalmia Fold Belt

Ophthalmia Fold Belt structures affect the Pilbara Craton basement and very low grade supracrustal rocks, up to, and including, the lower Wyloo Group (Tyler, 1991; Thorne and Seymour, 1991; Martin and Morris, 2010). These structures include regional scale, en-echelon, open to tight, upright folds; e.g. the Hardey Syncline, Turner Syncline, and Rocklea Dome (Frontispiece 1; Plate 1). These structures are cut by 2010 Ma, northwest-trending dolerite dykes (Müller et al., 2005), and are overprinted by younger Asburton Fold Belt structures. Ophthalmia Fold Belt structures show decreasing strain when traced from southwest to northeast.

Three pre- and one post- lower Wyloo Group Ophthalmian events are recognized. The earliest structures, F_{1oph}, are represented by localized, though widely distributed, tight to isoclinal, bedding-parallel folds that are refolded by the later regional-scale Ophthalmian folds (Tyler, 1991). Martin and Morris (2010) record a minimum of three phases of roughly east–west trending Ophthalmian folds in the Hardey syncline. The earliest of these, F_{2opth} (F_{1oph} of Martin and Morris, 2010), affected all strata up to, and including, the middle Kazput Formation; however, these folds are truncated by the unconformity at the base of the upper Kazput Formation. Subsequent F_{3oph} folds (F_{2oph} of Martin and Morris, 2010) are open and upright, and affected all strata up to, and including, the upper Kazput Formation, but are truncated by the unconformity at the base of the lower Wyloo Group. Later F_{4opth} folding (F_{3oph} of Martin and Morris, 2010) post-dates the c. 2210 Ma dolerite sills that intrude the Beasley River Quartzite, but are cut by c. 2010 Ma northwest-trending dolerite dykes (Müller et al., 2005).

Martin and Morris (2010) also record the presence of a younger folding event that refolds the Hardey Syncline. Although it could be Ophthalmian in age, the absolute timing of this event is unclear, and it may be related to younger deformation; e.g. the Panhandle event (Taylor et al., 2001) or Capricorn Orogeny.

Ashburton Fold Belt

Ashburton Fold Belt structures affect the Pilbara Craton basement and very low grade supracrustal rocks, up to, and including, the lower Capricorn Group. These structures overprint those belonging to the earlier Ophthalmia Fold Belt (Tyler and Thorne, 1990; Thorne and Seymour, 1991; Martin and Morris, 2010). One pre- Capricorn Group event (D_{1ash} /M_{1ash}) and two post- Capricorn Group – pre- Edmund Group events (D_{2ash} /M_{2ash} and D_{3ash}) are recognized within the Ashburton Fold Belt. The timing of D_{1ash} /M_{1ash} was between c. 1806 and c. 1786 Ma, the latter being the age of the post- D_{1ash} Boolaloo Granodiorite (Krapež and McNaughton, 1999; Martin et al., 2005). D_{2ash}/M_{2ash} occurred between c. 1786 and c. 1738 Ma, the younger age limit being set by the age of gold mineralization at the Mount Olympus deposit (Sener et al., 2005). The youngest event, D_{3ash}, occurred between c. 1738 and c. 1620 Ma, based on the minimum age of

D_{2ash}/M_{2ash} and the maximum age of the overlying Edmund Group (Martin et al., 2005).

Thorne and Seymour (1991) recognized three structural zones (A, B, and C) within the Ashburton Fold Belt, based on the geometry of the D_{2ash} structures and the preservation of D_{1ash} structures. Zone A is dominated by dextral strike-slip faulting and refolding of Ophthalmia Fold Belt folds along the southwestern Pilbara margin. Zone B is developed in the Ashburton Formation, northeast of the Baring Downs Fault. It represents a relatively high-strain zone formed during D_{2ash}. As a result of this, the recognition of D_{1ash} structures within Zone B is generally difficult, because strong overprinting by D_{2ash} has resulted in the early cleavage (S_{1ash}) being coaxial, and often coplanar, with the later fabric (S_{2ash}). Zone C occupies the remainder of the Ashburton Fold Belt, between the southwestern boundary of Zone B and the Edmund Group unconformity. It is distinguished from Zone B by its generally lower level of D_{2ash} strain leading to the better preservation of D_{1ash} structures, and also by the presence of large-scale F_{2ash} folds and dextral strike-slip faults. Zone C also preserves evidence of D_{3ash} structures in the western Capricorn Range.

Ashburton Fold Belt D_{1ash}/M_{1ash}

Most of the evidence for the D_{1ash} deformation is based on the widespread S_{1ash} foliation — the marked angular unconformity between the Ashburton Formation and the Capricorn Group — and rare F_{1ash} folds (Thorne and Seymour, 1991; Martin et al., 2005). In many outcrops, evidence for D_{1ash} is present in the form of an early S_{1ash} cleavage developed subparallel to bedding. This cleavage is often crenulated by S_{2ash}, and with the increase in metamorphic grade in southwestern parts of the fold belt, it develops into a metamorphic schistosity.

In the Capricorn Range, the marked angular unconformity at the base of the Capricorn Group provides clear evidence that the Ashburton Formation was folded prior to deposition of the Capricorn Group. In addition, the Ashburton Formation shows a well-developed S_{1ash} penetrative cleavage that is not developed in the overlying Capricorn Group (Thorne and Seymour, 1991). At the eastern end of the Capricorn Range, the basal unconformity of the Capricorn Group dips north at 50° as a result of D_{2ash} folding. The S_{1ash} cleavage in the underlying Ashburton Formation dips 15–45° south, whereas bedding dips (and youngs) southward at 0–30°. The rotation of bedding and S_{1ash} to their pre-D_{2a} orientation indicates that the tight F_{1ash} fold was characterized by a steeply southward-dipping axial surface.

The metamorphic grade is low throughout most of the Ashburton Basin; however, there is a general increase in grade and intensity of schistosity towards the west and southwest. Thorne and Seymour (1991) note that much of the Ashburton Basin is characterized by the quartz–chlorite–muscovite(–sericite) mineral assemblage in pelitic and psammitic rocks. To the southwest of the Capricorn Range, medium-grade metamorphosed equivalents of the Ashburton Formation are represented by quartz–muscovite–biotite–cordierite–andalusite–garnet schists. Textural evidence suggests that porphyroblastic minerals (biotite, andalusite, cordierite, and garnet) grew both during and after the D_{1ash} deformation event, overgrowing a quartz, muscovite, and chlorite groundmass. The metamorphic schistosity (S_{1ash}) is typically deformed by F_{2ash} folds and crenulation cleavage.

Ashburton Fold Belt D_{2ash}/M_{2ash}

Most obvious folding and faulting in the Ashburton Fold Belt results from the second deformation event, D_{2ash} (Thorne and Seymour, 1991; Martin et al., 2005). Within Zone B, D_{2ash} deformation has resulted in tight to isoclinal, non-cylindrical F_{2ash} folds, with wavelengths of 5–200 m. Folds trend west to northwest, and are associated with a pronounced axial-plane cleavage (S_{2ash}) that generally dips 60–90° to the southwest or northeast. Within the main body of Ashburton Formation rocks, faults are generally associated with subparallel quartz veins, and are frequently observed to cut out all, or part, of the northern limb of the F_{2ash} folds. This fact, coupled with lack of marker horizons in the Ashburton Formation and the tight to isoclinal folding, creates a false impression of a simple stratigraphy with southwesterly dipping beds throughout much of Zone B. In such cases, evidence for F_{2ash} folding comes from local reversals in younging direction, and the presence of isolated F_{2ash} fold closures within the otherwise uniformly dipping Ashburton Formation. F_{2ash} folds in Zone C are large (100–6000 m wavelength), non-cylindrical, and trend west to northwest. Most plunge 10–40° (up to 80° locally) to the southeast or northwest. Axial planes dip steeply to the southwest or northeast. Close to the northern margin of Zone C, folds are open to tight (or locally isoclinal), but are generally more open in central and southwestern parts of the fold belt. S_{2ash} is a penetrative slaty cleavage in the more easterly outcrops, but is present as a crenulation cleavage further west.

Numerous west-northwesterly to north-northwesterly trending strike-slip faults are either parallel to the F_{2ash} fold axes, or crosscut them at a shallow angle. The most prominent of these faults are the Nanjilgardy, Baring Downs, and Blair Faults. Locally, a dextral displacement of up to 3 km can be measured. However, in general, the lack of marker horizons within the Ashburton Formation makes it difficult to accurately assess the amount of relative movement. The northern margin of the Capricorn Range is locally marked by a steep southward-dipping fault. Many faults are marked by a line of en echelon quartz veins, dipping 30–90° northeast or southwest. Locally, they are associated with a second suite of steeply dipping veins that trend between north-northwest and north-northeast. Most veins consist of equant to prismatic, subhedral to anhedral quartz, with irregular goethite vugs (after sulfide). Locally, quartz crystals are kinked as a result of progressive fault movement. Most of the copper, gold, lead, and silver mineralization discovered to date in the Ashburton Fold Belt is associated with D_{2ash} faults and quartz veins.

Low-grade metamorphism accompanied D_{2ash}, causing the retrogression of biotite to chlorite and andalusite to sericite, and the growth of porphyroblastic muscovite.

Ashburton Fold Belt D_{3a}

In the western Capricorn Range, the traces of F_{2ash} folds in the Capricorn Group are folded such that the regional west-northwest trend swings firstly southwest, and then west-northwest near Irregully Creek. Locally, the fold limbs are cut by a steep, southwesterly dipping fracture cleavage. The geometry of the F_{3ash} fold structure suggests it may have formed in response to a localized late-stage sinistral movement, on a pair of strike-slip faults that occur along the northern margin of the Capricorn Range and beneath the northern edge of Edmund Group outcrop.

Refererences

Blake, TS 1984, The lower Fortescue Group of the northern Pilbara Craton — stratigraphy and paleogeography, *in* Archaean and Proterozoic basins of the Pilbara, Western Australia — evolution and mineralization potential *edited by* JR Muhling, DI Groves and TS Blake: University of Western Australia, Geology Department and University Extension, Publication no. 9, p. 123–143.

Blake, TS 1993, Late Archaean crustal extension, sedimentary basin formation, flood basalt volcanism, and continental rifting. The Nullagine and Mount Jope Supersequences, Western Australia: Precambrian Research, v. 60, p. 185–241.

Blake, TS 2001, Cyclic continental mafic tuff and flood basalt volcanism in the Late Archaean Nullagine and Mount Jape Supersequences in the eastern Pilbara, Western Australia: Precambrian Research, v. 107, p. 139–177.

Blake, TS and Barley, ME 1992, Tectonic evolution of the Late Archaean to Early Proterozoic Mount Bruce Megasequence Set, Western Australia: Tectonics, v. 11, p. 1415–1425.

Blake, TS, Buick, R, Brown, SJA and Barley, ME 2004, Geochronology of a Late Archean flood basalt province in the Pilbara Craton, Australia: constraints on basin evolution, volcanic and sedimentary accumulation, and continental drift rates: Precambrian Research, v. 133, p. 143–173.

Cawood, PA and Tyler, IM 2004, Assembling and reactivating the Proterozoic Capricorn Orogen: lithotectonic elements, orogenies, and significance: Precambrian Research, v. 128, p. 201–218.

Doyle, MG, Krapež, B and Barley, ME 2001, Volcanic facies architecture of the Woongarra Large Igneous Province, *in* 4th International Archean Symposium Extended Abstracts *edited by* KF Cassidy, JM Dunphy and MJ Van Kranendonk: Geoscience Australia, Record 2001/37, p. 149–150.

Evans, DAD, Sircombe, KN, Wingate, MTD, Doyle, M, McCarthy, M, Pidgeon, RT and Van Niekerk, HS 2003, Revised geochronology of magmatism in the western Capricorn Orogen at 1805–1785 Ma: diachroneity of the Pilbara–Yilgarn collision: Australian Journal of Earth Sciences, v. 50, p. 853–864.

Gee, RD 1979, Structure and tectonic style of the Western Australian Shield: Tectonophysics, v. 58, p. 327–369.

Hall, CE, Powell, CMcA and Bryant, J 2001, Basin setting and age of the Late Palaeoproterozoic Capricorn Formation, Western Australia: Australian Journal of Earth Sciences, v. 48, p. 731–744.

Hickman, AH and Van Kranendonk, MJ 2008, Archean crustal evolution and mineralization of the northern Pilbara Craton — a field guide: Geological Survey of Western Australia, Record 2008/13, 79p.

Horwitz, RC and Smith, RE 1978, Bridging the Yilgarn and Pilbara blocks, Western Australia: Precambrian Research, v. 6, p. 293–322.

Johnson, SP, Sheppard, S, Rasmussen, B, Muhling, JR, Fletcher, IR, Wingate, MTD, Kirkland, CL and Pirajno, F 2009, Meso- to Neoproterozoic reworking in the Gascoyne Complex and what it means for mineral exploration, *in* GSWA 2009 extended abstracts: promoting the prospectivity of Western Australia: Geological Survey of Western Australia, Record 2009/2, p. 23–25.

Johnson, SP, Sheppard, S, Rasmussen, B, Wingate, MTD, Kirkland, CL, Muhling, JR, Fletcher, IR and Belousova, E 2010, The Glenburgh Orogeny as a record of Paleoproterozoic continent–continent collision: Geological Survey of Western Australia, Record 2010/5, 54p.

Johnson, SP, Thorne, AM, Cutten, HN, Tyler, IM and Blay, O 2011a, Geology of the Gascoyne Province, *in* Capricorn Orogen seismic and magnetotelluric (MT) workshop 2011: extended abstracts *edited by* SP Johnson, AM Thorne and IM Tyler: Geological Survey of Western Australia, Record 2011/25, p. 27–40.

Johnson, SP, Sheppard, S, Rasmussen, B, Wingate, MTD, Kirkland, CL, Muhling, JR, Fletcher, IR and Belousova, EA 2011b, Two collisions, two sutures: punctuated pre-1950 Ma assembly of the West Australian Craton during the Ophthalmian and Glenburgh Orogenies: Precambrian Research, v. 189, no. 3–4, p. 239–262, doi: 10.1016/j.precamres.2011.07.011.

Kennett, BLN, Tyler, IM, Maher, J, Holzschuh, J, Fomin, T and Costelloe, RD 2011, The Capricorn seismic survey: experimental design, acquisition, and processing, *in* Capricorn Orogen seismic and magnetotelluric (MT) workshop 2011: extended abstracts *edited by* SP Johnson, AM Thorne and IM Tyler: Geological Survey of Western Australia, Record 2011/25, p. 1–6.

Krapež, B and McNaughton, NJ 1999, SHRIMP zircon U–Pb age and tectonic significance of the Palaeoproterozoic Boolaloo Granodiorite in the Ashburton Province, Western Australia: Australian Journal of Earth Sciences, v. 46, p. 283–287.

Martin, DMcB 1999, Depositional setting and implications of Paleoproterozoic glaciomarine sedimentation in the Hamersley Province, Western Australia: Geological Society of America, Bulletin, v. 111, p. 189–203.

Martin, DM, Li, ZX, Nemchin, AA and Powell, CMcA 1998, A pre-2.2 Ga age for giant hematite orebodies of the Hamersley Province, Australia?: Economic Geology, v. 93, p. 1084–1090.

Martin, DM, Powell, CMcA and George, AD 2000, Stratigraphic architecture and evolution of the early Paleoproterozoic McGrath Trough, Western Australia: Precambrian Research, v. 99, p. 33–64.

Martin, DMcB, Sheppard, S and Thorne, AM 2005, Geology of the Maroonah, Ullawarra, Capricorn, Mangaroon, Edmund, and Elliott Creek 1:100 000 sheets: Western Australia Geological Survey, 1:100 000 Geological Series Explanatory Notes, 65p.

Martin, DM and Morris, PA 2010, Tectonic setting and regional implications of ca. 2.2 Ga mafic magmatism in the southern Hamersley Province, Western Australia: Australian Journal of Earth Sciences, v. 57, no. 7, p. 911–931.

Morris, RC and Horwitz, RC 1983, The origin of the iron formation- rich Hamersley Group of Western Australia — deposition on a platform: Precambrian Research, v. 21, p. 273–297.

Muhling, JR 1988, The nature of Proterozoic reworking of early Archaean gneisses, Mukalo Creek Area, southern Gascoyne Province, Western Australia: Precambrian Research, v. 40–41 (The Early to Middle Proterozoic of Australia), p. 341–362.

Müller, SG, Krapež, B, Barley, ME and Fletcher, IR 2005, Giant iron-ore deposits of the Hamersley province related to breakup of Paleoproterozoic Australia: new insights from in situ SHRIMP dating of baddeleyite from mafic intrusions: Geology, v. 33, p. 577–580.

Occhipinti, SA, Sheppard, S, Myers, JS, Tyler, IM and Nelson, DR 2001, Archaean and Palaeoproterozoic geology of the Narryer Terrane (Yilgarn Craton) and southern Gascoyne Complex (Capricorn Orogen), Western Australia — a field guide: Geological Survey of Western Australia, Record 2001/8, 70p.

Occhipinti, SA, Sheppard, S, Passchier, C, Tyler, IM and Nelson, DR 2004, Palaeoproterozoic crustal accretion and collision in the southern Capricorn Orogen: the Glenburgh Orogeny: Precambrian Research, v. 128, p. 237–255.

Rasmussen, B, Fletcher, IR and Sheppard, S 2005, Isotopic dating of the migration of a low-grade metamorphic front during orogenesis: Geology, v. 33, p. 773–776.

Sener, AK, Young, C, Groves, DI, Krapež, B and Fletcher, I 2005, Major orogenic episode associated with Cordilleran-style tectonics related to the assembly of Paleoproterozoic Australia?: Geology, v. 33, no. 3, p. 225–228.

Sheppard, S, Occhipinti, SA and Tyler, IM 2004, A 2005–1970 Ma Andean-type batholith in the southern Gascoyne Complex, Western Australia: Precambrian Research, v. 128 (Assembling the Palaeoproterozoic Capricorn Orogen), p. 257–277.

Sheppard, S, Occhipinti, SA and Nelson, DR 2005, Intracontinental reworking in the Capricorn Orogen, Western Australia: the 1680–1620 Ma Mangaroon Orogeny: Australian Journal of Earth Sciences, v. 52, p. 443–460.

Sheppard, S, Rasmussen, B, Muhling, JR, Farrell, TR and Fletcher, IR 2007, Grenvillian-aged orogenesis in the Palaeoproterozoic Gascoyne Complex, Western Australia: 1030–950 Ma reworking of the Proterozoic Capricorn Orogen: Journal of Metamorphic Geology, v. 25, p. 477–494.

Sheppard, S, Johnson, SP, Wingate, MTD, Kirkland, CL and Pirajno, F 2010a, Explanatory Notes for the Gascoyne Province: Geological Survey of Western Australia, 336p.

Sheppard, S, Bodorkos, S, Johnson, SP, Wingate, MTD and Kirkland, CL 2010b, The Paleoproterozoic Capricorn Orogeny: intracontinental reworking not continent–continent collision: Geological Survey of Western Australia, Report 108, 33p.

Simonson, BM and Hassler, SW 1997, Revised correlations in the Early Precambrian Hamersley Basin based on a horizon of resedimented impact spherules: Australian Journal of Earth Sciences, v. 44, p. 37–48.

Simonson, BM, Schubel, KA and Hassler, SW 1993, Carbonate sedimentology of the early Precambrian Hamersley Group of Western Australia: Precambrian Research, v. 60, p. 287–336.

Sircombe, KN 2002, Reconnaissance detrital zircon geochronology provenance of the Palaeoproterozoic Ashburton Formation: implications for Pilbara and Yilgarn amalgamation, *in* Geoscience 2002: Expanding Horizons. Abstracts of the 16th Australian Geological Convention *edited by* VP Preiss: Adelaide Convention Centre, Adelaide, South Australia, 1–5 July 2002, p. 147.

Sircombe, KN 2003, Age of the Mt Boggola volcanic succession and further geochronological constraint on the Ashburton Basin, Western Australia: Australian Journal of Earth Sciences, v. 50, p. 967–974.

Taylor, D, Dalstra, HJ, Harding, AE, Broadbent, GC and Barley, ME 2001, Genesis of high-grade hematite orebodies of the Hamersley Province, Western Australia: Economic Geology v. 96, p. 837–873.

Thorne, AM and Trendall, AF 2001, The geology of the Fortescue Group, Pilbara Craton, Western Australia: Geological Survey of Western Australia, Bulletin 144, 249p.

Thorne, AM and Seymour, DB 1991, Geology of the Ashburton Basin, Western Australia: Geological Survey of Western Australia, Bulletin 139, 141p.

Thorne, AM and Tyler, IM 1996, Geology of the Rocklea 1:100 000 sheet: Western Australia Geological Survey, 1:100 000 Geological Series Explanatory Notes, 15p.

Trendall, AF 1976, Striated and faceted boulders from the Turee Creek Formation — evidence for a possible Huronian glaciation on the Australian continent, *in* Annual report for the year 1975: Geological Survey of Western Australia, Perth, Western Australia, p. 88–92.

Trendall, AF 1990 Hamersley Basin, *in* Geology and mineral resources of Western Australia: Geological Survey of Western Australia, Memoir 3, p. 163–189.

Trendall, AF 1995, The Woongarra Rhyolite — a giant lavalike felsic sheet in the Hamersley Basin of Western Australia: Western Australia Geological Survey, Report 42, 70p.

Trendall, AF and Blockley, JG 1970, The iron formations of the Precambrian Hamersley Group, Western Australia, with special reference to the associated crocidolite: Western Australia Geological Survey, Bulletin 119, 366p.

Trendall, AF, Compston, W, Nelson, DR, de Laeter, JR and Bennett, VC 2004, SHRIMP zircon ages constraining the depositional age of the Hamersley Group, Western Australia: Australian Journal of Earth Sciences, v. 51, p. 621–644.

Tyler, IM and Thorne, AM 1990, The northern margin of the Capricorn Orogen, Western Australia — an example of an Early Proterozoic collision zone: Journal of Structural Geology, v. 12, p. 685–701.

Tyler, IM 1991, The geology of the Sylvania Inlier and southeast Hamersley Basin: Western Australia Geological Survey, Bulletin 138, 108p.

Preliminary interpretation of deep seismic reflection line 10GA–CP1: crustal architecture of the northern Capricorn Orogen

by

AM Thorne, IM Tyler, RJ Korsch[1], SP Johnson, JW Brett, HN Cutten, O Blay, BLN Kennett[2], RS Blewett[1], A Joly[3], MC Dentith[3], ARA Aitken[3], J Holzschuh[1], JA Goodwin[1], M Salmon[2], A Reading[4], and G Boren[5]

Introduction and aims of the seismic survey

Seismic reflection line 10GA–CP1 is oriented approximately north-northeast–south-southwest, broadly normal to the strike of the major geological structures in the northern Capricorn Orogen (Frontispieces 1–3; Plate 1; Thorne et al., 2011). It traverses rocks of the Fortescue and Hamersley Groups in the Turner and Hardey Synclines, and granite–greenstones of the Pilbara Craton in the Rocklea Dome, before crossing the Nanjilgardy Fault system into the Ashburton Basin to the south. Based on the known stratigraphy, stacking all the Archean and Paleoproterozoic supracrustal units present in the northern Capricorn Orogen gives a maximum cumulative thickness of ~26 km. The total thickness of the stratigraphy along 10GA–CP1 is probably less than 20 km, as the transect only passes through a small part of the Capricorn Group, and as the 4 km maximum thickness for the Turee Creek Group is only preserved locally in the Hardey Syncline.

The principal objectives of seismic reflection line 10GA–CP1 were to determine:

- the nature of reactivated growth faults that formed during deposition of the Fortescue Group in the southern Pilbara region
- the character of major faults, e.g. the Nanjilgardy Fault, that mark the boundary between the Pilbara Craton and the Ashburton Basin
- the crustal architecture of the Ashburton Basin — is it consistent with current tectonic models for the orogen?
- the deep crustal structure and nature of the Mohorovičić discontinuity ('the Moho') beneath the northern Capricorn Orogen (discussed by Kennett, 2011).

The preliminary interpretation of seismic transect 10GA–CP1 is presented in two sections. In the first section, an interpretation is presented based upon the nature of the seismic reflection data, and constrained by outcrop geology along the section line, as well as the gravity and magnetic data for the region. In the second section, the first interpretation is re-assessed in the light of additional regional aeromagnetic, gravity, and magnetotelluric datasets, and the results of regional geological mapping elsewhere in the northern Capricorn Orogen.

10GA–CP1: preliminary seismic interpretation

Turner Syncline to Baring Downs Fault

Northeast of the Baring Downs Fault, the Moho is weakly defined and has a gentle, undulating character, at a variable depth of 11.5 – 12.3 s two-way travel time (TWT) or 34–37 km (Fig. 1). The crust is thinnest beneath the Turner Syncline and Rocklea Dome, and thickest between the Nanjilgardy and Baring Downs Faults. Beneath the Archean to Paleoproterozoic supracrustal rocks, the crust shows a broad two-fold subdivision into a generally weakly reflective upper crust, corresponding to the exposed granite–greenstones of the Pilbara Craton, and a moderately reflective lower crust referred to as the Carlathunda Seismic Province (Korsch et al., 2011). The boundary between these crustal divisions is undulating and offset by the major faults, but generally occurs at a depth of 4–7 s TWT (12–21 km).

1 Minerals and Natural Hazards Division, Geoscience Australia, GPO Box 378, Canberra, ACT 2601.

2 Research School of Earth Sciences, The Australian National University, Canberra ACT 0200.

3 Centre for Exploration Targeting, School of Earth and Environment, The University of Western Australia, 35 Stirling Highway, Crawley, WA 6009.

4 School of Earth Sciences and CODES Centre of Excellence, University of Tasmania, Private Bag 79, Hobart, TAS 7001.

5 Centre for Tectonics, Resources and Exploration, University of Adelaide, Adelaide, SA 5005.

In addition to the Baring Downs Fault, three other major crustal structures — the Nanjilgardy Fault, Soda Fault, and Moona Fault — are imaged in the seismic data (Fig. 1). With the possible exception of the Moona Fault, these structures are interpreted to extend through the crust to the Moho. The Baring Downs Fault is imaged as a moderately steep, broadly northeasterly dipping structure in upper crustal levels, but becomes asymptotically northeasterly dipping towards the Moho. The Nanjilgardy Fault is a single, steep, north- to northeast-dipping structure in the middle- to lower-crustal levels, but splays upwards into a complex, transpressive flower structure defined by steep to flat-lying, northeast- or southwest-dipping, minor faults. Both the Moona and Soda Well Faults are steep to vertical close to the surface, but flatten out to form irregular, northeasterly dipping listric structures in the middle to lower crust.

At the northeastern end of 10GA–CP1 (Fig. 2), the Fortescue Group dips gently to the southwest, and is imaged in the north as a series of weak to strong, layered reflections. Here, three units can be recognized within the Fortescue Group, based on their seismic reflectivity: a lower layer of weak reflections 0.25 s TWT (~0.8 km) thick; a middle layer of strong reflections 0.7 s TWT (~2.2 km) thick; and an upper layer of weak reflections 0.5 s TWT (~1.4 km) thick. The lower seismic layer cannot be tied to the outcrop geology, but possibly corresponds to sedimentary rocks of the Hardey Formation. The middle layer equates to the mostly basaltic rocks of the Boongal, Pyradie, and lower Bunjinah Formations, whereas the upper layer includes the upper Bunjinah Formation and Jeerinah Formation. Although the seismic reflections lose some of their definition beneath the Turner Syncline, they suggest a southwesterly thickening of the Fortescue Group from about 1.5 s TWT (~4.5 km) to about 2 TWT (~6 km) approaching the Moona Fault. Some loss of seismic definition also occurs on the southwestern limb of the Turner Syncline, where the Fortescue Group appears to have a maximum thickness of about 1.7 s TWT (~5 km).

Seismic data suggests that a section of the Hamersley Group about 1 s TWT (~3 km) thick is preserved in the Turner Syncline. The reflections corresponding to this unit are poorly defined on the northeastern limb, but are stronger near the syncline axis and the southwestern limb.

Pilbara Craton granite–greenstones in the Rocklea Dome are generally weakly reflective, although a number of prominent southwest-dipping to flat-lying reflections are recorded at depth, unconformably underlying the Fortescue Group. These reflections are interpreted as discontinuous greenstone sheets within the granitic crust. A prominent, steeply north-dipping mylonite zone, the Mithgoondy Shear (Frontispiece 1), is exposed in surface outcrops of the Rocklea Dome, but is not observed in the seismic profile.

A thick, almost complete, succession of the Fortescue Group outcrops on the southwestern limb of the Rocklea Dome, and is cut by the Karra Well and Soda Faults. Despite this, the succession is poorly imaged in the seismic profile, probably as a result of complex near-surface conditions. Further west, between the Soda and Nanjilgardy Faults, a succession of weakly to strongly reflective lower and middle Fortescue Group rocks 1.7 s TWT (~5 km) thick is interpreted to overlie the weakly reflective granite–greenstone rocks. Here, the strongest reflections are from the lower 1.3 s TWT (~4 km) of the stratigraphy, whereas the subhorizontal dip of the reflections is caused by the trace of 10GA–CP1 being parallel to the local geological strike.

The stratigraphic succession between the Nanjilgardy and Baring Downs Faults (Fig. 3) has been difficult to interpret from the seismic reflection data. Surface outcrops consist of a fold- and fault-repeated succession of rocks of the upper Wyloo Group, consisting of the Mount McGrath Formation, Duck Creek Dolomite, and Ashburton Formation, whereas a thick succession of lower Wyloo Group rocks occurs along-strike to the northwest. In the seismic profile, the overall structural elements are delineated; however, the stratigraphy below the Duck Creek Dolomite is often poorly defined, with significant lateral variation in reflective character. Preliminary interpretation of these data suggest a marked thickening of the lower Wyloo Group (from 0.3 – 1.3 s TWT, or 1–4 km) and upper Wyloo Group (from 0.3 – 1.3 s TWT, or 1–4 km) towards the Baring Downs Fault. In this area, the lower Wyloo Group can be interpreted to directly overlie granite–greenstone basement rocks. The nature of the stratigraphy below the Mount McGrath Formation, in the flower structure of the Nanjilgardy Fault, has not been determined due to the weak reflections in this area.

Baring Downs Fault to the southern limit of 10GA–CP1

Within this part of the transect (Fig. 3), the depth to Moho shows little variation, ranging from about 12.3 s TWT (~37 km) at the Baring Downs Fault, to about 13 s TWT (~39 km) near the southern end of 10GA–CP1 (Frontispiece 1). Beneath the supracrustal succession, mid- to lower-crustal levels can be subdivided into a generally strongly reflective upper crust, and a weakly reflective lower crust. The boundary between these divisions is undulating, and generally occurs at a depth of 8.3 – 9.5 s TWT (25 – 27.5 km). This seismic structure contrasts markedly with that present northeast of the Baring Downs Fault, and has accordingly been interpreted as a separate seismic entity, the Bandee Seismic Province (Korsch et al., 2011). The nature of this crust is unknown, as the Bandee Seismic Province is not exposed in the Capricorn Orogen.

Several major faults were identified in the upper crust and supracrustal succession, although none of these structures could be traced below a depth of about 4.5 s TWT (~13.5 km). Most faults are moderately to steeply southward-dipping in the upper parts of the profile, although the Blair and Beasley Faults become flatter, but still southward-dipping, at depth. Major faults preserve either an extensional or thrust sense of movement.

The surface geology of the Bandee Seismic Province comprises polyphase-deformed Ashburton Formation, although this structural complexity is not imaged in the

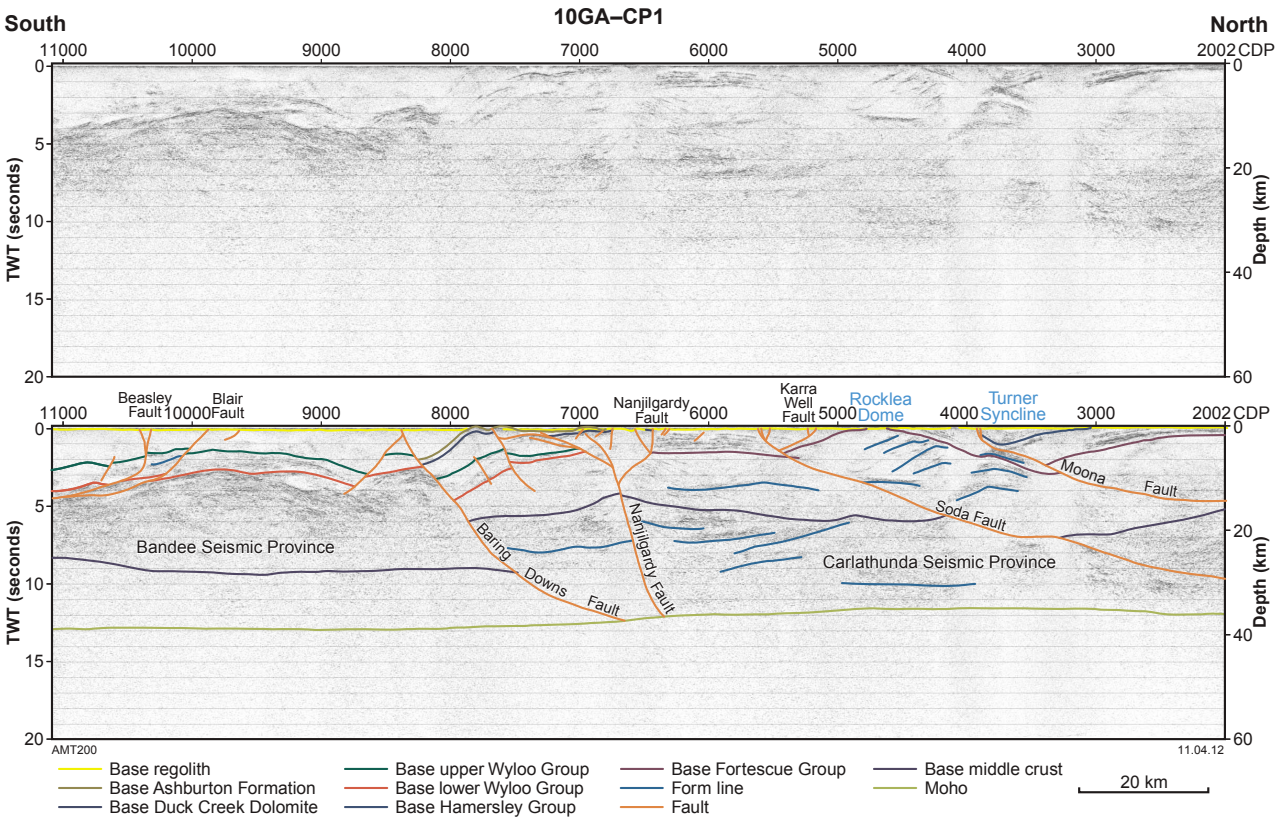

Figure 1. Migrated seismic section for line 10GA–CP1 across the northern Capricorn Orogen. Display shows vertical scale equal to the horizontal scale, assuming a crustal velocity of 6000 m/s. Common Depth Point (CDP) locations are shown in Frontispiece 1 (100 CDP = 2 km).

subsurface, probably because of a lack of continuous reflective markers within the stratigraphy (Fig. 2). The generally poor reflective response in this part of the section has also made it difficult to subdivide the upper Wyloo Group south of the Baring Downs Fault.

The reflective response is stronger below the interpreted base of the upper Wyloo Group, and the crustal architecture is imaged as a broad, faulted, upright anticline, whose axis lies immediately north of the Blair Fault. The thick (1 – 1.3 s TWT, or 3–4 km), weakly to strongly reflective layer that immediately underlies the Ashburton Formation is interpreted to be the lower Wyloo Group, with the high reflectivity of this layer caused by the Cheela Springs Basalt. Reflective layers beneath the interpreted lower Wyloo Group also show a broad anticlinal structure. Although these reflections could be due to an underlying succession of Hamersley and Fortescue Group rocks, the presence of numerous internal angular relationships is a feature not seen in this part of the stratigraphy elsewhere in the seismic profile.

Discussion of seismic interpretation

Seismic reflection data indicate a crustal thickness of about 11.7 – 12 s TWT (34–36 km) for the exposed southern part of the Pilbara Craton (Fig. 3, top). This is close to the values of 30 km ± 2km and 34 km obtained by the passive seismic studies of Reading and Kennett (2003), and Reading et al. (2012) for locations in the general vicinity, and also within the 28–37 km range reported for the southern Pilbara from the seismic reflection and refraction study of Drummond (1983).

Our deep seismic study has highlighted major differences between mid- to lower-crustal levels of the Pilbara Craton along 10GA–CP1. Upper-crustal granite–greenstone rocks, which occur northeast of the Baring Downs Fault, do not appear to be present south of this structure. Similarly, the middle- to deep-crustal levels, corresponding to the Carlathunda and Bandee Seismic Provinces, are quite different in their reflective character. These differences suggest that the combined granite–greenstone and underlying Carlathunda Seismic Province were once separate from the Bandee Seismic Province, but became juxtaposed along the line of the Baring Downs Fault. The timing of this amalgamation is uncertain, but must have pre-dated deposition of the lower Wyloo Group. This event may have occurred in the early stages of the 2215–2145 Ma Ophthalmian Orogeny, although the level of Ophthalmian deformation on the exposed Pilbara margin is not consistent with the presence of a major crustal suture along the line of the Baring Downs Fault. A more likely interpretation is that this suture pre-dates the Fortescue Group, and represents a southern terrane boundary analogous to those described from the northern Pilbara Craton (Hickman and Van Kranendonk, 2008; Hickman et al., 2010).

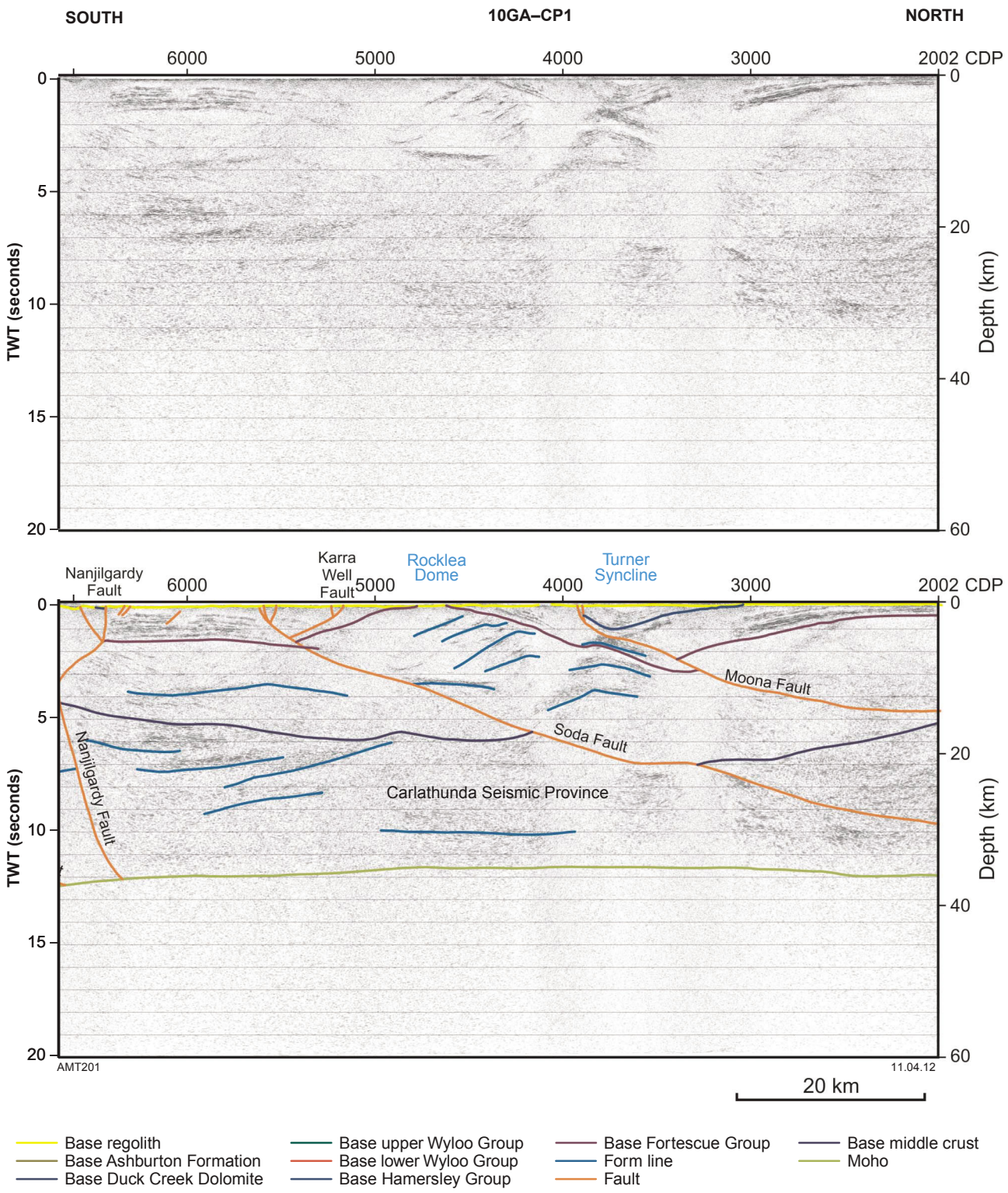

Figure 2. Clip of line 10GA–CP1, showing the crustal architecture between the Turner Syncline and the Nanjilgardy Fault. Display shows vertical scale equal to the horizontal scale, assuming a crustal velocity of 6000 m/s. Common Depth Point (CDP) locations are shown in Frontispiece 1 (100 CDP = 2 km).

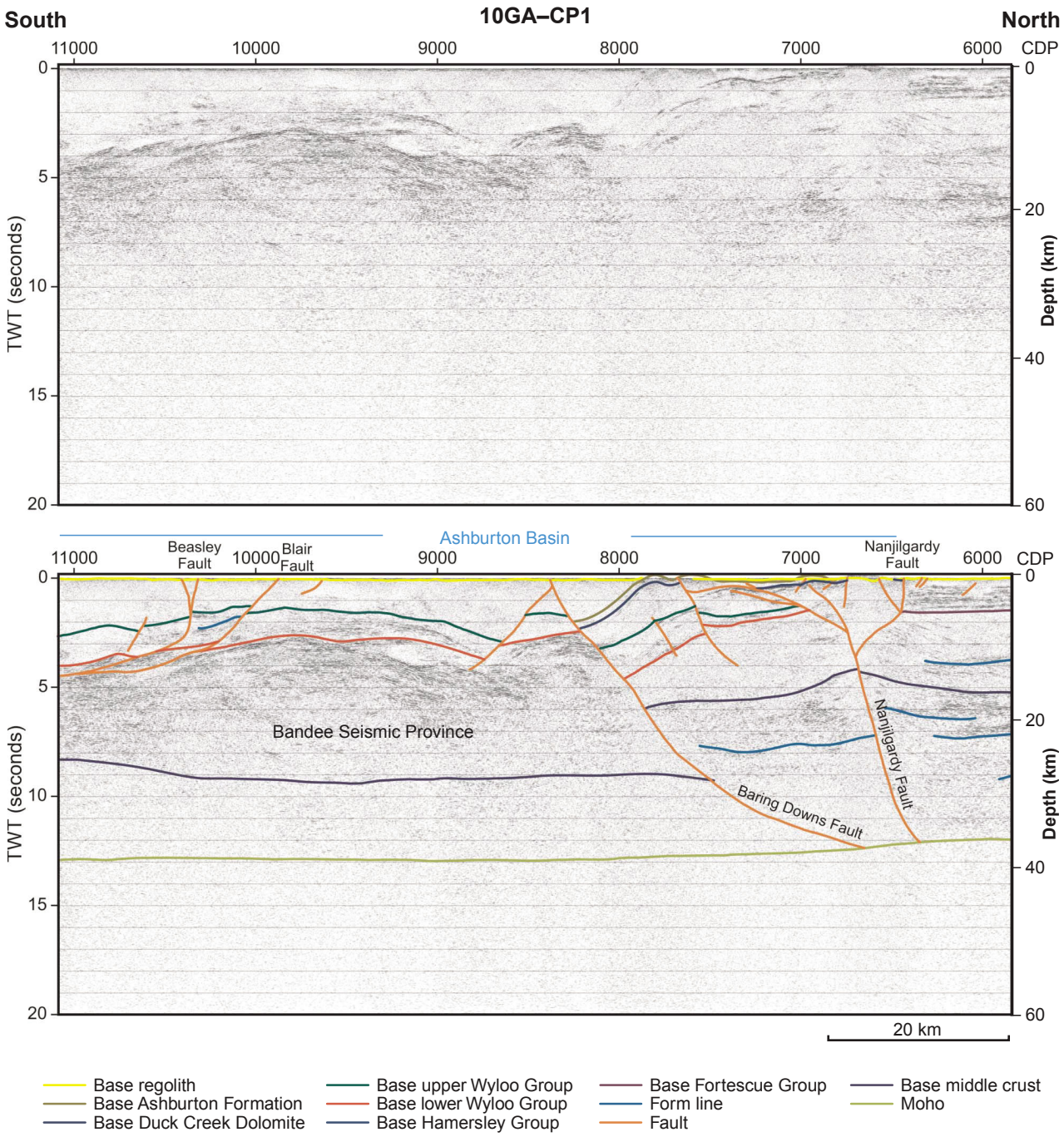

Figure 3. Clip of line 10GA–CP1, showing the crustal architecture between the Nanjilgardy Fault and the central Ashburton Basin. Display shows vertical scale equal to the horizontal scale, assuming a crustal velocity of 6000 m/s. Common Depth Point (CDP) locations are shown in Frontispiece 1 (100 CDP = 2 km).

Seismic profile 10GA–CP1 has delineated the northward-dipping attitude of the Baring Downs, Nanjilgardy, Soda, and Moona Faults. This is in contrast to previous interpretations that suggested that the major faults in the south central Pilbara Craton are steeply south-dipping (Thorne and Seymour, 1991). Syn- Fortescue Group growth faults in the southern Pilbara have also been postulated as south-dipping (Thorne and Trendall, 2001), a view not supported by the seismic data, which instead indicates that the Fortescue Group thickens from about 1.5 s TWT to roughly 2 s TWT (4.5 – 6 km) when traced in a southwesterly direction from the northeastern limb of the Turner Syncline towards the Moona Fault. The presence of north-dipping faults in the south central Pilbara has to be reconciled with the south-dipping, northward verging, structural fabric present in the southeastern Hamersley Basin (Tyler and Thorne, 1990; Tyler, 1991). This switch in fault orientation may take place across the eastern margin of the Turee Creek Syncline, where a marked change in the style of Ophthalmian deformation occurs, and which may mark the location of a related, buried, fossil transfer structure (Tyler, 1991; Plate 2).

Seismic profile 10GA–CP1 also represents a major advance in our understanding of the deep crustal structure beneath the Ashburton Basin. This area is now seen to mark the change from the north-dipping structural style of the south central Pilbara, to the south-dipping geometries characteristic of the southern Capricorn Orogen. The Ophthalmian suture between the Pilbara Craton (including the Bandee Seismic Province) and the Glenburgh Terrane is not observed on 10GA–CP1, being located south of the exposed Ashburton Basin, at the Lyons River Fault (Johnson et al., 2011; Korsch et al., 2011). Extensional and thrust faults, which cut both the lower and upper Wyloo Groups, may represent Ophthalmian structures that were subsequently reactivated during the 1820–1770 Ma Capricorn Orogeny. The strong Ashburton Fold Belt (Capricorn Orogeny) deformation recorded in surface outcrops of the Ashburton Formation does not appear to be present in the underlying lower Wyloo Group, which is imaged as a relatively continuous, although faulted, layer. This relationship suggests the possibility that the contact between the lower Wyloo Group and the Ashburton Formation is a significant structural decollement.

10GA–CP1 preliminary interpretation: additional geological and geophysical constraints

The previously discussed seismic interpretation of 10GA–CP1 (Fig. 4a) represents a major advance in the understanding of the crustal architecture of the northern Capricorn Orogen. However, there are aspects of the seismic interpretation south of the Nanjilgardy Fault, particularly whether or not the Hamersley and Fortescue Groups are present south of the Nanjilgardy Fault, that are at odds with other lines of evidence. These additional lines of evidence are summarized below.

- Both the surface geology and the regional gravity data suggest that the section between the Nanjilgardy and Baring Downs Faults is a down-faulted, westward continuation of the Bellary Dome. Since a complete Fortescue and Hamersley Group stratigraphy is exposed in the Bellary Dome (Thorne et al., 1991a), these rocks should also be present in the equivalent part of the 10GA–CP1 profile.
- The upper Hamersley Group is exposed immediately south of the Nanjilgardy Fault at Mount Maquire, southeast of Paraburdoo (Thorne and Tyler, 1993). A complete succession of Hamersley and Fortescue Group rocks is also preserved further east, on the southern flank of the Sylvania Inlier (Tyler et al., 1990).
- A broad aeromagnetic anomaly is present within the central Ashburton Basin, which coincides with the anticlinal crest indicated on the 10GA–CP1 seismic profile. The broad scale, uniform nature of this anomaly suggests it has a deep-seated source, below the strongly deformed and stratigraphically dismembered Ashburton Formation, which extends down to a minimum depth of 1.5 s TWT (~4.5 km). Geophysical modelling carried out as part of this study suggests that the aeromagnetic anomaly could be caused by a very strongly magnetic unit, such as the Hamersley Group, occurring at a depth of 9.5 – 10 km. This modelled depth is similar to the 8–11 km depth expected for the Hamersley Group based on the position of the basal contact of the lower Wyloo Group on the seismic profile.
- The results of a recent magnetotelluric study (Heinsen et al., 2011) indicate the presence a conductive layer at depth beneath the Ashburton Basin.
- There are no features of the Fortescue and Hamersley Group stratigraphy that suggest proximity to a southern basin margin at the Nanjilgardy Fault (Seymour et al., 1988; Thorne et al., 1991b; Thorne and Trendall, 2001). This stratigraphy, totalling almost 10 km in thickness, would have to have been stripped from the area south of the Nanjilgardy Fault prior to the deposition of the lower Wyloo Group.
- Paleocurrent and provenance data suggest that during deposition of the middle to upper Turee Creek Group, the Hamersley Group was distally exposed to the south of the present-day Pilbara margin (Thorne and Seymour, 1991; Martin et al., 2000).

In addition to the arguments listed above, other lines of evidence relate to the interpretation of the lower and upper Wyloo Group in the 10GA–CP1 seismic profile.

- Terminating the 1 km thick Duck Creek Dolomite at the Baring Downs Fault does not agree with the presence of mapped exposures of Duck Creek Dolomite in the central Ashburton Basin on eastern Turee Creek map sheet (Thorne et al., 1991a).
- The seismic interpretation of 10GA–CP1 shows the lower Wyloo Group varying in thickness from about 0.3 – 1.3 s TWT (1–4 km) between the Najilgardy and Baring Downs Faults. A similar thickness variation is interpreted for the Mount McGrath Formation (upper Wyloo Group). Although these thickness changes

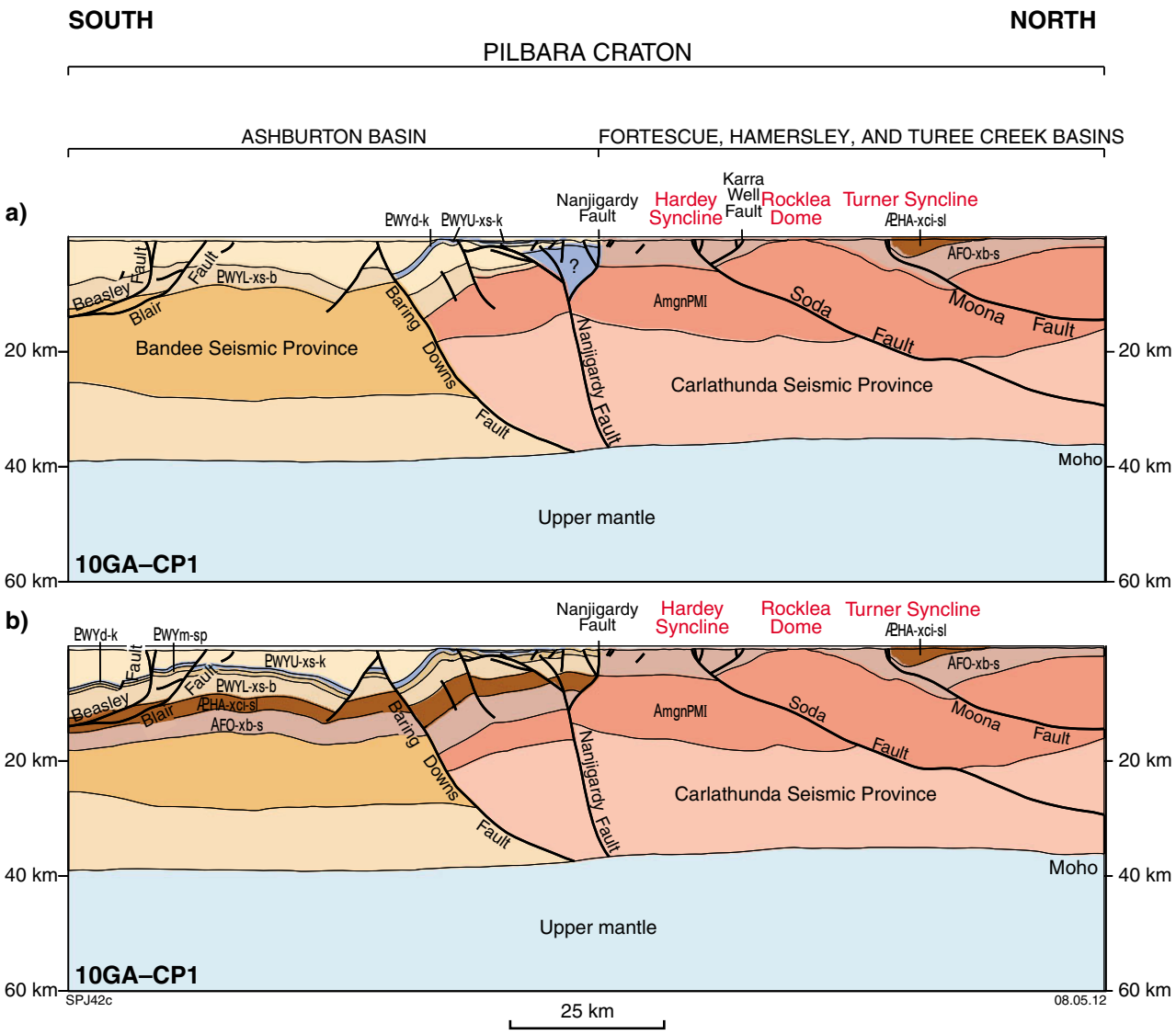

Figure 4. **Preliminary interpretations of seismic line 10GA–CP1: a) preliminary seismic interpretation; b) alternative preliminary geological interpretation. This interpretation is based on that shown in Figure 2, but uses additional geological and geophysical evidence to show the likely distribution of the Fortescue, Hamersley, and upper Wyloo Groups south of the Nanjilgardy Fault. Abbreviations: AmgnPMI — Pilbara Craton, AFO-xb-s — Fortescue Group, Æ-HA-xci-sl — Hamersley Group, PWYL-xs-b — lower Wyloo Group, PWYU-xs-k — upper Wyloo Group, PWYm-sp — Mount McGrath Formation, PWYd-k — Duck Creek Dolomite.**

cannot be ruled out entirely, they do not match with observations from adjacent surface outcrops, which indicate relatively consistent thicknesses of ~3 km and ~1.2 km for the lower Wyloo Group and Mount McGrath Formation, respectively (Thorne and Seymour, 1991).

10GA–CP1: alternative preliminary interpretation

Figure 4b is an alternative cross-section for 10GA–CP1, which is based on the seismic data, but also tries to address the problems with the preliminary seismic interpretation south of the Nanjilgardy Fault, cited above. Geological evidence suggests that the Duck Creek Dolomite, and possibly the Mount McGrath Formation, underlie the Ashburton Formation south of the Baring Downs Fault; however, these units cannot be distinguished on the basis of their seismic reflectance. Similarly, there is geological and geophysical evidence to suggest that the Hamersley and Fortescue Groups underlie the lower Wyloo Group between the Nanjilgardy Fault and the southern end of 10GA–CP1. Based on their known thicknesses, the positions of the Hamersley and Fortescue Groups on the seismic profile appear to coincide with a complexly structured, moderately reflective layer below the lower Wyloo Group. Although this layer does not have the

same reflective signature as the exposed Hamersley and Fortescue Group rocks seen at the northern end of 10GA–CP1, this may be due to an increased structural complexity and, in particular, the presence of numerous low-angle faults, beneath the Ashburton Basin. A similar explanation may also account for the difficulties in interpreting the seismic signature of supracrustal rocks between the Nanjilgardy and Baring Downs Faults.

The revised interpretation shows the Hamersley and Fortescue Groups extending from the exposed Pilbara Craton, across the Baring Downs Fault, to the southern Ashburton Basin. This succession overlies, and must therefore post-date, the boundary between the Bandee Seismic Province and the combined Pilbara granite–greenstone – Carlathunda Seismic Province, providing further support that this contact represents an Archean crustal suture within the Pilbara Craton.

References

Drummond, BJ 1983, Detailed seismic velocity/depth models of the upper lithosphere of the Pilbara craton, northwest Australia: BMR Journal of Geology and Geophysics, v. 8, p. 35–51.

Heinson, G, Boren, G, Ross, J, Campanya, J, Thiel, S and Selway, K 2011, The Capricorn magnetotelluric (MT) transect, *in* Capricorn Orogen seismic and magnetotelluric (MT) workshop 2011: extended abstracts *edited by* SP Johnson, AM Thorne and IM Tyler: Geological Survey of Western Australia, Record 2011/25, p. 75–100.

Hickman, AH and Van Kranendonk, MJ 2008, Archean crustal evolution and mineralization of the northern Pilbara Craton — a fieldguide: Geological Survey of Western Australia, Record 2008/13, 79p.

Hickman, AH, Smithies, RH and Tyler, IM 2010, Evolution of active plate margins: West Pilbara Superterrane, De Grey Superbasin, and the Fortescue and Hamersley Basins — a field guide: Geological Survey of Western Australia, Record 2010/3, 74p.

Johnson, SP, Cutten, HN, Tyler, IM, Korsch, RJ, Thorne, AM, Blay, O, Kennett, BLN, Blewitt, RS, Joly, A, Dentith, MC, Aitken, ARA, Goodwin, JA, Salmon, M, Reading, A, Boren, G, Ross, J, Costelloe, RD and Fomin, T 2011, Preliminary interpretation of deep seismic reflection lines 10GA–CP2 and 10GA–CP3: crustal architecture of the Gascoyne Province, and Edmund and Collier Basins, *in* Capricorn Orogen seismic and magnetotelluric (MT) workshop 2011: extended abstracts *edited by* SP Johnson, AM Thorne and IM Tyler: Geological Survey of Western Australia, Record 2011/25, p. 49–60.

Kennett, BLN 2011, Understanding the lithosphere in the vicinity of the Capricorn seismic lines from passive seismic studies, *in* Capricorn Orogen seismic and magnetotelluric (MT) workshop 2011: extended abstracts *edited by* SP Johnson, AM Thorne and IM Tyler: Geological Survey of Western Australia, Record 2011/25, p. 101–106.

Korsch, RJ, Johnson, SP, Tyler, IM, Thorne, AM, Blewett, RS, Cutten, HN, Joly, A, Dentith, MC, Aitken, ARA, Goodwin, JA and Kennett, BLN 2011, Geodynamic implications of the Capricorn deep seismic survey: from the Pilbara Craton to the Yilgarn Craton, *in* Capricorn Orogen seismic and magnetotelluric (MT) workshop 2011: extended abstracts *edited by* SP Johnson, AM Thorne and IM Tyler: Geological Survey of Western Australia, Record 2011/25, p. 107–114.

Martin, DM, Powell, CMcA and George, AD 2000, Stratigraphic architecture and evolution of the early Paleoproterozoic McGrath Trough, Western Australia: Precambrian Research, v. 99, p. 33–64.

Reading, AM and Kennett, BLN 2003, Lithospheric structure of the Pilbara Craton, Capricorn Orogen and northern Yilgarn Craton, Western Australia, from tele-seismic receiver functions: Australian Journal of Earth Sciences, v. 50, p. 439–445.

Reading, AM, Tkalčić, H, Kennett, BLN, Johnson, SP and Sheppard, S 2012, Seismic structure of the crust and uppermost mantle of the Capricorn and Paterson Orogens and adjacent cratons, Western Australia, from passive seismic transects: Precambrian Research, v. 196–197, p. 295–308.

Seymour, DB, Thorne, AM and Blight, DF 1988, Wyloo, Western Australia (2nd edition): Geological Survey of Western Australia, 1:250 000 Geological Series Explanatory Notes, 36p.

Thorne, AM and Seymour, DB 1991, Geology of the Ashburton Basin, Western Australia: Geological Survey of Western Australia, Bulletin 139, 141p.

Thorne, AM, Tyler, IM, Hunter, WM and Seymour, DB 1991a, Turee Creek, WA Sheet SF 50-15 (2nd edition): Geological Survey of Western Australia, 1:250 000 Geological Series.

Thorne, AM, Tyler, IM and Hunter, WM 1991b, Turee Creek, Western Australia (2nd edition): Geological Survey of Western Australia, 1:250 000 Geological Series Explanatory Notes, 29p.

Thorne, AM and Tyler, IM 1993, Paraburdoo, WA Sheet 2451: Geological Survey of Western Australia, 1:100 000 Geological Series.

Thorne, AM and Trendall, AF 2001, Geology of the Fortescue Group, Pilbara Craton, Western Australia: Geological Survey of Western Australia, Bulletin 144, 249p.

Thorne, AM, Johnson, SP, Tyler, IM, Cutten, HN and Blay, O 2011, Geology of the northern Capricorn Orogen, *in* Capricorn Orogen seismic and magnetotelluric (MT) workshop 2011: extended abstracts *edited by* SP Johnson, AM Thorne and IM Tyler: Geological Survey of Western Australia, Record 2011/25, p. 7–18.

Tyler, IM, Hunter, WM and Williams, IR 1990, Newman, WA Sheet SF 50-16 (2nd edition): Geological Survey of Western Australia, 1:250 000 Geological Series.

Tyler, IM and Thorne, AM 1990, The northern margin of the Capricorn Orogen, Western Australia — an example of an early Proterozoic collision zone: Journal of Structural Geology, v. 12, p. 685–701.

Tyler, IM 1991, The geology of the Sylvania Inlier and the southeast Hamersley Basin: Geological Survey of Western Australia, Bulletin 138, 108p.

Geology of the Gascoyne Province

by

SP Johnson, AM Thorne, HN Cutten, IM Tyler, and O Blay

Introduction

The Gascoyne Province lies at the western end of the Capricorn Orogen, and includes a range of Neoarchean to Paleoproterozoic gneisses, granites, and metasedimentary basins that record the amalgamation of the Archean Pilbara and Yilgarn Cratons to form the West Australian Craton, and over one billion years of subsequent intracontinental crustal reworking. During these multiple reworking events, different parts of the Gascoyne Province have responded differently to deformation, metamorphism, and magmatism. This has led to the subdivision of the province into several fault or shear zone bounded, easterly–southeasterly trending structural and metamorphic zones (Frontispiece 1–3; Fig. 1; Sheppard et al., 2010b).

The oldest crust in the Gascoyne Province is the Glenburgh Terrane, which is exposed only within the southern part of the province (Frontispiece 1–3; Plate 1). The southern boundary is marked by the Errabiddy Shear Zone, a high-strain zone up to 25 km wide that contains imbricated slices of reworked Yilgarn Craton. The northern margin of the Glenburgh Terrane is not exposed, but is interpreted from various geophysical data to coincide roughly with the Talga Fault (Frontispiece 2; Selway, 2008; Selway et al., 2009), implying that the terrane also forms basement to the northern part of the province. During subsequent crustal reworking, the Glenburgh Terrane was intruded by various generations of granitic magmas and overlain by numerous metasedimentary basins, some of which have been deformed at low- to medium-metamorphic grades. During these multiple tectonomagmatic reworking events, deformation, metamorphism, and magmatism were focused into discrete easterly–southeasterly trending tectonic corridors (structural and metamorphic zones), each of which is bounded by a major fault or shear zone (Frontispiece 1; Fig. 1; Sheppard et al., 2010b). Variable uplift on major faults across the province has then juxtaposed blocks of contrasting crustal depth.

The Glenburgh Terrane and assembly of the West Australian Craton

The Glenburgh Terrane comprises: (i) a basement of heterogeneous granitic gneisses (the Halfway Gneiss) with ages between c. 2555 and c. 2430 Ma; (ii) an overlying package of continent-derived siliciclastic metasedimentary rocks (the 2240–2125 Ma Moogie Metamorphics); (iii) a c. 2000 Ma belt of metagranitic rocks (the Dalgaringa Supersuite), which are interpreted to have formed in a continental-margin volcanic arc; and (iv) arc-related metasedimentary rocks (the 2000–1955 Ma Camel Hills Metamorphics) that are in tectonic contact with both the arc rocks and the deformed northern margin of the Yilgarn Craton. The oldest tectonic unit, the Halfway Gneiss, consists of heterogeneous, variably pegmatite-banded, granitic gneisses. The protoliths have crystallization ages between c. 2555 and c. 2430 Ma, but also contain abundant older inherited zircons, some of which are as old as c. 3447 Ma (Johnson et al., 2011c). Although no older crust (>2555 Ma) is exposed, the Lu–Hf compositions and crustal model ages of both magmatic and inherited zircons indicate a long crustal history ranging back to c. 3700 Ma (Johnson et al., 2011c). These isotopic data also demonstrate that large parts of the terrane, presumably representing the mid and lower crust (none of these rocks are currently exposed), formed via juvenile crustal growth processes between c. 2730 and c. 2600 Ma (Johnson et al., 2011c). Formation of the 2555–2430 Ma gneisses occurred mainly by the in situ reworking of these older crustal components (Johnson et al., 2011c). A comparison of the U–Pb zircon ages and zircon-Hf isotopic compositions of the Halfway Gneiss with those of the bounding Pilbara and Yilgarn Cratons indicates that the Halfway Gneiss (and thus the Glenburgh Terrane) is exotic to, and evolved independently from, these cratons (Johnson et al., 2011c). The Glenburgh Terrane is interpreted to have collided and accreted with the Pilbara Craton during the 2215–2145 Ma Ophthalmian Orogeny (Occhipinti et al., 2004; Johnson et al., 2010, 2011a,c).

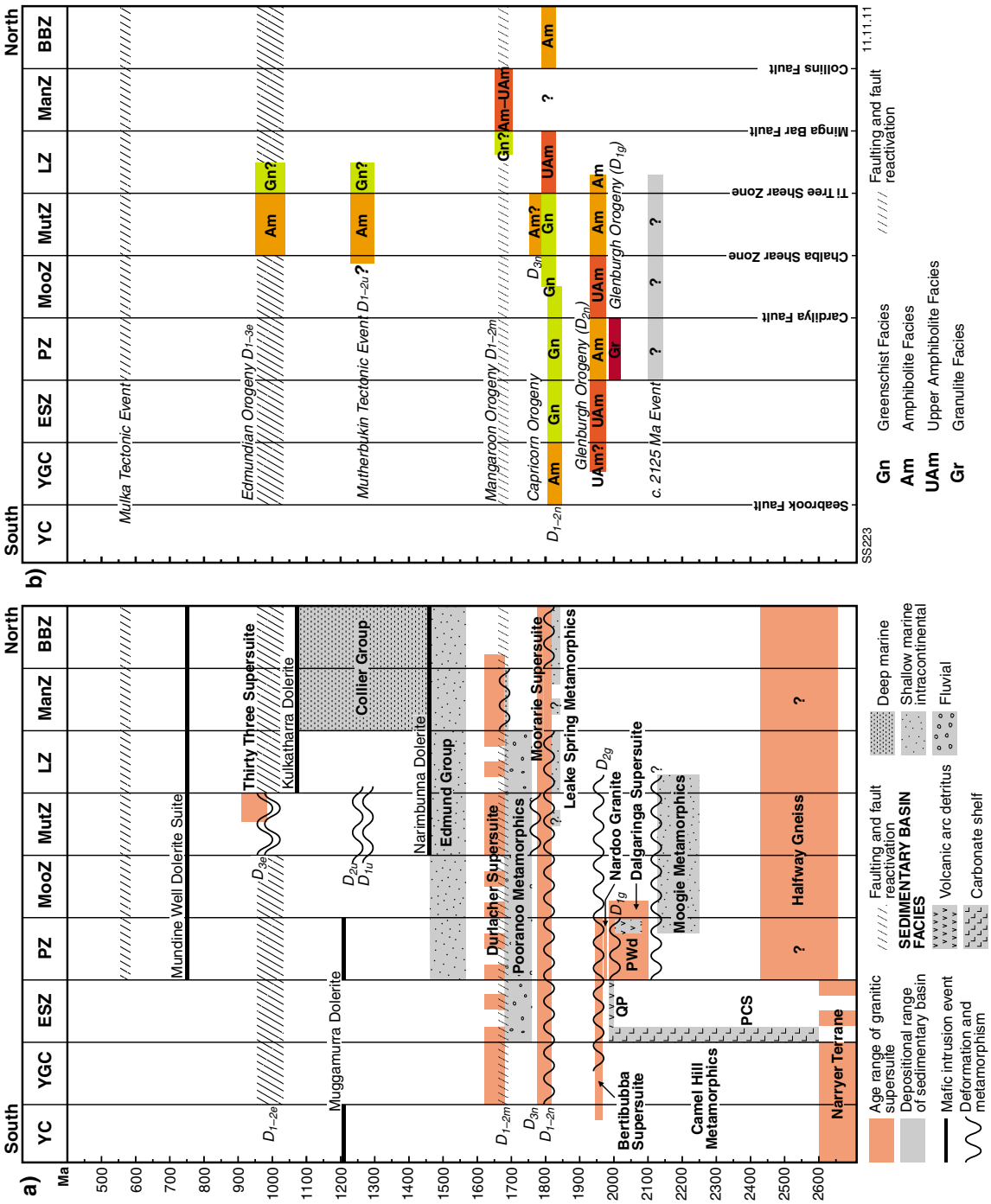

Figure 1. Time–space plot for the Gascoyne Province. Zone boundary abbreviations: BBZ — Boora Boora Zone; ESZ — Errabiddy Shear Zone; LZ — Limejuice Zone; ManZ — Mangaroon Zone; MooZ — Mooloo Zone; MutZ — Mutherbukin Zone; PZ — Paradise Zone; YC — Yilgarn Craton; YGC — Yarlarweelor Gneiss Complex. Abbreviations in time–space plot: PCS — Petter Calc-silicate; QP — Quartpot Pelite; PWd — Paradise Well diatexite.

The Moogie Metamorphics are dominated by psammitic schists, the protoliths to which were deposited across the Glenburgh Terrane sometime between c. 2240 and c. 2125 Ma. The timing of deposition is essentially coincident with the 2215–2145 Ma Ophthalmian Orogeny, and these protoliths are interpreted to represent a pro-foreland basin deposited in response to uplift of the southern Pilbara Craton margin during the collision and accretion of the Glenburgh Terrane with the Pilbara Craton (Fig. 2; Occhipinti et al., 2004; Johnson et al., 2010, 2011a). The Moogie Metamorphics are probably roughly time-equivalent to the Beasley River Quartzite of the lower Wyloo Group, which was deposited in a retro-foreland basin during the Ophthalmian Orogeny (Fig. 2; Martin and Morris, 2010).

Following this collision on the northern margin of the Glenburgh Terrane, continental-margin arc-magmatic activity was initiated along the southern margin at c. 2080 Ma (Fig. 2; Johnson et al., 2010, 2011a). Although magmatic rocks with ages between c. 2080 and c. 2005 Ma are not exposed within the province, detrital and inherited zircons of this age, with slightly evolved Lu–Hf compositions, are abundant within the volcanoclastic metasediments of the 2000–1955 Ma Camel Hills Metamorphics (Johnson et al., 2010, 2011a), and within the granitic gneisses of the 2005–1985 Ma Dalgaringa Supersuite.

The Dalgaringa Supersuite is exposed in the southern part of the province, within the Paradise Zone (Frontispiece 1–3; Plate 1), and comprises massive, foliated, and gneissic granitic rocks that have major-, trace-, and rare earth element (REE) concentrations consistent with formation in a supra-subduction zone setting (Sheppard et al., 2004). Their whole-rock Sm–Nd, and magmatic zircon Lu–Hf, isotopic signatures indicate the incorporation of Neoarchean granitic gneisses with isotopic compositions similar to those of the Halfway Gneiss (Sheppard et al., 2004; Johnson et al., 2011a), suggesting that magmatism occurred in a continental-margin arc, termed the Dalgaringa Arc, which formed along the southern margin of the Glenburgh Terrane (Fig. 2). This magmatic event records the progressive closure and northward subduction of an oceanic tract under the combined Pilbara Craton – Glenburgh Terrane. The older parts of the Dalgaringa Supersuite (2005–1985 Ma), including lenses of pelitic diatexite and mafic granulite, were deformed and metamorphosed at high temperatures and pressures during the D_{1g} event (2005–1985 Ma) of the 2005–1950 Ma Glenburgh Orogeny. This event is interpreted to reflect the construction of the arc in the middle crust (Johnson et al., 2010, 2011a).

Terminal ocean closure, the collision between the Pilbara Craton – Glenburgh Terrane and the Yilgarn Craton, and the formation of the West Australian Craton, all took place during the 1965–1950 Ma D_{2g} event of the Glenburgh Orogeny (Johnson et al., 2010, 2011a). The collision resulted in the imbrication of the northern Yilgarn Craton margin with Glenburgh Terrane lithologies along the Errabiddy Shear Zone (Frontispiece 1–3; Fig. 2; Plate 1), and the high-grade tectonometamorphism of metasedimentary and meta-igneous rocks along the southern margin of the Glenburgh Terrane. The D_{2g} event was accompanied by the intrusion of granitic stocks and dykes of the 1965–1945 Ma Bertibubba Supersuite. These granitic rocks are the first common magmatic element of the northern margin of the Yilgarn Craton, the Yarlarweelor Gneiss Complex, the Errabiddy Shear Zone, and the Paradise Zone of the Glenburgh Terrane. Therefore, suturing of the combined Pilbara Craton – Glenburgh Terrane with the Yilgarn Craton, and thus the assembly of the West Australian Craton, was complete by this time (Fig. 2).

Intracontinental magmatism and repeated crustal reworking

Subsequent to the assembly of the West Australian Craton during the Glenburgh Orogeny, the history of the Capricorn Orogen is dominated by more than one billion years of episodic intracontinental reworking and reactivation. These multiple crustal events took place during the 1820–1770 Ma Capricorn Orogeny, the 1680–1620 Ma Mangaroon Orogeny, the 1385–1200 Ma Mutherbukin Tectonic Event, the 1030–955 Ma Edmundian Orogeny, and the c. 570 Ma Mulka Tectonic Event.

The 1820–1770 Ma Capricorn Orogeny

Although the Capricorn Orogeny had been widely interpreted to be the result of oblique collision between the Yilgarn and Pilbara Cratons (Myers, 1990; Tyler and Thorne, 1990; Krapež, 1999; Evans et al., 2003), most of these models were based largely on interpretations of poorly dated metasedimentary successions in the northern part of the orogen, or else did not take into account the ages, spatial distribution, and composition of granitic magmatism in the Gascoyne Province. The recognition of pre-1950 Ma tectonometamorphic events associated with the assembly of the West Australian Craton also negate a Capricorn Orogeny aged collision. Structures and metamorphic mineral assemblages related to the Capricorn Orogeny, and granites of the accompanying Moorarie Supersuite, are recognized across the province and in adjacent tectonic units such as the Ashburton Basin to the north, the Yarlarweelor Gneiss Complex and Errabiddy Shear Zone to the south, and the Padbury, Bryah, and Yerrida Basins to the east (Thorne and Seymour, 1991; Occhipinti et al., 1998; Sheppard and Swager, 1999; Occhipinti and Myers, 1999; Krapež and McNaughton, 1999; Pirajno et al., 2000; Sheppard et al., 2003; Martin et al., 2005; Sheppard et al., 2011). The orogeny is characterized by extensive deformation at low- to medium-metamorphic grades, and was accompanied by the intrusion of voluminous, felsic magmatic stocks and plutons, including the Minnie Creek batholith in the central part of the province (Fig. 3).

Three main tectonothermal events are recognized in the Gascoyne Province (D_{1n}, D_{2n}, and D_{3n}). The oldest event (D_{1n}) is recorded in the Yarlarweelor Gneiss Complex, Errabiddy Shear Zone, and southern part of the Mooloo Zone, occurring between c. 1820 and c. 1810 Ma. This event is dominated by intense upright to isoclinal folds,

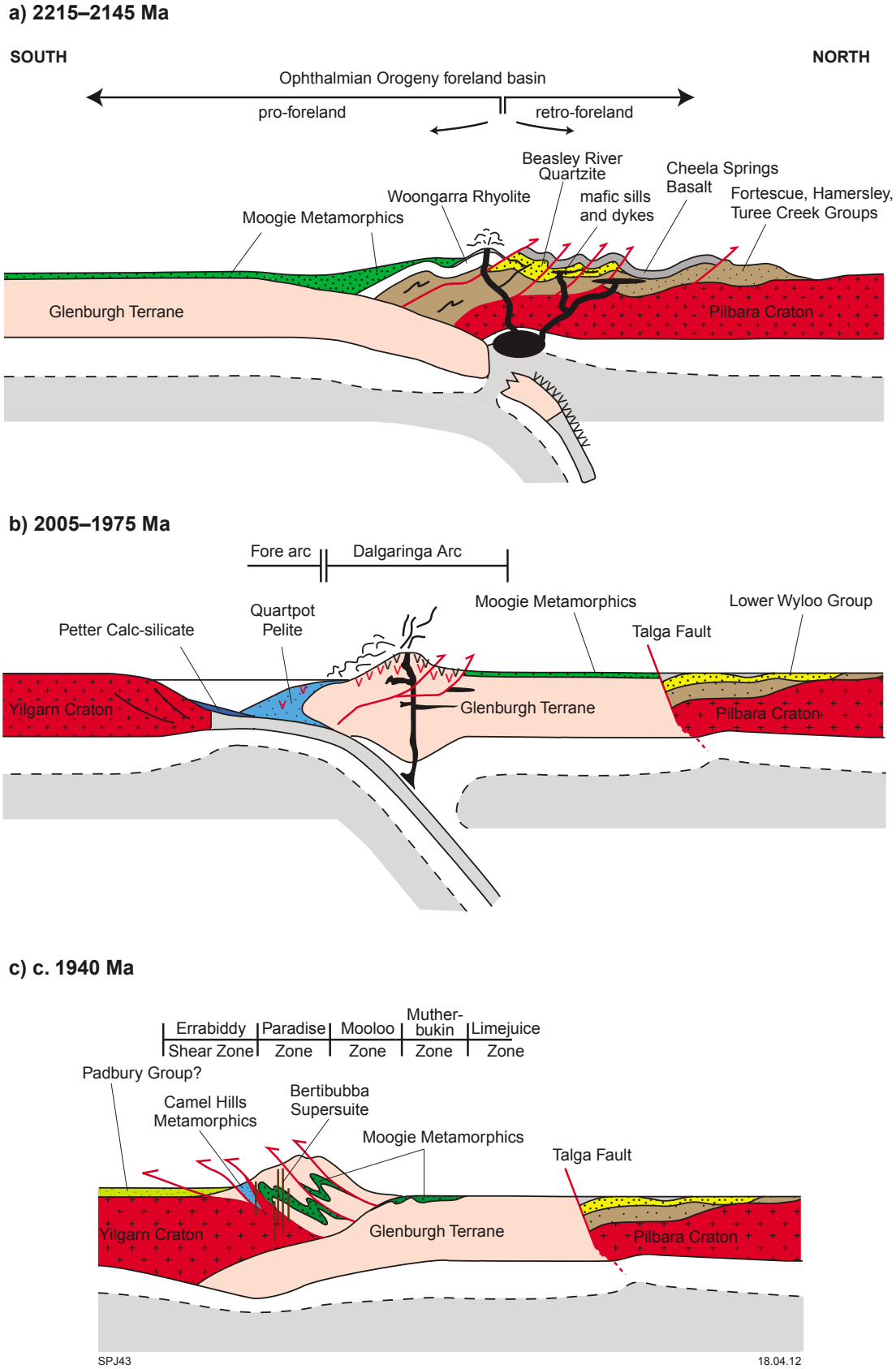

Figure 2. Schematic cross sections showing possible tectonic settings for the deposition of: a) the Moogie Metamorphics during the 2215–2145 Ma Ophthalmian Orogeny, modified from Martin and Morris (2010); b) the Camel Hills Metamorphics during the 2005–1975 Ma period of the Glenburgh Orogeny; and c) the post-collisional architecture at c. 1940 Ma, modified from Cawood and Tyler (2004). Note that cross sections are not intended to infer orthogonal collision or plate motions between the tectonic blocks or cratons.

with the production of an intense foliation or gneissic fabric. Apart from the Yarlarweelor Gneiss Complex, where metamorphism peaked in the upper amphibolite facies (Sheppard and Swager, 1999), metamorphism during this event was generally of greenschist-facies grade, and was responsible for the wholescale retrogression of high-grade metamorphic minerals formed during the Glenburgh Orogeny. Tectonometamorphism was accompanied by the intrusion of extensive sheets and stocks of granodiorite and monzogranite.

In the central part of the province, the main tectonic event is represented by D_{2n}, which is dated to between c. 1808 and c. 1786 Ma, and was synchronous with the intrusion of the Minnie Creek batholith. Due to subsequent structural and metamorphic overprinting, the structures and mineral assemblages associated with D_{2n} are commonly difficult to identify, especially in the Mutherbukin Zone; however, in the Limejuice Zone, inclusions and rafts of pelitic and semipelitic material (belonging to the 1840–1810 Ma Leake Spring Metamorphics) found within granites of the Minnie Creek batholith commonly contain a strong gneissic fabric or schistosity. Although the peak mineral assemblages have been wholly retrogressed, they probably contained andalusite as a porphyroblastic phase. In the southeastern portion of the Minnie Creek batholith, the appearance of cordierite indicates metamorphism at higher temperatures. Gneissic fabrics are also developed in granites of the Minnie Creek batholith, such as the Middle Spring Granite. Based on the age of undeformed granites that crosscut the strongly deformed Middle Spring Granite, the D_{2n} event in the batholith as a whole appears to have been a very short lived event, occurring between c. 1788 and c. 1786 Ma (Sheppard et al., 2010b; Geological Survey of Western Australia, 2011).

Throughout the province, granites of the Moorarie Supersuite mostly range from about 61 wt% SiO_2 to 77 wt% SiO_2, although the Minnie Creek batholith also includes some mafic–ultramafic intrusions and mafic inclusions. The granites show a wide range in initial εNd values, extending from -1.7 to -14.3, although most have initial εNd values between -1.7 and -8.1. The most evolved compositions, between -11.6 and -14.3, belong to very silicic, leucocratic, pegmatitic granites in the Yarlarweelor Gneiss Complex that were derived from the melting of Archean crust (Sheppard et al., 2003). Granites from individual regions show a more restricted range of values (Fig. 3a). Minnie Creek batholith granites have initial εNd values of -1.7 to -5.5, which are less negative than coeval granites to the north and south (-4.0 to -8.1; Fig. 3), and on the whole have younger T_{DM} model ages (between 2570 and 2250 Ma) than contemporaneous granites elsewhere in the province. These data imply a more juvenile source for the Minnie Creek batholith. The presence of gabbros and widespread mafic inclusions in this batholith's granites suggests that this juvenile component was probably derived directly from the mantle. However, all of the granites, including those of the Minnie Creek batholith, have much lower εNd values than depleted mantle at this time (~+6, using the depleted mantle model of Goldstein et al. (1984)), implying that the granites themselves were derived largely by melting older crust, which must have included components older than c. 2570 Ma; i.e. the Yarlarweelor Gneiss Complex of the Yilgarn Craton, and the Halfway Gneiss of the Glenburgh Terrane.

The third tectonic event, D_{3n}, is only recognized in the Limejuice Zone, where D_{2n} gneissic fabrics and foliations in the Minnie Creek batholith and associated pelitic inclusions are folded about upright, local- to regional-scale, close to tight folds. A well-developed crenulation cleavage is developed parallel to these macroscopic F_{3n} fold traces, and is defined by a lower-greenschist facies mineral assemblage. Low Th/U metamorphic or hydrothermal zircon rims, obtained from quartzites in the Mutherbukin Zone, have been dated at c. 1772 Ma (Johnson et al., 2010, 2011a). Although zircon-rim growth cannot be directly related to any tectonic fabric, it is possible that they record hydrothermal fluid flow during the D_{3n} event.

On a regional scale, deformation and metamorphism associated with the main D_{2n} event in the central part of the Gascoyne Province was synchronous with deformation and metamorphism in the Ashburton Fold Belt and Boora Boora Zone to the north. In the Boora Boora Zone, metasedimentary rocks of the Leake Spring Metamorphics are interpreted to grade northwards into lower-grade metasedimentary rocks of the upper Wyloo Group, particularly the Ashburton Formation (Williams, 1986; Myers, 1990). In the Ashburton Fold Belt, D_{1ash} is dated to between c. 1806 and c. 1786 Ma, which occurred before the deposition of the Capricorn Group. D_{2ash} occurred between c. 1786 and c. 1738 Ma, after deposition of the Capricorn Group. Both events occurred at low- to medium-metamorphic grade, peaking during M_{1a} with the production of garnet, cordierite, and andalusite in pelitic schists. Both events are also associated with the generation of local- to regional-scale tight to isoclinal folds and associated strike-slip faults.

The spatial and temporal patterns of deformation, metamorphism, magmatism, and sedimentation, along with the geochemical and isotopic composition of the granites in the Gascoyne Province, are best explained by intracontinental reworking during the Capricorn Orogeny (Sheppard et al., 2010a,b), rather than by continental collision during the assembly of the West Australian Craton. Although the tectonic driver of the Capricorn Orogeny is unknown, it is possible that tectonism was in response to plate-margin stresses associated with the collision of the West Australian and North Australian Cratons during the 1795–1760 Ma Yapungku Orogeny.

The 1680–1620 Ma Mangaroon Orogeny

The Mangaroon Orogeny encompasses complex and progressive deformation, metamorphism, sedimentation, and granite magmatism. Structures and metamorphic assemblages related to the orogeny appear to be restricted entirely to the Mangaroon Zone in the northern part of the Gascoyne Province, although granite magmatism (the Durlacher Supersuite) and sedimentation (the Pooranoo Metamorphics) took place across the entire province.

The Pooranoo Metamorphics contain a well-defined stratigraphy consisting of a lower succession of fluvial

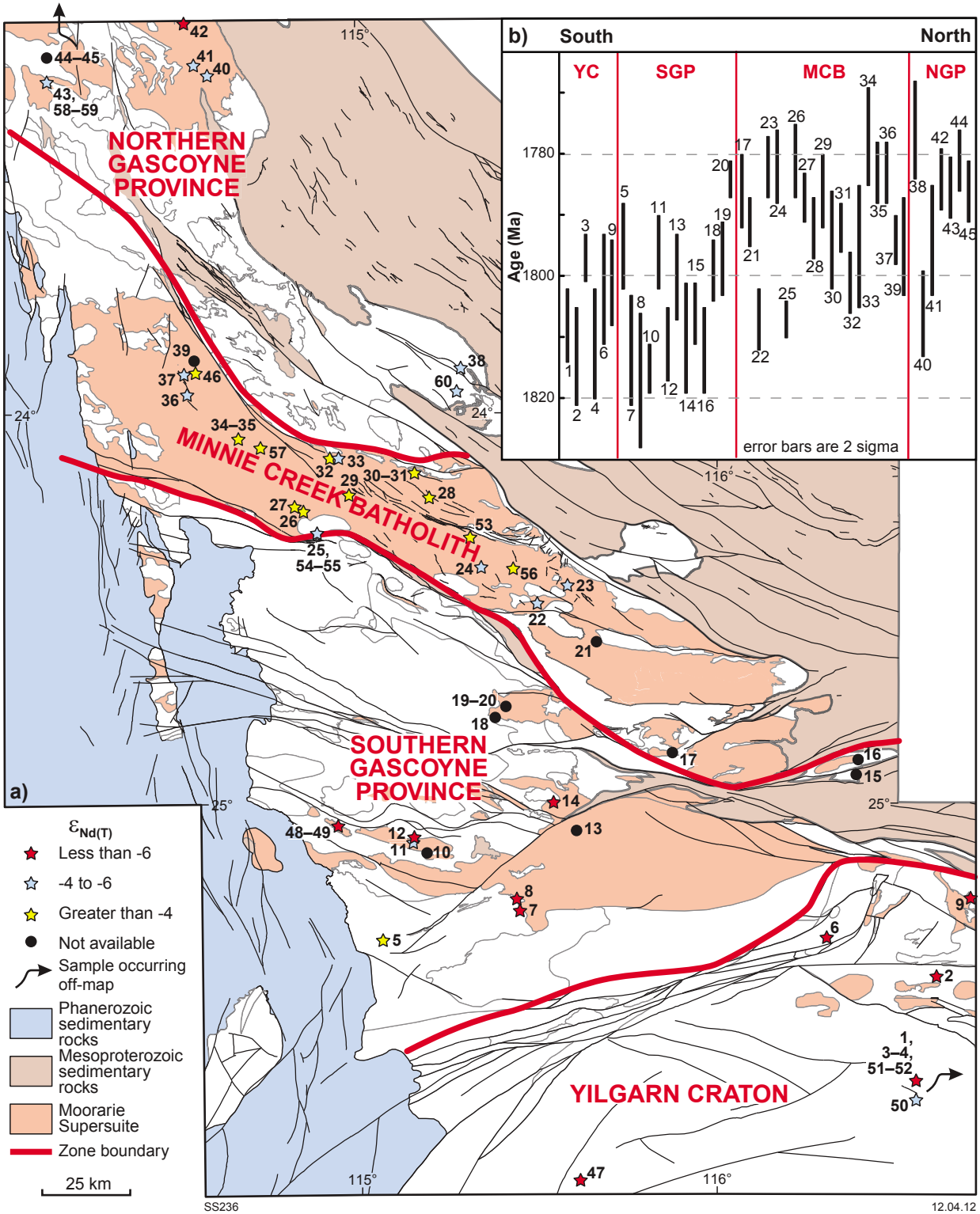

Figure 3. **Summary of: (a) whole-rock Nd isotope compositions; and (b) SHRIMP U–Pb zircon ages for granites of the Moorarie Supersuite from south to north. Age data from Perring et al. (1996), Krapež and McNaughton (1999), Evans et al. (2003), and Geological Survey of Western Australia (2011). Numbers on part (a) refer to sample numbers in part (b). Key to abbreviations: YC — reworked Yilgarn Craton; SGP — southern Gascoyne Province; MCB — Minnie Creek batholith; NGP — northern Gascoyne Province.**

conglomerates and sandstones up to 700 m thick, overlain by shallow-marine sandstones. This basal package is known as the Mount James Subgroup, and is present from the Errabiddy Shear Zone through to the Limejuice Zone (Frontispiece 1–3; Plate 1). In the northern part of the Limejuice Zone and throughout the Mangaroon Zone, these rocks grade upwards into turbiditic sandstones, siltstones, and shales that appear to mark a deepening of the basin to the north. SHRIMP U–Pb geochronology of detrital zircons from the Mount James Subgroup indicate that these sediments were deposited after c. 1760 Ma, but prior to deformation and the intrusion of Durlacher Supersuite granites at c. 1670 Ma. The depositional age of the turbiditic rocks in the Mangaroon Zone is well constrained by the youngest detrital zircon population at 1680 ± 13 Ma, and by granite plutons that intruded the metasedimentary rocks at 1677 ± 5 Ma (Sheppard et al., 2005), indicating a very short time-span between sedimentation, high-grade metamorphism, and granite magmatism.

In the Mangaroon Zone, deformation and metamorphism has been divided into two events (D_{1m} and D_{2m}), which were probably broadly associated with the intrusion of voluminous granite plutons of the Durlacher Supersuite. During D_{1m}, between c. 1680 and c. 1677 Ma, the Pooranoo Metamorphics were metamorphosed in the upper amphibolite facies, and characterized by the production of gneissic fabrics and extensive melting of pelitic and semipelitic rocks, although the grade of metamorphism appears to be lower in the northern half of the Mangaroon Zone where migmatites are less common. The D_{2m} event appears to have immediately followed the D_{1m} event, and was responsible for the production of a pervasive schistosity, metre- to kilometre-scale upright folds, and the retrogression of D_{1m} metamorphic minerals to greenschist-facies assemblages. Many granites of the Durlacher Supersuite with igneous crystallization ages of c. 1675 Ma or older were deformed during D_{2m}. The lack of megascopic compressional structures during the low-pressure, high-temperature metamorphism of D_{1m}, and the near-synchronous timing of basin deposition and granite intrusion, both suggest that the Mangaroon Zone was under extensional crustal regimes during this event.

After the termination of D_{1m} and D_{2m} deformation and metamorphism, granitic magmatism ceased in the Mangaroon Zone and stepped across into the other parts of the Gascoyne Province, especially the Mutherbukin Zone. Large volumes of megacrystic K-feldspar-phyric monzogranite and leucocratic tourmaline-bearing monzogranite were emplaced between c. 1670 and c. 1650 Ma, although the Discretion Granite, a pluton of granite in the Yarlarweelor Gneiss Complex, has been dated at c. 1620 Ma. Deformational structures and metamorphic assemblages associated with this younger period (1670–1620 Ma) of magmatism have yet to be identified in the Gascoyne Province. However, $^{40}Ar/^{39}Ar$ age determinations of c. 1950 Ma have been obtained on sericite from strongly cleaved metamudstones from the Earaheedy Basin in the southern part of the orogen (Pirajno et al., 2009b), and on muscovite from regional-scale extensional faults within the Sylvania Inlier along the northern margin of the orogen (Sheppard et al., 2006).

Similar to the Capricorn Orogeny, the nature, style, and timing of deformation, metamorphism, sedimentation, and granite magmatism suggest that the Mangaroon Orogeny was an intraplate event, the driver of which is currently unknown.

Mesoproterozoic sedimentation and tectonism

Following the Mangaroon Orogeny, mostly fine-grained siliciclastic sediments and carbonates were deposited, firstly in the Edmund Basin and then within the Collier Basin, both of which unconformably overlie the Gascoyne Province (Frontispiece 1; Plate 1). A detailed description of the stratigraphy and tectonic history of these basins is provided by Cutten et al. (2011).

Both the Edmund and Collier Basins were deposited as a response to the intracratonic reactivation of the Capricorn Orogen, and the sedimentation, at least in the lower part of the Edmund Group, appears to have been controlled principally by the Talga Fault (Martin and Thorne, 2004; Martin et al., 2008). However, structures or metamorphic assemblages associated with this intracratonic reactivation have yet to be identified within the Gascoyne Province. The upper part of the Edmund Basin, specifically the Ullawarra Formation, contains thin felsic tuffs dated at c. 1460 Ma (Cutten et al., 2011; Geological Survey of Western Australia, 2011), the ages of which are within uncertainty of the abundant c. 1465 Ma dolerite sills that intrude the upper parts of the basin (Wingate, 2002; Cutten et al., 2011). These dates provide a younger age limit for sedimentation, the older limit being provided by the age of Gascoyne Province basement (c. 1620 Ma), upon which the basin was unconformably deposited. The Collier Basin was deposited unconformably on both the Gascoyne Province basement and the Edmund Basin (Frontispiece 1; Plate 1), and was not affected by the 1385–1200 Ma Mutherbukin Tectonic Event, indicating deposition after c. 1200 Ma. As both the Edmund and Collier Basins were intruded by c. 1070 Ma dolerite sills of the Warakurna Large Igneous Province (Morris and Pirajno, 2002; Wingate et al., 2004), this set of sills provides a younger age limit for deposition of the Collier Basin.

The 1385–1200 Ma Mutherbukin Tectonic Event

The Mutherbukin Tectonic Event is a poorly defined tectonothermal event, known primarily from the Mutherbukin Zone in the central part of the Gascoyne Province (Johnson et al., 2011b). However, hydrothermal alteration and faulting also affected rocks of the Edmund Basin.

In the Gascoyne Province, mineral assemblages and tectonic fabrics related to the Mutherbukin Tectonic Event occur within a 50 km wide corridor, bounded by the Ti Tree and Chalba Shear Zones, lying directly south of the Minnie Creek batholith (Frontispiece 1–3; Fig. 4; Plate 1). However, discrete narrow shear zones of this age are also present within, and to the north of, the Minnie Creek batholith. The primary expression of this event is

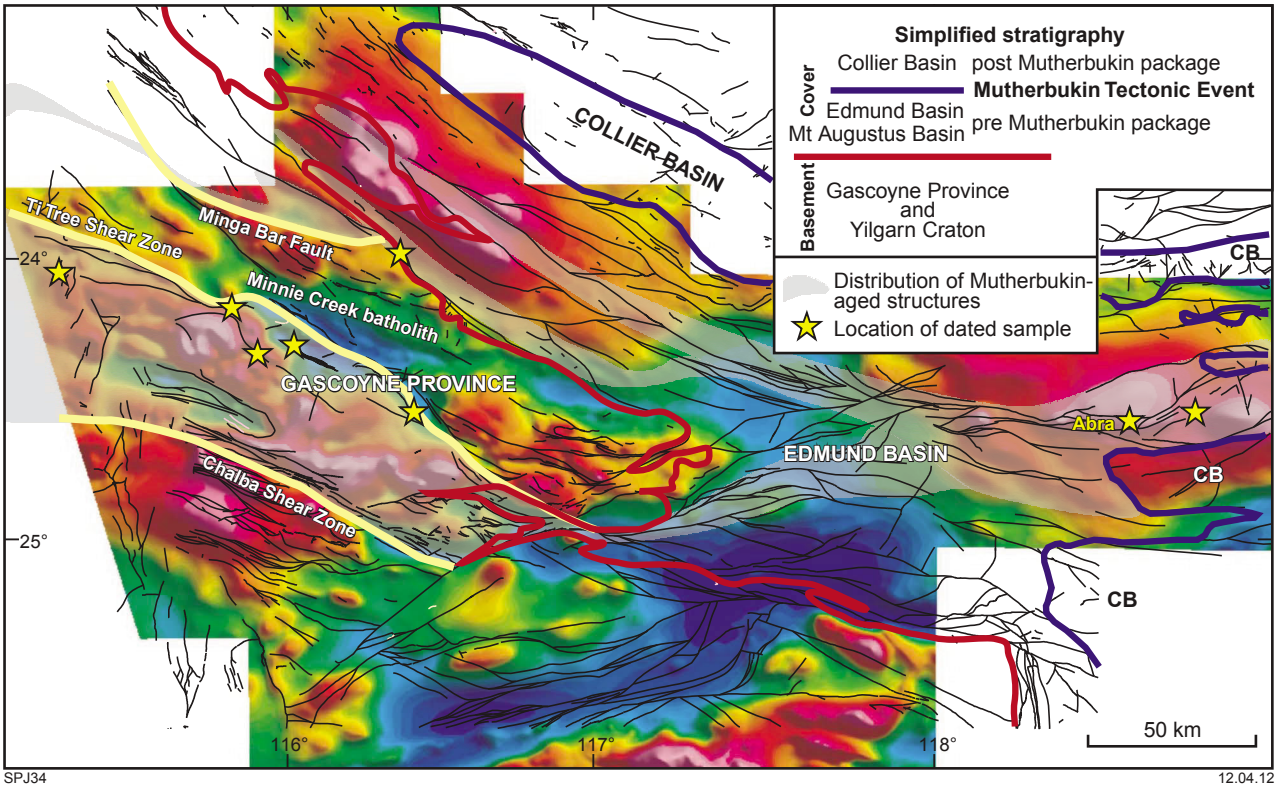

Figure 4. Regional distribution of Mutherbukin-aged structures. The mapped 1:100 000 scale surface structures are overlain on a 2000 m upward-continuation model of 400 m line-spaced reduced-to-pole aeromagnetic data. The stratigraphy of the region has been divided into three main packages: Gascoyne Province basement, and overlying sedimentary cover rocks, with the cover rocks divided into pre-Mutherbukin (Mount Augustus and Edmund Basins) and post-Mutherbukin (Collier Basin) packages.

a strong schistosity in the metasedimentary rocks, and a widely developed foliation or gneissic banding within metamorphosed granites. Garnet and staurolite-bearing semipelitic schists on the south side of the Minnie Creek batholith pass into upper-amphibolite facies granitic gneisses of the 1680–1620 Ma Durlacher Supersuite that are interpreted to have been emplaced in the mid crust. These gneisses locally preserve evidence for in situ melting. Both the metasedimentary rocks and gneissic granites contain a strong, shallow, east-plunging mineral lineation parallel to the hinges of decametre- to kilometre-scale, shear-related folds. Abundant shear sense indicators in both the schists and granitic gneisses reveal sinistral transtensional shear regimes. Dating of metamorphic monazite, mainly from garnet–staurolite schists, from widely spaced localities provides a range of ages between c. 1280 and c. 1200 Ma, interpreted as the age of deformation and metamorphism (Johnson et al., 2011b).

Field evidence for Mutherbukin-age deformation in the sedimentary rocks of the Edmund Group and the underlying Mount Augustus Sandstone is more cryptic, due to its very low metamorphic grade and restriction to narrow shear zones and faults that were reactivated during the 1030–955 Ma Edmundian Orogeny and c. 570 Ma Mulka Tectonic Event. However, Mutherbukin-aged hydrothermal monazite and xenotime within these sedimentary rocks indicates that they were subject to low-grade metamorphism and hydrothermal alteration during this event (Rasmussen et al., 2010; Johnson et al., 2011c). Furthermore, many faults within the Edmund Group rocks have large, sinistral, strike-slip offsets, although only small offsets are seen in rocks of the overlying Collier Group, suggesting that the main faulting event was of Mutherbukin age. This has been confirmed by the dating of authogenic illite from a fault gouge, yielding a $^{40}K/^{40}Ar$ date of 1171 ± 25 Ma (GSWA, unpublished data).

Abra is a major polymetallic lead–silver–copper–gold deposit within the lower part of the Edmund Basin, which has been interpreted as part of a hydrothermal breccia-pipe system (Pirajno et al., 2009a). The geochronology of the deposit and surrounding sedimentary host rocks is complex; however, primary mineralization, or secondary upgrading of the polymetallic ore, appears to have occurred during the Mutherbukin Tectonic Event (Rasmussen et al., 2010; Cutten et al., 2011). Irrespective of these geochronological complexities, the ages obtained from phosphate dating demonstrate that this part of the Edmund Basin underwent a prolonged period of low-grade metamorphism, hydrothermal activity, and faulting at a time when low- to medium-grade metamorphism and deformation was also affecting the underlying Gascoyne Province basement.

The Mutherbukin Tectonic Event may have been a relatively protracted intracontinental oblique strike-slip event, or series of events (1385–1200 Ma), the driver of which is currently unknown. During the event, near-continuous shearing and faulting were accompanied by regional-scale hydrothermal fluid flow. The geological, geochronological, and geophysical data demonstrate that the major Mutherbukin-aged structures in the Gascoyne Province basement extend into the overlying Edmund Basin, albeit at a much lower metamorphic and structural grade (Fig. 4). Regional-scale faulting and the transport of hydrothermal fluids from the mid to upper crust, appear to have played a critical role in the formation or upgrading of the Abra polymetallic deposit.

The 1030–955 Ma Edmundian Orogeny

The latest Mesoproterozoic to earliest Neoproterozoic Edmundian Orogeny is best known for widespread folding and low-grade metamorphism in the Edmund and Collier Basins (Martin and Thorne, 2004), although the orogeny was also responsible for reworking a southeast-striking corridor between the Chalba and Ti Tree Shear Zones in the Gascoyne Province (Frontispiece 1–3; Plate 1). Within this zone, garnet–staurolite or garnet–andalusite porphyroblasts were developed in the pelitic and semipelitic rocks of the Leake Spring Metamorphics, Pooranoo Metamorphics, and Ullawarra Formation of the Edmund Group (Frontispiece 1). In rocks of the Gascoyne Province, three events (D_{1e}, D_{2e}, and D_{3e}) have been attributed to the Edmundian Orogeny, although it is not clear how these relate to the three Edmundian Orogeny events (D_{1e}, D_{2e}, and D_{3e}) identified in the Edmund and Collier Basins (Martin and Thorne, 2004). These events were accompanied and post-dated by leucocratic granite stocks and sheets, and REE-bearing pegmatites, of the 1030–925 Ma Thirty Three Supersuite.

The first of these events in the Gascoyne Province (D_{1e}) is preserved only as inclusion trails within syn-D_{2e} metamorphic porphyroblasts. Kilometre-scale upright folds, and a crenulation schistosity that folds the earlier D_{2e} fabrics, characterize the D_{3e} event. Monazite and xenotime, which grew during amphibolite-facies metamorphism along the northern margin of the Mutherbukin Zone, have been dated at 1030–995 Ma (Sheppard et al., 2007). The older age of c. 1030 Ma is interpreted to date the timing of D_{1e}, whereas the bulk of the phosphate ages, which lie between c. 1005 and c. 995 Ma, are interpreted to date peak amphibolite-facies metamorphism during D_{2e}. Sheppard et al. (2007) estimated pressure–temperature conditions of 3–5 kbar and 500–550°C for the garnet–staurolite-bearing schists. Further south, in the central part of the Mutherbukin Zone, melt-filled pockets that developed within a c. 1665 Ma metamonzogranite cut the main gneissic fabrics associated with the Mutherbukin Tectonic Event. Metamorphic zircons (as rims around older igneous cores) extracted from these melt pockets are contemporaneous with the D_{2e} monazite and xenotime ages of c. 1000 Ma. Upright folding and a schistosity that formed during D_{3e} are only loosely constrained to between 995 and 955 Ma (Sheppard et al., 2007), the younger limit defined by an undeformed REE-bearing pegmatite that cuts the crenulation schistosity.

Porphyritic metamonzogranites, REE-bearing pegmatites, and leucocratic tourmaline-bearing granites of the 1030–925 Ma Thirty Three Supersuite were intruded during and after the Edmundian Orogeny, and are currently only known from the northern part of the Mutherbukin Zone (Frontispiece 1–3; Plate 1). The granites are typically leucocratic and locally tourmaline-rich, ranging in composition from granodiorite to monzogranite. Most of the pegmatites are composed of quartz, feldspar, and tourmaline, although some REE-rich, bismuth-bearing pegmatites are locally common. All phases of the Thirty Three Supersuite are generally zircon poor, but dating of magmatic monazite and xenotime from both the granites and pegmatites provide a wide range of ages between c. 1030 and c. 925 Ma. However, due to limited data, it is not clear whether this age range represents a single period of protracted magmatism or several discrete intrusion pulses.

The interval between 1050 and 1000 Ma is commonly thought to mark the assembly of the Rodinia supercontinent (e.g. Li et al., 2008, and references therein), of which the Australian continent may have been an integral part. Collision between the eastern margin of Australia and a partly assembled Rodinia is estimated at c. 1000 Ma (Li et al., 2008), the timing of which coincides with the growth of peak metamorphic phases during the Edmundian Orogeny. However, in all reconstructions of Rodinia (e.g. Pisarevsky et al., 2003; Li et al., 2008), the western margin of the West Australian Craton is shown to face an open ocean. If so, then the deformation and metamorphism associated with the Edmundian Orogeny may have been a response to plate reorganization and collisions elsewhere in Rodinia, since no other impinging crustal block was present to the west.

The c. 570 Ma Mulka Tectonic Event

The Mulka Tectonic Event is responsible for a series of anastomosing shear zones or faults that cut rocks of the Gascoyne Province and Edmund and Collier Groups across the southwestern part of the Capricorn Orogen (Frontispiece 1; Plate 1). This tectonic event is characterized by fault reactivation, rather than reworking. Mulka-aged faults are generally concentrated within discrete corridors such as the Chalba and Ti Tree Shear Zones (Frontispiece 1–3; Fig. 5a,b), the largest of these being the Chalba Shear Zone – Clere Fault (Frontispiece 1; Plate 1). The shear zones and faults display consistent dextral strike-slip kinematics. Most faults and shear zones range from a few centimetres to several tens of metres wide, and have dextral offsets generally in the order of 10–100 m, commonly displacing c. 755 Ma dykes of the Mundine Well Dolerite Suite (Fig. 5a). An estimate of fault offsets across the region (Fig. 5c) shows both that displacements across individual faults in these zones be as large as 1–4 km, but also that smaller-scale movements, in the order of 100–500 m, across a greater density of faults can lead to significant cumulative regional-scale displacements; e.g. up to 35 km dextral displacement across the 5–10 km wide Chalba Shear Zone (Fig. 5a,c).

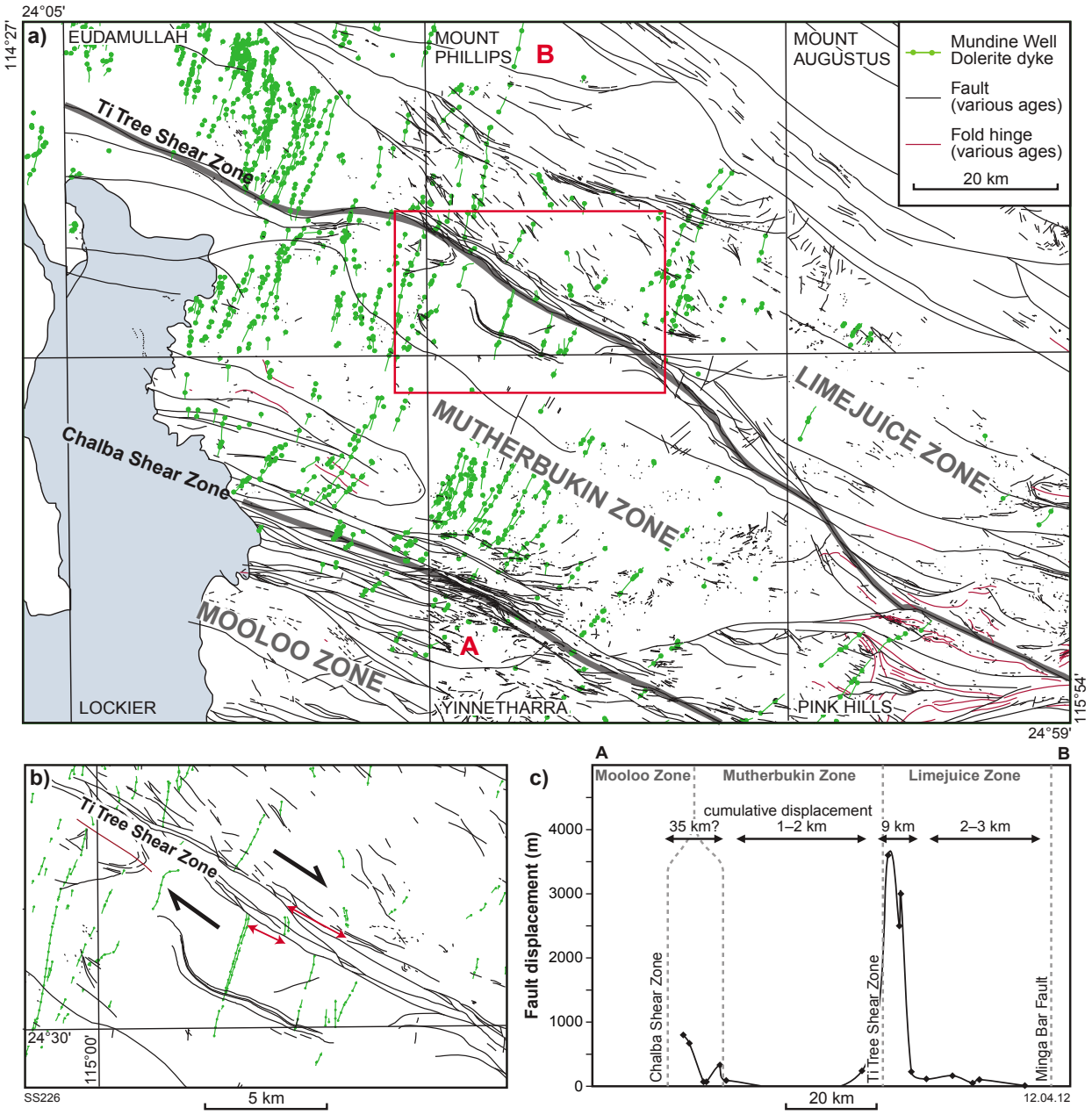

Figure 5. a) Map of the central part of the Gascoyne Province showing Mulka-aged (c. 570 Ma) fault displacements on c. 755 Ma Mundine Well Dolerite Suite dykes. Location of enlarged map (b) is shown by the highlighted box. The location of the calculated fault offsets along A and B, as shown in graph (c), is also marked on the main map.

White mica in the S-planes of an S–C fabric in the Chalba Shear Zone has been dated in situ using the $^{40}Ar/^{39}Ar$ method, yielding a single age of 570 ± 10 Ma (Bodorkos and Wingate, 2007). In the southern part of the province, faults belonging to the Mulka Tectonic Event appear to have been sinistrally offset by 15–20 km across a single discrete fault known as the Deadman Fault (Frontispiece 1–3; Plate 1). The age of this fault is not precisely known, but it may relate either to the late stages of the Mulka Tectonic Event, or to Phanerozoic extensional processes that accommodated the deposition of the Southern Carnarvon Basin to the west. The Mulka Tectonic Event is coeval with the Petermann, Paterson, and King Leopold Orogenies, and reflects an episode of 'pan-Gondwana' intracontinental reactivation.

Crustal architecture and fault reactivation

The different fault and shear zone bounded structural/metamorphic zones of the Gascoyne Province juxtapose rocks from various crustal levels (Fig. 6). An isostatic

analysis of the regional gravity field suggests that the Gascoyne Province topography is significantly overcompensated, presumably due to intense erosion during the Mesozoic and Cenozoic (Hackney, 2004). However, various lines of geological evidence indicates that the current crustal architecture of the province is a much older, Proterozoic feature.

The Errabiddy Shear Zone and Cardilya Fault

The Errabiddy Shear Zone (Frontispiece 1–3; Plate 1) is the suture zone between the Glenburgh Terrane and the Yilgarn Craton, specifically the Narryer Terrane. Rocks in this zone were deformed and metamorphosed in the upper-amphibolite facies during the 2005–1950 Ma Glenburgh Orogeny (Occhipinti et al., 2004; Johnson et al., 2010, 2011a,d), whereas those of the Narryer Terrane were metamorphosed up to the granulite facies during the Archean. However, some of the Archean gneisses show evidence for high-grade metamorphism during the Glenburgh Orogeny (Muhling, 1986, 1988; Muhling et al., 2008). The precise dating of metamorphic monazite from high-grade rocks in the Errabiddy Shear Zone indicate that juxtaposition occurred during the collisional phase (D_{2g} at 1965–1950 Ma) of the Glenburgh Orogeny (Johnson et al., 2010, 2011a). Subsequent reworking and uplift across the Errabiddy Shear Zone is recorded by several $^{40}Ar/^{39}Ar$ mica dates between 960–820 Ma (Occhipinti, 2007).

The Cardilya Fault separates the Paradise and Mooloo Zones. The Paradise Zone contains upper amphibolite to granulite-facies gneisses of the Dalgaringa Supersuite, and the Mooloo Zone contains mid- to upper-amphibolite facies rocks of the Halfway Gneiss and Moogie Metamorphics (Frontispiece 1–3; Fig. 6; Plate 1; Johnson et al., 2010, 2011a). Rocks within the Mooloo Zone were significantly retrogressed in the greenschist facies during the 1820–1770 Ma Capricorn Orogeny, but those within the Paradise Zone were essentially unaffected (Occhipinti et al., 2004; Johnson et al., 2010; Sheppard et al., 2010b; Johnson et al., 2011a). Furthermore, during the Capricorn Orogeny, the Cardilya Fault appears to have been a conduit for the intrusion of voluminous Moorarie Supersuite granitic magmas, essentially sealing any large-scale movements on the fault. Although this fault is a principal crustal structure related to the assembly of the West Australian Craton, reactivation and uplift of upper-mid crustal rocks in the Mooloo Zone must have taken place during the Capricorn Orogeny. The truncation of c. 755 Ma aged dolerite dykes of the Mundine Well Dolerite Suite at the eastern end of the Cardilya Fault, close to where the fault is truncated by the Clere Fault (Frontispiece 1–3; Plate 1), suggests that this fault may have been partly reactivated during the c. 570 Ma Mulka Tectonic Event.

The Limejuice Zone, Ti Tree Shear Zone, and Lyons River Fault

The mapped surface geology of the Minnie Creek batholith in the Limejuice Zone indicates the presence of abundant, lower-greenschist facies grade inclusions of the 1840–1810 Ma Leake Spring Metamorphics (Frontispiece 1; Plate 1). The low to very low metamorphic grade of these inclusions demonstrates not only that the batholith was emplaced at upper crustal levels, but also that it has remained a highstand within the Gascoyne Province basement since its intrusion at c. 1800 Ma. During the 1680–1620 Ma Mangaroon Orogeny, the Lyons River, Minnie Creek, and Minga Bar Faults (Frontispiece 1–3; Plate 1) must have been active, in order to partition sedimentation, deformation, and granite magmatism to the north and into the Mangaroon Zone. Equally, the Lyons River Fault, Godfrey Fault, and Ti Tree Shear Zone must have been active during the 1385–1200 Ma Mutherbukin Tectonic Event in order to partition deformation to the north and south of the Limejuice Zone.

Since both the low-grade upper-crustal rocks of the Limejuice Zone, and the high-grade rocks of the Mangaroon Zone, are unconformably overlain by sediments of the Edmund Basin (Frontispiece 1; Plate 1), juxtaposition and exhumation must have occurred after high-grade D_{1m} metamorphism of the Mangaroon Orogeny (1680–1675 Ma), but before the deposition of the Edmund Basin at ≤1620Ma. This uplift event is recorded by the intense retrograde replacement of high-grade metamorphic minerals in diatexites of the Pooranoo Metamorphics during the 1675–1650 Ma D_{2m} event of the Mangaroon Orogeny (Sheppard et al., 2005).

Both the Minga Bar Fault and Lyons River Fault show evidence of younger reactivation. The southerly extension of the Minga Bar Fault cuts and offsets mafic dykes of the c. 755 Ma Mundine Well Dolerite Suite (Frontispiece 1–3; Plate 1), indicating that that this fault was reactivated during the c. 570 Ma Mulka Tectonic Event. The truncation of folded Edmund Group rocks by the Lyons River Fault demonstrates that this fault was reactivated during the 1385–1280 Ma Mutherbukin Tectonic Event and/or the 1030–955 Ma Edmundian Orogeny.

The Mutherbukin Zone and the Chalba Shear Zone

The Mutherbukin Zone exposes rocks of various crustal levels. Semipelitic schists of the 1840–1810 Ma Leake Spring Metamorphics and the 1760–1680 Ma Pooranoo Metamorphics (specifically the Mount James Subgroup) show a gradual increase in metamorphic grade southward, away from the Ti Tree Shear Zone (Fig. 6). These pass exclusively into the very strongly deformed plutonic rocks of the 1680–1620 Ma Durlacher Supersuite, which in the central part of the zone show evidence for in situ melting (Johnson et al., 2011b). The highest metamorphic grades attained are in the central part of the zone, which forms the core of a kilometre-scale mid-crustal extensional sheath fold (Fig. 6). Tectonometamorphism is related to the 1385–1200 Ma Mutherbukin Tectonic Event (Johnson et al., 2011b), although a narrow strip of staurolite-grade schists along the southern margin of the Ti Tree Shear Zone in the Nardoo Hills region also indicate metamorphism during the 1030–955 Ma Edmundian Orogeny (Sheppard et al., 2007).

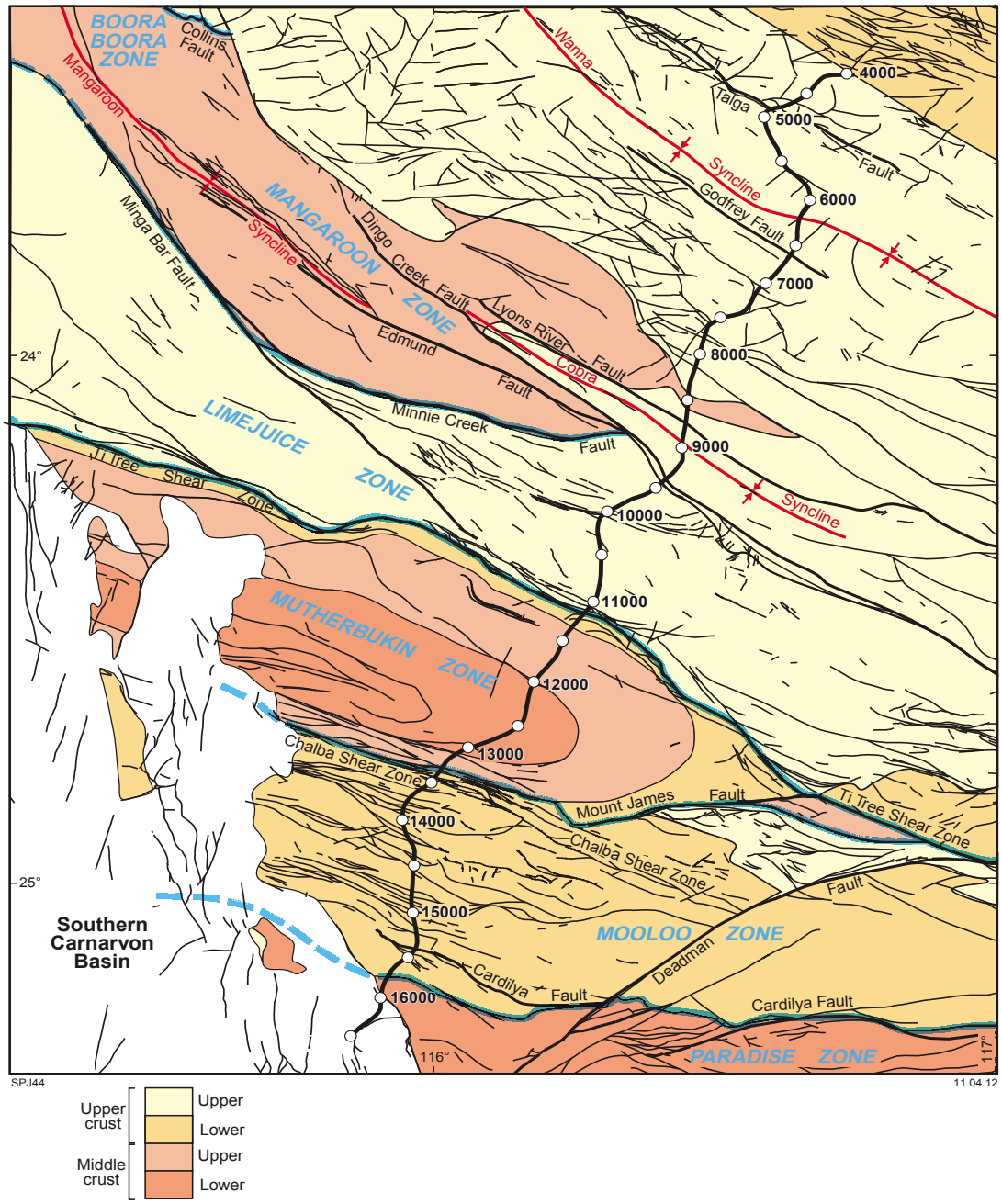

Figure 6. Schematic map of relative crustal levels across the Gascoyne Province

At depth, the Ti Tree Shear Zone has been shown to merge with the Lyons River Fault, and is interpreted to be the suture zone between the Glenburgh Terrane and Pilbara Craton (Bandee Seismic Province; Johnson et al., 2011d). This structure shows a long and punctuated history of reactivation, as shown by the tectonometamorphic history of the rocks within the Mutherbukin Zone and adjoining Limejuice Zone. The differential exhumation of these rocks presumably took place during the Mutherbukin Tectonic Event, as the structural fabrics that define the regional-scale southeast-plunging sheath fold (Fig. 6) are of this age.

The dextral offset, across the Chalba Shear Zone, of mafic dykes belonging to the c. 755 Ma Mundine Well Dolerite Suite indicates that this fault was active during the c. 570 Ma Mulka Tectonic Event. The total cumulative dextral offset across this 5–10 km wide zone is in excess of 35 km (Sheppard et al., 2010b). However, since Mutherbukin-aged tectonometamorphism has yet to be identified south of the Chalba Shear Zone, it is possible that this structure is a much older feature, reactivated during the Mulka Tectonic Event.

The Talga and Godfrey Faults

As shown by the seismic reflection data (Johnson et al., 2011d), the Talga Fault is a south-dipping structure. Its dominant listric normal character was obtained during extensional reactivation, when it formed part of a major system of half grabens facilitating the deposition of sediments into the Edmund Basin (Martin and Thorne, 2004; Martin, 2006; Cutten et al., 2011). Thus, extensional reactivation on this and other half graben-bounding faults, such as the Godfrey Fault, must have occurred shortly after uplift and juxtaposition of the rocks within the Mangaroon and Limejuice Zones; i.e. at c. 1620 Ma. Extension on these faults continued until the cessation of Edmund Basin deposition at c. 1465 Ma, implying an almost continuous period of fault activation and reactivation from the beginning of the Mangaroon Orogeny at c. 1680 Ma, through to the culmination of basin deposition at c. 1465 Ma.

Summary

The subparallel orientation, seismic character, and tectonic history of these major zone-bounding faults indicate that they are principal crustal features, such as suture zones and crustal-scale shear zones, originally related to the assembly of the West Australian Craton during the 2215–2145 Ma Ophthalmian and 2005–1950 Ma Glenburgh Orogenies. Their subsequent tectonic history is one of constant reactivation during greater than one billion years of episodic crustal reworking. These inherent crustal-scale features have facilitated the partitioning of deformation, metamorphism, magmatism, and possibly mineralization, to the point where the present-day architecture of the Gascoyne Province has ultimately been influenced by events that took place some 2200 to 1950 million years ago.

References

Bodorkos, S and Wingate, MTD 2007, The contribution of geochronology to GSWA's mapping programs: current perspectives and future directions, *in* GSWA 2007 extended abstracts: promoting the prospectivity of Western Australia: Geological Survey of Western Australia, Record 2007/2, p. 10–11.

Cawood, PA and Tyler, IM 2004, Assembling and reactivating the Proterozoic Capricorn Orogen: lithotectonic elements, orogenies, and significance: Precambrian Research, v. 128, p. 201–218.

Cutten, HN, Thorne, AM and Johnson, SP 2011, Geology of the Edmund and Collier Groups, *in* Capricorn Orogen seismic and magnetotelluric (MT) workshop 2011: extended abstracts *edited by* SP Johnson, AM Thorne and IM Tyler: Geological Survey of Western Australia, Record 2011/25, p. 41–48.

Evans, DAD, Sircombe, KN, Wingate, MTD, Doyle, M, McCarthy, M, Pidgeon, RT and Van Niekerk, HS 2003, Revised geochronology of magmatism in the western Capricorn Orogen at 1805–1785 Ma: diachroneity of the Pilbara–Yilgarn collision: Australian Journal of Earth Sciences, v. 50, no. 6, p. 853–864.

Geological Survey of Western Australia 2011, Compilation of geochronology information, 2011 update: Geological Survey of Western Australia, digital data product.

Goldstein, SL, O'Nions, RK and Hamilton, PJ 1984, A Sm–Nd study of atmospheric dusts and particulates from major river systems: Earth and Planetary Science Letters, v. 70, p. 221–236.

Hackney, R 2004, Gravity anomalies, crustal structure and isostasy associated with the Proterozoic Capricorn Orogen, Western Australia: Precambrian Research, v. 128, no. 3–4, p. 219–236, doi: 10.1016/j.precamres.2003.09.012.

Johnson, SP, Sheppard, S, Rasmussen, B, Wingate, MTD, Kirkland, CL, Muhling, JR, Fletcher, IR and Belousova, E 2010, The Glenburgh Orogeny as a record of Paleoproterozoic continent–continent collision: Geological Survey of Western Australia, Record 2010/5, 54p.

Johnson, SP, Sheppard, S, Rasmussen, B, Wingate, MTD, Kirkland, CL, Muhling, JR, Fletcher, IR and Belousova, EA 2011a, Two collisions, two sutures: punctuated pre-1950 Ma assembly of the West Australian Craton during the Ophthalmian and Glenburgh Orogenies: Precambrian Research, v. 189, no. 3–4, p. 239–262, doi: 10.1016/j.precamres.2011.07.011.

Johnson, SP, Sheppard, S, Thorne, AM, Rasmussen, B, Fletcher, IR, Wingate, MTD and Cutten, HN 2011b, The role of the 1280–1250 Ma Mutherbukin Tectonic Event in shaping the crustal architecture and mineralization history of the Capricorn Orogen, *in* GSWA 2011 extended abstracts: promoting the prospectivity of Western Australia: Geological Survey of Western Australia, Record 2011/2, p. 1–3.

Johnson, SP, Sheppard, S, Wingate, MTD, Kirkland, CL and Belousova, EA 2011c, Temporal and hafnium isotopic evolution of the Glenburgh Terrane basement: an exotic crustal fragment in the Capricorn Orogen: Geological Survey of Western Australia, Report 110, 27p.

Johnson, SP, Cutten, HN, Tyler, IM, Korsch, RJ, Thorne, AM, Blay, O, Kennett, BLN, Blewitt, RS, Joly, A, Dentith, MC, Aitkin, ARA, Goodwin, JA, Salmon, M, Reading, A, Boren, G, Ross, J, Costello, RD and Fomin, T 2011d, Preliminary interpretation of deep seismic reflection lines 10GA–CP2 and 10GA–CP3: crustal architecture of the Gascoyne Province and Edmund and Collier Basins, *in* Capricorn Orogen seismic and magnetotelluric (MT) workshop 2011: extended abstracts *edited by* SP Johnson, AM Thorne and IM Tyler: Geological Survey of Western Australia, Record 2011/25, p. 49–60.

Krapež, B 1999, Stratigraphic record of an Atlantic-type global tectonic cycle in the Palaeoproterozoic Ashburton Province of Western Australia: Australian Journal of Earth Sciences, v. 46, p. 71–87.

Krapež, B and McNaughton, NJ 1999, SHRIMP zircon U–Pb age and tectonic significance of the Palaeoproterozoic Boolaloo Granodiorite in the Ashburton Province, Western Australia: Australian Journal of Earth Sciences, v. 46, p. 283–287.

Li, ZX, Bogdanova, SV, Collins, AS, Davidson, A, De Waele, B, Ernst, RE, Fitzsimons, ICW, Fuck, RA, Gladkochub, DP, Jacobs, J, Karlstrom, KE, Lu, S, Natapov, LM, Pease, V, Pisarevsky, SA, Thrane, K and Vernikovsky, V 2008, Assembly, configuration, and break-up history of Rodinia: a synthesis: Precambrian Research, v. 160, no. 1–2, p. 179–210, DOI: 10.1016/j.precamres.2007.04.021.

Martin, DM 2006, The provenance record of the Bangemall Supergroup and implications for the Mesoproterozoic tectonic history of Western Australia, *in* GSWA 2006 extended abstracts: promoting the prospectivity of Western Australia: Geological Survey of Western Australia, Record 2006/3, p. 15–16.

Martin, DM and Morris, PA 2010, Tectonic setting and regional implications of ca 2.2 Ga mafic magmatism in the southern Hamersley Province, Western Australia: Australian Journal of Earth Sciences, v. 57, no. 7, p. 911–931.

Martin, DM, Sheppard, S and Thorne, AM 2005, Geology of the Maroonah, Ullawarra, Capricorn, Mangaroon, Edmund, and Elliott Creek 1:100 000 sheets: Geological Survey of Western Australia, 1:100 000 Geological Series Explanatory Notes, 65p.

Martin, DM, Sircombe, KN, Thorne, AM, Cawood, PA and Nemchin, AA 2008, Provenance history of the Bangemall Supergroup and implications for the Mesoproterozoic paleogeography of the West Australian Craton: Precambrian Research, v. 166, no. 1–4 (Assembling Australia: Proterozoic building of a continent), p. 93–110.

Martin, DM and Thorne, AM 2004, Tectonic setting and basin evolution of the Bangemall Supergroup in the northwestern Capricorn Orogen: Precambrian Research, v. 128, p. 385–409.

Morris, PA and Pirajno, F 2002, A Mesoproterozoic large igneous province in central Western Australia, *in* GSWA 2002 extended abstracts: GSWA online: Geological Survey of Western Australia, Report 2002/5, p. 23–25.

Muhling, JR 1986, Tectonothermal history of the Mukalo Creek Area, Southern Gascoyne Province, Western Australia: crustal evolution of Archaean gneisses reworked during Proterozoic orogenesis: University of Western Australia, Perth, Western Australia, PhD thesis (unpublished), 320p.

Muhling, JR 1988, The nature of Proterozoic reworking of early Archaean gneisses, Mukalo Creek area, southern Gascoyne Province, Western Australia: Precambrian Research, v. 40–41 (The Early to Middle Proterozoic of Australia), p. 341–362.

Muhling, JR, Fletcher, IR and Rasmussen, B 2008, Dating high-grade metamorphic events in the Narryer Terrane by U–Pb SHRIMP analysis of monazite and zircon: Geological Society of Australia; Australian Earth Sciences Convention (AESC) 2008: New Generation Advances in Geoscience, Perth, Western Australia, 20 July 2008; Abstracts v. 89, p. 180.

Myers, JS 1990, Precambrian tectonic evolution of part of Gondwana, southwestern Australia: Geology, v. 18, p. 537–540.

Occhipinti, SA 2007, Neoproterozoic reworking in the Paleoproterozoic Capricorn Orogen: evidence from $^{40}Ar/^{39}Ar$ ages: Geological Survey of Western Australia, Record 2007/10, 41p.

Occhipinti, SA and Myers, JS 1999, Geology of the Moorarie 1:100 000 sheet: Geological Survey of Western Australia, 1:100 000 Geological Series Explanatory Notes, 20p.

Occhipinti, SA, Myers, JS and Swager, CP 1998, Geology of the Padbury 1:100 000 sheet: Geological Survey of Western Australia, 1:100 000 Geological Series Explanatory Notes, 29p.

Occhipinti, SA, Sheppard, S, Passchier, C, Tyler, IM and Nelson, DR 2004, Palaeoproterozoic crustal accretion and collision in the southern Capricorn Orogen: the Glenburgh Orogeny: Precambrian Research, v. 128, p. 237–255.

Perring, CS, Barnes, SJ and Hill, RET 1996, Geochemistry of komatiites from Forrestania, Southern Cross Province, Western Australia: evidence for crustal contamination: Lithos, v. 37, p. 181–197.

Pirajno, F, Hell, A, Thorne, AM and Cutten, HN 2009a, The Abra deposit: a breccia-pipe polymetallic mineral system in the Edmund Basin, Capricorn Orogen: implications for mineral exploration, *in* GSWA 2009 extended abstracts: promoting the prospectivity of Western Australia: Geological Survey of Western Australia, Record 2009/2, p. 31–33.

Pirajno, F, Hocking, RM, Reddy, SM and Jones, JA 2009b, A review of the geology and geodynamic evolution of the Palaeoproterozoic Earaheedy Basin, Western Australia: Earth-Science Reviews, v. 94, p. 39–77.

Pirajno, F, Occhipinti, SA and Swager, CP 2000, Geology and mineralization of the Palaeoproterozoic Bryah and Padbury Basins, Western Australia: Geological Survey of Western Australia, Report 59, 52p.

Pisarevsky, SA, Wingate, MTD, Powell, CM, Johnson, SP and Evans, DAD 2003, Models of Rodinia assembly and fragmentation: Geological Society, London, Special Publications, v. 206, no. 1, p. 35–55.

Rasmussen, B, Fletcher, IR, Muhling, JR, Thorne, AM, Cutten, HN, Pirajno, F and Hell, A 2010, In situ U–Pb monazite and xenotime geochronology of the Abra polymetallic deposit and associated sedimentary and volcanic rocks, Bangemall Supergroup, Western Australia: Geological Survey of Western Australia, Record 2010/12, 31p.

Selway, K 2008, Magnetotelluric investigation into the electrical structure of the Capricorn Orogen, Western Australia: Geological Survey of Western Australia, Record 2007/16, 39p.

Selway, K, Sheppard, S, Thorne, AM, Johnson, SP and Groenewald, PB 2009, Identifying the lithospheric structure of a Precambrian orogen using magnetotellurics: the Capricorn Orogen, Western Australia: Precambrian Research, v. 168, p. 185–196.

Sheppard, S, Bodorkos, S, Johnson, SP, Wingate, MTD and Kirkland, CL 2010a, The Paleoproterozoic Capricorn Orogeny: intracontinental reworking not continent–continent collision: Geological Survey of Western Australia, Report 108, 33p.

Sheppard, S, Farrell, TR, Bodorkos, S, Hollingsworth, D, Tyler, IM and Pirajno, F 2006, Late Paleoproterozoic (1680–1620 Ma) sedimentation, magmatism, and tectonism in the Capricorn Orogen, *in* GSWA 2006 extended abstracts: promoting the prospectivity of Western Australia: Geological Survey of Western Australia, Record 2006/3, p. 11–12.

Sheppard, S, Johnson, SP, Wingate, MTD, Kirkland, CL and Pirajno, F 2010b, Explanatory Notes for the Gascoyne Province: Geological Survey of Western Australia, Perth, Western Australia, 336p.

Sheppard, S, Occhipinti, SA and Johnson, SP 2011, Landor, WA Sheet 2247 (2nd edition): Geological Survey of Western Australia, 1:100 000 Geological Series.

Sheppard, S, Occhipinti, SA and Nelson, DR 2005, Intracontinental reworking in the Capricorn Orogen, Western Australia: the 1680–1620 Ma Mangaroon Orogeny: Australian Journal of Earth Sciences, v. 52, p. 443–460.

Sheppard, S, Occhipinti, SA and Tyler, IM 2003, The relationship between tectonism and composition of granitoid magmas, Yarlarweelor Gneiss Complex, Western Australia: Lithos, v. 66, p. 133–154.

Sheppard, S, Occhipinti, SA and Tyler, IM 2004, A 2005–1970 Ma Andean-type batholith in the southern Gascoyne Complex, Western Australia: Precambrian Research, v. 128 (Assembling the Palaeoproterozoic Capricorn Orogen), p. 257–277.

Sheppard, S, Rasmussen, B, Muhling, JR, Farrell, TR and Fletcher, IR 2007, Grenvillian-aged orogenesis in the Palaeoproterozoic Gascoyne Complex, Western Australia: 1030–950 Ma reworking of the Proterozoic Capricorn Orogen: Journal of Metamorphic Geology, v. 25, p. 477–494.

Sheppard, S and Swager, CP 1999, Geology of the Marquis 1:100 000 sheet: Geological Survey of Western Australia, 1:100 000 Geological Series Explanatory Notes, 21p.

Thorne, AM and Seymour, DB 1991, Geology of the Ashburton Basin, Western Australia: Geological Survey of Western Australia, Bulletin 139, 141p.

Tyler, IM and Thorne, AM 1990, Capricorn Orogen — structural evolution of the northern margin, *in* Geology and mineral resources of Western Australia: Geological Survey of Western Australia, Memoir 3, p. 223–232.

Williams, SJ 1986, Geology of the Gascoyne Province, Western Australia: Geological Survey of Western Australia, Report 15, 85p.

Wingate, MTD 2002, Age and palaeomagnetism of dolerite sills of the Bangemall Supergroup on the Edmund 1:250 000 sheet, Western Australia: Geological Survey of Western Australia, Record 2002/4, 48p.

Wingate, MTD, Pirajno, F and Morris, PA 2004, Warakurna large igneous province: a new Mesoproterozoic large igneous province in west-central Australia: Geology, v. 32, no. 2, p. 105–108.

Geology of the Edmund and Collier Groups

by

HN Cutten, AM Thorne, and SP Johnson

Introduction

Low-grade metasedimentary rocks of the Paleoproterozoic to Mesoproterozoic Edmund and Collier Groups represent the youngest depositional element within the Capricorn Orogen (Fig. 1). The succession comprises 4–10 km of mainly fine-grained siliciclastic and carbonate sedimentary rocks that were deposited in a variety of shelf to basinal environments (Martin and Thorne, 2004). Sediments in the Edmund Basin were deposited unconformably on granitic rocks of the Gascoyne Province sometime between c. 1620 and c. 1465 Ma. Sediments in the unconformably overlying Collier Basin were deposited across both the Gascoyne Province basement and locally deformed sedimentary rocks of the Edmund Basin sometime between c. 1200 and c. 1070 Ma. The Edmund Basin (Fig. 1) extends from the Pingandy Shelf in the north, and continues south across the Talga Fault as a rift-graben structure over 180 km in width (northeast–southwest) and 400 km in length (northwest–southeast). The Collier Basin is relatively restricted in the west, where it is only 30 km wide (Fig. 1); however, the basin widens significantly to the east to a maximum of ~200 km.

The main depositional and structural elements of the basins were controlled principally by movements on the Talga, Godfrey, Lyons River, Edmund, and Minga Bar Faults, and the Ti Tree Shear Zone (Frontispiece 1–3; Plate 1). Deposition within the Edmund Basin was controlled mainly by normal movements on the Talga Fault (Martin and Thorne, 2004), with the basin fill dramatically thickening to the southwest from the Pingandy Shelf. Deposition in the Collier Basin appears to have been less influenced by significant fault movements (Martin and Thorne, 2004). Subsequent basin inversion took place during the 1385–1200 Ma Mutherbukin Tectonic Event and the 1030–955 Ma Edmundian Orogeny (Frontispiece 1; Plate 1). Minor fault reactivation took place during the c. 570 Ma Mulka Tectonic Event. The structural architecture of the basins, including the Wanna, Cobra, and Ti Tree Synclines, and associated faults (Frontispiece 1–3; Plate 1), parallel the main northwest–southeast to east–west structural trends within the underlying Gascoyne Province basement (Johnson et al., 2011a), and indicate a regional-scale control on deformation and basin inversion.

Edmund and Collier Basins: stratigraphy and age constraints

The Edmund and Collier Groups comprise 4–10 km of siliciclastic and carbonate metasedimentary rocks that have been subdivided into 14 formations, grouped into six depositional packages (Figure 2 of this report, based on Martin and Thorne, 2004). Each package is separated by an unconformity or basal marine-flooding surface (Martin and Thorne, 2004).

The Edmund Group unconformably overlies granites of the 1680–1620 Ma Durlacher Supersuite of the Gascoyne Province (Sheppard et al., 2010), providing a maximum age of c. 1620 Ma for deposition. However, in the eastern part of the basin, the sediments are largely deposited on weathered granitic rocks of the 1820–1775 Ma Moorarie Supersuite (Occhipinti and Myers, 1999; Martin et al., 2005).

The Ullawarra Formation, within the uppermost package (Package 4) of the Edmund Group, locally contains volcaniclastic rocks, magmatic zircons from which have been dated, using the U–Pb SHRIMP technique, at 1463 ± 8 Ma (Wingate et al., 2010), and which provides a youngest age limit for deposition. The age of these volcaniclastic rocks are within uncertainty of those for voluminous dolerite sills of the Narimbunna Dolerite, dated between c. 1500 and c. 1465 Ma (Wingate et al., 2002, in prep.), which intrude the upper packages of the Edmund Group.

The depositional age of the overlying Collier Group is poorly constrained. Both the Edmund and Collier Basins are intruded by voluminous dolerite sills of the Kulkatharra Dolerite, which are related to the c. 1070 Ma Warakurna Large Igneous Province (Wingate et al., 2002). These sills therefore provide an upper age constraint for Collier Group deposition. The lower age constraint is provided by structural relationships that suggest that the sediments of the Collier Group were not affected by the 1385–1200 Ma Mutherbukin Tectonic Event (Johnson et al., 2011a); thus, deposition occurred between c. 1200 and c. 1070 Ma.

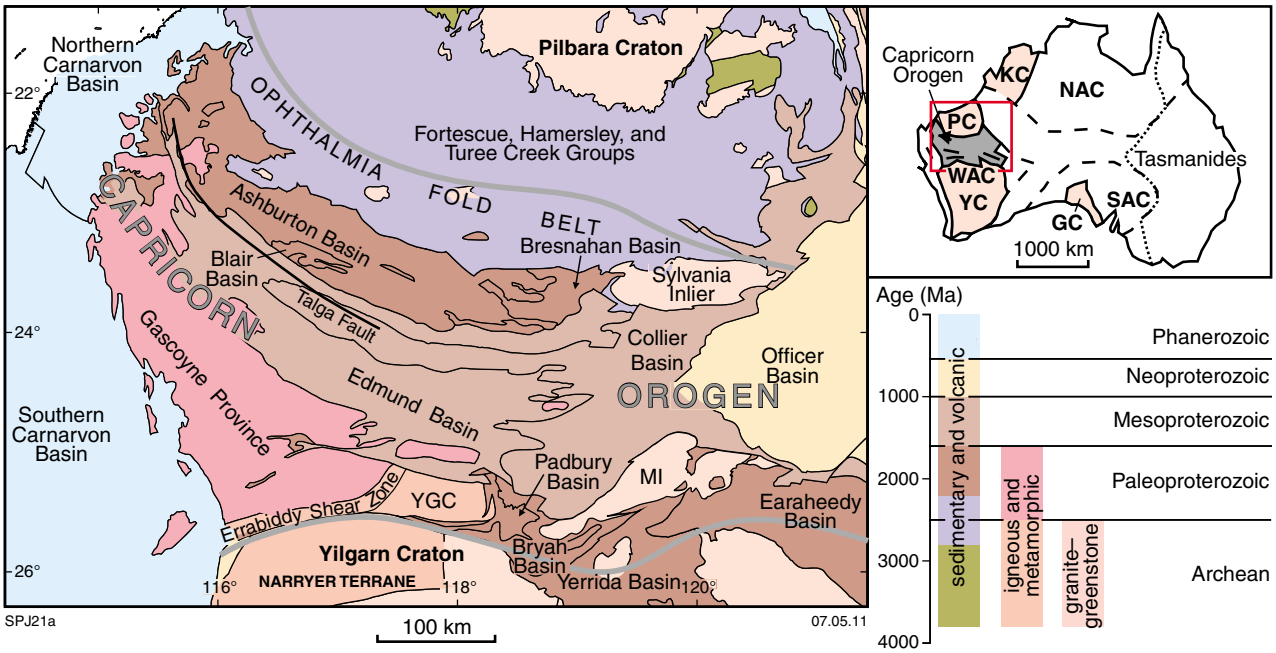

Figure 1. Location of seismic line 10GA–CP2 and the Edmund and Collier Basins in the Capricorn Orogen

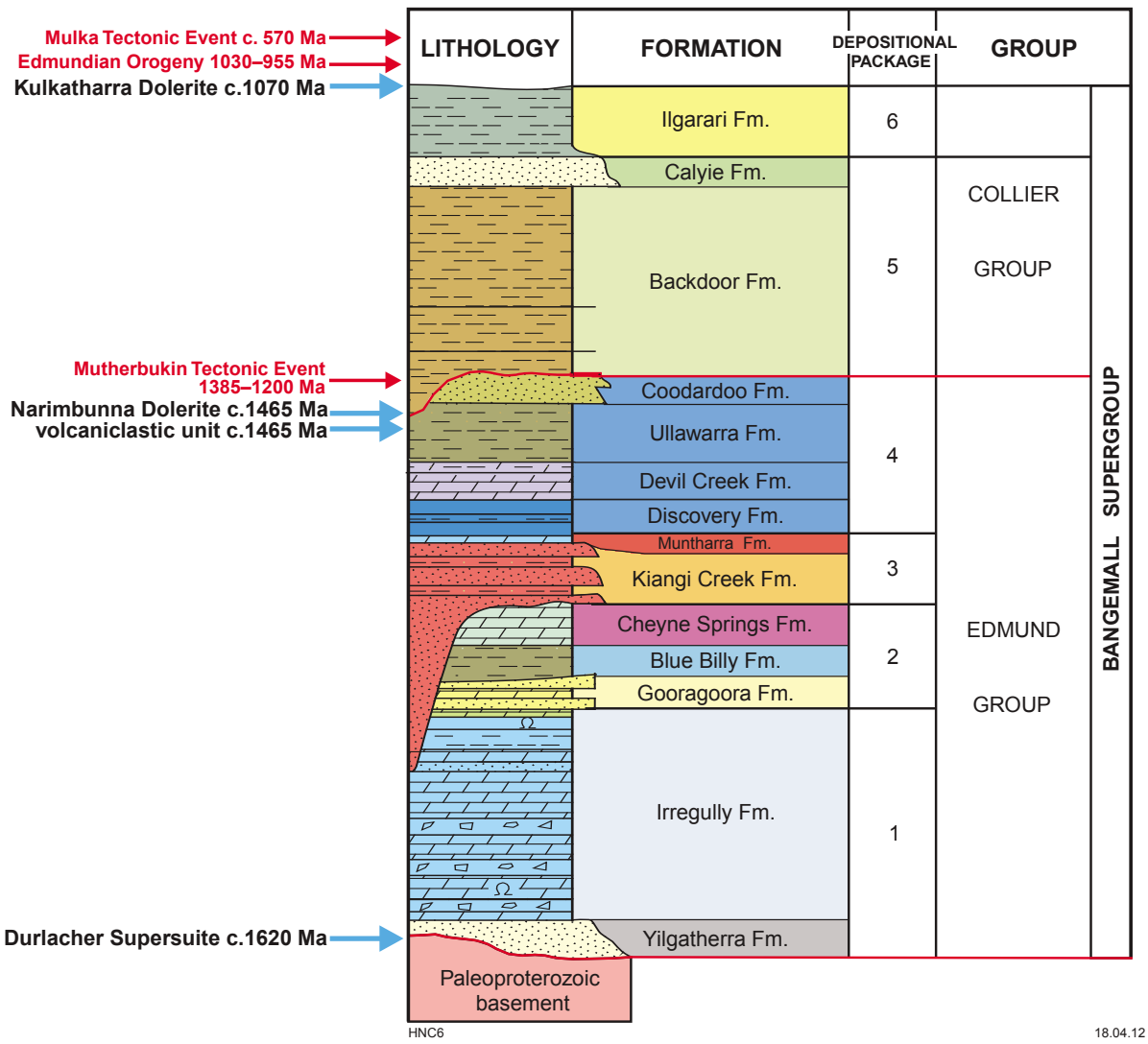

Figure 2. Stratigraphy of the Edmund and Collier Groups

U–Pb SHRIMP dating of detrital zircons from the Edmund Group reveal prominent age modes in the 1850–1600 Ma range, consistent with detritus from the northern Gascoyne Province and coeval sedimentary basins (Martin et al., 2008). Some samples also have prominent age modes in the 2780–2450 Ma range, consistent with detritus from the Fortescue and Hamersley Groups of southern Pilbara (Martin et al., 2008). In the Edmund Group, the dominant age modes become progressively older higher up in the succession, suggesting unroofing of the underlying basement rocks. In contrast, the dominant modes of the Collier Group become younger higher in the succession, recording progressive unroofing of the underlying Edmund Group. Ongoing Lu–Hf isotope studies of the same detrital zircon suite identified first-cycle transportation from the Gascoyne Province to the Wyloo and Capricorn Groups (2200–1800 Ma), and possibly on to the Besnahan Group (?1680 Ma), with second-cycle transportation from these older sedimentary basins into the Edmund Group (GSWA, unpublished results).

Edmund Basin

Package 1

Package 1 of the Edmund Group comprises mainly fluvial to shallow-marine sandstones and siltstones (Yilgatherra Formation), conformably overlain by siliciclastic and carbonate rocks (Irregully Formation). These were deposited in a half-graben formed by normal movements largely on the Talga, Lyons River, and Minga Bar Faults. On the Pingandy Shelf, these deposits are up to 400 m thick, and were deposited in fluvial to peritidal environments. Paleocurrent directions indicate that the sediments were sourced predominantly from the northeast (Martin et al., 2008). South of the Talga Fault, up to 3 km of sediments were deposited in fluvial, marine shelf, and marine-slope environments. Paleocurrent directions suggest that the sediments were sourced from local basement highs, with the predominant source to the southwest (Martin et al., 2008).

Package 2

Package 2 has an apparent conformable contact with the underlying Irregully Formation, and initially represents a prograding deltaic environment propagating from the northwestern part of the Edmund Basin. Planar-laminated siltstones grade upwards into fine- to coarse-grained, massive to trough cross-stratified sandstones (Gooragoora Formation) that range in thickness from 10–150 m. Deposition was controlled by continued normal movements, initially on the Talga Fault and later on the Lyons River Fault, and was accompanied by a rise in sea level. The basin then expanded to the southeast with the deposition of between 30–500 m of pyritic carbonaceous siltstones and turbidite sandstones (Blue Billy Formation) in a deep-water anoxic shelf environment. Infill of the basin led to the deposition of 50–300 m of siliciclastic and calcareous sediments (Cheyne Springs Formation) in a distal subtidal environment.

Paleocurrent directions in the prograding delta indicate that sediment was sourced from the northwest, although higher in the succession sediment supply was from the northeast and normal to the basin margin (Martin et al., 2008).

Package 3

The deposition of Package 3 followed an extended hiatus and considerable erosional thinning of the underlying sediments (Packages 1 and 2). In the eastern part of the Edmund Basin, conglomerates and coarse-grained sandstones of the basal Kiangi Creek Formation were deposited in an alluvial-fan environment. These deposits are truncated by an erosional marine-flooding surface, and overlain by pebbly sandstones and interbedded siltstones and sandstones deposited in a fan-delta environment. In the western part of the basin, these units pass into 50–2600 m of deep-shelf siltstones, and interbedded turbiditic sandstones with local amalgamated turbidites, mass-flow quartz sandstones, and planar-laminated carbonaceous siltstones. Here, deposition was controlled by progressive normal movements on the Talga, Lyons River, Edmund, and Minga Bar Faults. In the eastern part of the basin, sediment deposition was accommodated by normal movements on the Quartzite Well and Mount Clere Faults. On the Pingandy Shelf, a locally developed, 30–50 m thick, dolostone (Muntharra Formation) represents the shelf-edge to basinal carbonate deposition during the waning of coarse-grained sediment supply. Paleocurrent directions in all parts of the basin indicate that the sediments were sourced from the northeast.

Package 4

The basal sediments of Package 4 were deposited following a major transgressive event. Although these sediments have a sharp contact with the upper units of Package 3, they truncate the underlying units at a very low angle. The basal deposits comprise 50–365 m of silicified, pyritic carbonaceous siltstones and black cherts (Discovery Formation). They are interpreted as an anoxic deposit that accumulated below storm wave base. These sediments are overlain by locally stromatolitic, dolograinstones and dolomudstones of the Devil Creek Formation. Deposition appears to have been controlled by reactivation of the Talga Fault, as the units thicken southward from 80–450 m, and record a change from subtidal to slope and basinal facies. The Devil Creek Formation is transitional upwards into the planar- and ripple-laminated siltstones and mudstones, with minor dolostones and fine- to medium-grained sandstones, of the Ullawarra Formation. This unit grades into turbiditic sandstones and parallel-planar siltstones (Curran Member). A similar southward thickening of units, from 100 m on the Pingandy Shelf to ~600 m south of the Talga Fault, is also observed. In the eastern part of the basin, volcaniclastic sediments dated at 1463 ± 8 Ma (Wingate et al., 2010) occur within the Ullawarra Formation. The uppermost unit of Package 4 comprises up to 200 m of medium to very thick bedded turbidite sandstones and minor siltstones (Coodardoo Formation).

The deposition of Package 4 appears to have been controlled by the reactivation of the Edmund Fault and

Mount Clere Fault in the south, and the Talga Fault in the north. Late-stage reactivation along the Lyons River and Quartzite Well Faults accommodated deposition of the Coodardoo Formation in a northwest–southeast oriented basin. Paleocurrent directions indicate that sediments in the Ullawarra Formation were sourced from the southeast along the axis of an earlier larger basin, but were sourced from the northwest for the deposition of the Coodardoo Formation, indicating a smaller, narrower basin in the area of the Wanna Syncline at this time.

In the latest depositional phase of Package 4, the Edmund Basin south of the Pingandy Shelf was intruded by voluminous dolerite sills of the c. 1465 Ma Narimbunna Dolerite. These sills have inflated the thickness of the basin by up to 2 km.

Collier Basin

Package 5

Deposition of Package 5, within the Collier Group, followed a drop in sea level and a erosional period of at least 85 million years, based on the older age limit of c. 1380 Ma for the Mutherbukin Event (Rasmussen et al., 2010). The lowermost unit comprises ~1500 m of laminated siltstones, with minor thin beds of fine-grained sandstone and thin-bedded dolomudstones (Backdoor Formation). These units were deposited in a progradational shallow-shelf and marginal delta-front, and were in turn overlain by ~200 m of interbedded medium- to coarse-grained sandstones and siltstones (Calyie Formation) deposited in a delta-top to delta-front environment. Paleocurrent directions suggest that the sediment supply was from the northeast for the Backdoor Formation, but from the southeast for the Calyie Formation.

Package 6

Package 6 comprises up to 700 m of parallel planar-laminated pyritic and carbonaceous siltstones and fine-grained sandstones, with minor limestones, and calcareous siltstones and cherts (Ilgarari Formation). These rocks represent marine-shelf facies deposits, and were laid down following a basin-wide marine transgression.

Following the deposition of the Collier Basin, rocks of both the Edmund and Collier Groups were intruded by voluminous dolerite sills of the c. 1070 Ma Kulkatharra Dolerite, which form part of the Warakurna Large Igneous Province. The local presence of pepperites within the Backdoor Formation indicates that some of the dolerites were intruded into wet sediments, suggesting that deposition of the Collier Group was closer to c. 1070 Ma than to c. 1200 Ma (Martin, 2003).

Deformation history

Deposition of the Edmund Basin appears to have been ultimately controlled by the primary orientation and repeated reactivation of major crustal structures in the underlying Gascoyne Province basement (Sheppard et al., 2010; Johnson et al., 2011a–c). Following the termination of the Mangaroon Orogeny at c. 1620 Ma, extensional reactivation, principally on the Talga and Godfrey Faults, formed half grabens into which the sediments were deposited. Basin inversion took place during the 1385–1200 Ma Mutherbukin Tectonic Event, before the deposition of the Collier Group. Folding and faulting of both the Edmund and Collier Basins took place during the 1030–955 Ma Edmundian Orogeny and the c. 570 Ma Mulka Tectonic Event.

Mutherbukin Tectonic Event

Medium-grade metamorphism and deformation associated with the 1385–1200 Ma Mutherbukin Tectonic Event has been recognized in the basement rocks of the Gascoyne Province (Johnson et al., 2011a,c). Evidence in the Edmund Basin is more limited due to the low to very low grade nature of metamorphism; however, rocks of both the Edmund and Mount Augustus Basins contain abundant 1385–1300 Ma aged hydrothermal monazite and xenotime (Rasmussen et al., 2010; Tyler et al., 2011). In addition, magmatic xenotime from the Tangadee Rhyolite has been dated at c. 1235 Ma (Rasmussen et al., 2010), and pyrite from the mineralized zone of the Abra deposit has been dated using the Re–Os system at c. 1280 Ma (GSWA, unpublished data).

Surface geological mapping in the eastern part of the basin (Cutten et al., 2010; Thorne and Cutten, 2011) demonstrates that many faults within the Edmund Group have large, sinistral, strike-slip offsets, but only small offsets in the overlying Collier Group, suggesting pre-Edmundian Orogeny (1030–955 Ma) movements. These features are replicated in the Wanna Syncline, where the intensity of faults is significantly greater in the Edmund Group (Fig. 3) than in the Collier Group, suggesting that the Collier Group was deposited at <1200 Ma, following the 1385–1200 Ma Mutherbukin Tectonic Event.

Due to the brittle nature of faulting in the Edmund Group, direct age constraints on the fault movements themselves are rare. However, authigenic illite from a fault gouge that displaces sandstone and siltstone beds of the Kiangi Creek Formation (Fig. 4) has been dated at 1171 ± 25 Ma using the $^{40}K/^{40}Ar$ method (GSWA, unpublished data). These results demonstrate that faulting and hydrothermal fluid flow during the Mutherbukin Tectonic Event affected rocks of the Edmund Basin.

Edmundian Orogeny

In the Edmund and Collier Basins, the 1030–955 Ma Edmundian Orogeny was responsible for low to very low grade metamorphism, reverse faulting, and transpressional folding (Martin and Thorne, 2004; Martin et al., 2005). Martin and Thorne (2004) identified three distinct deformation events (D_{1e}, D_{2e}, and D_{3e}), although the latter (D_{3e}) is now considered to be related to the c. 570 Mulka Tectonic Event. It is currently unclear how the main folding and faulting events (D_{1e} and D_{2e}) in the Edmund and Collier Basins relate to regional amphibolite-grade metamorphism and deformation in the basement rocks of the Gascoyne Province (Sheppard et al., 2007). During this

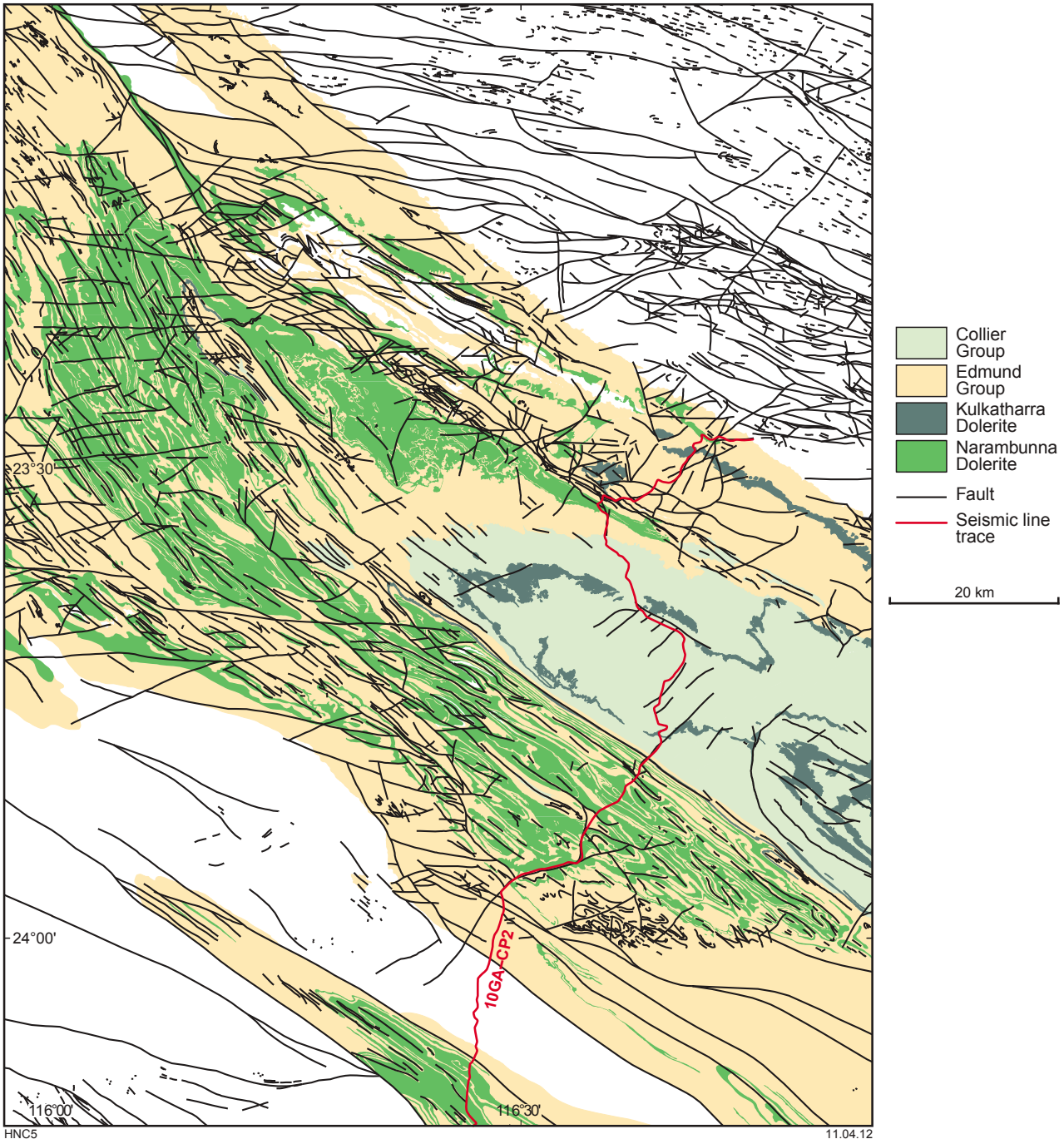

Figure 3. Map illustrating the greater abundance of fault traces in the Edmund Group as compared to the Collier Group.

Figure 4. Fault with 50 cm reverse displacement of sandstone and siltstone beds of Kiangi Creek Formation, and with a 5 cm fault gouge (TANGADEE 1:100 000 map sheet; Thorne and Cutten, 2010).

event, the Gascoyne Province was intruded by leucocratic granites and pegmatites of the 1030–925 Ma Thirty Three Supersuite (Sheppard et al., 2010; Johnson et al., 2011a).

In the Edmund and Collier Basins, the fold and fault structures trend west–east to northwest–southeast, and are concordant with both the general basin architecture and the regional-scale structures in the underlying Gascoyne Province basement. The surface expression of these faults is usually limited to the presence of eroded valleys filled with regolith between offset ridges of Edmund–Collier strata. Because fault planes are very rarely exposed, it is difficult to determine if lateral offset is truly strike-slip, or only apparently so, due to normal or reverse offset (Fig. 5). Faults are often evident as zones of quartz veining up to 50 m wide, or as zones of brecciated quartz in an ironstone matrix (Fig. 6). Minor faults with well-developed slickensides or thin fault gouges are seen to offset strata rarely (Figs 4 and 7).

Folds are generally upright and open, but are tightened adjacent to faults, and generally plunge gently to the northwest or southeast. Martin et al. (2005) identified a main D_{1e} event resulting from northeast–southwest compression, although in the northwest, also documented local evidence of an earlier episode of north-northwesterly directed compression, possibly occurring during the Mutherbukin Tectonic Event. Here, reverse faulting and northeast-trending folds have been refolded by the main northeast–southwest D_{1e} compression. A D_{1e} axial planar cleavage is also locally developed, although absent in most rocks of the Edmund and Collier Groups. A later D_{2e} event is apparent from the often curvilinear axial traces of the F_{1e} folds, which Martin et al. (2005) identified as the result of a weak east-southeast to west-northwest compression.

Mulka Tectonic event

The Mulka Tectonic Event (c. 570 Ma) is evident from late-stage, dextral, brittle–ductile faults and shears, and associated quartz veins, developed in rocks of the Edmund and Collier Groups and the Gascoyne Province. These commonly have well-developed dextral strike-slip shear-sense indicators, and show dextral offset of dolerite dykes belonging to the c. 755 Ma Mundine Well Dolerite

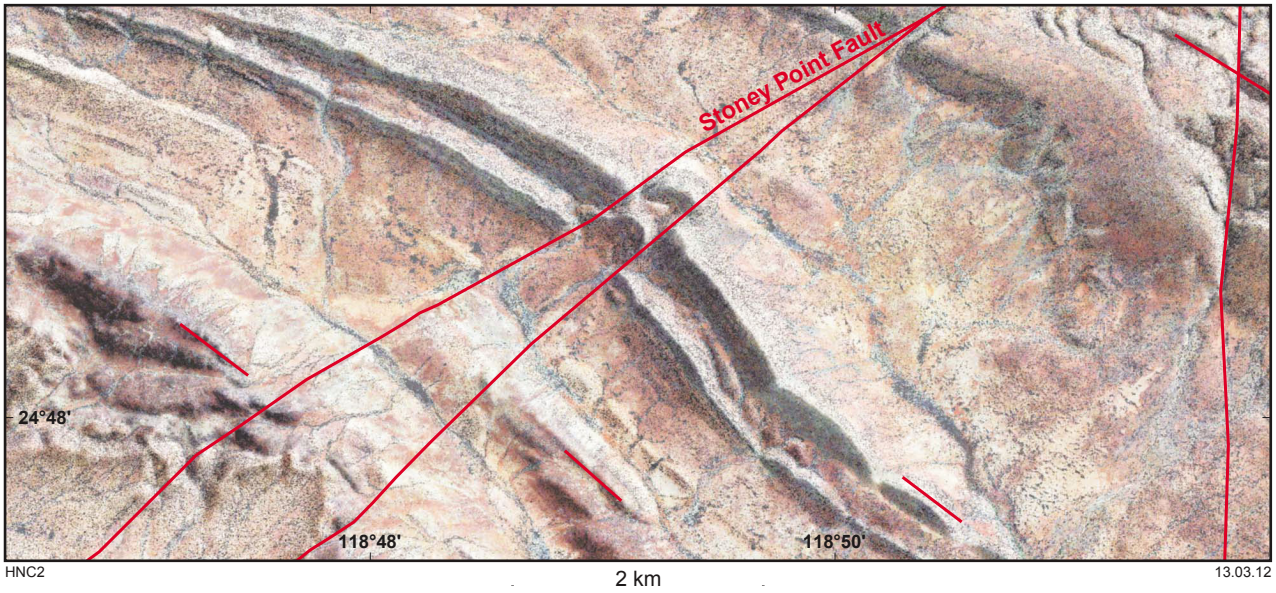

Figure 5. Hillshade-DTM image of northeast-trending fault offset (post- Edmundian Orogeny) on northeast margin of Calyie Syncline, displacing rocks of the Calyie Formation (CALYIE 1:100 000 map sheet; Cutten et al., 2010).

Figure 6. Brecciated quartz in an ironstone matrix, Quartzite Well Fault (MULGUL 1:100 000 map sheet; Thorne and Cutten, 2011)

Suite (Sheppard et al., 2010; Johnson et al., 2011a). Fault movement has been dated at c. 570 Ma, based on in situ $^{40}Ar/^{39}Ar$ geochronology on newly grown muscovite in a small dextral shear zone (Bodorkos and Wingate, 2007).

Figure 7. Slickensides showing reverse movement on an east-northeast trending fault, displacing rocks of the Yilgatherra Formation (MOUNT EGERTON 1:100 000 map sheet; Cutten et al., 2011).

References

Bodorkos, S and Wingate, MTD 2007, The contribution of geochronology to GSWA's mapping programs: current perspectives and future directions, *in* GSWA 2007 extended abstracts: promoting the prospectivity of Western Australia: Geological Survey of Western Australia, Record 2007/2, p. 10–11.

Cutten, HN, Thorne, AM and Blay, OA 2011, Mount Egerton, WA Sheet 2448: Geological Survey of Western Australia, 1:100 000 Geological Series.

Cutten, HN, Thorne, AM and Sheppard, S 2010, Calyie, WA Sheet 2648: Geological Survey of Western Australia, 1:100 000 Geological Series.

Johnson, SP, Thorne, AM, Cutten, HN, Tyler, IM and Blay, O 2011a, Geology of the Gascoyne Province, *in* Capricorn Orogen seismic and magnetotelluric (MT) workshop 2011: extended abstracts *edited by* SP Johnson, AM Thorne and IM Tyler: Geological Survey of Western Australia, Record 2011/25, p. 27–40.

Johnson, SP, Cutten, HN, Tyler, IM, Korsch, RJ, Thorne, AM, Blay, O, Kennett, BLN, Blewett, RS, Joly, A, Dentith, MC, Aitken, ARA, Goodwin, JA, Salmon, M, Reading, A, Boren, G, Ross, J, Costelloe, RD and Fomin, T 2011b, Preliminary interpretation of deep seismic reflection lines 10GA–CP2 and 10GA–CP3: crustal architecture of the Gascoyne Province, and Edmund and Collier Basins, *in* Capricorn Orogen seismic and magnetotelluric (MT) workshop 2011: extended abstracts *edited by* SP Johnson, AM Thorne and IM Tyler: Geological Survey of Western Australia, Record 2011/25, p. 49–60.

Johnson, SP, Sheppard, S, Thorne, AM, Rasmussen, B, Fletcher, IR, Wingate, MTD and Cutten, HN 2011c, The role of the 1280–1250 Ma Mutherbukin Tectonic Event in shaping the crustal architecture and mineralization history of the Capricorn Orogen, *in* GSWA 2011 extended abstracts: promoting the prospectivity of Western Australia: Geological Survey of Western Australia, Record 2011/2, p. 1–3.

Martin, DM 2003, Peperite in the Backdoor Formation and its significance to the age and tectonic evolution of the Bangemall Supergroup, *in* Geological Survey of Western Australia Annual Review 2002–03: Geological Survey of Western Australia, Perth, Western Australia, p. 53–59.

Martin, DM, Sheppard, S and Thorne, AM 2005, Geology of the Maroonah, Ullawarra, Capricorn, Mangaroon, Edmund, and Elliott Creek 1:100 000 sheets: Geological Survey of Western Australia, 1:100 000 Geological Series Explanatory Notes, 65p.

Martin, DM, Sircombe, KN, Thorne, AM, Cawood, PA and Nemchin, AA 2008, Provenance history of the Bangemall Supergroup and implications for the Mesoproterozoic paleogeography of the West Australian Craton: Precambrian Research, v. 166, no. 1–4 (Assembling Australia: Proterozoic building of a continent), p. 93–110.

Martin, DM and Thorne, AM 2004, Tectonic setting and basin evolution of the Bangemall Supergroup in the northwestern Capricorn Orogen: Precambrian Research, v. 128, p. 385–409.

Occhipinti, SA and Myers, JS 1999, Geology of the Moorarie 1:100 000 sheet: Geological Survey of Western Australia, 1:100 000 Geological Series Explanatory Notes, 20p.

Rasmussen, B, Fletcher, IR, Muhling, JR, Thorne, AM, Cutten, HN, Pirajno, F and Hell, A 2010, In situ U–Pb monazite and xenotime geochronology of the Abra polymetallic deposit and associated sedimentary and volcanic rocks, Bangemall Supergroup, Western Australia: Geological Survey of Western Australia, Record 2010/12, 31p.

Sheppard, S, Johnson, SP, Wingate, MTD, Kirkland, CL and Pirajno, F 2010, Explanatory Notes for the Gascoyne Province: Geological Survey of Western Australia, Perth, Western Australia, 336p.

Sheppard, S, Rasmussen, B, Muhling, JR, Farrell, TR and Fletcher, IR 2007, Grenvillian-aged orogenesis in the Palaeoproterozoic Gascoyne Complex, Western Australia: 1030–950 Ma reworking of the Proterozoic Capricorn Orogen: Journal of Metamorphic Geology, v. 25, p. 477–494.

Thorne, AM and Cutten, HN 2010, Tangadee, WA Sheet 2649: Geological Survey of Western Australia, 1:100 000 Geological Series.

Thorne, AM and Cutten, HN 2011, Mulgul, WA Sheet 2548: Geological Survey of Western Australia, 1:100 000 Geological Series.

Tyler, IM, Johnson, SP, Thorne, AM and Cutten, HN 2011, Implications of the Capricorn deep seismic survey for mineral systems, *in* Capricorn Orogen seismic and magnetotelluric (MT) workshop 2011: extended abstracts *edited by* SP Johnson, AM Thorne and IM Tyler: Geological Survey of Western Australia, Record 2011/25, p. 115–120

Wingate, MTD, Kirkland, CL and Cutten, HN in prep, 143445: dolerite sill, Waldburg Homestead; Geochronology Record: Geological Survey of Western Australia.

Wingate, MTD, Kirkland, CL and Thorne, AM 2010, 149019: felsic volcaniclastic rock, Tangadee Road; Geochronology Record 875: Geological Survey of Western Australia, 4p.

Wingate, MTD, Pisarevsky, SA and Evans, DAD 2002, Rodinia connections between Australia and Laurentia: no SWEAT, no AUSWUS?: Terra Nova, v. 14, p. 121–128.

Preliminary interpretation of deep seismic reflection lines 10GA–CP2 and 10GA–CP3: crustal architecture of the Gascoyne Province, and Edmund and Collier Basins

by

SP Johnson, HN Cutten, IM Tyler, RJ Korsch[1], AM Thorne, O Blay, BLN Kennett[2], RS Blewett[1], A Joly[3], MC Dentith[3], ARA Aitken[3], JA Goodwin[1], M Salmon[2], A Reading[4], G Boren[5], J Ross[5], RD Costelloe[1], and T Fomin[1]

Introduction and aims of the seismic survey

The Capricorn Orogen in Western Australia records both the punctuated assembly of the Pilbara and Yilgarn Cratons to form the West Australian Craton, and over one billion years of subsequent intracratonic reworking and basin formation (Cawood and Tyler, 2004; Sheppard et al., 2010). The orogen is over 1000 km long, and includes the passive margin deposits of both the Pilbara and Yilgarn Cratons, variably deformed and metamorphosed granitic and metasedimentary rocks of the Gascoyne Province, and both the sedimentary and low-grade metasedimentary rocks that overly these three tectonic units (Frontispiece 1; Plate 1; Cawood and Tyler, 2004; Sheppard et al., 2010).

A deep seismic reflection survey through the Capricorn Orogen, consisting of three lines (10GA–CP1, 10GA–CP2, and 10GA–CP3; Frontispiece 1), was acquired during 2010 by Geoscience Australia and Australian National Seismic Imaging Resource (ANSIR), in collaboration with Geological Survey of Western Australia (GSWA). All three lines were processed by the Seismic Acquisition and Processing Section of the Minerals and Natural Hazards Division, Geoscience Australia. Details of the data acquisition and processing are provided by Kennett et al. (2011).

1 Minerals and Natural Hazards Division, Geoscience Australia, GPO Box 378, Canberra, ACT 2601.

2 Research School of Earth Sciences, The Australian National University, Canberra ACT 0200.

3 Centre for Exploration Targeting, School of Earth and Environment, The University of Western Australia, 35 Stirling Highway, Crawley, WA 6009.

4 School of Earth Sciences and CODES Centre of Excellence, University of Tasmania, Private Bag 79, Hobart, TAS 7001.

5 Centre for Tectonics, Resources and Exploration, University of Adelaide, Adelaide, SA 5005.

The southern two lines, 10GA–CP2 and 10GA–CP3 (Frontispieces 1–3), provide a transect through the Gascoyne Province, and Edmund and Collier Basins, totalling 383 line-km. Both lines are oriented approximately north–south, and are perpendicular to the major faults and regional-scale structures (Frontispiece 1–3; Plate 1). The geology of the Gascoyne Province, and of the Edmund and Collier Basins, are documented in detail by Johnson et al. (2011a) and Cutten et al. (2011), respectively. Because of the lack of road access, it was not possible to have a single, continuous survey line through the region. Instead, the end of line 10GA–CP2 is offset from 10GA–CP3 by ~80km along the strike of the orogen (Frontispiece 1; Plate 1). Line 10GA–CP2 starts at the contact between the Edmund Group and Ashburton Basin, crosses the Talga Fault, and finishes within the Dalgaringa Supersuite to the north of the Errabiddy Shear Zone. Line 10GA–CP3, designed to cross the Errabiddy Shear Zone, begins in the Dalgaringa Supersuite and finishes within the Narryer Terrane of the Yilgarn Craton (Frontispiece 1; Plate 1). Considering that the surface geology and geological history of the Gascoyne Province, and of the Edmund and Collier Basins are relatively well understood (e.g. Johnson et al., 2011a; Cutten et al., 2011), the main aim of lines 10GA–CP2 and 10GA–CP3 within the broader objectives of the Capricorn Orogen transect (Kennett et al., 2011) were to establish:

1. the location and orientation of the major crustal terrane-bounding faults, including the suture between the Yilgarn Craton and Gascoyne Province (located at the Errabiddy Shear Zone), and the suture between the Pilbara Craton and the Gascoyne Province (possibly located at the Talga Fault)

2. the depth and shape of the Minnie Creek batholith, and other Proterozoic granite intrusions

3. the deep crustal structure of the Edmund and Collier Basins, and nature of major growth faults; e.g. the Talga Fault.

Here, we report the results of an initial geological interpretation of these two seismic lines, and the resulting implications for the crustal architecture of the Gascoyne

Province, and Edmund and Collier Basins, as well as the processes related to the punctuated assembly of the West Australian Craton and multiple periods of subsequent crustal reactivation and reworking.

Preliminary interpretation of seismic lines 10GA–CP2 and 10GA–CP3

Both seismic lines (Figs 1 and 2) provide images through the crust and upper mantle, down to 20 seconds two-way travel time (s TWT) (~60 km). The crust in both lines is moderately reflective and several major crustal structures can be identified. The location and character of the Mohorovičić discontinuity ('the Moho') varies considerably across the two lines. Under the Gascoyne Province, in 10GA–CP2, the Moho is deep and undulating, varying between 12 and 15.3 s TWT (36–46 km), and continues this trend into the northern part of 10GA–CP3, where the Moho is at 15 s TWT (~45 km) deep. In the south of 10GA–CP3, we interpret the presence of a double Moho, formed by the thrusting of the Glenburgh Terrane under the Narryer Terrane along the Cardilya Fault (Korsch et al., 2011). The upper mantle, below the Moho, is essentially non-reflective within both seismic lines. Features such as granite batholiths and sedimentary basins can be observed in the upper 0–5 s TWT (~15 km) of the crust (Figs 1 and 2).

The Gascoyne Province has been divided into several fault- or shear-bounded, easterly–southeasterly trending structural and metamorphic zones (Frontispieces 2–3; Sheppard et al., 2010). Although each zone shares a common, province-wide tectonostratigraphic assemblage, each has also been shaped by a characteristic and unique combination of deformational, metamorphic, and magmatic events, which reflects different responses to the multiple reworking events in the Gascoyne Province (Sheppard et al., 2010; Johnson et al., 2011a). Some of the major zone-bounding structures have also affected rocks of the Edmund and Collier Basins (Cutten et al., 2011). The major structures that define the boundaries of each zone are prominent in both regional gravity and aeromagnetic images (Frontispeices 2 and 3), although the attitudes, depth extents, and kinematic histories of these structures are not yet well known. The most important structures are the Collins and Talga Faults; the composite Minga Bar and Minnie Creek Faults; the Ti Tree, Chalba, and Errabiddy Shear Zones; and the Cardilya Fault (Frontispieces 1–3; Plate 1); although not all were intersected during this seismic survey. All the major structures imaged dip moderately to the south, and generally steepen in the upper crust. Some structures, such as the Ti Tree Shear Zone, Lyons River Fault, Godfrey Fault, Talga Fault, and Cardilya Fault, transect the entire crustal profile and root in the Moho (Figs 1 and 2). In line 10GA–CP3, the Errabiddy Shear Zone dips moderately to the north, where it soles onto the south-dipping Cardilya Fault (Fig. 2).

Crustal terranes and seismic provinces

On the basis of seismic character and surface geology, Korsch et al. (2011) identified three terranes and seismic crustal provinces within the two lines, most of which are separated by major structures that coincide with the mapped surface faults or shear zones that define the major zone boundaries of the Gascoyne Province (Johnson et al., 2011a). The seismic character of these terranes and seismic provinces is described in detail by Korsch et al. (2011), and as such, only a summary of their geometric relationships is presented here.

Within line 10GA–CP3, the Narryer Terrane, which forms part of the northern Yilgarn Craton, is separated from the Glenburgh Terrane by a series of anastomosing, north-dipping faults known as the Errabiddy Shear Zone, and a single, moderately south-dipping fault called the Cardilya Fault (Figs 1 and 2). These two fault systems also segment the Glenburgh Terrane into two crustal elements:

1. The Dalgaringa Supersuite, including the Nardoo Granite, which, at the surface, represents the exhumed mid-crustal portions of a continental-margin arc known as the Dalgaringa Arc (Johnson et al., 2010, 2011a,b), and which occurs structurally above both the Errabiddy Shear Zone and the Cardilya Fault (that is, the hangingwall).

2. The remainder of the Glenburgh Terrane, including the basement gneisses into which the continental-margin arc magmas were intruded, which occur in the footwall of the Cardilya Fault, lying structurally below the Narryer Terrane.

The lower crust beneath the Glenburgh Terrane is only very weakly reflective, and has been interpreted as a distinct crustal entity from the overlying Glenburgh Terrane (Korsch et al., 2011). This portion of crust, termed the MacAdam Seismic Province (Korsch et al., 2011), is up to 5.5 s TWT (~16.5 km) thick, and is bounded by the Lyons River Fault in the north and the lower crustal component of the Glenburgh Terrane in the south (Figs 1 and 2). As this crust is not exposed at the surface, neither its age nor composition are known.

Within line 10GA–CP2, the Glenburgh Terrane is separated from the Bandee Seismic Province by the moderately south-dipping Lyons River Fault (Fig. 1). This fault splays into the Ti Tree Shear Zone, with both faults dissecting rocks of the Moorarie and Durlacher Supersuites, plus the sedimentary rocks of the Edmund Basin, in the upper crust (Figs 1 and 2).

Since rocks of the Bandee Seismic Province are not exposed at the surface, it is impossible to determine if this province is similar to the Glenburgh Terrane in terms of its age, lithological makeup, and composition. Its differing seismic character suggests that it may in fact be a separate terrane, forming part of the southern extension of the Pilbara Craton (Thorne et al., 2011a; Korsch et al., 2011).

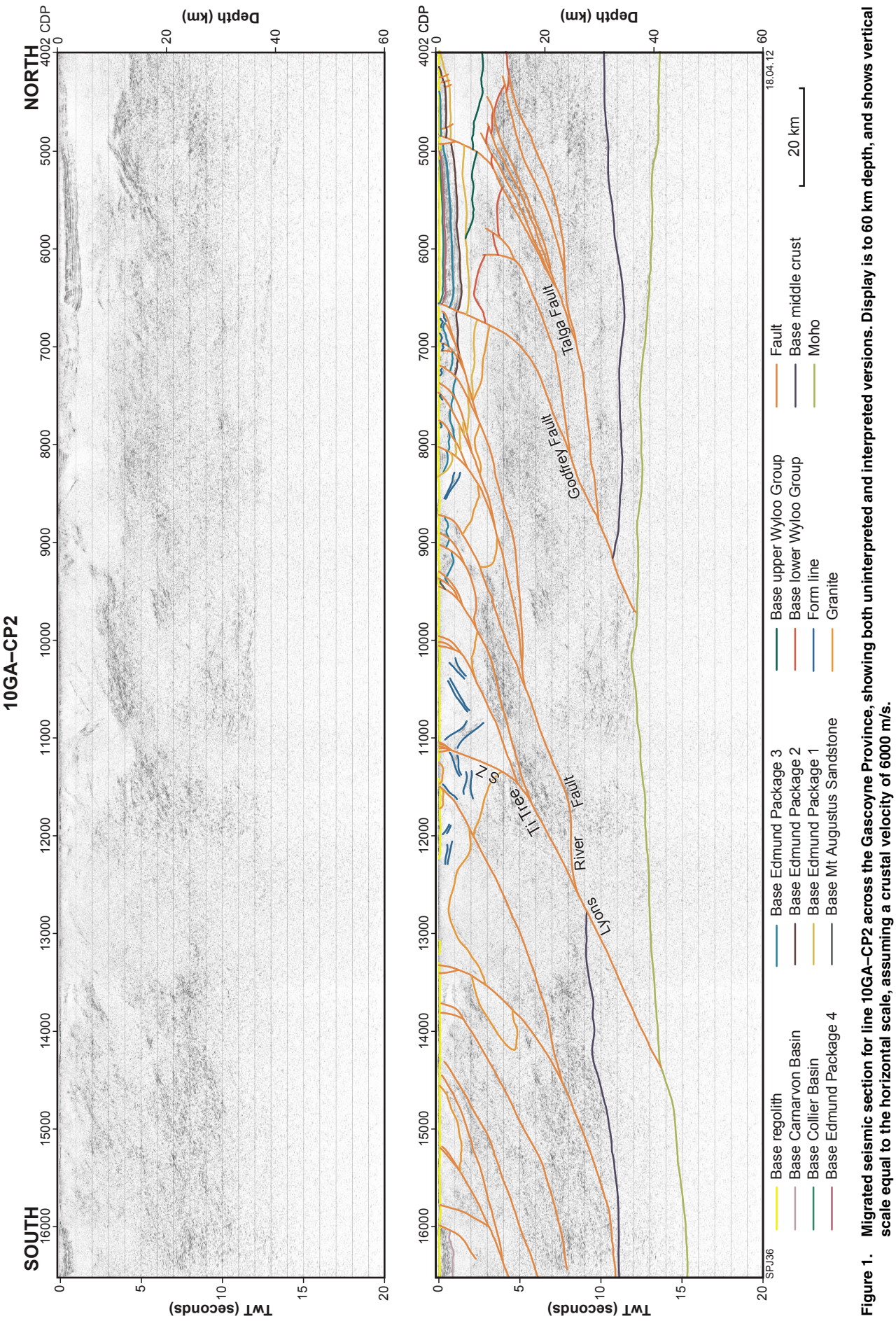

Figure 1. Migrated seismic section for line 10GA–CP2 across the Gascoyne Province, showing both uninterpreted and interpreted versions. Display is to 60 km depth, and shows vertical scale equal to the horizontal scale, assuming a crustal velocity of 6000 m/s.

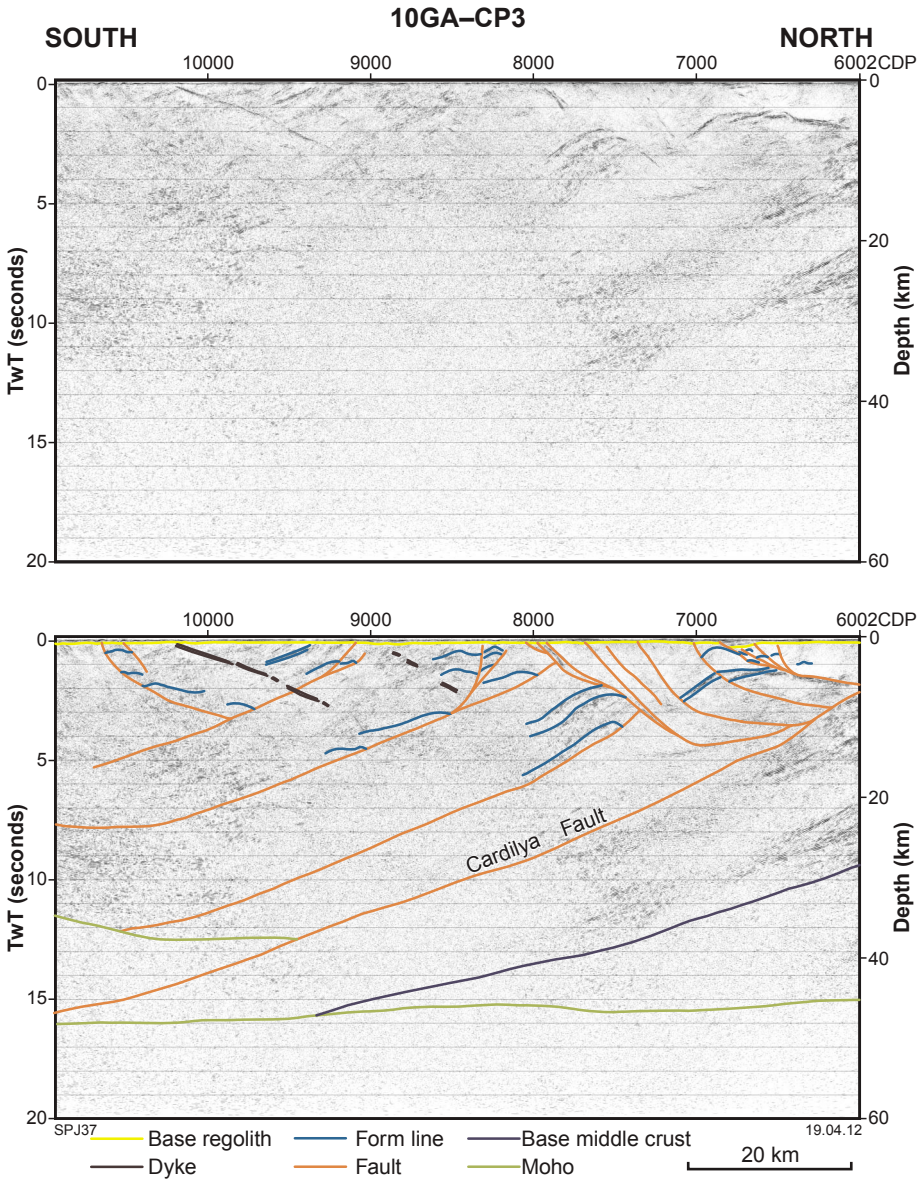

Figure 2. Migrated seismic section for line 10GA–CP3, showing both uninterpreted and interpreted versions. Display is to 60 km depth, and shows vertical scale equal to the horizontal scale, assuming a crustal velocity of 6000 m/s.

Towards the northern end of 10GA–CP2, the Bandee Seismic Province is cut by the moderately south-dipping Talga and Godfrey Faults, which transect the entire crustal profile, and root in the Moho.

Suture zones

The geological history of the Gascoyne Province indicates that the West Australian Craton was assembled from at least three distinct and unrelated tectonic blocks (the Pilbara and Yilgarn Cratons, and the Glenburgh Terrane of the Gascoyne Province), thus requiring the presence of two suture zones (Occhipinti et al., 2004; Johnson et al., 2010, 2011a,b). This punctuated assembly history records the collision, or accretion, of the Glenburgh Terrane with the southern margin of the Pilbara Craton during the 2215–2145 Ma Ophthalmian Orogeny, followed by the collision of this combined entity with the northern margin of the Yilgarn Craton during the 2005–1950 Ma Glenburgh Orogeny (Occhipinti et al., 2004; Johnson et al., 2010, 2011a,b).

Pilbara Craton and Bandee Seismic Province – Glenburgh Terrane suture

Due to the extensive cover of the Ashburton, Edmund, and Collier Basins, the suture between the Pilbara Craton – Bandee Seismic Province and Glenburgh Terrane is

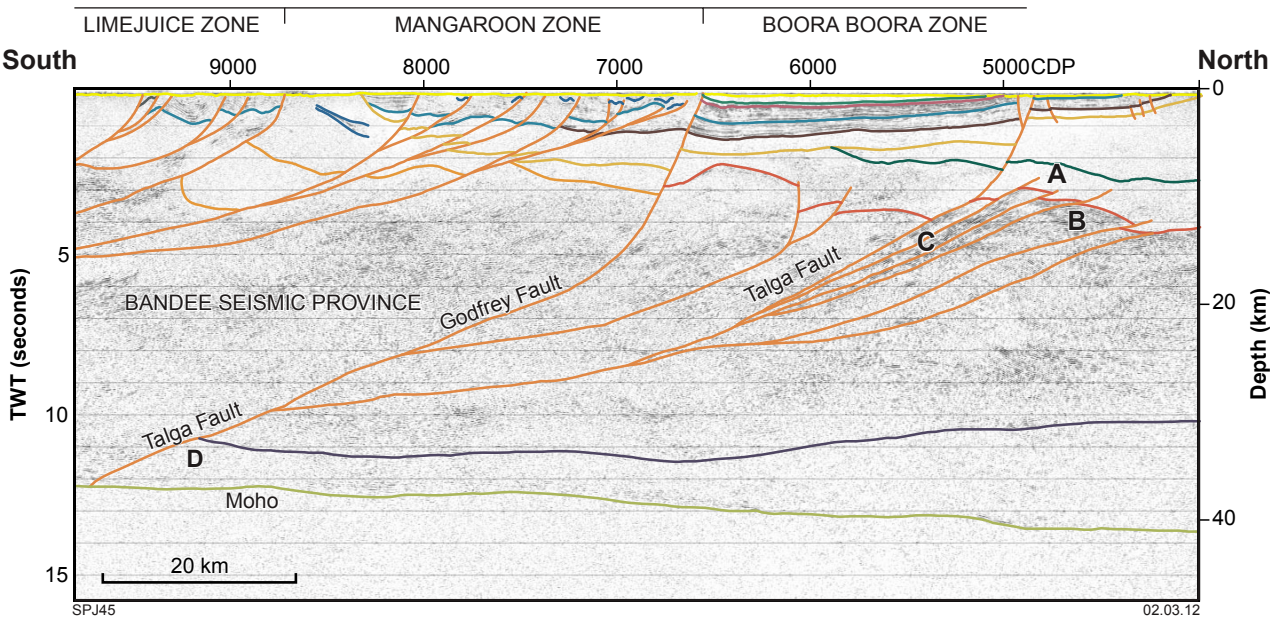

Figure 3. Interpreted migrated seismic section of part of line 10GA–CP2, showing the attitude and orientation of the Talga and Godfrey Faults.

not exposed (Frontispiece 1; Plate 1), although prior to the present seismic and magnetotelluric (MT) surveys, various geophysical data (Abdulah, 2007; Selway, 2008; Selway et al., 2009; Kennett, 2011) with limited horizontal resolution had implied that the suture was a vertical, or steeply north-dipping, structure approximately coincident with the mapped surface expression of the Talga Fault. However, in line 10GA–CP2 (Fig. 1), the Talga Fault does not appear to separate crust of differing seismic character (that is, it may be an intra- seismic province fault), and so is not likely to represent a suture zone. If not this structure, then the suture is probably located further south, at the Lyons River Fault, which separates the Glenburgh Terrane from the Bandee Seismic Province (Korsch et al., 2011).

The Talga Fault

In contrast to the various pre-existing geophysical data (Abdulah, 2007; Selway, 2008; Selway et al., 2009; Kennett, 2011), the seismic data presented in line 10GA–CP2 show the Talga Fault to be a listric, south-dipping structure, which joins with the Godfrey Fault before intersecting the Moho at 12.3 s TWT (~37 km) (Figs 1 and 3).

Although this fault does not appear to separate crust of differing seismic character, several other lines of evidence suggest that it may be a significant structure relating to the collision between the Pilbara Craton and the Glenburgh Terrane. The offset of seismic reflections across the fault in 10GA–CP2 show that its present expression is as a south-dipping listric fault that offsets rocks as young as the 1620–1465 Ma Edmund Group. The current listric nature of the fault is most likely a late Paleoproterozoic to Mesoproterozoic feature, formed by the reactivation of older structures to accommodate the deposition of sediments in the Edmund Basin (see below and Cutten et al., 2011). From 3–7 s TWT (9–21 km), the Talga Fault is parallel to, and forms part of, an imbricate set of faults (area A in Fig. 3) that reorient (area C in Fig. 3) a region of horizontal seismic reflections to the north (area B in Fig. 3), indicating that it is a zone of intense deformation. The faults offset only the lower stratigraphic units of the lower Wyloo Group, suggesting that they are of Ophthalmian age (equivalent in age to the c. 2210 Ma Cheela Springs Basalt in the lower Wyloo Group; Martin et al., 1998; Martin and Morris, 2010), whereas the northward-directed thrust sense of movement is parallel to the transport direction of exposed northward-verging thrusts in the Ophthalmia Fold and Thrust Belt (Tyler, 1991; Thorne et al., 2011b). Furthermore, non-reflective lower crust on the north side of the Talga–Godfrey Faults (area D in Fig. 3) does not occur to the south, implying that, at least in the lower crust, the Talga–Godfrey Faults offset and juxtapose crust of differing seismic character.

Therefore, the Talga Fault appears to be a major crustal shear zone that forms part of a north-verging fold and thrust system active during the Ophthalmian Orogeny.

The Lyons River Fault

The Glenburgh Terrane is well exposed in the Mooloo Zone, and fragmentary outcrops are present in the southern part of the Limejuice Zone (Johnson et al., 2011a–c; Frontispiece 1; Plate 1). Basement to the 1820–1775 Ma Moorarie Supersuite and 1680–1620 Ma Durlacher Supersuite in the northern part of the Gascoyne Province (i.e. the Bandee Seismic Province) is not exposed, and thus, the northerly extent of the Glenburgh Terrane is unknown. A recent MT survey showed no significant

electrical contrast between the Glenburgh Terrane in the south, and unexposed basement north of the Limejuice Zone, and it was concluded that the Glenburgh Terrane extended north up to the Talga Fault, thus forming basement to the entire Gascoyne Province (Selway, 2008; Selway et al., 2009).

Although the seismic character of the upper and middle crust of both the Glenburgh Terrane and Bandee Seismic Province are relatively similar in line 10GA–CP2, the Glenburgh Terrane is characterized by a non-reflective lower crust, the MacAdam Seismic Province (Korsch et al., 2011). In contrast, the lower crust of the Bandee Seismic Province south of the Talga Fault is highly reflective, locally showing gentle folding in the seismic reflections (area A in Fig. 4). The contact between the two regions is defined by the Lyons River Fault, the Ti Tree Shear Zone, and a zone of strong seismic reflections parallel to these faults (areas B and C in Fig. 4). Furthermore, there is a significant step in the Moho where the Lyons River Fault intersects the upper mantle (Fig. 4).

These observations suggest that the Lyons River Fault represents a major crustal suture in the central part of the Gascoyne Province (Korsch et al., 2011). At the surface, this structure is represented by the Lyons River, Minnie Creek, and Minga Bar Faults (Frontispiece 1–3; Plate 1); nevertheless, all three faults have been extensively reworked during younger orogenic and magmatic events (Sheppard et al., 2005, 2010; Johnson et al., 2011a). Thus, direct age constraints for the timing of collision/accretion of the Bandee Seismic Province – Pilbara Craton with the Glenburgh Terrane along this structure are poor. The upper age limit can be defined by the youngest rocks of the Halfway Gneiss, which forms the basement to the Glenburgh Terrane, at c. 2430 Ma (Johnson et al., 2011a,c). The younger age limit is taken to be 2240–2125 Ma, the depositional age of the Moogie Metamorphics, which unconformably overlie the Glenburgh Terrane. These metasedimentary rocks were sourced partly from the Fortescue, Hamersley, and Turee Creek Groups on the southern margin of the Pilbara Craton (Johnson et al., 2011a–c) and thus, the Bandee Seismic Province and Glenburgh Terrane must have been sutured by this time. Based on these observations, the Lyons River Fault is likely to form the principal Ophthalmian-aged suture between the Pilbara Craton – Bandee Seismic Province and the Glenburgh Terrane.

Glenburgh Terrane – Yilgarn Craton suture

Based on both geological (e.g. Johnson et al., 2011a) and geophysical observations (Hackney, 2004; Selway, 2008; Selway et al., 2009; Reading et al., 2012), the Errabiddy Shear Zone is interpreted to be the suture between the Glenburgh Terrane and the Narryer Terrane of the Yilgarn Craton. A previous MT survey across this zone showed a clear electrical contrast between the Gascoyne Province and Yilgarn Craton, with the contact dipping 45° to the south (Selway, 2008; Selway et al., 2009). Regional gravity anomalies and geoid lows in this area have been interpreted to indicate thickened crust under this part of the orogen (Hackney, 2004); passive seismic data not only confirm the existence of this thickened crust, but also indicate the presence of a double crust or double Moho in the region (Reading et al., 2012).

The seismic data presented from 10GA–CP3 (Fig. 2) and the southern part of line 10GA–CP2 (Fig. 1) show that the Narryer Terrane is separated from the Glenburgh Terrane by the north-dipping Errabiddy Shear Zone, and the south-dipping Cardilya Fault, the two fault systems intersecting at CDP 6300 on line 10GA–CP3 at 3.3 s TWT (~10 km) depth. The Cardilya Fault transects the entire crust, can be imaged down to 15.5 s TWT (~46.5 km), and is interpreted to offset the Moho, which under the Narryer Terrane is much shallower at 12.5 s TWT (~37.5 km) depth (Figs 2 and 5). These results are comparable to those obtained by passive-seismic methods (Reading et al., 2012). At the northern end of line 10GA–CP3, the footwall of the Cardilya Fault is marked by a thick package, up to 3 s TWT (~9 km) thick, of strong seismic reflections (area A in Fig. 5) that are parallel to the fault. Similar packages are also observed adjacent to the boundary with the MacAdam Seismic Province (area B in Fig. 5).

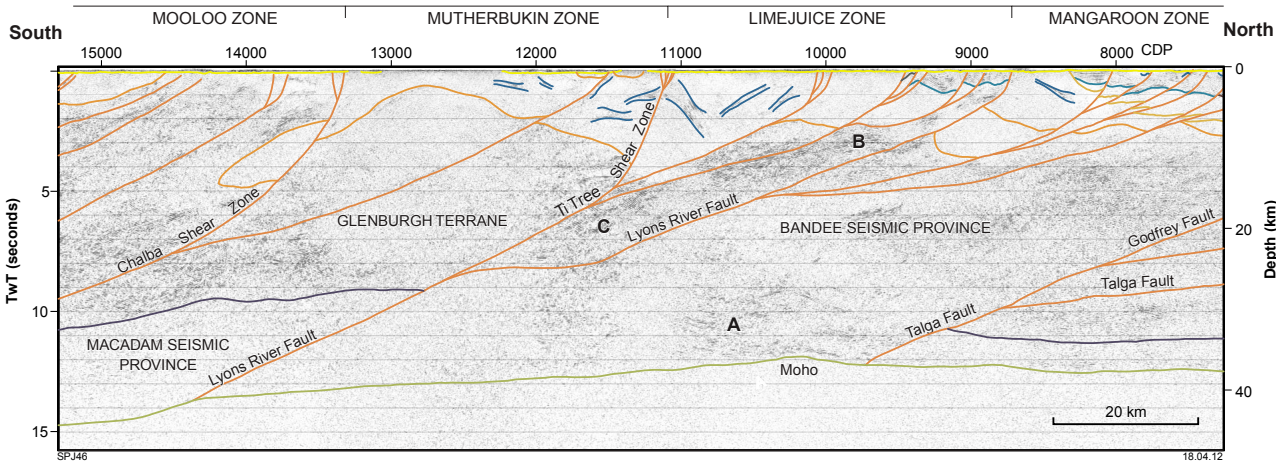

Figure 4. Interpreted migrated seismic section of part of line 10GA–CP2, showing the location of the suture zone between the Glenburgh Terrane and Bandee Seismic Province at the Lyons River Fault.

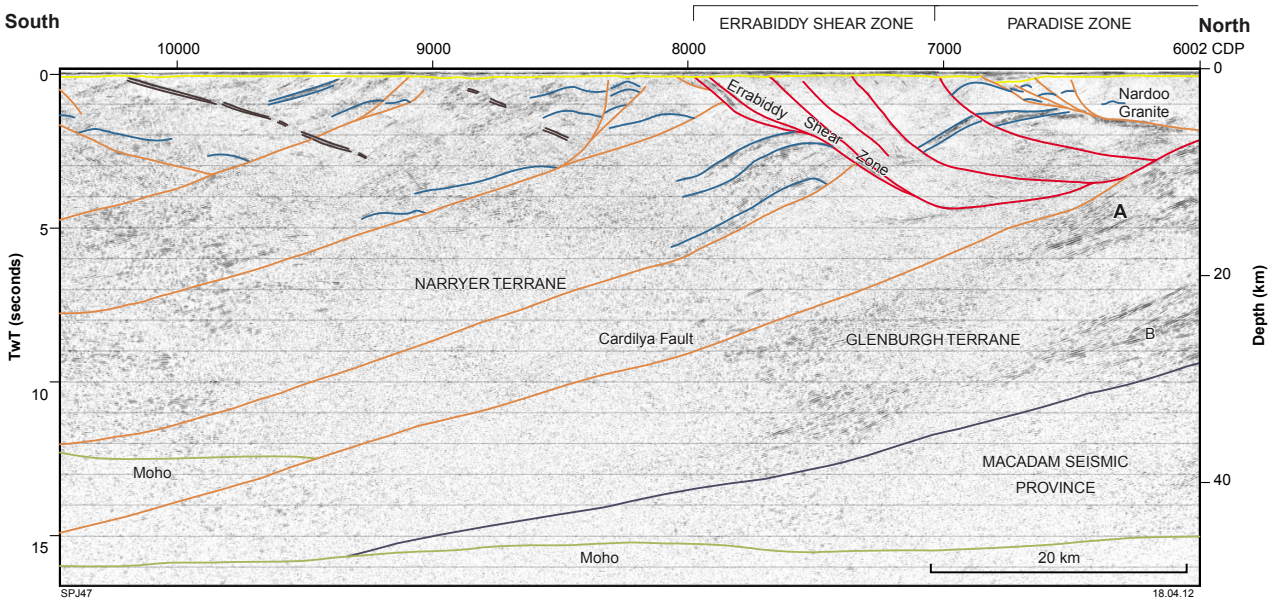

Figure 5. Interpreted migrated seismic section of part of line 10GA–CP3, showing the relationships between the Errabiddy Shear Zone and Cardilya Fault.

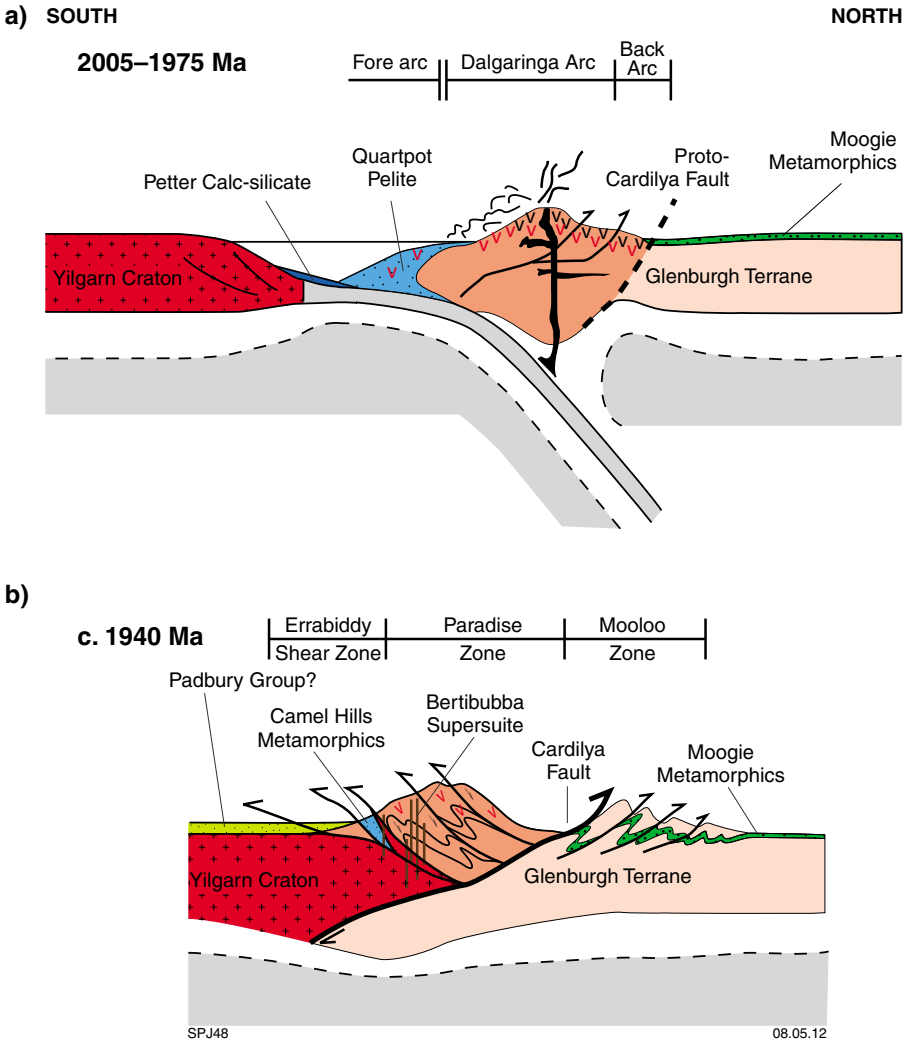

Figure 6. Schematic cross sections, showing the evolution of the Dalgaringa Arc and the formation of the Errabiddy Shear Zone and Cardilya Fault.

These areas are interpreted to represent strongly deformed parts of the Glenburgh Terrane. Lithological variations within the Errabiddy Shear Zone, such as imbricate slices of Narryer Terrane, or intrusions of the Bertibubba Supersuite (Johnson et al., 2011a), cannot be differentiated seismically. However, areas of low seismic reflectivity north of CDP 6800 in the upper 3.5 s TWT (~10.5 km) of the crust most likely represent composite plutons of weakly deformed Nardoo Granite (Sheppard et al., 2004, 2010; Johnson et al., 2011a).

The crustal architecture of this suture zone, as imaged in line 10GA–CP3, is significantly complex, something predicted in part by the surface geology (see fig. 3 of Cawood and Tyler, 2004; Sheppard et al., 2004) and geophysical data (Hackney, 2004; Selway, 2008; Selway et al., 2009; Reading et al., 2012). Although both major terrane-bounding structures are related to the Glenburgh Terrane – Yilgarn Craton collision, their geometric relationships suggest that the Cardilya Fault post-dates the formation of the Errabiddy Shear Zone. The imbrication of lithologies from the Glenburgh Terrane and Yilgarn Craton along the Errabiddy Shear Zone suggest that this earlier structure is probably the suture zone. This interpretation is consistent with the presence of continental-margin arc magmatic rocks of the Dalgaringa Supersuite to the north of the north-dipping Errabiddy Shear Zone, implying northward-directed subduction under the southern margin of the Glenburgh Terrane (Sheppard et al., 2004; Johnson et al., 2010, 2011a,b). Following the initial collision and interleaving of lithologies along the Errabiddy Shear Zone, this zone was reworked by the Cardilya Fault, which underthrust the southern margin of the Glenburgh Terrane beneath the Narryer Terrane (Sheppard et al., 2003; Cawood and Tyler, 2004). The geological history of this fault is poorly known from surface mapping, as it is both poorly exposed, and has been extensively intruded by younger magmatic rocks of the 1820–1775 Ma Moorarie Supersuite (Frontispiece 1; Plate 1). However, the fault that occurs between the magmatic-arc rocks of the Dalgaringa Supersuite, and the basement gneisses of the Glenburgh Terrane into which they were intruded (Frontispiece 1; Plate 1), is located in the former back-arc region of the Dalgaringa Arc. The proto-Cardilya Fault may have been established during a period of back-arc crustal thinning (Fig. 6). During the collision, this thinned crust may have ruptured, resulting in the underthrusting of the Glenburgh Terrane beneath the Yilgarn Craton (Fig. 6).

Alternatively, the Narryer Terrane may have been obducted onto the Glenburgh Terrane at the present site of the Cardilya Fault during the collision. During the post-collisional phase of the Glenburgh Orogeny, there was backthrusting along the Errabiddy Shear Zone, with a slice of the Glenburgh Terrane being thrust back to the south over the upper part of the Narryer Terrane.

Batholiths and granite intrusions

Within both the Glenburgh Terrane and upper crust of the Bandee Seismic Province, the upper 5 s TWT (~15 km) of the crust is defined by numerous, irregular, and seismically non-reflective bodies (Figs 1, 2, and 7), which are indicated by the mapped surface geology (Frontispiece 1; Plate 1) to be granite plutons of the 1820–1775 Ma Moorarie Supersuite and 1680–1620 Ma Durlacher Supersuite.

In the Mutherbukin Zone (Frontispiece 1–3; Fig. 7; Plate 1), a single pluton belonging to the 1680–1620 Ma Durlacher Supersuite is imaged between the Chalba and Ti Tree Shear Zones (CDPs 11075–13325). The pluton has a concave, presumably intrusive, basal contact with the underlying Glenburgh Terrane (Fig. 7). The pluton ranges in thickness from 0.6 s TWT (~1.8 km) in the centre of the Mutherbukin Zone, to 3.8 s TWT (~11.5 km) at its northerly contact where it is truncated by the Ti Tree Shear Zone. The pluton thins rapidly by about 2 s TWT (~6 km) on the southern side of the Chalba Shear Zone, where it has been downthrown across this fault to the south. Weak seismic reflections within and beneath the intrusion are parallel to the concave basal contact, suggesting that the shape and orientation of the pluton is due to folding during the Mutherbukin Tectonic Event (Johnson et al., 2011a). Prior to folding, the pluton would have been a flat-lying or gently dipping, tabular body greater than, or equal to, 11.5 km at its thickest.

In the Limejuice Zone, the Minnie Creek batholith (Frontispiece 1; Fig. 7; Plate 1; Johnson et al., 2011a) is imaged north of the Ti Tree Shear Zone at CDP 11075, and is interpreted to continue northward, underlying rocks of the Edmund Basin in the Cobra Syncline to CDP 8975 (Figs 3 and 8). North of the Edmund Fault at CDP 9450, the batholith is cut by numerous listric normal faults, which have produced a series of rotated (southwest-side down) half grabens. The Minnie Creek batholith has not been imaged north of these half grabens (between CDP 8975 and the Lyons River Fault at CDP 8725), where the area is dominated by rocks of high seismic reflectivity (Fig. 8). The base of the Minnie Creek batholith is mostly interpreted as a fault contact, but between CDP 10400 and 9900, the batholith has a relatively sharp, flat, possibly intrusive contact with the underlying Glenburgh Terrane. In this section, the batholith has a thickness of 2.25 s TWT (~6.75 km), but its maximum thickness, immediately north of the Ti Tree Shear Zone, is 6 s TWT (~18 km); nevertheless, as the basal contact in this region is tectonic in origin, it is possible that the Minnie Creek batholith has been thickened during folding or faulting.

At several localities within the batholith (e.g. CDP 11000, 10500, and 10300), planar regions of highly seismically reflective material dip at moderate angle toward the batholith centre. At the surface, these bodies have been shown to be kilometre-scale rafts of low-metamorphic grade pelitic and semipelitic schist belonging to the 1840–1810 Ma Leake Spring Metamorphics (Frontispiece 1; Plate 1; Johnson et al., 2011a). These rafts are also evident in the northern part of the Durlacher Supersuite pluton to the south of the Ti Tree Shear Zone (e.g. at CDP 11200 and CDP 11500), although none are exposed at the surface. These packages, some of which are up to 8 km in length, most likely represent vestiges of a formerly coherent sedimentary succession (Leake Spring Metamorphics), into which the granites were intruded. The preservation of these tabular metasedimentary packages suggest that the batholith may have formed by a series of

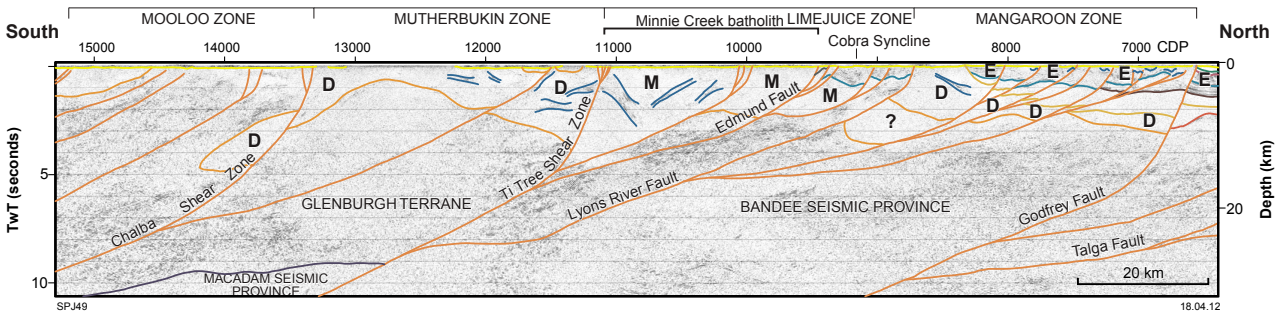

Figure 7. Interpreted migrated seismic section of part of line 10GA–CP2, showing the location and shape of granitic plutons and batholiths in the upper 15 km (5 s TWT) of the crust. Abbreviations used: D — Durlacher Supersuite; E — Edmund Group; M — Moorarie Supersuite.

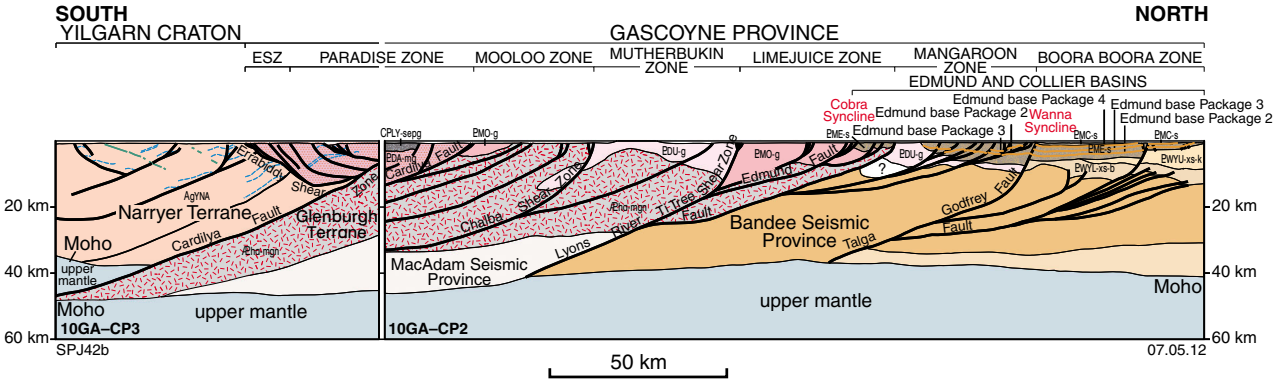

Figure 8. Geological interpretation of seismic lines 10GA–CP2 and 10GA–CP3

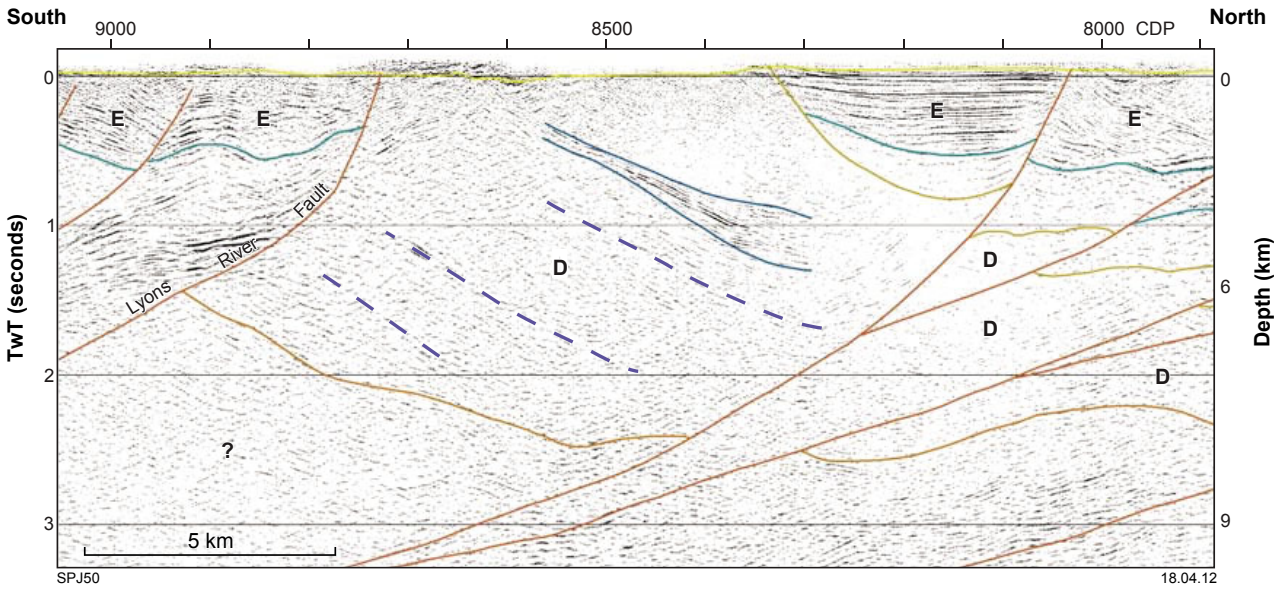

Figure 9. Interpreted migrated seismic section of part of line 10GA–CP2, showing the architecture of the Mangaroon Zone, including the raft of metasedimentary material that is parallel to other weak seismic reflections (shown as dashed blue lines) within the granitic body. Abbreviations used: D — Durlacher Supersuite; E — Edmund Group.

sheet-like plutons, an interpretation supported in part by field evidence, which indicates that many of the granites in the Moorarie Supersuite in the Limejuice Zone have sheet-like geometries (Sheppard et al., 2010).

In the Mangaroon Zone, the seismic reflection data presented in seismic line 10GA–CP2 (Figs 1 and 7) show weakly reflective crust, interpreted as granite plutons of the 1860–1620 Ma Durlacher Supersuite, bounded by the Lyons River Fault in the south (CDP 8720), and the Godfrey Fault to the north (CDP 6575; Fig. 7). The area north of CDP 8300 is covered by extensive sedimentary rocks of the Edmund Basin, and there are no surface exposures of basement rocks in this region (Frontispiece 1; Plate 1). The largest volume of granitic material occurs in the central part of the Mangaroon Zone, between CDP 8750 and 8300, where it is ~2.5 s TWT (~7.5 km) thick (Fig. 9). The granite contains a 6 km long package of moderately north-dipping, seismically reflective material (CDP 8550–8300) similar to the metasedimentary rafts in the Minnie Creek batholith further south. The reflective package also parallels numerous other weak seismic reflections that occur throughout the granite body (Fig. 9), which are interpreted to reflect relict sedimentary or lithological layering of the 1760–1680 Ma Pooranoo Metamorphics. The presence of parallel seismic reflections down to ~2.0 s TWT indicates that the Pooranoo basin was at least ~6 km thick.

Farther north, in the area underlying the Edmund Basin (south of the Godfrey Fault; Fig. 7), it is difficult to determine if the non-reflective packages are granites of the Moorarie or Durlacher Supersuites, and for simplicity they are tentatively shown as a continuation of the interlayered granitic and metasedimentary material of Durlacher Supersuite and Pooranoo Metamorphics. Rare outcrops of strongly deformed granite belonging to the Moorarie Supersuite (the Gooche Gneiss; Frontispiece 1; Plate 1), formed a basement onto which the Pooranoo Metamorphics were deposited (Sheppard et al., 2005, 2010).

Architecture of the Edmund and Collier Basins

Line 10GA–CP2 crosses the Edmund and Collier Basins (Frontispiece 1; Plate 1), revealing the subsurface architecture necessary to understand their depositional and tectonic evolution. Although the succession in the Collier Basin, which is only present in the Wanna Syncline, is relatively thin (<0.25 s TWT; ~750 m), both basins are well imaged in line GA10–CP2 (Fig. 10). The maximum thickness of the Edmund Basin is 2.25 s TWT (~6.75 km) on the southern side of the Godfrey Fault. A relatively large package, up to 1 s TWT (~3 km) thick, of highly seismically reflective material occurs between the base of Package 2 and the top of Package 4 (Fig. 10); these reflections are interpreted to be abundant dolerite sills of the c. 1465 Ma Narimbunna Dolerite and c. 1070 Ma Kulkatharra Dolerite, which intrude the upper parts of the Edmund Basin (Cutten et al., 2011).

Three principal structures, the Talga, Godfrey, and Lyons River Faults, appear to have controlled the depositional architecture of the Edmund Basin (Fig. 10). Extensional movement on these faults formed three half graben structures, into which sediments of the Edmund Basin were deposited (Martin and Thorne, 2004), and across which significant sediment thickness variations are evident. On the Pingandy Shelf, to the north of the Talga Fault (Fig. 10), the maximum thickness of Packages 1 and 2 are ~0.5 s TWT (~1.5 km), whereas to the south they increase to ~1.25 s TWT (~3.75 km). Across the Godfrey Fault, Packages 1 and 2 increase from 2.0 s TWT (~6 km) to >2.75 s TWT (~8.25 km) thick. Packages 1 and 2 are consistently thicker in the hangingwall of the basin-bounding extensional faults, suggesting that extensional downthrow on these major faults was toward the southwest. Packages 1 and 2 are not present south of CDP 8300, presumably having been incised and eroded away prior to the deposition of Packages 3 and 4 (Martin et al., 2008; Cutten et al., 2011). In this region, Package 3 is at least 1 s TWT (~3km) thick.

Between the Godfrey Fault (CDP 6575) and the Edmund Fault (CDP 9465), the Edmund Basin (Package 3) is intensely folded, with numerous imbricate thrust faults truncating the limbs of the tight, upright folds (Fig. 10). This corridor of intense deformation has been mapped in the surface geology (Frontispiece 1; Plate 1), and does not appear to have significantly affected rocks of the Collier Basin, suggesting either that the deformation is related to the pre- Collier Basin, 1385–1200 Ma Mutherbukin Tectonic Event, or that the Godfrey Fault acted as a backstop to the northward-propagating thrust system during the 1030–955 Ma Edmundian Orogeny.

The seismic data show that the depositional architecture and subsequent structural inversion of the Edmund Basin was controlled by pre-existing major crustal structures in the underlying Gascoyne Province. Reactivation of these structures as extensional faults accommodated the deposition of the sediments in the Edmund Basin, whereas subsequent reactivation as thrust faults inverted the basin.

Summary

Figure 8 (also see Plate 2) shows a complete cross section through the Gascoyne Province, based on the interpretation of seismic reflection data presented in lines 10GA–CP2 (Fig. 1) and 10GA–CP3 (Fig. 2). The main suture zones are shown to be the Lyons River Fault, separating the Pilbara Craton – Bandee Seismic Province from the Glenburgh Terrane, and the Errabiddy Shear Zone – Cardilya Fault, which separates the Glenburgh Terrane from the Narryer Terrane (Yilgarn Craton). Therefore, the West Australian Craton can be shown to consist of three separate tectonic units, juxtaposed at two suture zones, as originally proposed by Occhipinti et al. (2004), Sheppard et al. (2004), and Johnson et al. (2011b). Plutonic rocks of the 1820–1775 Ma Moorarie Supersuite and 1680–1620 Ma Durlacher Supersuite are imaged in the upper crust of the Glenburgh Terrane and Bandee Seismic Province (Fig. 8). At the northern end of line 10GA–CP2 (Fig. 8), the depositional architecture of the Edmund and Collier Basins has also been resolved, and indicates that deposition of these basins was controlled by the reactivation of older, crustal-scale faults.

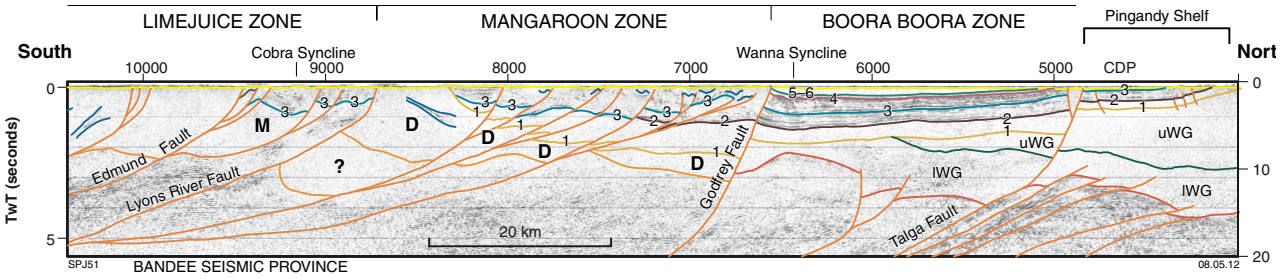

Figure 10. Interpreted migrated seismic section of part of line 10GA–CP2, showing the extent of the Edmund Basin. The base of individual packages of the Edmund Group are also shown. Abbreviations used: M — Moorarie Supersuite; D — Durlacher Supersuite; IWG — lower Wyloo Group ; uWG — upper Wyloo Group

References

Abdulah, A 2007, Seismic body wave attenuation tomography beneath the Australasian region: Australian National University, Canberra, Australian Capital Territory, PhD thesis (unpublished), 163p.

Cawood, PA and Tyler, IM 2004, Assembling and reactivating the Proterozoic Capricorn Orogen: lithotectonic elements, orogenies, and significance: Precambrian Research, v. 128, p. 201–218.

Cutten, HN, Thorne, AM and Johnson, SP 2011, Geology of the Edmund and Collier Groups, *in* Capricorn Orogen seismic and magnetotelluric (MT) workshop 2011: extended abstracts *edited by* SP Johnson, AM Thorne and IM Tyler: Geological Survey of Western Australia, Record 2011/25, p. 41–48.

Hackney, R 2004, Gravity anomalies, crustal structure and isostasy associated with the Proterozoic Capricorn Orogen, Western Australia: Precambrian Research, v. 128, no. 3–4, p. 219–236, doi: 10.1016/j.precamres.2003.09.012.

Johnson, SP, Sheppard, S, Rasmussen, B, Wingate, MTD, Kirkland, CL, Muhling, JR, Fletcher, IR and Belousova, E 2010, The Glenburgh Orogeny as a record of Paleoproterozoic continent–continent collision: Geological Survey of Western Australia, Record 2010/5, 54p.

Johnson, SP, Thorne, AM, Cutten, HN, Tyler, IM and Blay, O 2011a, Geology of the Gascoyne Province, in Capricorn Orogen seismic and magnetotelluric (MT) workshop 2011: extended abstracts *edited by* SP Johnson, AM Thorne and IM Tyler: Geological Survey of Western Australia, Record 2011/25, p. 27–40.

Johnson, SP, Sheppard, S, Rasmussen, B, Wingate, MTD, Kirkland, CL, Muhling, JR, Fletcher, IR and Belousova, EA 2011b, Two collisions, two sutures: punctuated pre-1950 Ma assembly of the West Australian Craton during the Ophthalmian and Glenburgh Orogenies: Precambrian Research, v. 189, no. 3–4, p. 239–262, doi: 10.1016/j.precamres.2011.07.011.

Johnson, SP, Sheppard, S, Wingate, MTD, Kirkland, CL and Belousova, EA 2011c, Temporal and hafnium isotopic evolution of the Glenburgh Terrane basement: an exotic crustal fragment in the Capricorn Orogen: Geological Survey of Western Australia, Report 110, 27p.

Kennett, BLN 2011, Understanding the lithosphere in the vicinity of the Capricorn seismic lines from passive seismic studies, *in* Capricorn Orogen seismic and magnetotelluric (MT) workshop 2011: extended abstracts *edited by* SP Johnson, AM Thorne and IM Tyler: Geological Survey of Western Australia, Record 2011/25, p. 101–107.

Kennett, BLN, Tyler, IM, Maher, J, Holzschuh, J, Fomin, T and Costelloe, RD 2011, The Capricorn seismic survey: experimental design, acquisition, and processing, *in* Capricorn Orogen seismic and magnetotelluric (MT) workshop 2011: extended abstracts *edited by* SP Johnson, AM Thorne and IM Tyler: Geological Survey of Western Australia, Record 2011/25, p. 1–6.

Korsch, RJ, Johnson, SP, Tyler, IM, Thorne, AM, Blewett, RS, Cutten, HN, Joly, A, Dentith, MC, Aitken, ARA, Goodwin, JA and Kennett, BLN 2011, Geodynamic implications of the Capricorn deep seismic survey: from the Pilbara Craton to the Yilgarn Craton, *in* Capricorn Orogen seismic and magnetotelluric (MT) workshop 2011: extended abstracts *edited by* SP Johnson, AM Thorne and IM Tyler: Geological Survey of Western Australia, Record 2011/25, p. 107–114.

Martin, DM, Li, ZX, Nemchin, AA and Powell, CM 1998, A pre-2.2 Ga age for giant hematite ores of the Hamersley Province, Australia: Economic Geology, v. 93, p. 1084–1090.

Martin, DM, Sircombe, KN, Thorne, AM, Cawood, PA and Nemchin, AA 2008, Provenance history of the Bangemall Supergroup and implications for the Mesoproterozoic paleogeography of the West Australian Craton: Precambrian Research, v. 166, no. 1–4 (Assembling Australia: Proterozoic building of a continent), p. 93–110.

Martin, DM and Morris, PA 2010, Tectonic setting and regional implications of ca 2.2 Ga mafic magmatism in the southern Hamersley Province, Western Australia: Australian Journal of Earth Sciences, v. 57, no. 7, p. 911–931.

Martin, DM and Thorne, AM 2004, Tectonic setting and basin evolution of the Bangemall Supergroup in the northwestern Capricorn Orogen: Precambrian Research, v. 128, p. 385–409.

Occhipinti, SA, Sheppard, S, Passchier, C, Tyler, IM and Nelson, DR 2004, Palaeoproterozoic crustal accretion and collision in the southern Capricorn Orogen: the Glenburgh Orogeny: Precambrian Research, v. 128, p. 237–255.

Reading, AM, Tkalčić, H, Kennett, BLN, Johnson, SP, Sheppard, S 2012, Seismic structure of the crust and uppermost mantle of the Capricorn and Paterson Orogens and adjacent cratons, Western Australia, from passive seismic transects: Precambrian Research, v. 196–197, p. 295–308.

Selway, K 2008, Magnetotelluric investigation into the electrical structure of the Capricorn Orogen, Western Australia: Geological Survey of Western Australia, Record 2007/16, 39p.

Selway, K, Sheppard, S, Thorne, AM, Johnson, SP and Groenewald, PB 2009, Identifying the lithospheric structure of a Precambrian orogen using magnetotellurics: the Capricorn Orogen, Western Australia: Precambrian Research, v. 168, p. 185–196.

Sheppard, S, Johnson, SP, Wingate, MTD, Kirkland, CL and Pirajno, F 2010, Explanatory Notes for the Gascoyne Province: Geological Survey of Western Australia, Perth, Western Australia, 336p.

Sheppard, S, Occhipinti, SA and Nelson, DR 2005, Intracontinental reworking in the Capricorn Orogen, Western Australia: the 1680–1620 Ma Mangaroon Orogeny: Australian Journal of Earth Sciences, v. 52, p. 443–460.

Sheppard, S, Occhipinti, SA and Tyler, IM 2004, A 2005–1970 Ma Andean-type batholith in the southern Gascoyne Complex, Western Australia: Precambrian Research, v. 128 (Assembling the Palaeoproterozoic Capricorn Orogen), p. 257–277.

Sheppard, S, Occhipinti, SA and Tyler, IM 2003, The relationship between tectonism and composition of granitoid magmas, Yarlarweelor Gneiss Complex, Western Australia: Lithos, v. 66, p. 133–154.

Thorne, AM, Tyler, IM, Korsch, RJ, Johnson, SP, Brett, JW, Cutten, HN, Blay, O, Kennett, BLN, Blewitt, RS, Joly, A, Dentith, MC, Aitken, ARA, Holzschuh, J, Goodwin, JA, Salmon, M, Reading, A and Boren, G 2011a, Preliminary interpretation of deep seismic reflection line 10GA–CP1: crustal architecture of the northern Capricorn Orogen, *in* Capricorn Orogen seismic and magnetotelluric (MT) workshop 2011: extended abstracts *edited by* SP Johnson, AM Thorne and IM Tyler: Geological Survey of Western Australia, Record 2011/25, p. 19–26.

Thorne, AM, Johnson, SP, Tyler, IM, Cutten, HN and Blay, O 2011b, Geology of the northern Capricorn Orogen, *in* Capricorn Orogen seismic and magnetotelluric (MT) workshop 2011: extended abstracts *edited by* SP Johnson, AM Thorne and IM Tyler: Geological Survey of Western Australia, Record 2011/25, p. 7–18.

Tyler, IM 1991, The geology of the Sylvania Inlier and southeast Hamersley Basin: Western Australia Geological Survey, Bulletin 138, 108p.

Potential-field interpretation of the Capricorn Orogen, Western Australia: worms, forward modelling, and 3D inversion

by

JA Goodwin[1]

Introduction

The deep seismic lines 10GA–CP1, 10GA–CP2, and 10GA–CP3, collected across the Capricorn Orogen by AuScope, the Geological Survey of Western Australia (GSWA), and Geoscience Australia (GA) (Kennett et al., 2011), extend from the Pilbara Craton in the north, across the Capricorn Orogen, to the Yilgarn Craton in the south. The aim of these seismic lines was to provide insight into the geological structure of the Capricorn Orogen, and to explore its relationship with the Pilbara and Yilgarn Cratons. To further aid interpretation, and to add value to the seismic data, an analysis of the potential-field data (gravity and magnetics) was also undertaken using a range of geophysical data analysis techniques. These consist of: multiscale edge detection (worms), forward modelling, and 3D inversion. By applying all three analysis techniques to the potential-field data, a number of geophysical terranes, major trends, and contrasting properties relating to the subsurface geology have been identified, allowing for a detailed comparison with the seismic interpretations provided by Thorne et al. (2011) and Johnson et al. (2011).

Interpretation techniques

All interpretation techniques were performed on gravity data extracted from the 3rd edition of the Gravity Anomaly Map of Australia (Bacchin et al., 2008), and on magnetic data extracted from the 5th edition of the Magnetic Anomaly Map of Australia (Milligan et al., 2010), with a variable reduction to the pole (RTP) applied.

Multiscale edge detection (worms)

Multiscale edge detection is a technique used to highlight areas of contrast in potential-field data (Archibald et al., 1999). These areas of contrast are represented as edges, referred to as worms, which are generated across a range of levels of upward continuation. When viewed together, the worms form 3D surfaces whose shapes and orientations are related to contrasting properties in the subsurface geology. Property contrasts in potential-field data are often the result of discontinuities or interfaces where contrasting rock materials occur, such as at faults, unconformities, or intrusive contacts.

Worms were generated for the Capricorn Orogen data using the multiscale edge detection function in Intrepid software (version 4.2.3). For both gravity and magnetic grids, 12 upward continuation levels, with each level varying by a factor of 1.4, were specified using the Canny points calculation method. A variable reduction to the pole (RTP) was applied to the magnetic grid before multiscale edge detection was undertaken. Features in the worms were delineated following the methods of Archibald et al. (1999) and Holden et al. (2000), who infer that higher continuation levels correspond to features at relatively greater depths, and that worm orientations relate to the orientation of contacts.

2.5D Forward modelling

2.5D forward modelling was carried out to test the validity of the interpreted seismic sections in relation to the magnetic and gravity data. 2.5D modelling is the process of modelling two-dimensional bodies in a three-dimensional space, by extending the strike length of a body to a distance that is large enough, perpendicular to the section, to avoid edge effects. Rock properties (density and magnetic susceptibility) are added to the interpreted bodies, and the modelled magnetic and gravity response is then compared to the observed response. A good fit between the modelled and observed indicates that the interpreted seismic sections are consistent with the magnetic and gravity data.

Gravity and magnetic data were extracted along the seismic line traverses using the dataset resampler tool in Intrepid. 2.5D forward models were then created using ModelVision v11.0 software, extending from 600 m above to 60 km below the datum. To better approximate the 3D nature of the bodies in a 2D environment, the models

1 Minerals and Natural Hazards Division, Geoscience Australia, GPO Box 378, Canberra ACT 2601.

were extended 120 km in strike length (60 km on either side of the line) and 60 km beyond the ends of the seismic line to avoid edge effects. For both gravity and magnetic data, an initial model was produced where the geometries identified in the seismic interpretation were used to constrain the architecture, and only the rock properties (density and magnetic susceptibility) were adjusted to achieve a fit with the observed data. A modified model was also produced, with both geometry and rock properties adjusted to achieve a fit. Rock property data from Emerson (1990), Telford et al. (1990), and Clark and Emerson (1991) were used as guides to assign density and magnetic susceptibility values. The effects of remnant magnetization were ignored as they are generally considered a minor component of the observed signal. The scales shown on the forward models are in kilometres, and assume that one second of two-way travel time (TWT) is equal to three kilometres depth (based on an average crustal velocity of 6000 m/s).

3D inversion

Inversion is a mathematical process used for acquiring a set of parameters that both describe a model and are consistent with a set of observations. In this case, the observations are the gravity and magnetic data, and the parameters describing the model are density and magnetic susceptibility, respectively.

3D inversions were performed with the University of British Columbia – Geophysical Inversion Facility's (UBC–GIF) inversion software — particularly the GRAV3D (version 3) and MAG3D (version 4) program libraries. The gravity and magnetic inversion methods outlined by Li and Oldenburg (1996, 1998) were used; however, the process of model-based trend removal has only been undertaken for the gravity data, not for the magnetic data. Inversions were performed at the National Computational Infrastructure (NCI) supercomputer facility (hosted by the Australian National University) with parallelized UBC–GIF software. For the magnetic inversions, a Curie Depth of 32 km was determined (assuming a Curie Temperature of 580°C), using a thermal conductivity estimate of 2.5 W/mK (Beardsmore and Cull, 2001, fig. 4.1.) and a heat flow of 45 mW/m^2 (Cull and Denham, 1979). Finally, the geothermal gradient was estimated at 18°C/km following the equation: Q (surface heat flow) = β (geothermal gradient) × λ (thermal conductivity). The inversions presented here are unconstrained and, as a result, they are not influenced by the seismic line interpretation or the surface geology. This also ensures that they are free from user bias.

Geophysical interpretation

Seismic line 10GA–CP1

The northern end of seismic line 10GA–CP1 is dominated by high-amplitude, short-wavelength magnetic anomalies, and high-amplitude gravity anomalies, both associated with banded iron-formations of the Hamersley Group (Fig. 1a,b). The Hamersley Group outcrops along the seismic line at the Turner Syncline, which is flanked on either side by a smooth textured, magnetic low correlating with the basalt-dominated Fortescue Group (Fig. 1a,c). Overprinting areas of the Fortescue Group are magnetic haloes, such as those seen between approximately CDPs 4100 and 5300, which correspond to the folded and faulted margins of the Rocklea Dome (Fig. 1a). Together, these features define a terrane separated from the southern end of the seismic line by the Nanjilgardy Fault.

A series of northwest-trending lineaments, observed in the magnetic data at the southern end of the seismic line, can be seen to overprint a broad wavelength, ovoid magnetic high (Fig. 1a). These lineaments are continuous, and can be traced northwest to outcrops of Leake Spring Metamorphics (Fig. 1a,c), which are inferred to be a correlative of the upper Wyloo Group (Cawood and Tyler, 2004; Sheppard et al., 2007). This interpretation is supported by the magnetic data, where irregularly shaped, high-amplitude anomalies coincide with outcrops of the Leake Spring Metamorphics before becoming increasingly linear, with lower amplitude responses, as they grade into the upper Wyloo Group to the southeast (Fig. 1a).

The Turner and Hardey Synclines, in the north of the study area, are visible in the both the gravity and magnetic worms, with upward continuation heights of 1400–28 930 m (Fig. 2). This suggests that the Hamersley Group is the dominant source of magnetic and gravity anomalies at the northern end of the seismic line. The large ovoid magnetic high identified in the magnetic data is delineated by magnetic worms in the south, with upward continuation levels of 14 760–56 703 m, which extend to outcrops of the Hamersley Group towards the northwest. The extension of these worms may indicate that this large ovoid magnetic high is related to the Hamersley Group. Approximately from CDPs 5500 to 6000, gravity worms, with upward continuation levels of 3842–56 703 m, define a southwest-dipping contact, possibly related to contrasting densities below the Fortescue Group, where south-dipping layers are observed in the seismic data (Thorne et al., 2011).

The Hamersley Group heavily influences both the 3D magnetic and gravity inversions, with a region of high magnetic susceptibility (≥0.1 SI) and high density (≥0.05 g/cm^3) occurring approximately between CDPs 3000 to 4000, and extending down to 15 km depth (Fig. 3). This body relates to the Turner Syncline, and has been forward modelled with a magnetic susceptibility of 0.20 – 0.40 SI and a thickness of approximately 2.5 km to match the seismic interpretation (Fig. 4; Thorne et al., 2011). As the effect of remnant magnetization in the Hamersley Group significantly increases the observed magnetic anomalies (Guo et al., 2011), only the shape of the wavelength has been matched by the forward model, not the amplitude.

Another region of high magnetic susceptibility (≥0.1 SI) and high density (≥0.05 g/cm^3) is observed between CDPs 6200 and 6800 in the magnetic inversion, and between CDPs 5500 and 6300 in the gravity inversion (Fig. 3). These anomalies are sourced from high density, high magnetic susceptibility rocks of the Hardey Syncline, which are located off the seismic line (see surface geology; Fig. 1c). As a result, this body has not been included in the forward modelling.

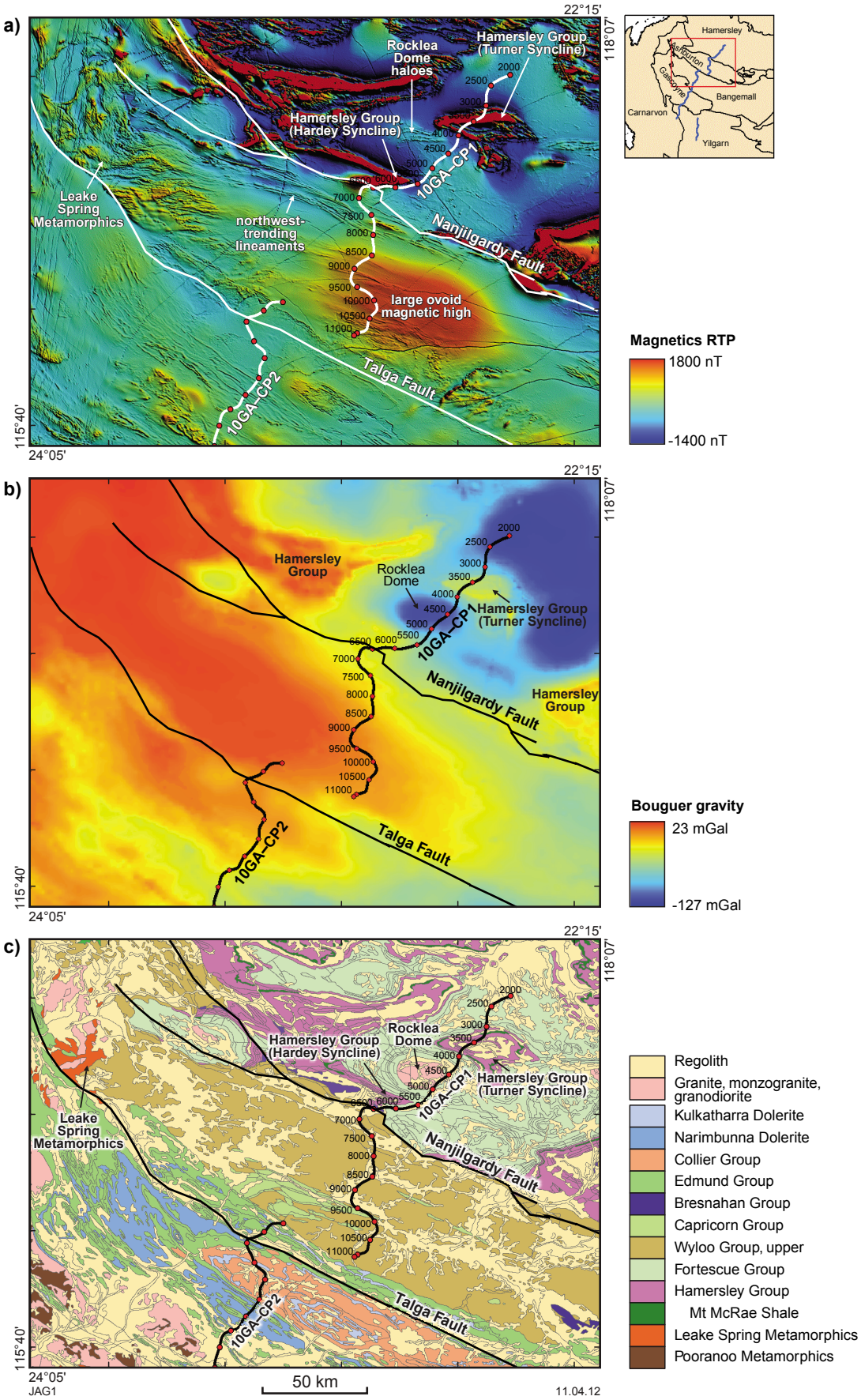

Figure 1. **a) Magnetic grid RTP (with values outside the 98th percentile removed, and sun shading from the northeast applied to highlight contrast in the data); b) bouguer gravity grid; c) 1:1 000 000 scale surface geology map covering seismic line 10GA–CP1.**

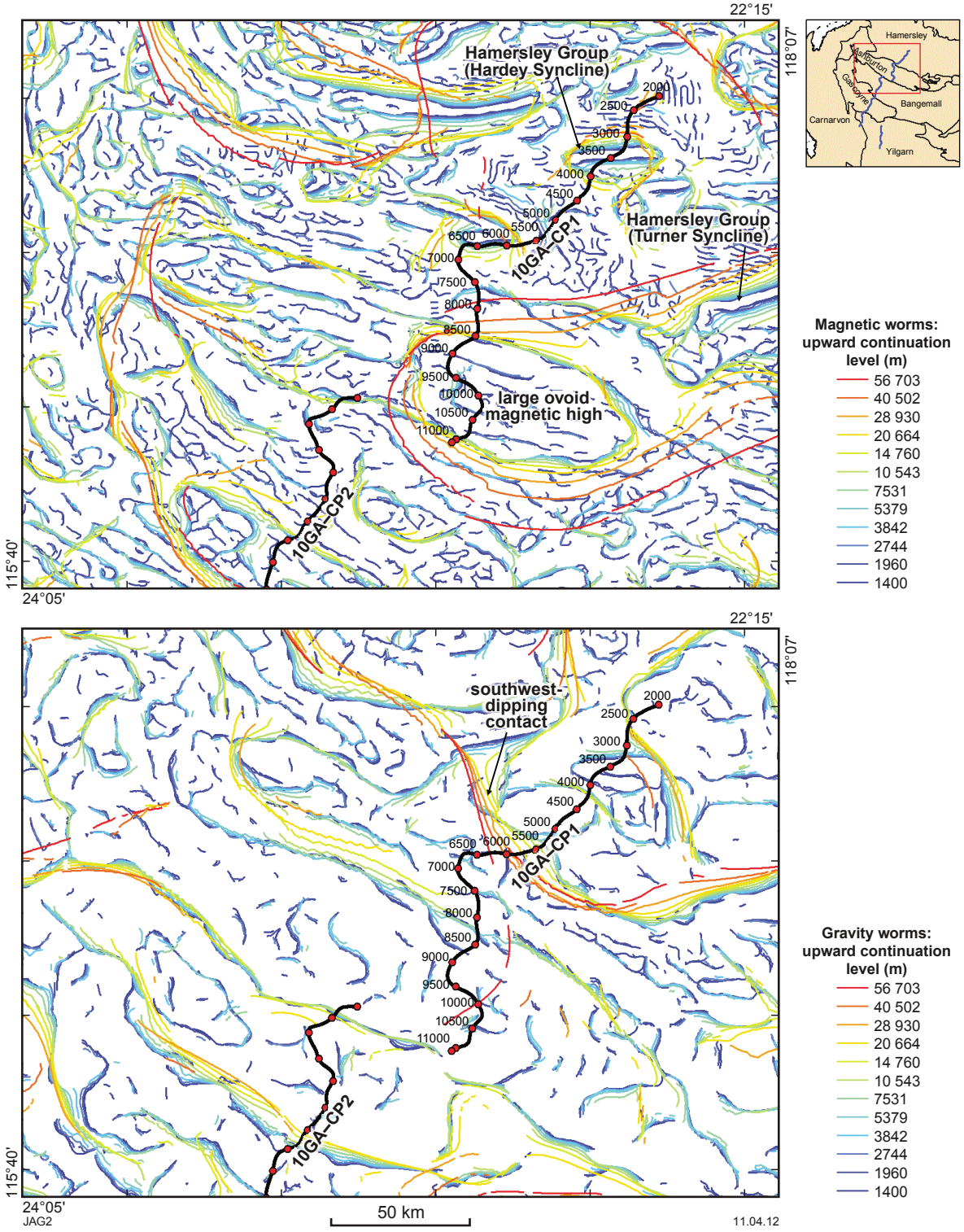

Figure 2. Worm images, covering seismic line 10GA–CP1, for magnetic (a) and gravity (b) data.

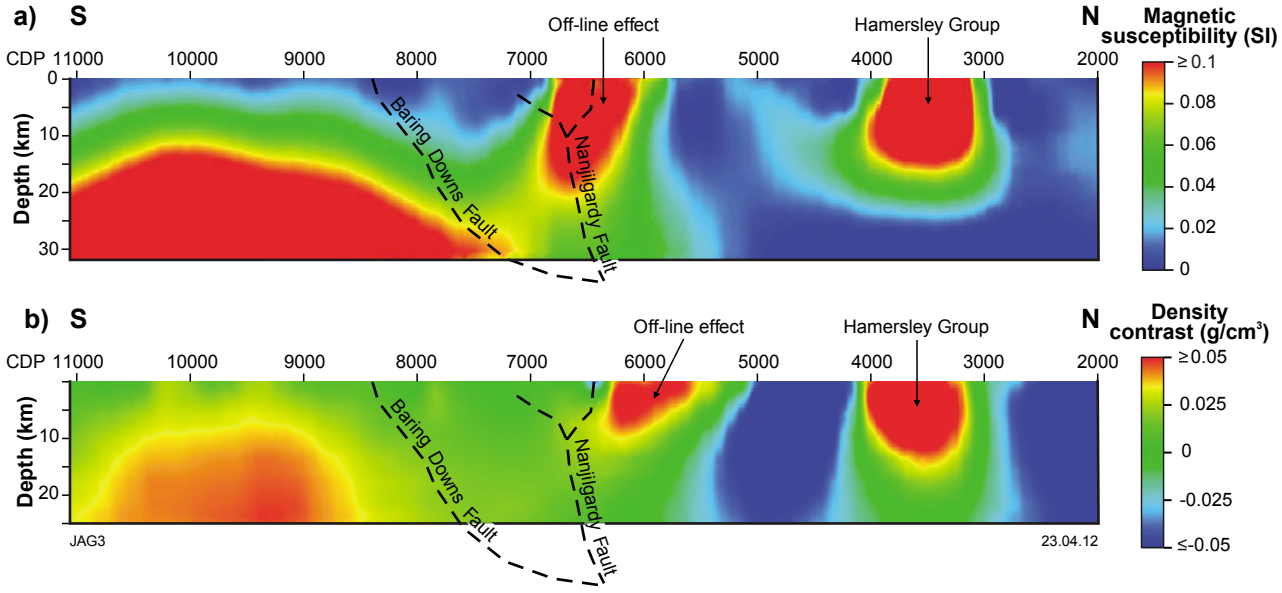

Figure 3. Inversion models extracted along seismic line 10GA–CP1: a) magnetic susceptibility model; b) density model.

At the southern end of seismic line 10GA–CP1, an upward doming body, ranging 12–25 km depth, and with a magnetic susceptibility of ≥0.1 SI, is observed in the magnetic inversion (Fig. 3). The northern margin of this magnetic body defines a north-dipping contact, consistent with the dip direction of the Baring Downs Fault, which itself is interpreted as a suture marking the southernmost extent of the granite–greenstone basement (Thorne et al., 2011). The gravity inversion also suggests that the Baring Downs Fault separates relatively denser units in the south from less dense units in the north (Fig. 3).

Two separate seismic interpretations have been suggested by Thorne et al. (2011) for seismic line 10GA–CP1, and these geometries have been used to create two different forward models — the initial interpretation (Fig. 4a) has a thicker Bandee Seismic Province, whereas the alternative interpretation (Fig. 4b) has the Hamersley and Fortescue Groups present above the Bandee Seismic Province (Fig. 4b). A third forward model, the modified interpretation, has also been created, in which the Hamersley Group in the south is closer to the surface than in the initial or alternative interpretations (Fig. 4c).

A regional gravity low, reaching −100 mGal, is observed at the northern end of the seismic line coinciding with the Pilbara Craton granite–greenstone terrane, and is forward modelled with densities of 2.60 – 2.72 g/cm^3 (Fig. 4). Nested within this gravity low is a broad-wavelength gravity high, reaching −43 mGal, associated with the overlying Hamersley Group (3.20 g/cm^3). The Hamersley Group itself has a short-wavelength gravity low nested within it, caused by a thin succession of the overlying Turee Creek Group (2.80 g/cm^3; Fig. 4).

Towards the southern end of seismic line 10GA–CP1, the regional gravity trend increases to −13 mGal, and this trend has been accounted for in the initial interpretation by attributing a density of 2.90 g/cm^3 to the Bandee Seismic Province (Fig. 4a). In both the alternative and modified interpretations (Fig. 4b,c), this increase in the gravity trend is accounted for by the Hamersley (3.20 g/cm^3) and Fortescue (2.90 g/cm^3) Groups. This increase in gravity also coincides with an increase in the regional magnetic trend, which peaks at 1250 nT in this area. This trend is accounted for by the Bandee Seismic Province (0.08 SI) in the initial interpretation, and by the Hamersley Group (0.10 – 0.20 SI) in the alternative and modified interpretations (Fig. 4). The regional magnetic high is best accounted for by the modified interpretation due to the upward doming geometry of the Hamersley Group (Fig. 4c). Of the three forward models presented here, the initial and modified models, seen in Figures 4a and 4c, respectively, show the best fit with the gravity and magnetic anomalies observed along the seismic line 10GA–CP1.

Seismic line 10GA–CP2

The Edmund Group covers the northern end of seismic line 10GA–CP2 and is intruded by sills of Narimbunna Dolerite (Cutten et al., 2011). These dolerite sills appear as northwest-trending undulations and cause short-wavelength magnetic anomalies throughout the extent of the Edmund Group (Fig. 5a). Mottled and irregular magnetic textures, associated with high-amplitude magnetic anomalies, are observed crossing the seismic line from CDPs 8000 to 8600 and from CDPs 9500 to 14000 (Fig. 5a), coinciding with outcrops of the Leake Spring Metamorphics (Fig. 5c). The Leake Spring Metamorphics are variably intruded and deformed by granites of the Moorarie and Durlacher Supersuites, which developed magnetic contact metamorphic aureoles. The bouguer gravity grid highlights high-amplitude anomalies

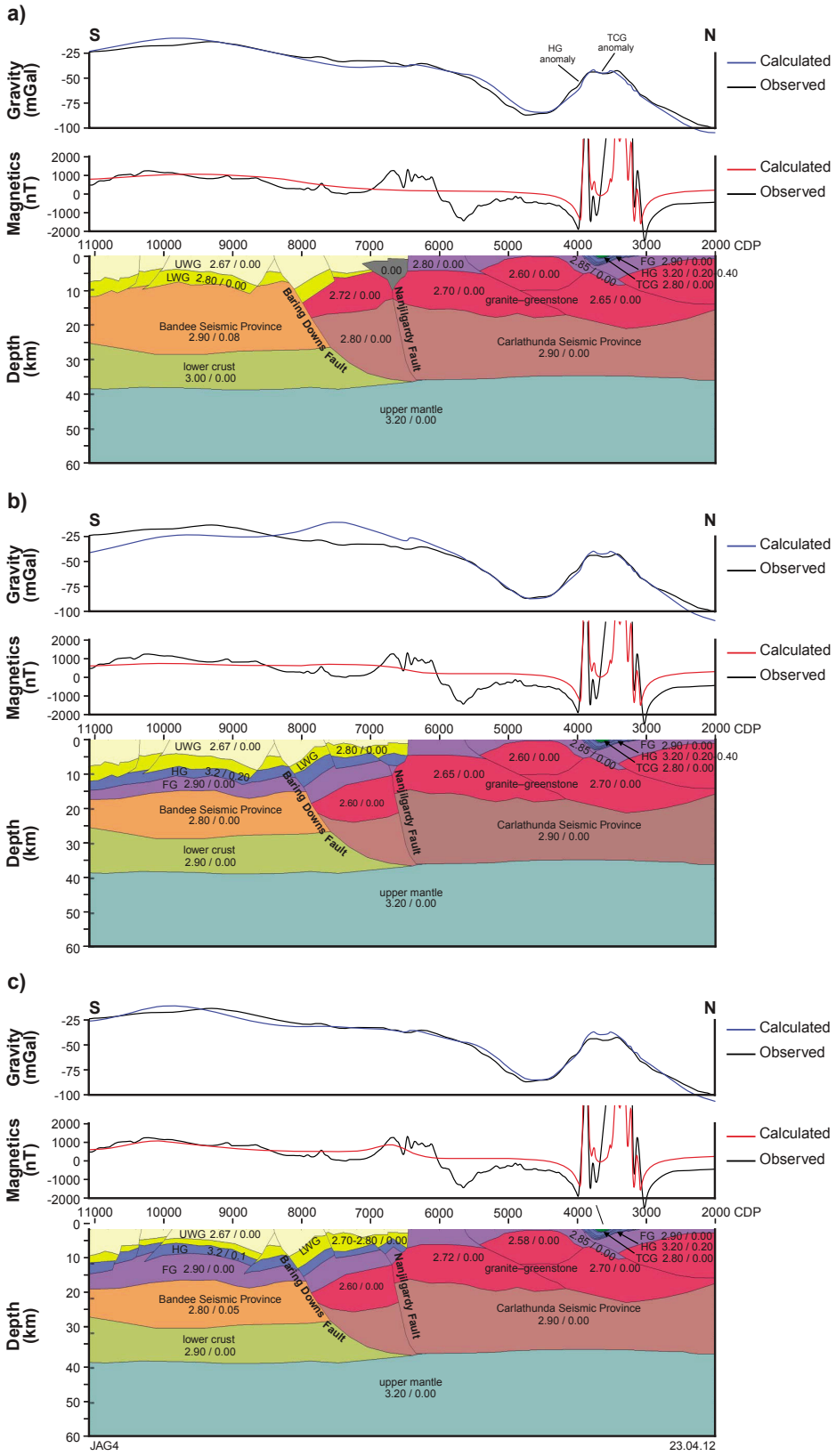

Figure 4. **Forward models for seismic line 10GA–CP1: a) initial interpretation using geometries described by Thorne et al. (2011); b) alternative interpretation using geometries described by Thorne et al. (2011); c) modified model, with the Hamersley Group in the south interpreted to be closer to the surface than in (b). Note that the outcropping Hamersley Group anomalies (between CDPs 3000 and 4000) exceed 5000 nT; to highlight variation in the southern section of the line, the scale for the observed magnetic profile was therefore set to a maximum of 3000 nT. Rock property values are listed on the figure as density (g/cm^3) / magnetic susceptibility (SI). Abbreviations used: FG — Fortescue Group; HG — Hamersley Group; TCG — Turee Creek Group; LWG — lower Wyloo Group; UWG — upper Wyloo Group.**

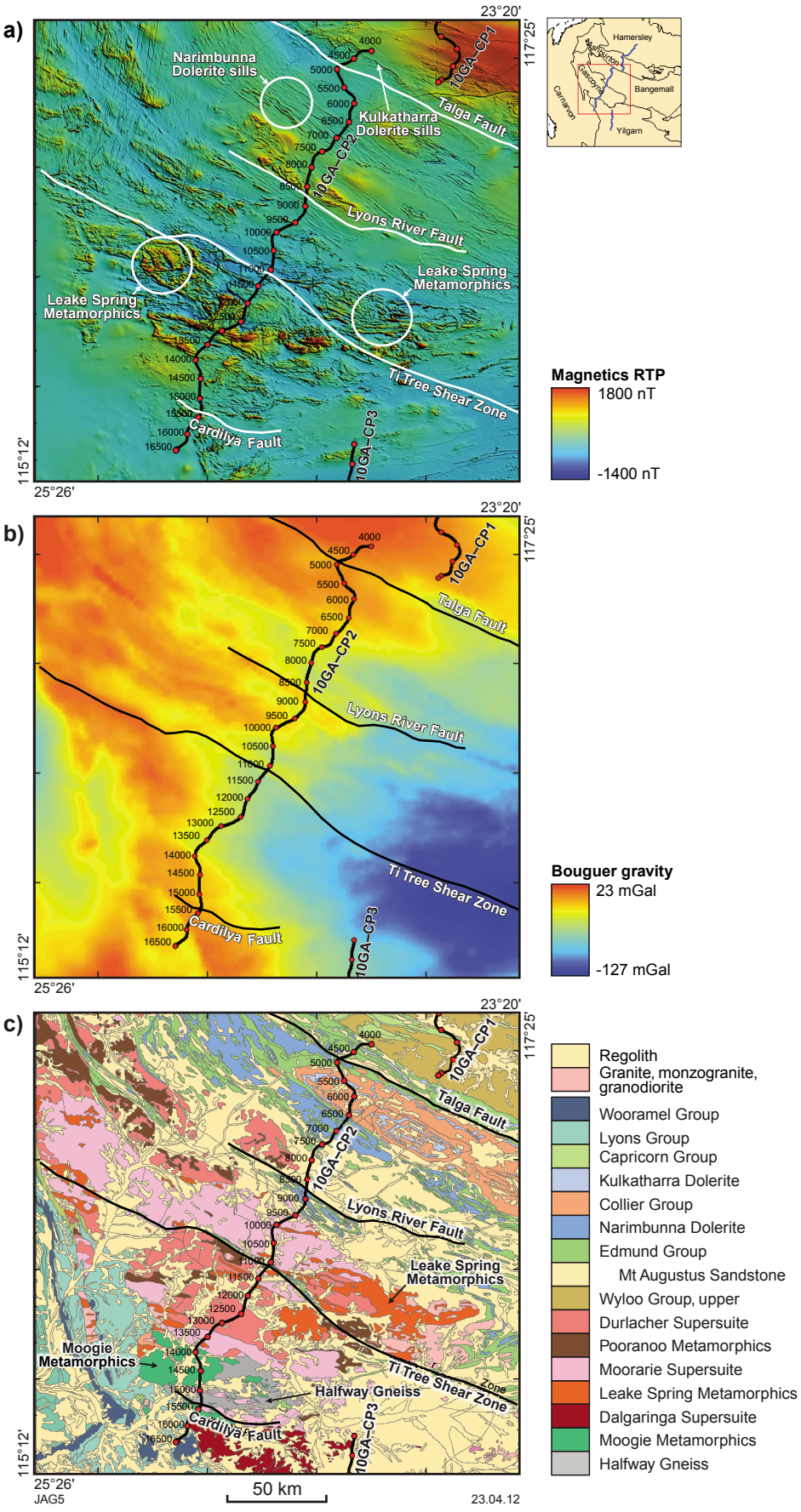

Figure 5. **a) Magnetic grid RTP (with values outside the 98th percentile removed, and sun shading from the northeast applied to highlight contrast in the data); b) bouguer gravity grid; c) 1:1 000 000 scale surface geology map covering seismic line 10GA–CP2.**

extending from the northwest, which splay out into fingers across seismic line 10GA–CP2, before grading into a regional gravity low in the southeast (Fig. 5b).

Three magnetic worms defining southwest-dipping contacts have been identified between CDPs 8600 to 9000, CDPs 11600 to 12000, and CDPs 14700 to 14900 (Fig. 6a). These contacts coincide with the Lyons River Fault, an unnamed fault, and the Cardilya Fault, respectively (Johnson et al., 2011), and suggest that these faults separate areas of contrasting magnetic susceptibility. In particular, the Lyons River and Cardilya Faults are suggested by Johnson et al. (2011) to be major sutures. Gravity worms, on the other hand, define a northeast-dipping contact between CDPs 7000 to 7500 (Fig. 6b), contradictory to the dominant southwest direction of faulting in this area, and perhaps related to a property contrast within or below the shallowly northwest-dipping layers of the Edmund Group.

The magnetic inversion defines a zone of relatively high magnetic susceptibility (0.04 – 0.07 SI) between CDPs 4000 and 10500, which correlates well with the interpreted extent of the Bandee Seismic Province (Fig. 7a). This zone also defines a south-dipping contact consistent with the Lyons River Fault, suggesting that this fault separates two areas of significantly different magnetic susceptibility. In the density inversion, four distinct low-density areas have been modelled at the surface, corresponding approximately with CDPs 8300, 9400, 10800, and 11500 (Fig. 7b). These areas correlate well with outcrops of granite and of the Mount Augustus Sandstone (Fig. 5c). A high density (≥0.05 g/cm^3), near-surface body located at CDPs 9000 is bound by the Lyons River Fault, and correlates well with the interpreted northernmost extent of the Glenburgh Terrane, as identified by Johnson et al. (2011).

Two forward models have been generated for seismic line 10GA–CP2; the first has geometries matched to the seismic interpretation from Johnson et al. (2011; Fig. 8a), and the second is a modified version, where extra detail has been added to produce a better fit with anomalies in the potential-field data (Fig. 8b).

The gravity profile of seismic line 10GA–CP2 peaks in the north with a high of −10 mGal (Fig. 8). Towards the centre of the line, a regional gravity low of −45 mGal is observed, and several short-wavelength, low-amplitude anomalies also occur, coinciding with granites of the Durlacher and Moorarie Supersuites (Fig. 8a,b). Areas where the Mount Augustus Sandstone outcrops also coincide with short-wavelength, low-amplitude gravity anomalies at CDPs 8300 and 9400 (Fig. 8b). Towards the southern end of the seismic line, another peak, of −20.5 mGal, occurs in the gravity data and has a broad-wavelength anomaly. This anomaly has been accounted for in the forward model by attributing densities of 2.78–2.80 g/cm^3 to the Glenburgh Terrane.

To increase the accuracy of the obtained models, a number of extra details were added to the interpretation provided by Johnson et al. (2011), including: the addition of dolerite sills within the Edmund Group to account for short-wavelength gravity and magnetic anomalies; the addition of the Leake Spring Metamorphics to account for short-wavelength, high-amplitude magnetic anomalies, particularly in the southern part of the seismic line; and the separation of the Moogie Metamorphics from the rest of the Glenburgh Terrane to account for the broad-wavelength gravity high (of −20.5 mGal) observed at the southern end of the seismic line (Fig. 8b).

Seismic line 10GA–CP3

The Dalgaringa Supersuite outcrops at the northern end of seismic line 10GA–CP3, and correlates with a smooth-textured region of magnetically low character that is overprinted by northeast-trending, short-wavelength anomalies at CDPs 6000–7500 (Fig. 9a,c). A similar magnetic character is seen at CDPs 7500–8000, although a northeast-trending gravity low is also observed in this area, corresponding with the extent of the Errabiddy Shear Zone (Fig. 9b). Beyond CDP 8000, the seismic line progresses into the Narryer Terrane, which is dominated by short-wavelength magnetic anomalies bearing a stippled texture. These magnetic anomalies correlate well with outcrops of the unit identified by the 1:1 000 000 scale Surface Geology Map of Australia as 'Banded Iron Formation 74257' (Raymond and Retter, 2010), which together form a regional fold, the hinge zone of which lies to the east of seismic line 10GA–CP3 (Fig. 9c).

The magnetic worms covering seismic line 10GA–CP3 delineate a major trend between CDPs 8000 and 9000, which at shallow upward continuation levels of 1400–5379 m, define a steeply north-dipping contact, before transitioning into a south-dipping contact at upward continuation levels of 7531–56 703 m (Fig. 10a). The position of these worms agree well with the northernmost extent of the Narryer Terrane as observed in the surface geology (Fig. 9a), and with the dip direction of faults in the seismic interpretation (Johnson et al., 2011). The gravity worms delineate another major trend at CDPs 6000, ranging from upward continuation levels of 1400–56 703 m, defining a steeply dipping undulating contact, possibly related to the Cardilya Fault (Fig. 10b).

The major feature observed in the magnetic inversion covering seismic line 10GA–CP3 is a high susceptibility (0.04 – 0.07 SI) body originating at the surface at CDP 8000, whose northern margin is south-dipping (Fig. 11a). This body coincides with the northern extent of the Narryer Terrane at the surface (Fig. 9c), and supports the interpretation of major south-dipping faults in the seismic data (Johnson et al., 2011). In particular, the high susceptibility body matches well with the dip direction of an unnamed fault, labelled 'Fault 1' in Figure 11. The gravity inversion also shows the Errabiddy Shear Zone, located between CDPs 7500 and 8000, as a low density (≤–0.05 g/cm^3) feature (Fig. 11b).

Following the interpretation of Johnson et al., (2011), an initial forward model was created for seismic line 10GA–CP3 (Fig. 12a). The initial interpretation separates part of the Dalgaringa Supersuite into sections, with density ranging from 2.60 – 2.75 g/cm^3, to account for the broad-wavelength gravity high of −52.2 mGal seen

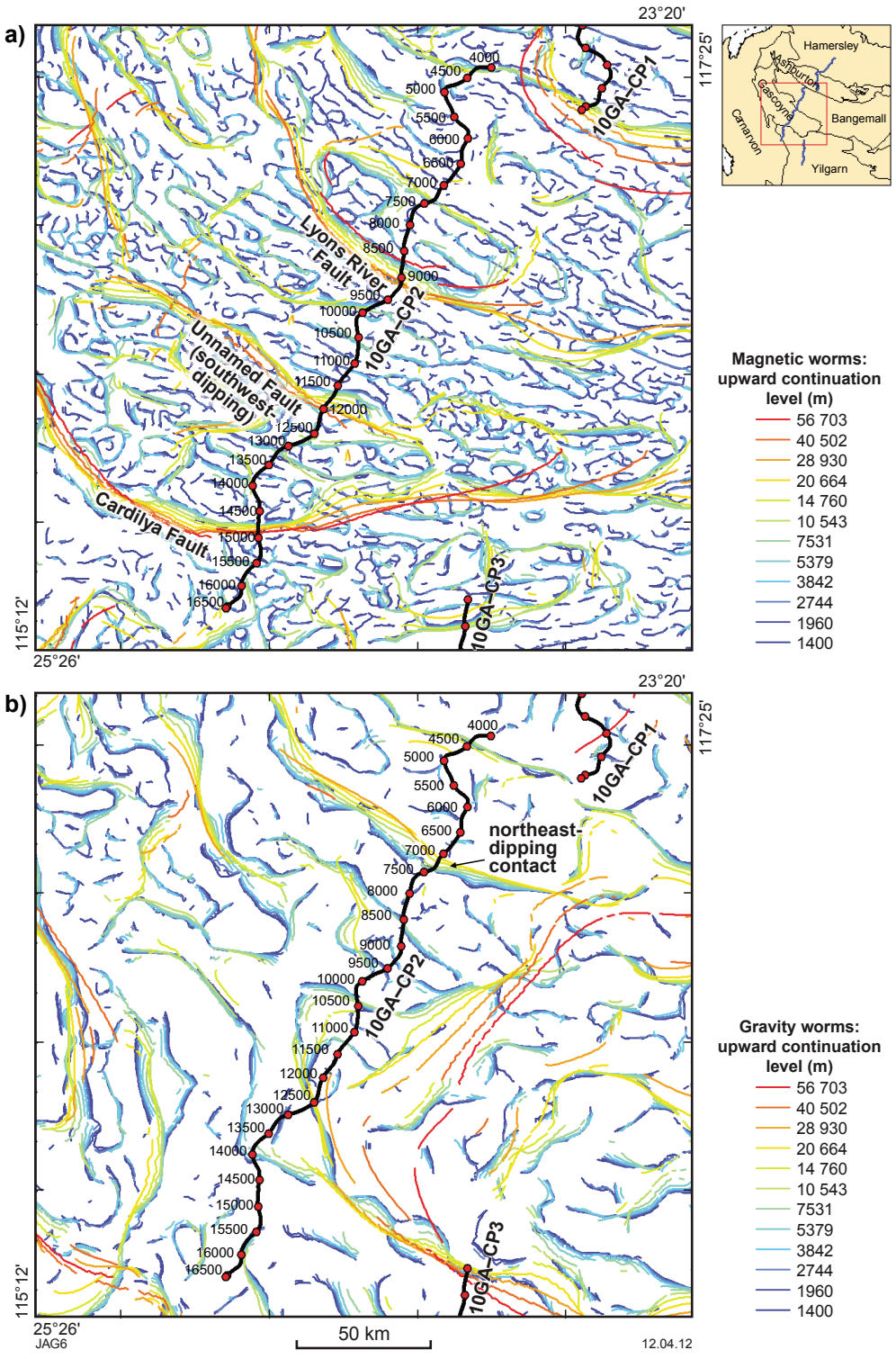

Figure 6. Worm images, covering seismic line 10GA–CP2, for magnetic (a) and gravity (b) data.

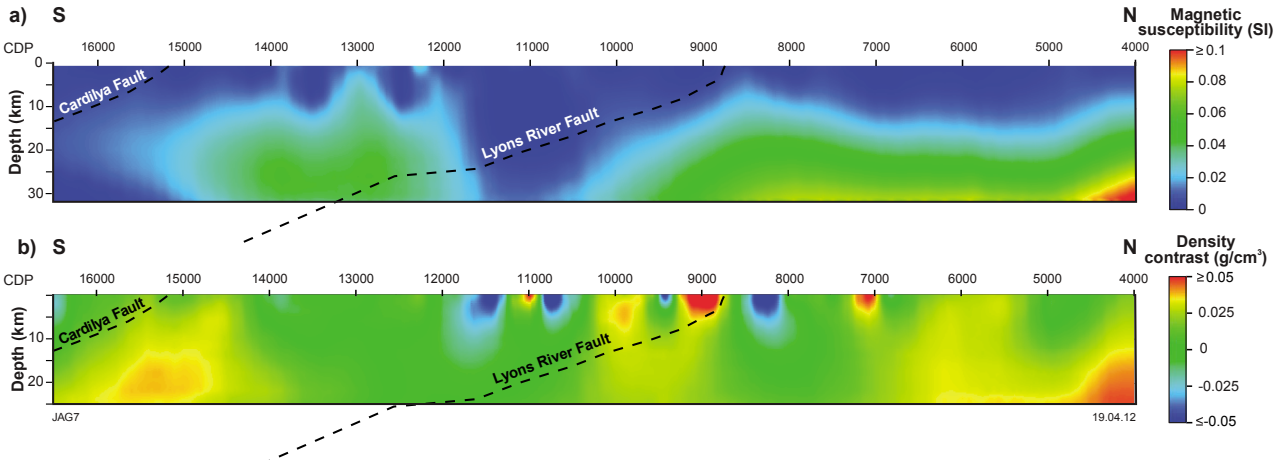

Figure 7. Inversion models extracted along seismic line 10GA–CP2: a) magnetic susceptibility model; b) density model.

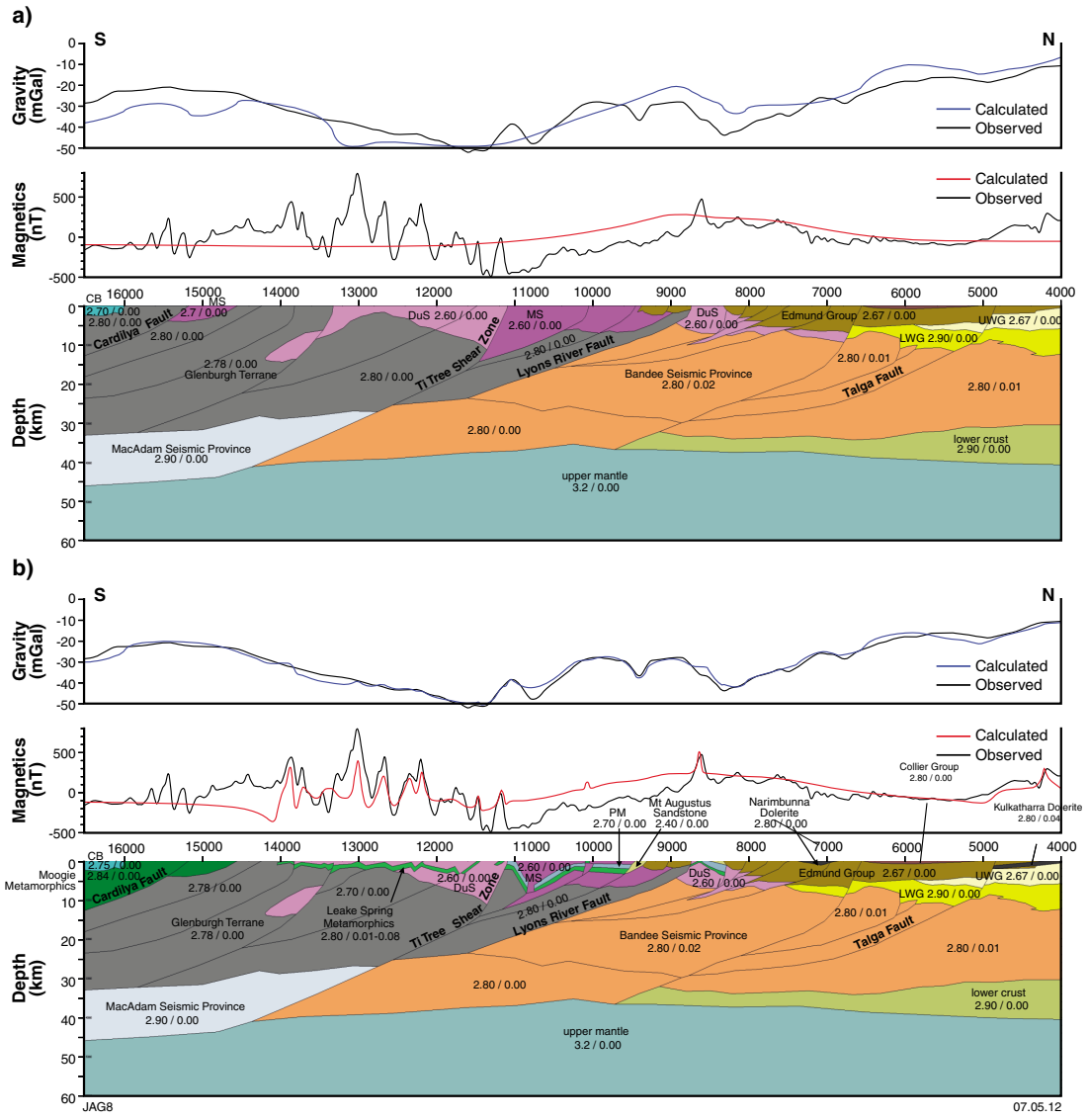

Figure 8. Forward models for seismic line 10GA–CP2: a) initial interpretation using geometries described by Johnson et al. (2011); and b) modified version of (a), altered to produce a better fit with the potential-field data. Rock property values are listed on the figure as density (g/cm³) / magnetic susceptibility (SI). Abbreviations used: PM — Pooranoo Metamorphics; MS — Moorarie Supersuite; DuS — Durlacher Supersuite; UWG — upper Wyloo Group; LWG — lower Wyloo Group; CB — Carnarvon Basin.

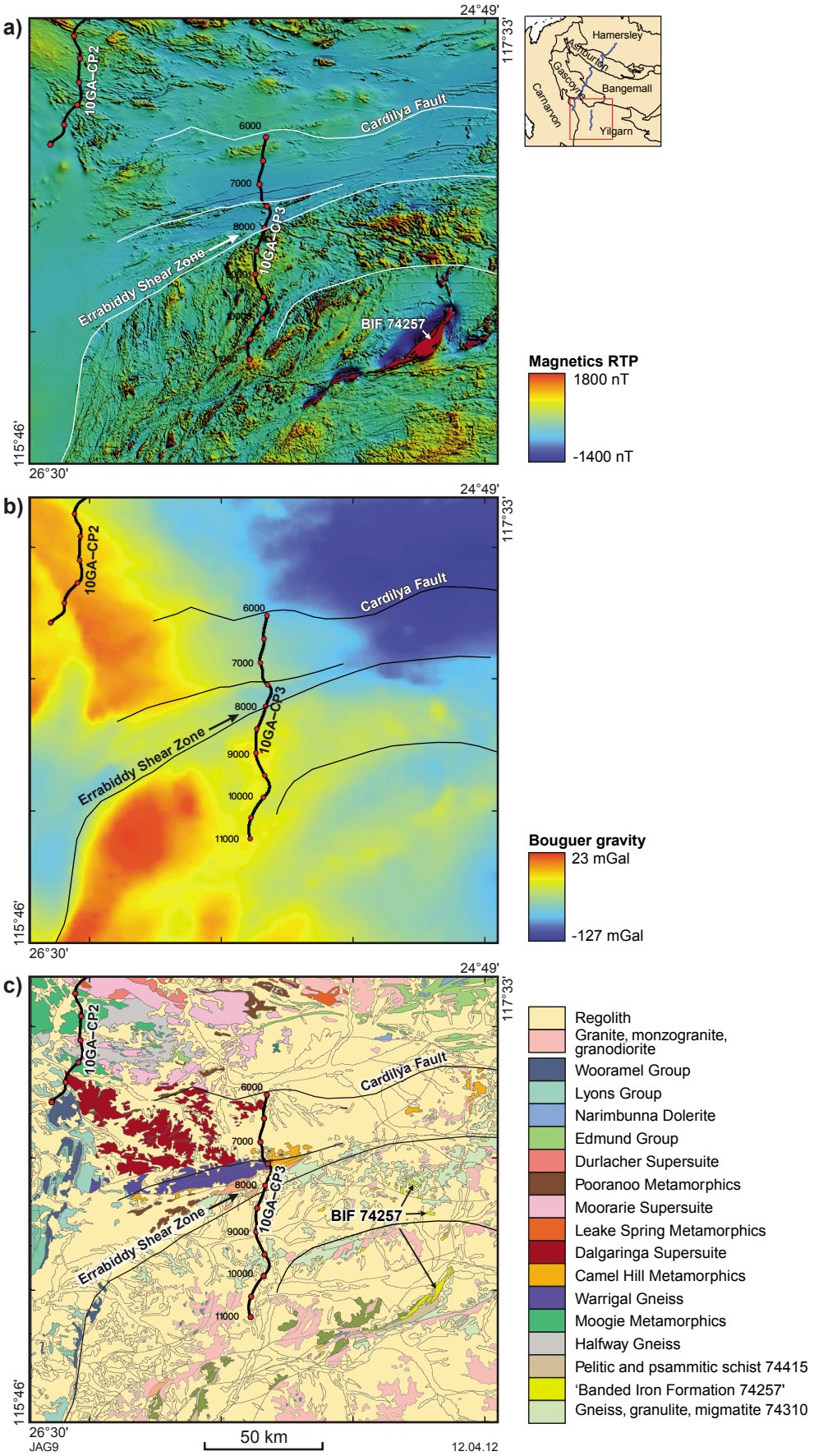

Figure 9. **a) Magnetic grid RTP (with values outside the 98th percentile removed, and sun shading from the northeast applied to highlight contrast in the data); b) bouguer gravity grid; c) 1:1 000 000 scale surface geology map covering seismic line 10GA–CP3.**

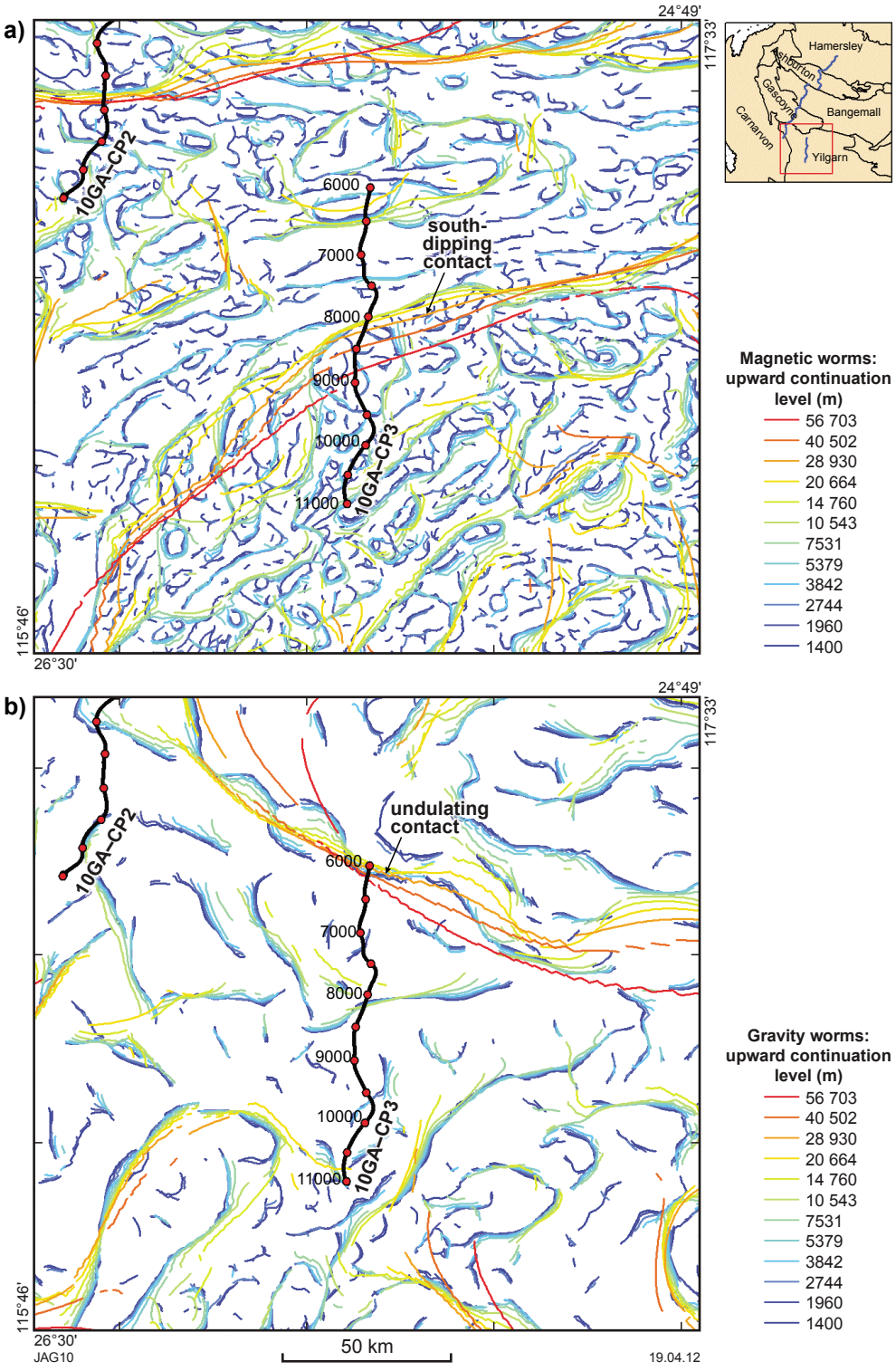

Figure 10. Worm images, covering seismic line 10GA–CP3, for magnetic (a) and gravity (b) data.

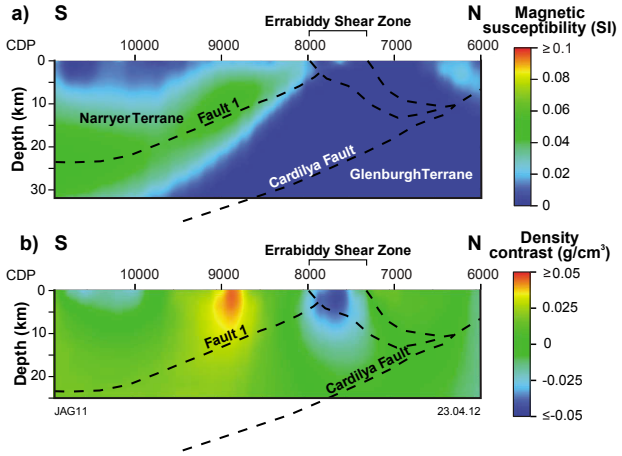

Figure 11. Inversion models extracted along seismic line 10GA–CP3: a) magnetic susceptibility model; b) density model.

at the northern end of the seismic line. Another possibility is shown in the modified interpretation, which accounts for this same gravity feature by placing a denser body of Moogie Metamorphics (2.90 g/cm^3) beneath the Dalgaringa Supersuite (Fig. 12b). The extent of this dense body of Moogie Metamorphics matches form lines observed in the seismic interpretation (Johnson et al., 2011).

In the initial forward model, the Narryer Terrane varies in density from 2.70 – 2.80 g/cm^3 to account for the gravity peak of −32.4 mGal, and in magnetic susceptibility from 0.00 – 0.02 SI to account for the relatively higher magnetic responses observed in the south of the study area (Fig. 12a). As part of the Narryer Terrane was modelled in the initial interpretation as being of low magnetic susceptibility, this section has been separated from the rest of the Narryer Terrane, forming a middle crust layer (0.00 SI) in the modified interpretation (Fig. 12b). This separation is supported by both the magnetic worms and magnetic inversion, which define a south-dipping body coinciding with ‘Fault 1’. It is also noted that short-wavelength, high-amplitude magnetic anomalies across the Narryer Terrane are not accounted for in the initial interpretation, and have been modelled using the 500 m thick, south-dipping beds of ‘Banded Iron Formation 74257’ (0.015 – 0.070 SI; Fig. 12b), based on the correlation of this unit with the magnetic anomalies mentioned above (see Fig. 9).

Conclusion

Using multiscale edge detection, 3D inversion, and 2.5D forward modelling, a number of geophysical terranes, contrasting properties, and major trends have been identified in the gravity and magnetic data covering the area of Capricorn Orogen seismic lines. The major sources of magnetic anomalies observed throughout the Capricorn

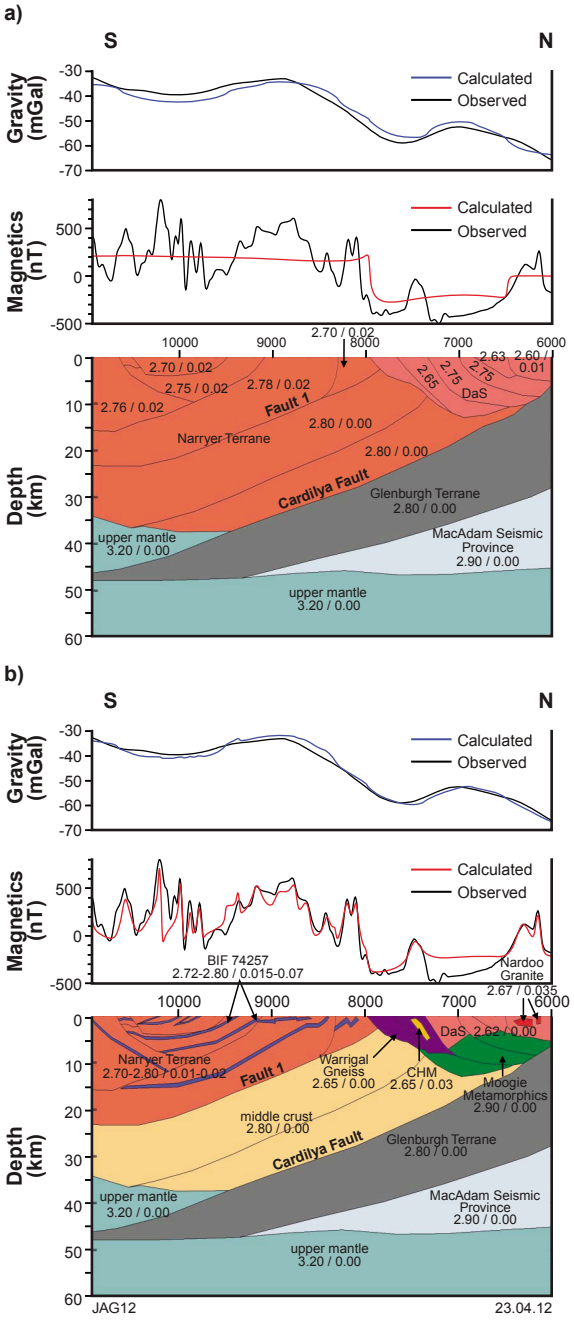

Figure 12. Forward models for seismic line 10GA–CP3: a) initial interpretation using geometries described by Johnson et al. (2011); and b) modified version of (a), altered to account for details observed in the potential-field data. Rock property values are listed on the figure as density (g/cm^3) / magnetic susceptibility (SI). Abbreviations used: CHM — Camel Hills Metamorphics; BIF — Banded Iron Formation; DaS — Dalgaringa Supersuite.

Orogen are attributed to the Hamersley Group, Bandee Seismic Province, Leake Spring Metamorphics, 'Banded Iron Formation 74257', and the Narryer Terrane.

Forward models generated using the geometries interpreted from the Capricorn seismic lines have indicated that these geometries can be modelled, using reasonable rock properties, to achieve a response that matches the observed potential-field data. This result indicates that the seismic interpretation is broadly consistent with the potential-field data. Nevertheless, further detail needed to be assumed for seismic lines 10GA–CP2 and 10GA–CP3, particularly to account for short-wavelength features observed in this potential-field data.

Two sutures identified in the seismic interpretation, the Baring Downs Fault and the Lyons River Fault, coincide with contacts between different magnetic terranes identified in the magnetic worms, 3D inversions, and forward models. A third suture, the Cardilya Fault, agrees with aspects of the gravity and magnetic worms, but does not agree with features identified in the inversions. In addition, an unnamed fault labelled 'Fault 1' (Fig. 12) is shown in the magnetic worms, 3D inversion, and modified forward model to separate a highly magnetic portion of the Narryer Terrane from a non-magnetic middle crust.

Acknowledgements

I would like to thank Richard Chopping, Russell Korsch, Malcolm Nicoll, and Richard Blewett for their assistance and insight. I would also like to thank Tony Meixner, Russell Korsch, and Richard Chopping for reviewing this extended abstract. Published with permission of the Chief Executive Officer, Geoscience Australia.

References

Archibald, NJ, Gow, P and Boschetti, F 1999, Multiscale edge analysis of potential field data: Exploration Geophysics, v. 30, p. 38–44.

Bacchin, M, Milligan, P, Tracey, R and Wynne, P 2008, Gravity Anomaly Map of the Australian Region (3rd edition): Geoscience Australia, Canberra, Australian Capital Territory, 1:5 000 000 scale map.

Beardsmore, GR and Cull, JP 2001, Crustal heat flow: a guide to measurement and modelling: Cambridge University Press, Cambridge, UK, 324p.

Cawood, PA and Tyler, IM 2004, Assembling and reactivating the Proterozoic Capricorn Orogen: lithotectonic elements, orogenies, and significance: Precambrian Research, v. 128, p. 201–218.

Clark, DA and Emerson, DW 1991, Notes on rock magnetization characteristics in applied geophysical studies: Exploration Geophysics, v. 22, p. 547–555.

Cull, JP and Denham, D 1979, Regional variations in Australian heat flow: BMR Journal of Australian Geology and Geophysics, v. 4, p. 1–13.

Cutten, HN, Thorne, AM and Johnson, SP 2011, Geology of the Edmund and Collier Groups, *in* Capricorn Orogen seismic and magnetotelluric (MT) workshop 2011: extended abstracts *edited by* SP Johnson, AM Thorne and IM Tyler: Geological Survey of Western Australia, Record 2011/25, p. 41–48.

Emerson, DW 1990, Notes on mass properties of rocks — density, porosity, permeability: Exploration Geophysics, v. 21, p. 209–216.

Guo, WW, Li, ZX and Dentith, MC 2011, Magnetic petrophysical results from the Hamersley Basin and their implications for interpretation of magnetic surveys: Australian Journal of Earth Sciences, v. 58, p. 317–333.

Holden, DJ, Archibald, NJ, Boschetti, F and Jessell, MW 2000, Inferring geological structures using wavelet-based multiscale edge analysis and forward models: Exploration Geophysics:, v. 31, p. 617–621.

Johnson, SP, Cutten, HN, Tyler, IM, Korsch, RJ, Thorne, AM, Blay, O, Kennett, BLN, Blewett, RS, Joly, A, Dentith, MC, Aitken, ARA, Goodwin, JA, Salmon, M, Reading, A, Boren, G, Ross, J, Costelloe, RD and Fomin, T 2011, Preliminary interpretation of deep seismic reflection lines 10GA–CP2 and 10GA–CP3: crustal architecture of the Gascoyne Province, and Edmund and Collier Basins, *in* Capricorn Orogen seismic and magnetotelluric (MT) workshop 2011: extended abstracts *edited by* SP Kohnson, AM Thorne and IM Tyler: Geological Survey of Western Australia, Record 2011/25, p. 49–60.

Kennett, BLN, Tyler, IM, Maher, J, Holzschuh, J, Fomin, T and Costelloe, RD 2011, The Capricorn seismic survey: experimental design, acquisition, and processing, *in* Capricorn Orogen seismic and magnetotelluric (MT) workshop 2011: extended abstracts *edited by* SP Johnson, AM Thorne and IM Tyler: Geological Survey of Western Australia, Record 2011/25, p. 1–6.

Li, Y and Oldenburg, DW 1996, 3-D inversion of magnetic data: Geophysics, v. 61, p. 394–408.

Li, Y and Oldenburg, DW 1998, 3-D inversion of gravity data: Geophysics, v. 63, p. 109–119.

Milligan, PR, Franklin, R, Minty, BRS, Richardson, LM and Percival, PJ 2010, Magnetic Anomaly Map of Australia (5th edition): Geoscience Australia, Canberra, Australian Capital Territory, 1:5 000 000 scale map.

Raymond, OL and Retter, AJ (editors) 2010, Surface geology of Australia, 2010 edition: Geoscience Australia, Commonwealth of Australia, Canberra, Australian Capital Territory, <http://www.ga.gov.au>, 1:1 000 000 scale digital dataset.

Sheppard, S, Rasmussen, B, Muhling, JR, Farrell, TR and Fletcher, IR 2007, Grenvillian-aged orogenesis in the Palaeoproterozoic Gascoyne Complex, Western Australia: 1030–950 Ma reworking of the Proterozoic Capricorn Orogen: Journal of Metamorphic Geology, v. 25, p. 477–494.

Telford, WM, Geldart, LP, Sheriff, RE and Sheriff, RE 1990, Applied geophysics: Cambridge University Press, Cambridge, UK, 792p.

Thorne, AM, Tyler, IM, Korsch, RJ, Johnson, SP, Brett, JW, Cutten, HN, Blay, O, Kennett, BLN, Blewett, RS, Joly, A, Dentith, MC, Aitken, ARA, Holzschuh, J, Goodwin, JA, Salmon, M, Reading, A and Boren, G 2011, Preliminary interpretation of deep seismic reflection line 10GA–CP1: crustal architecture of the northern Capricorn Orogen, *in* Capricorn Orogen seismic and magnetotelluric (MT) workshop 2011: extended abstracts *edited by* SP Johnson, AM Thorne and IM Tyler: Geological Survey of Western Australia, Record 2011/25, p. 19–26.

The Capricorn Orogen magnetotelluric (MT) transect

by

G Heinson[1], G Boren[1], J Ross[1], J Campanya[1], S Thiel[1], and K Selway[1]

Introduction

In April and May 2010, deep reflection-seismic data were collected along three lines in the Capricorn Orogen, funded through the Western Australian Government's Royalties for Regions Exploration Incentive Scheme (EIS) and the Australian Federal Government's National Earth Science Infrastructure Program (AuScope). The main objectives of these seismic lines were to image:

1. the overall structure and dip of the suture between the Yilgarn Craton and Gascoyne Province (Errabiddy Shear Zone)
2. the depth and shape of the Minnie Creek batholith
3. the nature of reactivated Fortescue Group growth faults in the southern Pilbara
4. the dip of the major faults that mark the boundary between the Pilbara Craton and the Ashburton Basin
5. the deep crustal structure of the Ashburton Basin
6. the deep crustal structure of the Edmund and Collier Basins, and the nature of major growth faults in these basins; e.g. the Talga Fault.

From October to November 2010, a magnetotelluric (MT) survey was conducted along the same transects as the Capricorn seismic lines. Broadband (200 – 0.005 Hz) MT sites were collected every 5 km, and long-period (0.1 – 0.0001 Hz) MT sites every 15 km. In total, 116 broadband and 40 long-period sites were collected over the three transects, spanning approximately 500 km. Like the seismic survey, the MT line was divided into three sections, denoted 10GA–CP1, 10GA–CP2, and 10GA–CP3. The MT results presented in this paper complement earlier long-period MT measurements (Fig. 1) conducted along similar transects by Selway et al. (2009).

[1] Centre for Tectonics, Resources and Exploration, University of Adelaide, Adelaide, SA 5005.

There are a number of aspects of MT measurements that make them very complementary to seismic methods.

1. MT signals have different depth penetrations, depending on frequency and on the resistivity of earth materials. The approximate depth of signal penetration into the Earth is known as the skin-depth. The skin-depth increases as frequencies decrease; skin-depth also increases as the resistivity increases.
2. The measurements are vector, which means they indicate the preferred orientation of electric current flow. Thus, MT measurements can delineate the dimensionality of Earth structures, and are sensitive to both lateral and vertical changes in geology.
3. MT measurements are sensitive to the volumetric properties of the crust and mantle, rather than being sensitive to boundaries. The primary physical property measured is electrical conductivity or its reciprocal, resistivity, and this can have changes of six of more orders of magnitude.
4. The MT method does not require an artificial source field, as the signals are all naturally occurring. Thus, the method measures just with receivers, making MT surveys relatively cheap to undertake.

The principal objectives of the MT survey were to complement the seismic reflection profiles, and to indicate any primary changes in electrical resistivity relating to the six objectives listed previously.

MT measurements

The magnetotelluric (MT) method has been in use for about 50 years, and is now a common technique used to analyse regional 2D and 3D transects (e.g. Simpson and Bahr, 2005). The principal objective of any MT survey is to measure variations in the electric field (E) and magnetic field (B) as time series (Figs 2 and 3).

Magnetic fields are measured as a time series using a magnetometer. These are vector measurements, oriented

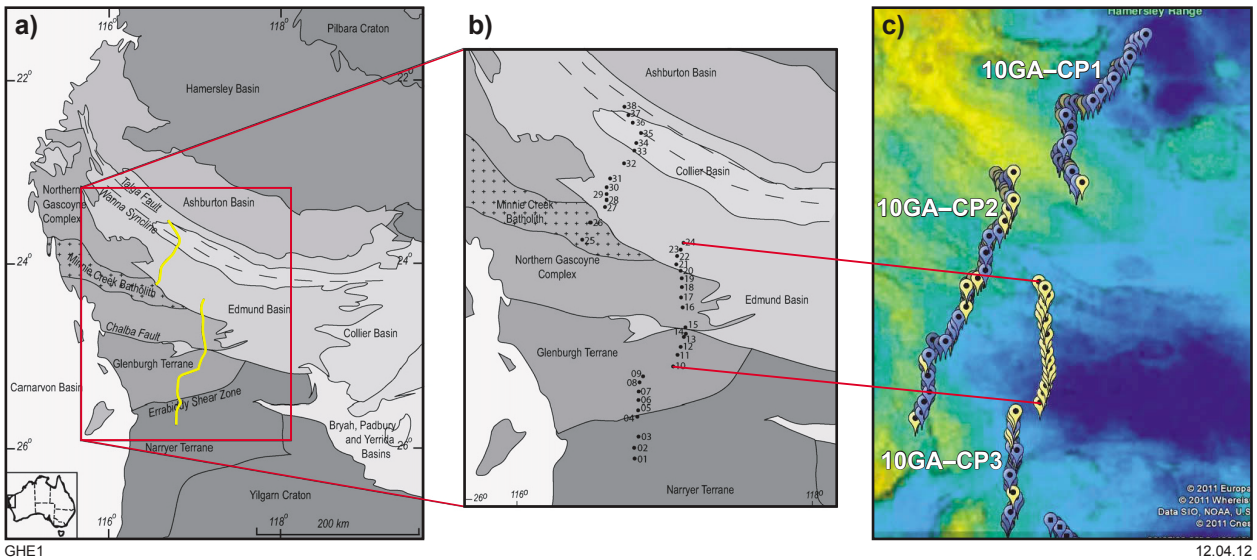

Figure 1. Profile map of survey: (a) regional scale geology, with survey lines from Selway et al. (2009), marked in yellow; (b) more detailed survey geology from Selway et al. (2009); (c) new broadband MT sites (blue) and long-period MT sites (yellow) plotted on top of a Bouguer gravity map of the region. The locations of the Selway et al. (2009) sites (which were long-period MT) are also shown. New sites were collected along lines 10GA–CP1, 10GA–CP2, and 10GA–CP3.

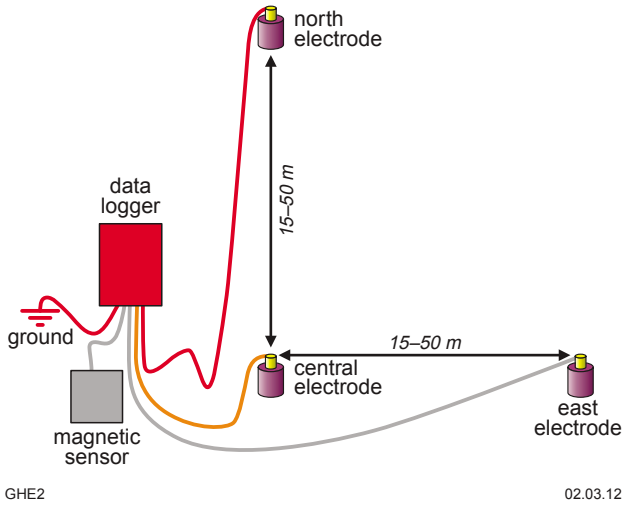

Figure 2. Typical layout of MT instrumentation.

in the direction of the sensor alignment. For broadband measurements, induction coils (LEMI120; <http://www.lemisensors.com/?q=lemi_120>) with the highest sensitivity, between 1000 and 0.001 Hz, were used. Only the two horizontal components, north and east orientations, are recorded (B_x, B_y).

For long-period measurements, a three-component fluxgate sensor (MAG03; <http://www.gmw.com/magnetic_measurements/Bartington/Mag-03.html>) was used, with sensitivity between about 0.1 Hz and DC. These three components are aligned north, east, and vertical (B_x, B_y, B_z).

The electric field is the voltage difference measured between two grounded electrodes, and is given as the voltage gradient (volts per metre; V/m). Typically, offsets are measured in microvolts (mV). Such measurements are vector in that they have both magnitude and direction; generally, electric field dipoles are established with one pair of electrodes orientated north–south (E_x), and the other pair oriented west–east (E_y).

Note that for the MT method, the important aspect of these magnetic and electric fields is that the fields change with time. The magnetic field changes are primarily due to external effects: at high frequencies (>1 Hz), the source fields are due to lightning strikes around the world, whereas at lower frequencies (<0.1 Hz), the source field are due to the interaction of the Earth's magnetic field with solar winds emanating from the sun. The bandwidth of 1 – 0.1 Hz is known as the dead-band, which typically contains little natural field signal.

The fundamental relationship linking the electric and magnetic fields in the frequency domain is given by the following equation.

$$\begin{pmatrix} E_x \\ E_y \end{pmatrix} = \begin{pmatrix} Z_{xx} & Z_{xx} \\ Z_{xx} & Z_{xx} \end{pmatrix} \begin{pmatrix} B_x \\ B_y \end{pmatrix} \quad (1)$$

In this equation, the matrix components B_x and B_y are the horizontal magnetic fields in the north (B_x) and east (B_y) directions, and can be considered, at first order, as input or source fields. The two horizontal electric-field components E_x and E_y are the equivalent orientations of the electric field, and are essentially the response of the Earth to inducting fields. Finally, the matrix [Z] is the impedance tensor, which contains information of the Earth as a filter, dependent primarily on electrical resistivity.

For a one-dimensional (1D) layered Earth, the impedance tensor is quite simple, with $Z_{xx} = Z_{yy} = 0$, and $Z_{xy} = -Z_{yx}$. Thus, the orthogonal components of the electric and magnetic fields are linked, and these responses can be written in terms of both an apparent resistivity, ρ_a (in ohm.m, or Ωm), as

$$\rho_a = \frac{0.2}{f}\left|\frac{E_x}{B_y}\right|^2 \quad (2)$$

and a phase angle (which is essentially the phase lag between the electric and magnetic fields), given by:

$$\phi = \tan^{-1}\left(\frac{E_x}{B_y}\right) \quad (3)$$

In these equations, f is the frequency of the signal.

For Earth structures that are relatively two-dimensional (2D) in that they change in electrical properties with depth and in one horizontal orientation, the impedance tensor [Z] can be mathematically rotated so that the observed fields are effectively resampled in directions parallel and perpendicular to the strike of the 2D geology; that is, $Z_{xx} = Z_{yy} = 0$, but $Z_{xy} \neq Z_{yx}$. In this case, the orientation of the fields can be defined as two modes: the TE mode, with the electric field parallel to the geological strike causing a resistivity variation; and the TM mode, in which the electric field is perpendicular to the strike of the geology. In many surveys, the TM mode is the most important, as the flow of electric currents across boundaries produces significant changes in apparent resistivity.

In many cases, the Earth is truly three-dimensional (3D) in that the electrical resistivity varies in both horizontal directions and vertically. In this case, $Z_{xx} \neq Z_{yy} \neq Z_{xy} \neq Z_{yx}$, and modelling is very difficult. The Earth may be anisotropic on a small scale; that is, a single piece of crust may conduct electricity better in one orientation than others.

The apparent resistivity and phase are measured at a wide range of frequencies, which translates to a wide range of depths and distances. The apparent resistivity can be considered as a weighted average of the resistivities to the skin-depth.

The skin-depth equation is given by:

$$\delta \approx 500\sqrt{\frac{\rho}{f}} \quad (4)$$

where the skin-depth (δ) is given in kilometres, and is approximately the depth at which the inducing field is about 30% of its surface value.

For long-period instruments, the vertical magnetic field component B_z is also measured. As for the horizontal electric field, the vertical field can be also considered as a response to the Earth from source field B_x and B_y, and is linked by the following equation:

$$\begin{pmatrix} B_z \end{pmatrix} = \begin{pmatrix} T_{xz} & T_{yz} \end{pmatrix}\begin{pmatrix} B_x \\ B_y \end{pmatrix} \quad (5)$$

The two transfer functions, T_{xz} and T_{yz}, relate the vertical field B_z to the horizontal components B_x and B_y, respectively.

Finally, there is the problem of static shift in MT soundings (Jones, 1988). Static shift is an effect that uniformly increases or decreases the apparent resistivity responses by a constant amount. The effect is due to very near-surface changes in resistivity that locally increase or decrease the electric field. There is an analogy to static in seismic methods, and indeed the static corrections used in each case may be linked.

Plotting of MT responses

In this paper, MT responses are plotted in three ways:

Firstly, the MT responses are presented as pseudosections. These sections show the MT responses in two modes, TE and TM, with apparent resistivity and phase plotted as a function of frequency and site location. The plots are colour contoured to give an approximate distance and depth scale, with lower frequencies penetrating deeper into the section than higher frequencies. As discussed previously, TE refers to the orientation in the 2D framework in which the electric field flows perpendicular to the 2D profile line, and hence parallel to the geological strike. TM, on the other hand, refers to the case in which the induced electric field is parallel to the 2D profile line, and hence perpendicular to the geological strike. The TM mode is often noted as being most sensitive to geological variations along the profiles (Wannamaker et al., 1984).

Secondly, the vertical field transfer functions of equation 5 are presented as what are known as induction arrows (Simpson and Bahr, 2005). As the transfer functions are complex numbers, each consists of an in-phase (or real) arrow, and an out-of-phase (or imaginary) arrow. The length of the arrow represents the size of the transfer functions, and the response to changes in lateral resistivity. These induction arrows are plotted in the Parkinson convention (Parkinson, 1962), which has the simple interpretation that real arrows point towards areas of low resistivity (and away from areas of high resistivity). These arrows are therefore very useful in demonstrating lateral resistivity changes.

Finally, data is also plotted as more complex phase tensors, which are also colour filled to indicate the primary electrical resistivity structure. For a detailed explanation of phase tensors, see Caldwell et al. (2004). The most important aspects of phase tensors are that they plot as circles for relatively uniform regions of resistivity, and are highly polarized as ellipses in more complex geology where there is a definite strike orientation in resistivity. The ellipses themselves have a 90° ambiguity, with either the major axis or the minor axis aligned with strike, depending on the geology.

Survey and data

In Appendix 1, the tables list the locations, elevations, and lines for both long-period and broadband MT sites.

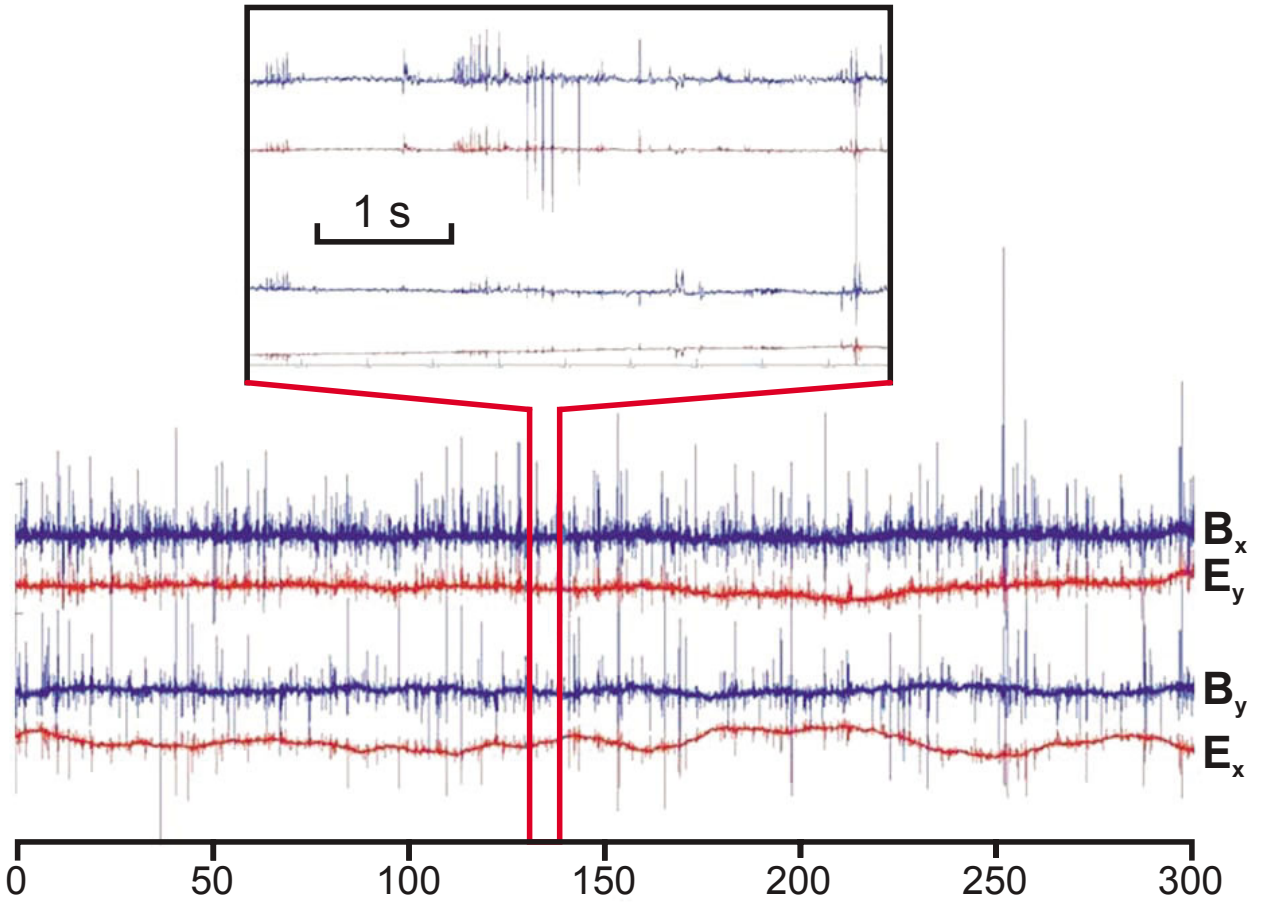

Figure 3. Typical MT time-series data for the four horizontal components of magnetic (B_x, B_y) and electric (E_x, E_y) fields. The lower figure covers 300 s of data, sampled at 1000 Hz. The inset figure is 5 s of the same dataset, illustrating the correlation between pairs of fields.

Typically, broadband sites were occupied for 2–3 days, and the long-period sites for 5–6 days. The figures in the Appendix indicate the duration of deployments.

Overall, instrumentation recorded high-quality time-series data. The time series were Fourier transformed to the frequency domain, and the impedance tensor [Z] (equation 1) and vertical field transfer function [T] (equation 5) determined at a wide range of frequencies. In turn, equation (1) was derived from the apparent resistivity and phases.

Processing was undertaken using the method of Chave et al. (1987), finally producing MT responses in the industry-standard Electronic Data Interchange (EDI) format.

Modelling and inversion

Modelling and inversion of data was undertaken using the commercial WinGLink package, which incorporates the 2D inversion code of Rodi and Mackie (2001). For each model shown, the primary parameters used in the inversion are listed in the figure caption. The models are all smooth or with minimum structure, and the philosophy is one of simplicity, in presenting the least complex resistivity structures compatible with the observed MT responses.

In the following three sections, the main attributes of the three lines are outlined in terms of their data plots and the best-fitting models. In the Discussion section, the models are assessed in terms of the principal objectives of the seismic survey. However, the model sections should all be considered works in progress, and are still being refined.

Line 10GA–CP1

Line 10GA–CP1 (approximately 150 km long) consists of 13 long-period and 39 broadband MT sites (Fig. 4). Data quality is good for all MT sites.

Figure 5 shows a plot of phase tensors for periods of 1 s and 10 s along this line. In crustal material of resistivity of 100 Ωm, the skin-depth is about 5 km for 1 s, and 15 km for 10 s. The ellipses, particularly at 10 s, are highly aligned with the geological strike in the southernmost section, but are more complex and variable in the north.

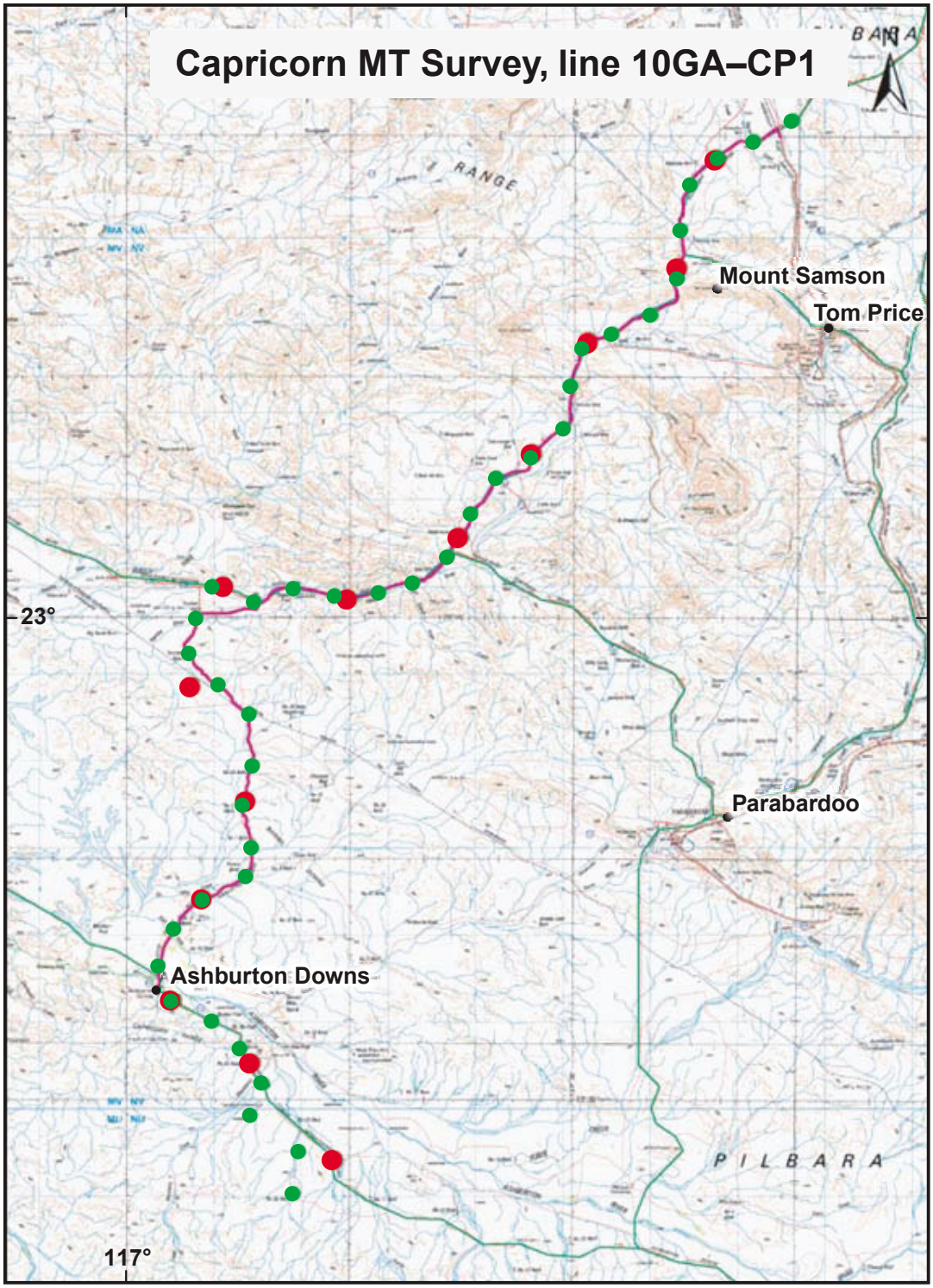

Figure 4. **Location of MT sites along the 10GA–CP1 profile. Broadband sites are shown in green, and are approximately 5 km apart; long-period MT sites are shown in red, and are 15 km apart. Appendix 1 lists the duration of the measurement at each site.**

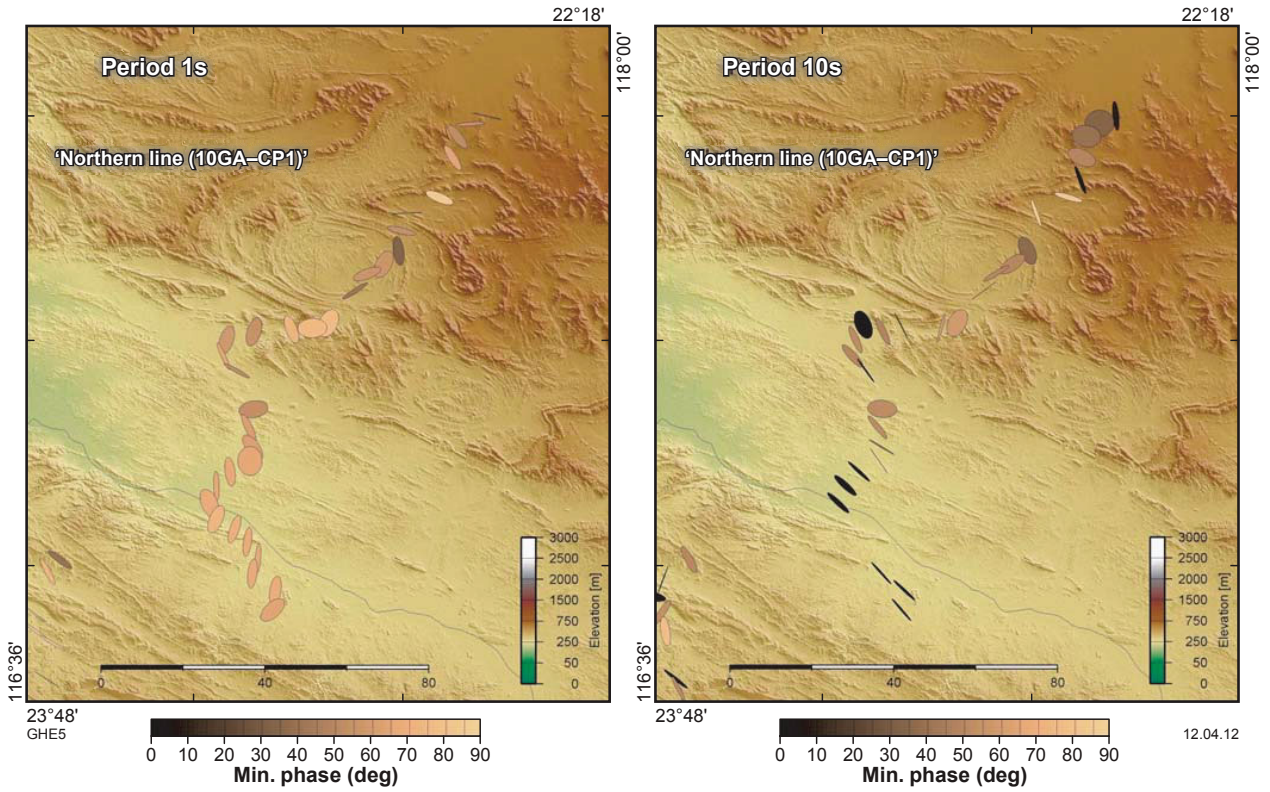

Figure 5. Phase tensors for line 10GA–CP1 for periods of 1 s and 10 s. Ellipses are aligned with geological strike, but note there is a 90° ambiguity in terms of the alignment with the major or minor axes. For crustal materials of resistivity 100 Ωm, the skin-depths are 5 km and 15 km, respectively. The minimum phase angles are indicative of primary electrical structure: high phases (>45°) indicate high resistivity over a much lower resistivity.

Despite this, the dominant feature of all these responses is that they are anisotropic and highly distorted.

Over longer periods, induction arrows indicate regional-scale MT responses. The vertical magnetic field was not recorded for broadband sites, so only the long-period sites, spaced 15 km apart, have induction arrows. Figure 6 shows the induction arrows for all three MT lines, for periods of 50 s, 500 s, and 5000 s. Again, for crustal material of resistivity of 100 Ωm, the skin-depths are 35 km, 110 km, and 350 km, respectively; such scale lengths can be considered in terms of the induction-scales vertically and horizontally. In other words, induction arrows at 50 s are sensitive to lateral changes in resistivity in the vicinity of 35 km away.

Note that on line 10GA–CP1 and along much of 10GA–CP2, the real arrows (red) at short periods are quite scattered (Fig. 6); however, along 10GA–CP3 the real arrows are much more uniform. At longer periods, there is a more regional trend for arrows to point to the northwest, presumably towards the deeper sediments of the Carnarvon Basin. A similar trend was noted by Selway et al. (2009) for the sites shown in Figure 1.

The broadband MT responses were inverted for 2D structure using the smooth model algorithm of Rodi and Mackie (2001). Responses were found to be approximately 2D and aligned with the strike of the geology and magnetic structures, but were quite 3D over some bandwidths. Additionally, there is evidence of significant static shift effects.

Figure 7 shows the 2D resistivity model that best fits the MT data from a bandwidth of 200 Hz – 0.1 Hz (10 s). The 39 broadband sites were carefully edited to remove bandwidths with obvious 3D effects. Inversions were run for a tau value of 0.1, with weighting on horizontal structure (alpha = 1.3) and 5% error bars. Static shifts were determined as part of the inversion, and the final model had a model misfit of about rms = 4. Figure 8 shows a pseudosection of the best-fits to the TM (with the electric field parallel to the line of the model) modes, in terms of both apparent resistivity and phase.

The most remarkable aspects of this model is that the resistivity structures are relatively uniform, and generally consists of a thin-conductive sedimentary layer at the top, then a very resistive layer (10 000 Ωm) of 2–10 km thickness, and finally a remarkably conductive (~1 Ωm) region (Fig. 7). In the model section, the structure below this conductive later is essentially unresolved, as the induced electric current do not flow any deeper; i.e. the conductive layer shields the deeper inductive response. Note too that many of the responses show evidence of 3D and possibly anisotropic conduction, which cannot be

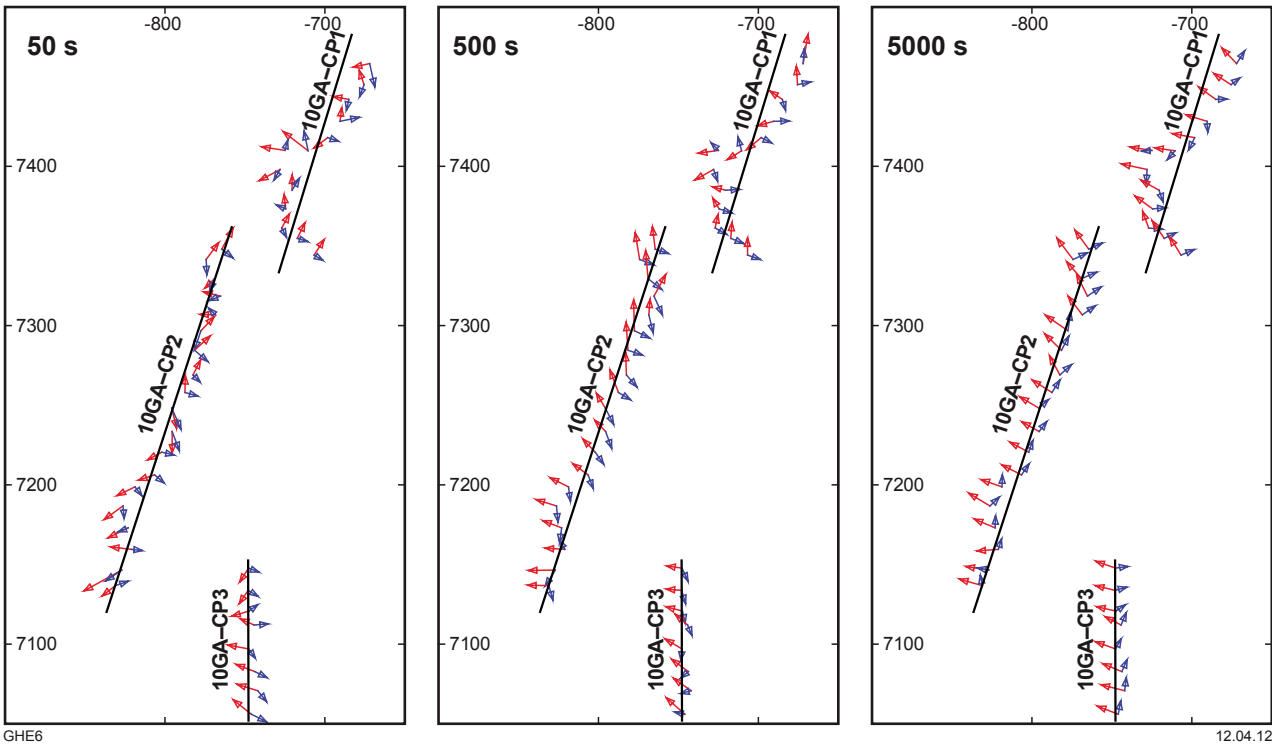

Figure 6. **Induction arrows at periods of 50 s, 500 s, and 5000 s for all three MT lines. The red arrows represent the in-phase (or real) component, whereas the blue arrows represent the out-of-phase (or imaginary) components. Both sets of arrows are plotted in the Parkinson convention, such that the real arrows point towards good conductors. The typical arrow size is quite small, with a magnitude of about 0.2.**

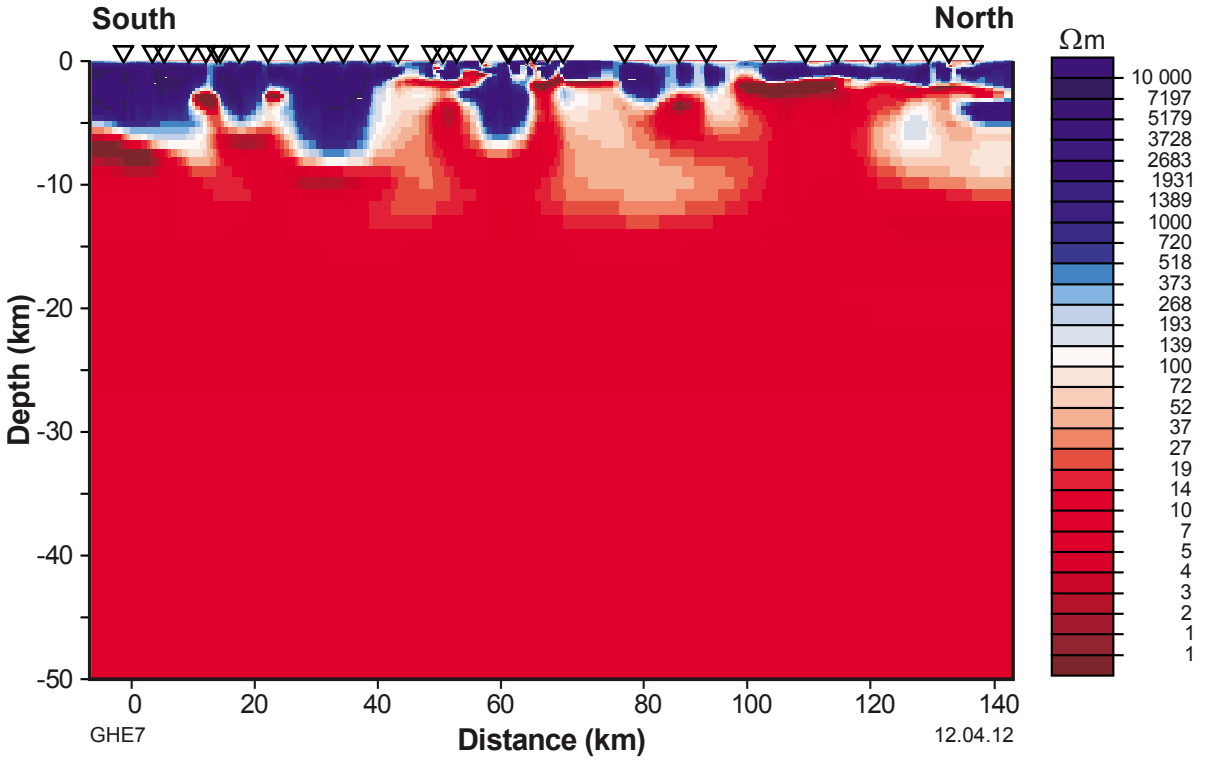

Figure 7. **2D resistivity section for line 10GA–CP1. The bandwidth of the inversion was 200 – 0.1 Hz, and the profile orientation was taken as being 30°E of geographic north (with geological strike perpendicular to the profile). The inversion achieved a misfit of about rms = 4 to both TE and TM mode data, with 5% errors and static shift as another model variable.**

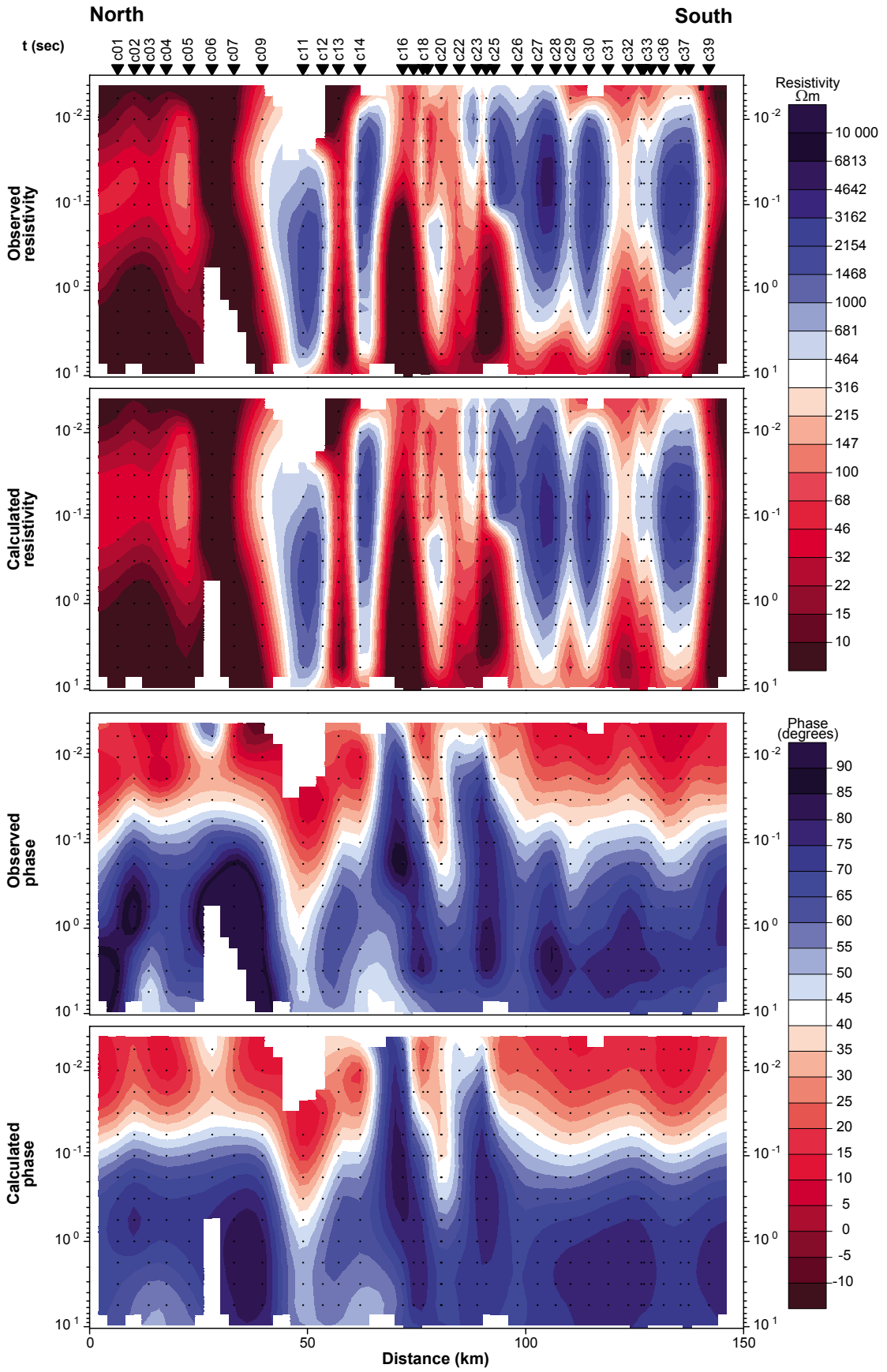

Figure 8. **Pseudosections for line 10GA–CP1 for the bandwidth 200 – 0.1 Hz. The top figure shows the observed TM mode apparent resistivity, and the second panel shows the calculated TM mode apparent resistivity for the model in Figure 7. Similarly, the bottom two figures show the observed and calculated phases.**

modelled with this 2D inversion approach. The southernmost section of this model shows a thicker resistive layer; this is consistent with the phase tensors seen in Figure 5, and which illustrate a change in characteristics at this point.

Long-period MT data were not modelled as the responses were generally of low quality at periods greater than 100 s and, moreover, were highly 3D. Interpretation of the low-quality responses at these long periods is made in terms of very small electric fields as the highly conducting layer effectively shorts out the induced electric currents.

Line 10GA–CP2

Line 10GA–CP2 was the longest section (approximately 250 km), with 19 long-period and 55 broadband MT sites deployed (Fig. 9).

Figure 10 shows a plot of phase tensors along this region for periods of 1 s and 10 s. There is a remarkable change in the phase tensor characteristics about halfway along the line. To the north, phase tensors are complex, but generally highly polarized. To the south, the phase tensors are generally more circular, which indicates lower order dimensionality. However, even in the southern section, there are elliptical phase tensors, particularly at longer periods in the south.

The characteristics of the induction arrows can be seen to change with increasing period (Fig. 6). At short periods, the arrows are quite scattered along the line, suggesting heterogeneity of electrical resistivity at a scale-length smaller than the survey. At longer periods, the real arrows all align to the northwest.

As for line 10GA–CP1, the broadband MT responses were inverted for 2D structure. Responses were found to have various amounts of static shift, were approximately 2D at frequencies higher than 0.1 Hz, and were aligned with the strike of both the geological and magnetic structures. However, at quite a few sites, some bandwidths were quite 3D. Figure 11 shows the best model obtained from an inversion of MT data in the bandwidth of 200 – 0.1 Hz (10 s). The 55 broadband sites were carefully edited to remove bandwidths with obvious 3D effects. As for Figure 7, inversions were run for a tau value of 0.1, with weighting on horizontal structure and 5% error bars. Static shifts were determined as part of the inversion, and the final model obtained a model misfit of about rms = 4. Figure 12 shows pseudosections of the best-fits to the observed TM (with the electric field parallel to the line of the model) modes, in terms of both apparent resistivity and phase.

The most remarkable aspects of this model is that the resistivity structure of the northern section is similar to the entirety of 10GA–CP1 (Fig. 11). In most parts, it consists of a thin-conductive sedimentary layer, followed by a very resistive layer (10 000 Ωm) 2–10 km thick, and finally a remarkably conductive (~1 Ωm) region at the base. In the model section, the structure below this conductive later is unresolved, as the induced electric current does not flow any deeper; i.e. the conductive layer shields the deeper responses. Many of the responses also show evidence of 3D and possibly anisotropic conduction that cannot be modelled with this 2D inversion approach.

However, in the southern part of 10GA–CP2, the crustal resistivity section shows a profound change where the phase tensors become more uniform (Fig. 10). The distinct electrical contrast between the Bandee Seismic Province and the Glenburgh Terrane dips at about the same angle as the Lyons River Fault, which is interpreted to be the suture zone between the Pilbara Craton and Glenburgh Terrane. Although there is evidence of conductive shear zones (which are coincident with some of the more polarized phase tensors in Figure 10), which may be related to the Ti Tree Shear Zone, the bulk of the crust is resistive (>1000 Ωm), which is considered more typical of Archean crustal profiles. The Minnie Creek batholith (as shown in Figure 1a and Frontispiece 1) was not resolved as a separate body, but its southern margin is coincident with a profound change in the crustal resistivity across the Lyons River Fault.

Again, long-period data was unable to modelled, due to the fact that data from sites in the north were of very low quality, and were 3D.

Line 10GA–CP3

Line 10GA–CP3 was the shortest (approximately 100 km), with eight long-period and 22 broadband MT sites deployed (Fig. 13).

Figure 14 shows a plot of phase tensors along this line for periods of 1 s and 10 s. These phase tensors are relatively uniform, with the only change occurring at the seventh site along the line, which indicates a more 2D structure. Interestingly, this site coincides approximately with the Errabiddy Shear Zone.

In Figure 6, the long-period induction arrows can be seen to be relatively uniform, but show a slight convergence to the north, indicating a conductive flow of current roughly aligned with the Errabiddy Shear Zone.

Broadband MT responses were again inverted for 2D structure (Fig. 15) using the same modelling parameters as for 10GA–CP1 (Fig. 7) and 10GA–CP2 (Fig. 11). Pseudosection fits are also shown for the TM mode in Figure 16. Overall, the MT responses are relatively simple, with the exception of the site directly on the shear zone, which exhibits a response indicating the strong channelling of electric currents.

The model section seen in Figure 15 is relatively simple and resistive (~1000 Ωm), but shows evidence of a conductive shear zone aligned with the Errabiddy Shear Zone. In this section, the shear zone does not fully intersect the surface, but coincides with a relatively broad (~10 km) region of low resistivity. The depth extent for this body is not clear from the modelling; although it appears to disappear at a depth of about 25 km, this is also about the skin-depth and from the broadband data the depth extent is unresolved. For most of the line, the resistive sections are imaged much deeper, as the skin-depths are much greater.

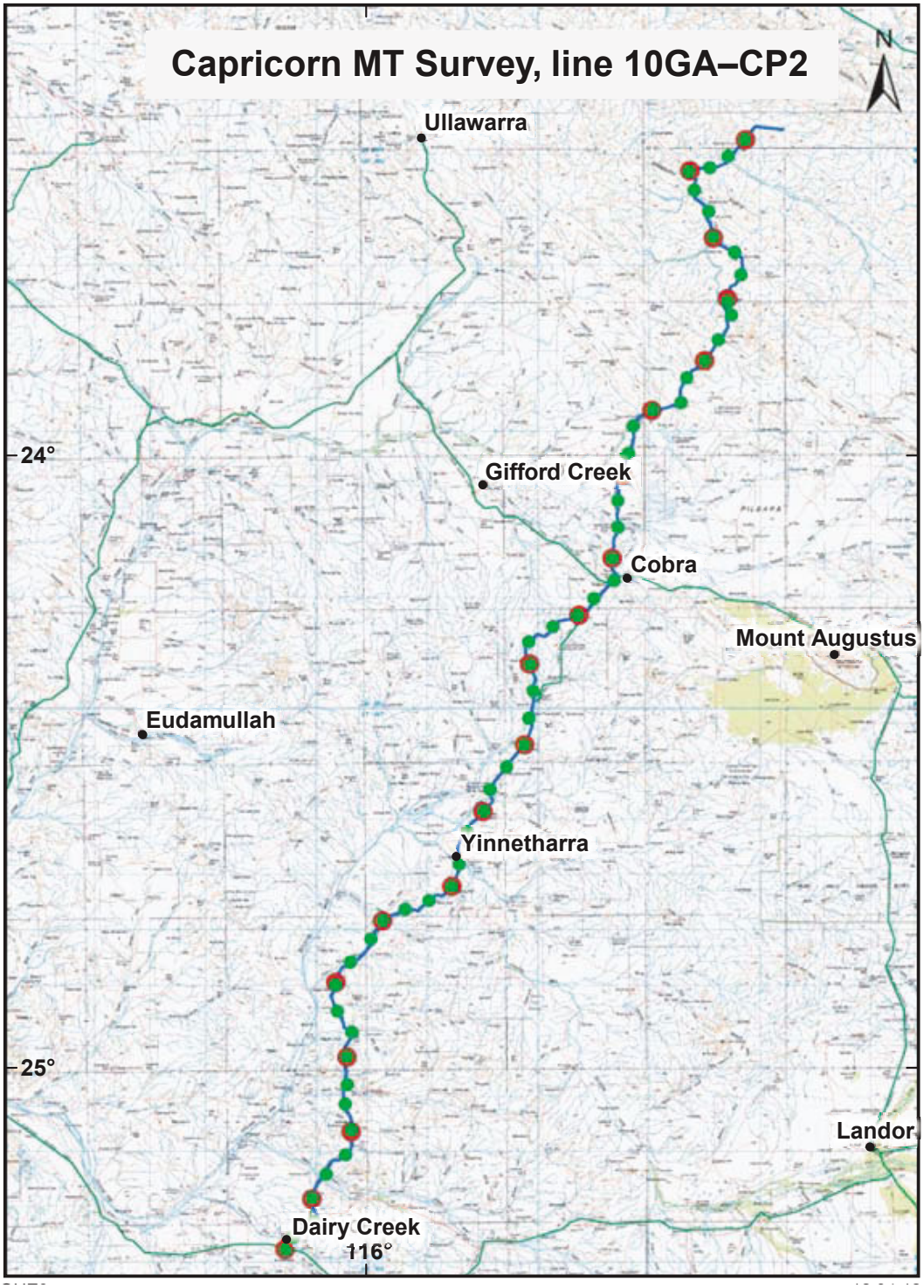

Figure 9. **Location of MT sites along the 10GA–CP2 profile. Broadband sites are shown in green, and are approximately 5 km apart; long-period MT sites are shown in red, and are 15 km apart. Appendix 1 lists the duration of the measurement at each site.**

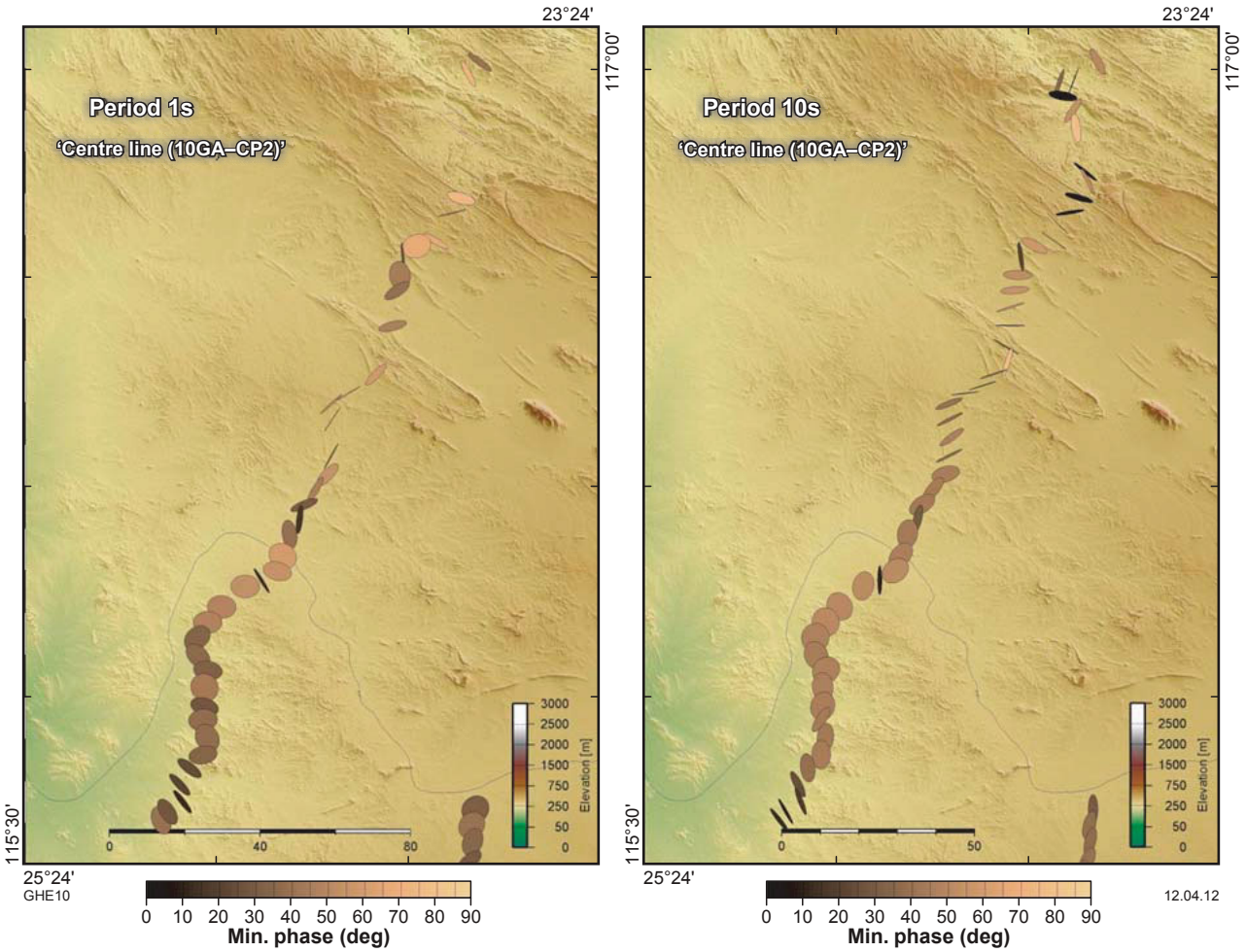

Figure 10. Phase tensors for line 10GA–CP2 for periods of 1 s and 10 s. Ellipses are aligned with geological strike, but note there is a 90° ambiguity in terms of the alignment with the major or minor axes. For crustal materials of resistivity 100 Ωm, the skin-depths are 5 km and 15 km, respectively. The minimum phase angles are indicative of primary electrical structure: high phases (>45°) indicate high resistivity over a much lower resistivity.

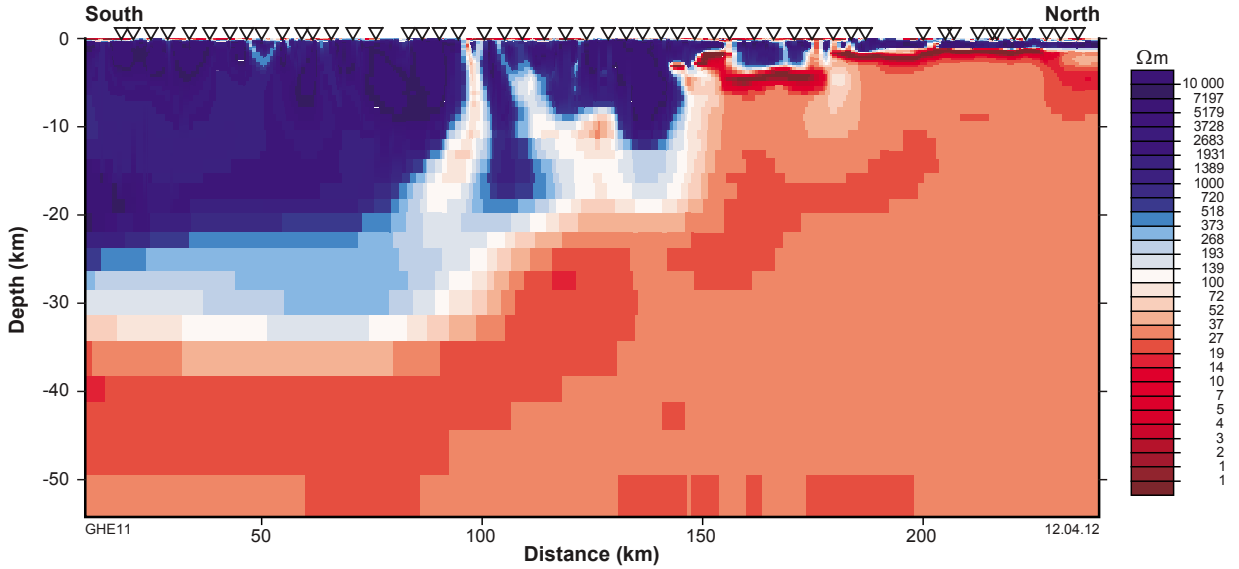

Figure 11. 2D resistivity section for line 10GA–CP2. The bandwidth of the inversion was 200 – 0.1 Hz, and the profile orientation was taken as being 30°E of geographic north (with geological strike perpendicular to the profile). The inversion achieved a misfit of about rms = 4 to both TE and TM mode data, with 5% errors and static shift as another model variable.

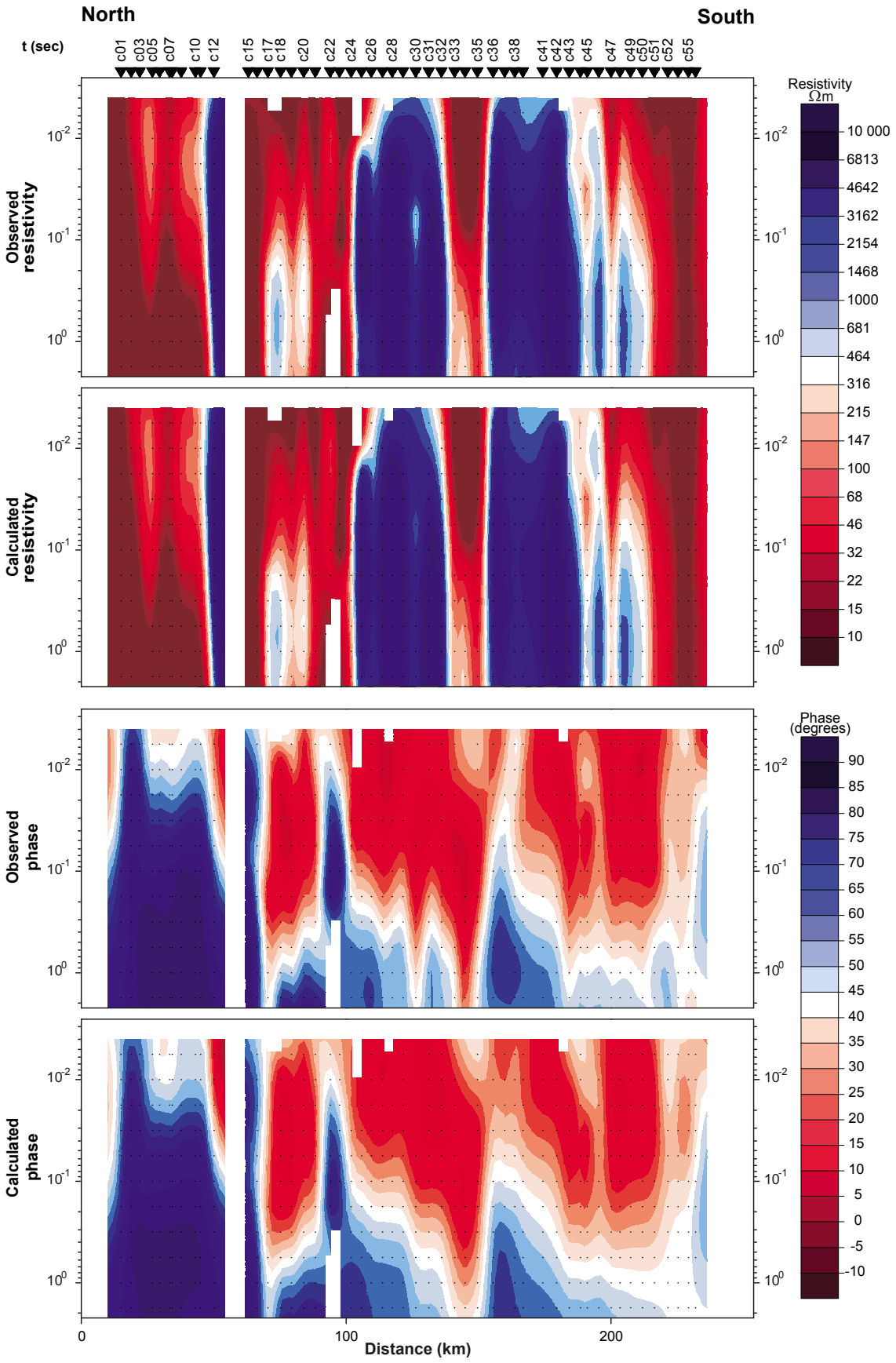

Figure 12. Pseudosections for line 10GA–CP2 for the bandwidth 200 – 0.1 Hz. The top figure shows the observed TM mode apparent resistivity, and the second panel shows the calculated TM mode apparent resistivity for the model in Figure 11. Similarly, the bottom two figures show the observed and calculated phases.

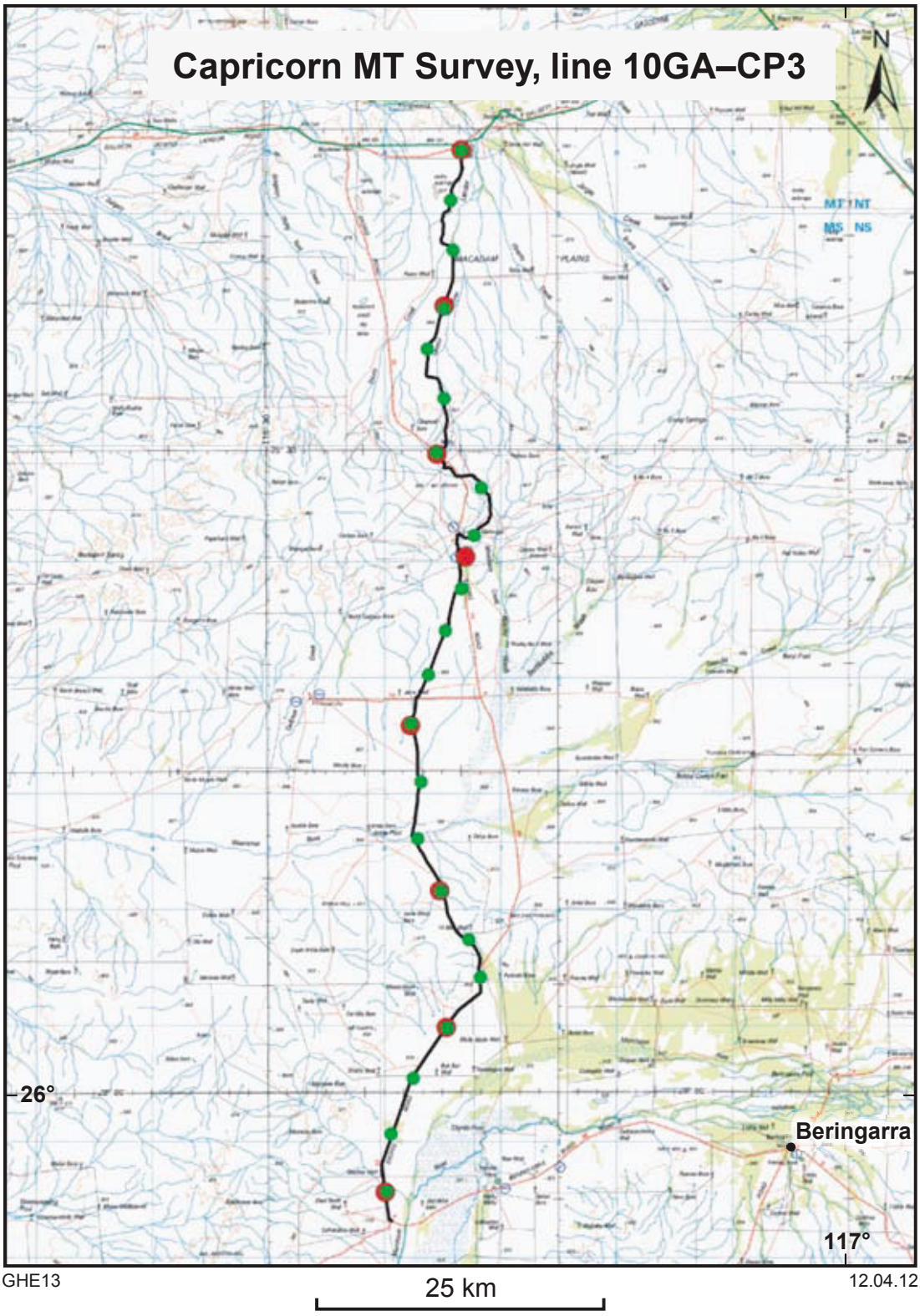

Figure 13. Location of MT sites along the 10GA–CP3 profile. Broadband sites are shown in green, and are approximately 5 km apart; long-period MT sites are shown in red, and are 15 km apart. Appendix 1 lists the duration of the measurement at each site.

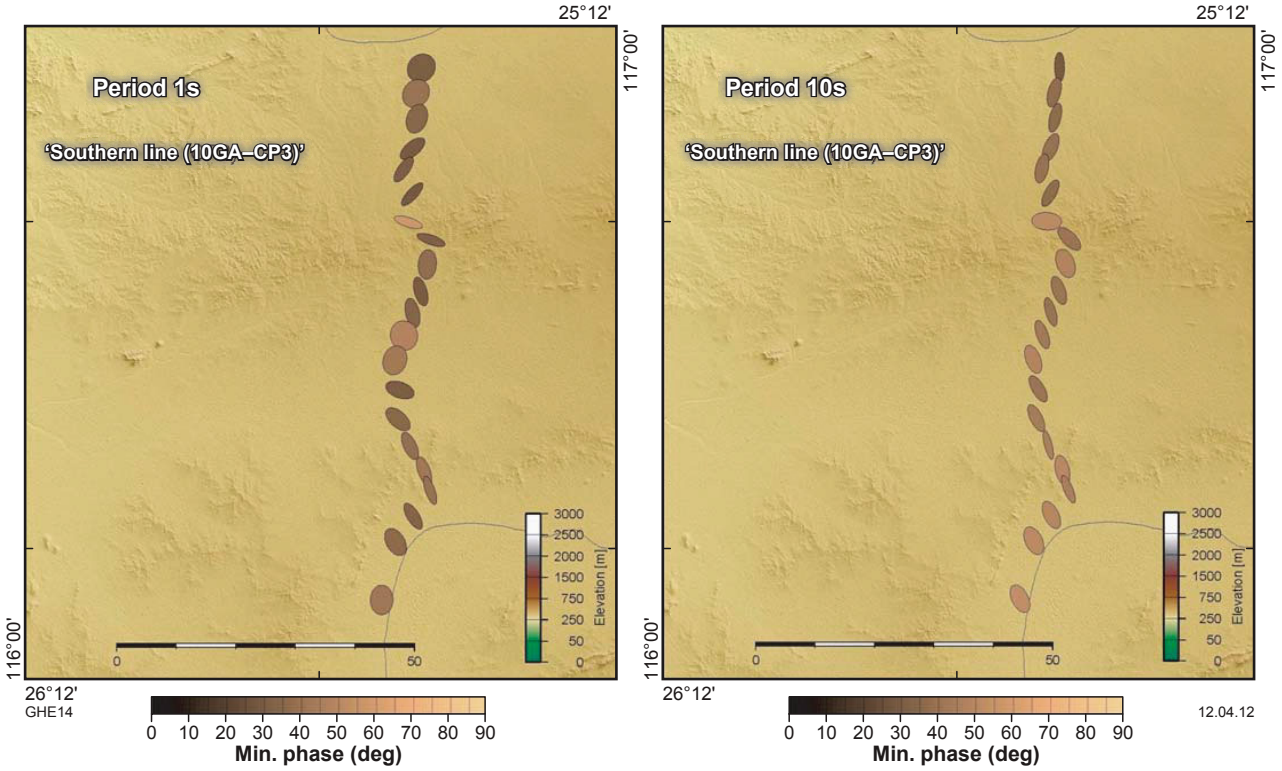

Figure 14: Phase tensors for line 10GA–CP3 for periods of 1 s and 10 s. Ellipses are aligned with geological strike, but note there is a 90° ambiguity in terms of the alignment with the major or minor axes. For crustal materials of resistivity 100 Ωm, the skin-depths are 5 km and 15 km, respectively. The minimum phase angles are indicative of primary electrical structure: low phases (<45°) indicate low resistivity over a much higher resistivity.

Long-period MT sites were also inverted. Only in this line section were long-period MT responses of high enough quality to a period of 10 000 s. Only seven of the eight long-period sites were modelled (Fig. 17), as the response at the site on the shear zone was very anisotropic. The most remarkable aspect of this model is that the low-resistivity region is imaged much deeper, and appears to dip towards the south when compared to the models for the other lines (Fig. 17).

Discussion and conclusion

Modelling is not complete, as the results from Selway et al. (2009) will be added to complement the current observations and there will be an attempt to improve the MT response estimation through the application of a number of processing refinements. However, it is unlikely that any new model will significantly differ from those presented here (Figs 7, 11, 15, and 17).

Figure 18 shows a composite model and a preliminary interpretation of the uppermost 25 km along the Capricorn study line, with the three profiles linked together. Figure 19 shows a composite model, for line 10GA–CP3 only, incorporating both the broadband and long-period MT sites to a depth of 200 km. Here, the outcomes are listed in terms of the primary seismic objectives.

1. The Errabiddy Shear Zone is clearly indentified in section 10GA–CP3 (Fig. 18), and appears as a zone of low resistivity, approximately 10 km wide, and extending to at least 25 km depth. The Shear Zone appears to be near-vertical, and exhibits some more complex geometry near the surface (Fig. 18). To examine the deep structure, a comparison, for line 10GA–CP3 only, of both the broadband and long-period MT sites to a depth of 200 km was made (Fig. 19). Although the long-period MT sites lack the resolution at depths of 50 km and more, there is an overall trend of a south-dipping structure evident in both the low-resistivity shear zone, and in the more resistive structures to the south.

2. The depth and geometry of the Minnie Creek batholith was not resolved, but it is noted that the location of this batholith is coincident with a profound change in the crustal resistivity along line 10GA–CP2, which in turn appears to be coincident with the Lyons River Fault.

3. The models resolve very little in terms of basin structure and faults in the Pilbara–Hamersley–Ashburton line, 10GA–CP1. This is primarily due to the low-resistivity structures observed at depths of 2–10 km. Thus, there is little quantitative information at present for the other objectives defined

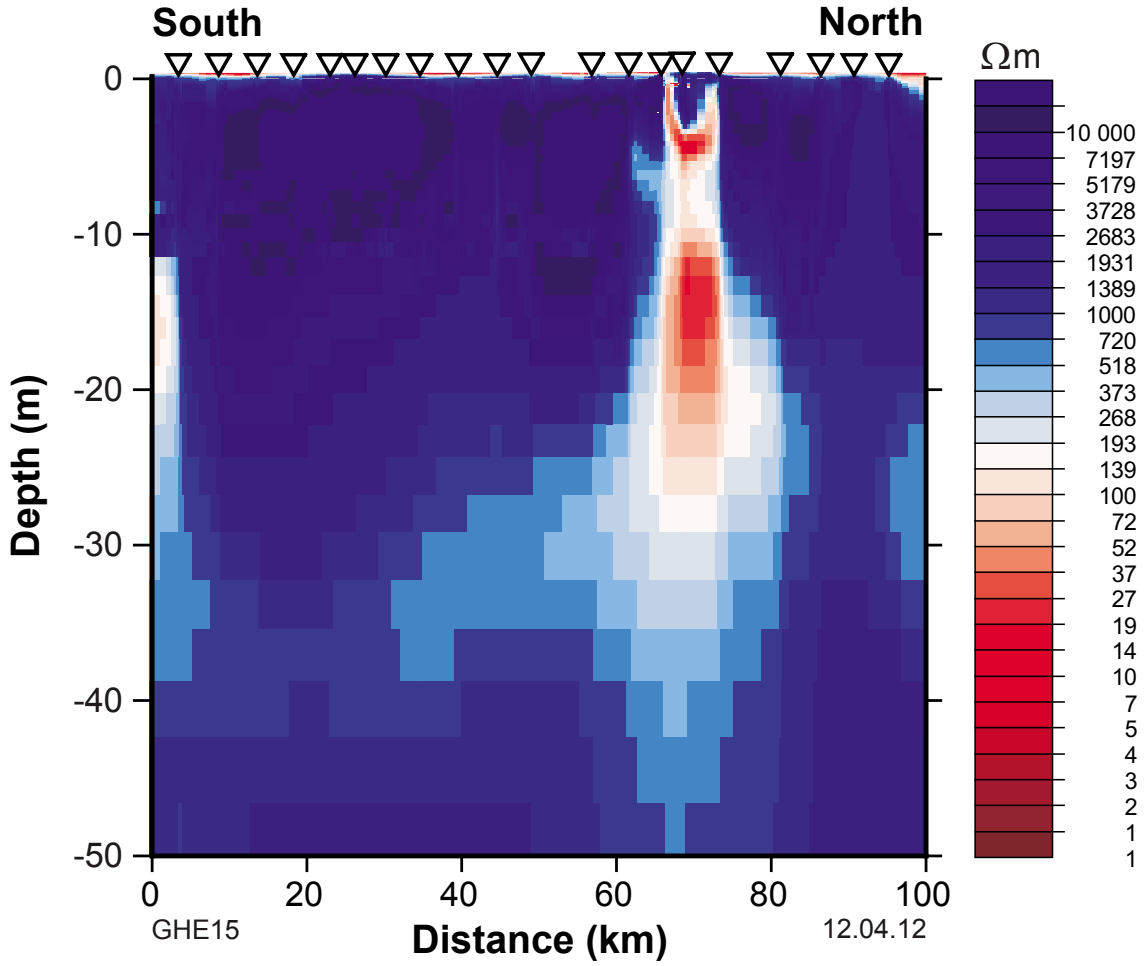

Figure 15. 2D resistivity section for line 10GA–CP3. The bandwidth of the inversion was 200 – 0.1 Hz, and the profile orientation was taken as being geographic north (with geological strike perpendicular to the profile). The inversion achieved a misfit of about rms = 4 to both TE and TM mode data, with 5% errors and static shift as another model variable.

for the Capricorn Seismic study, although a closer comparison with the interpreted seismic section may yield important new constraints on these structures.

Acknowledgement

We acknowledge the Western Australian Government's Exploration Incentive Scheme (EIS) and the Australia Federal Government's National Earth Science Infrastructure Program (AuScope) for funding of the MT program; and GSWA and Geoscience Australia are thanked for providing significant logistical support for fieldwork. The authors gratefully acknowledge the pastoralists and Aboriginal communities from the survey region for allowing us land access. We are indebted to the many station owners along this profile that provided accommodation for the field crews, and thereby made the survey achievable. The University of Adelaide is thanked for the ongoing technical, administrative, and research support that makes this, and other surveys, feasible.

References

Caldwell, TG, Bibby, HM and Brown, C 2004, The magnetotelluric phase tensor: Geophysical Journal International, v. 158, no. 2, p. 457–469.

Chave, AD, Thompson, DJ and Ander, ME 1987, On the robust estimation of power spectra, coherences and transfer functions: Journal of Geophysical Research — Solid Earth, v. 92, p. 633–648.

Jones, AG 1988, Static shift of magnetotelluric data and its removal in a sedimentary basin environment: Geophysics, v. 53, p. 967–978.

Parkinson, WD 1962, The influence of continents and oceans on geomagnetic variations: Geophysical Journal of the Royal Astronomical Society, v. 6, p. 441–449.

Rodi, W and Mackie, RL 2001, Nonlinear conjugate gradients algorithm for 2-D magnetotelluric inversion: Geophysics, v. 66, no. 1, p. 174–187.

Selway, K, Sheppard, S, Thorne, AM, Johnson, SP and Groenewald, PB 2009, Identifying the lithospheric structure of a Precambrian orogen using magnetotellurics: The Capricorn Orogen, Western Australia: Precambrian Research, v. 168, p. 185–196.

Simpson, F and Bahr, K 2005, Practical Magnetotellurics: Cambridge University Press, Cambridge, UK, 270p.

Wannamaker, PE, Hohmann, GW and Ward, SH 1984, Magnetotelluric responses of three-dimensional bodies in layered earths: Geophysics, v. 49, p. 1517–1533.

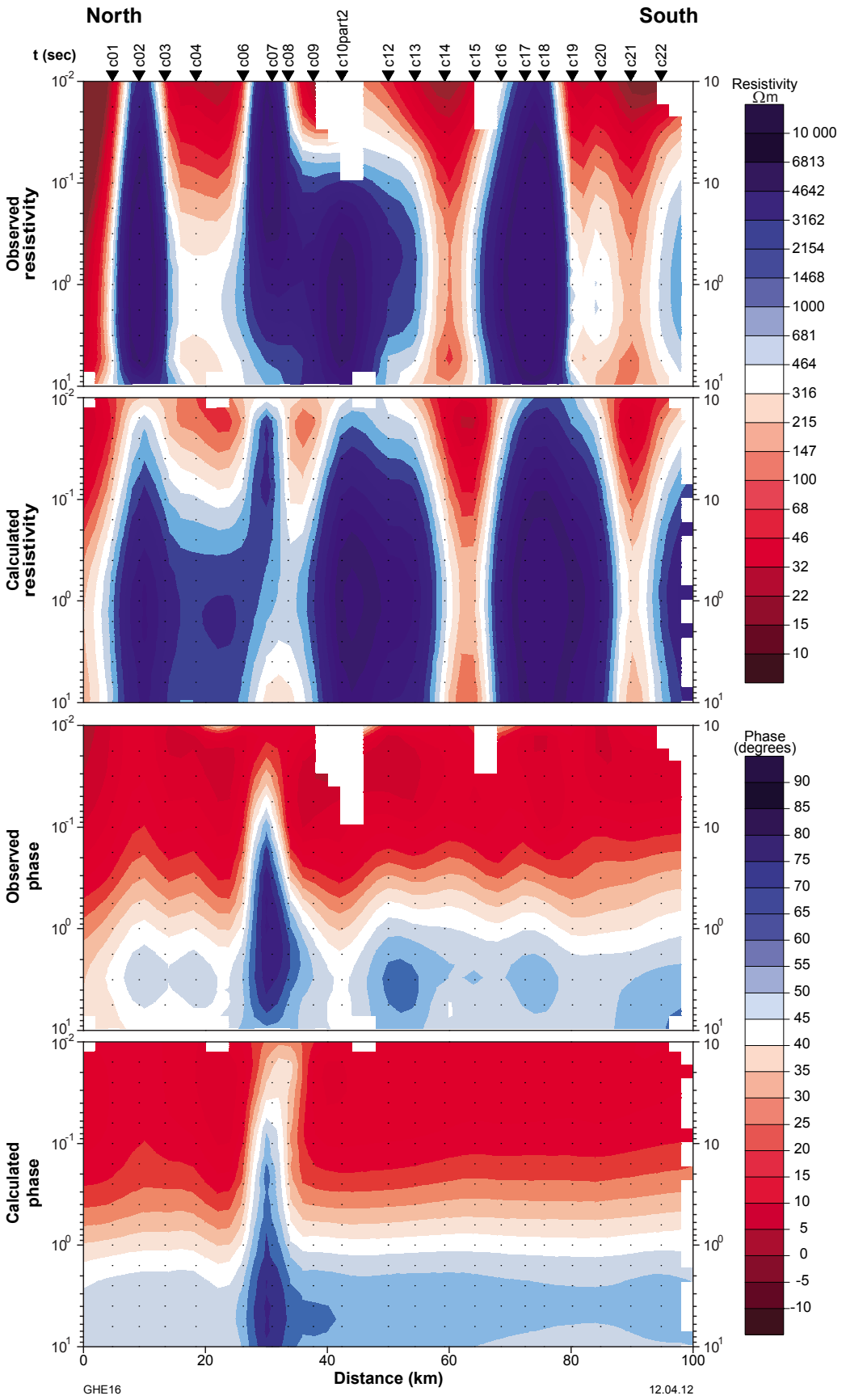

Figure 16. Pseudosections for line 10GA–CP3 for the bandwidth 200 – 0.1 Hz. The top figure shows the observed TM mode apparent resistivity, and the second panel shows the calculated TM mode apparent resistivity for the model in Figure 15. Similarly, the bottom two figures show the observed and calculated phases.

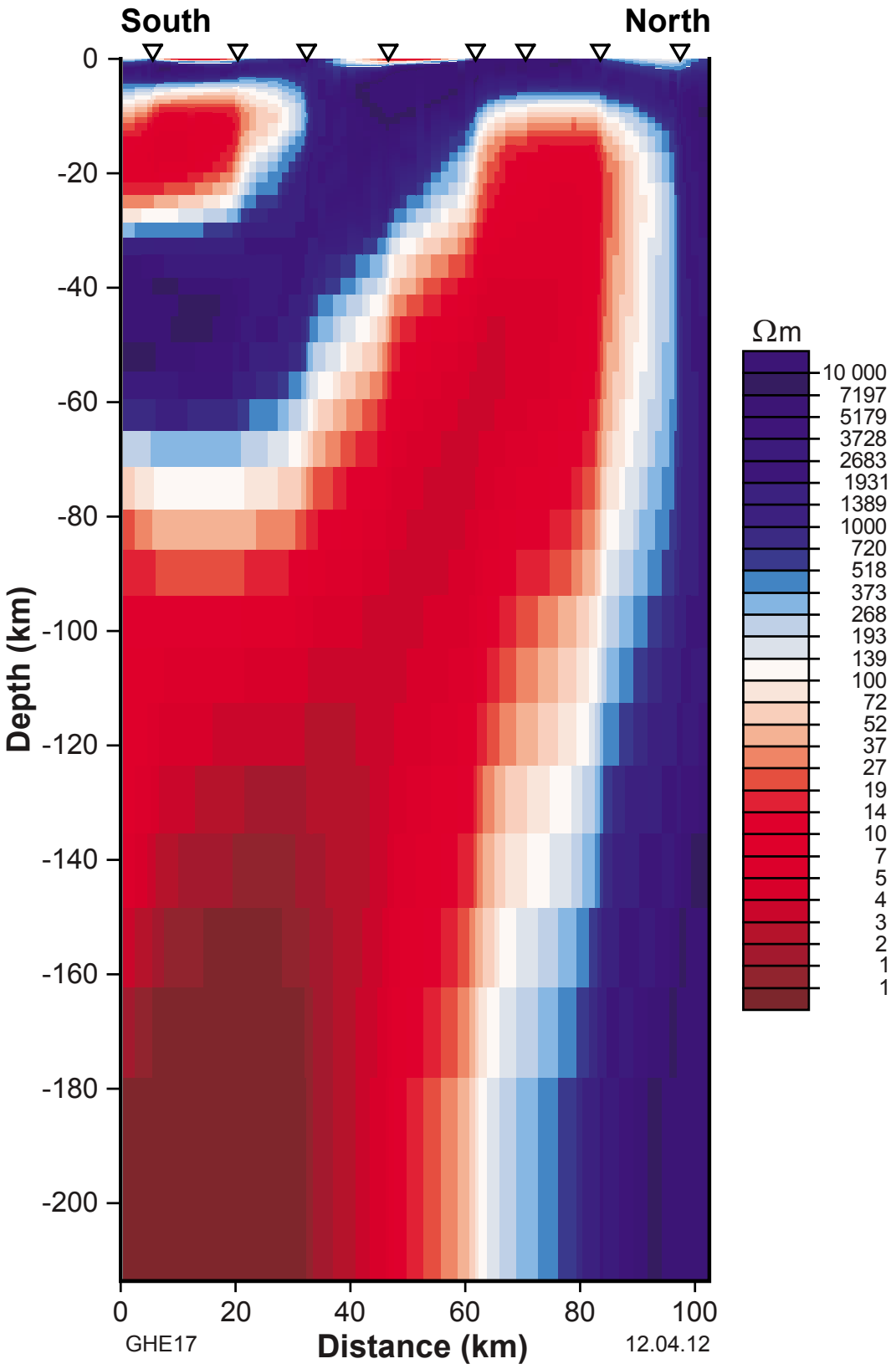

Figure 17. Deep resistivity structure beneath line 10GA–CP3. Note that there is a change in colour scale (compared to Figures 7, 11, and 15), such that the minimum is now 100 Ωm.

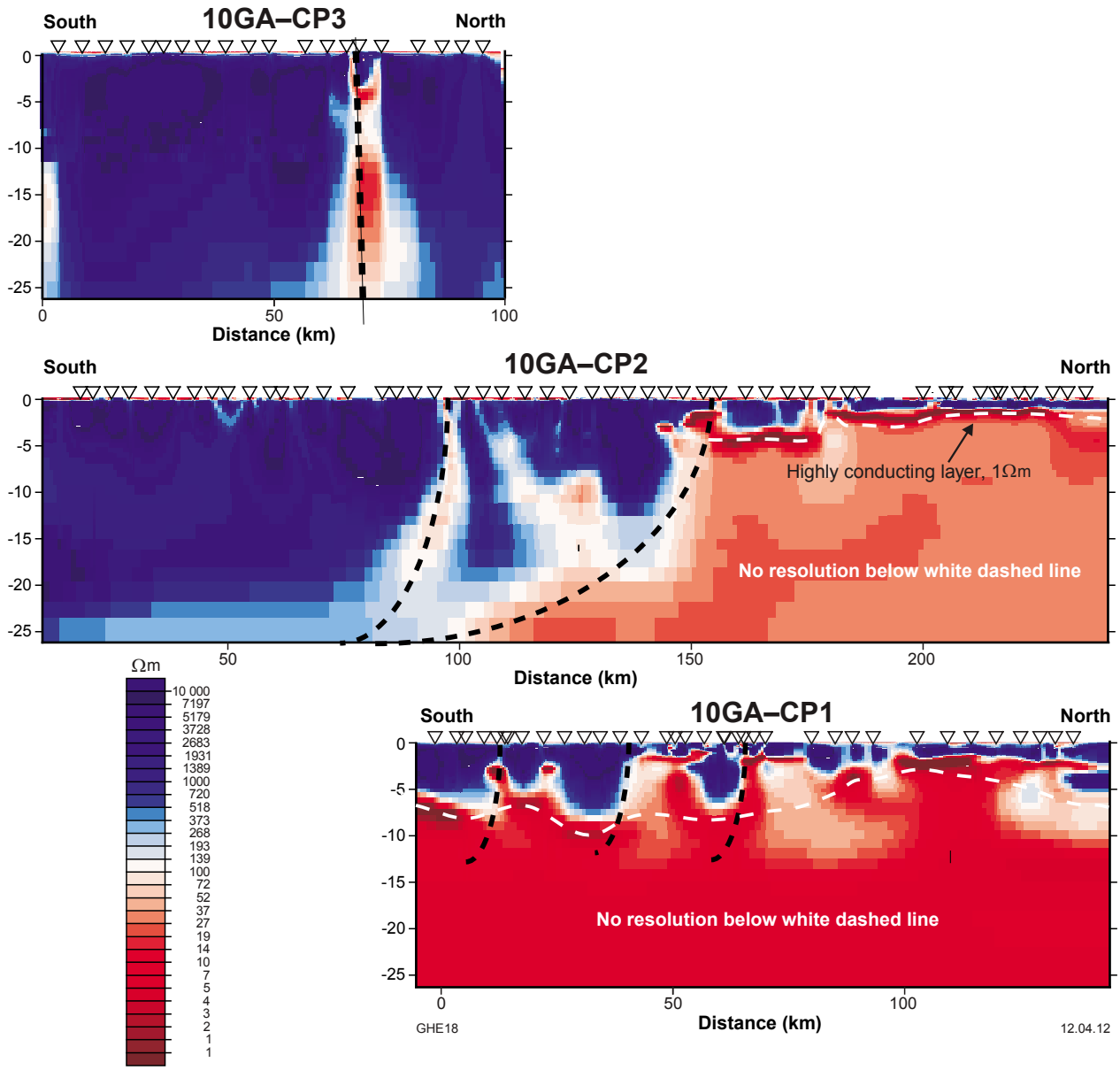

Figure 18. Preliminary interpretation of the three MT sections to a depth of 25 km.

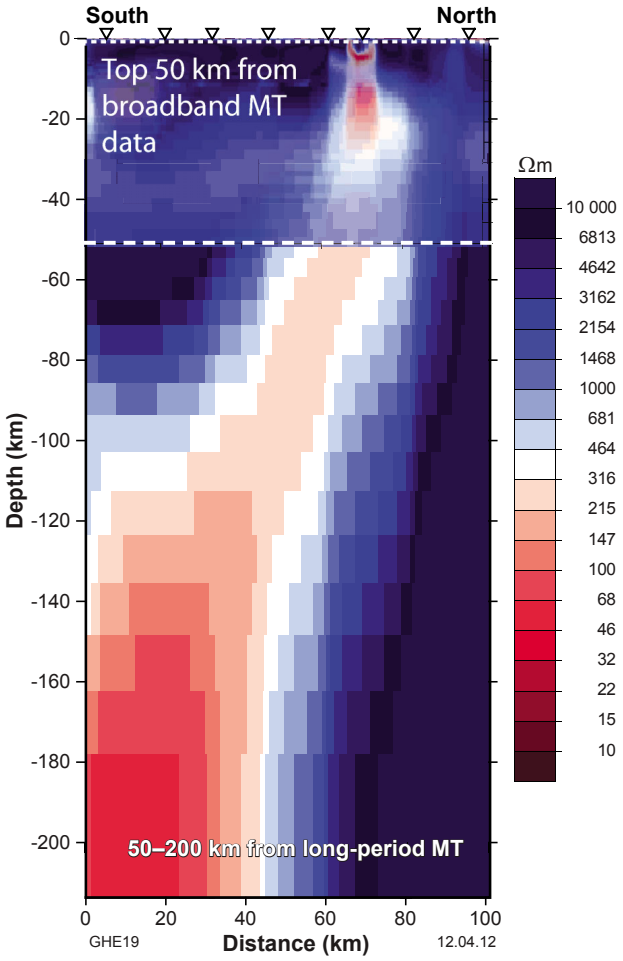

Figure 19. Broadband (top) and long-period (bottom) models for line 10GA–CP3, both at approximately the same scale.

Appendix 1

Station	Long		Lat		Decimal Coordinates					
Station	(°)	(')	(°)	(')	Long (°) Longitude_dd	Lat (°) Latitude_dd	Elevation	Easting	Northing	Zone
CP1B01	117	44.557	22	28.985	117.743	-22.483	639	513511	7513511	50
CP1B02	117	41.973	22	30.269	117.700	-22.504	634	571950	7511164	50
CP1B03	117	39.599	22	31.305	117.660	-22.522	642	567873	7509270	50
CP1B04	117	37.738	22	33.001	117.629	-22.550	653.7	564672	7506156	50
CP1B05	117	37.092	22	35.821	117.618	-22.597	603.9	563542	7500957	50
CP1B06	117	36.898	22	38.822	117.615	-22.647	584	563188	7495421	50
CP1B07	117	35.164	22	41.127	117.586	-22.685	585	560198	7491177	50
CP1B08	117	32.543	22	42.304	117.542	-22.705	544	555704	7489029	50
CP1B09	117	30.541	22	43.191	117.509	-22.720	526.9	552267	7487401	50
CP1B10	117	29.76	22	45.547	117.496	-22.759	516.9	550920	7486061	50
CP1B11	117	29.293	22	48.213	117.488	-22.804	473.4	550107	7478144	50
CP1B12	117	27.17	22	50.012	117.453	-22.834	451	546463	7474836	50
CP1B13	117	24.806	22	51.271	117.413	-22.855	448	542415	7472526	50
CP1B14	117	23.091	22	53.521	117.385	-22.892	433	539471	7468384	50
CP1B15	117	21.559	22	56.19	117.359	-22.937	398.4	536842	7463465	50
CP1B16	117	19.234	22	57.836	117.321	-22.964	381	532860	7460438	50
CP1B17	117	16.944	22	58.46	117.282	-22.974	366	528947	7459294	50
CP1B18	117	13.974	22	58.632	117.233	-22.977	349	523871	7458986	50
CP1B19	117	11.206	22	58.193	117.187	-22.970	343	519142	7459802	50
CP1B20	117	8.569	22	58.982	117.143	-22.983	318.4	514639	7458350	50
CP1B21	117	5.769	22	58.073	117.096	-22.968	305.6	509854	7460033	50
CP1B22	117	4.676	23	0.025	117.078	-23.000	295.2	507986	7456432	50
CP1B23	117	4.204	23	2.219	117.070	-23.037	285	507179	7452387	50
CP1B24	117	6.148	23	4.177	117.102	-23.070	290	510495	7448770	50
CP1B25	117	8.246	23	6	117.137	-23.100	285	514074	7445411	50
CP1B26	117	8.475	23	9.233	117.141	-23.154	279	514460	7439440	50
CP1B27	117	7.831	23	11.656	117.131	-23.194	260	513358	7434967	50
CP1B28	117	8.421	23	14.329	117.140	-23.239	256	514358	7430037	50
CP1B29	117	8.023	23	16.131	117.134	-23.269	240	513675	7426713	50
CP1B30	117	5.168	23	17.56	117.086	-23.293	238	508808	7424079	50
CP1B31	117	3.189	23	19.408	117.053	-23.323	235	505433	7420671	50
CP1B32	117	2.179	23	21.7	117.036	-23.362	237	503713	7416442	50
CP1B33	117	3.161	23	23.853	117.053	-23.398	242	505384	7412470	50
CP1B34	117	5.778	23	25.152	117.096	-23.419	240	509838	7410071	50
CP1B35	117	7.668	23	26.823	117.128	-23.447	250	513054	7406985	50
CP1B36	117	9.175	23	29.01	117.153	-23.484	248	515615	7402946	50
CP1B37	117	8.359	23	30.997	117.139	-23.517	258	514224	7399279	50
CP1B38	117	11.644	23	33.251	117.194	-23.554	263	519805	7395118	50
CP1B39	117	11.246	23	35.846	117.187	-23.597	276	519124	7390329	50

Station	Long		Lat		Decimal Coordinates					
	(°)	(')	(°)	(')	Long (°)	Lat (°)				
Station					Longitude_dd	Latitude_dd	Elevation	Easting	Northing	Zone
CP2B01	116	40.803	23	29	116.680	-23.486	339	467330	7402597	50
CP2B02	116	39.032	23	31	116.651	-23.513	304	464321	7399642	50
CP2B03	116	37.068	23	32	116.618	-23.532	290	460987	7397544	50
CP2B04	116	34.838	23	32	116.581	-23.538	281	457194	7396905	50
CP2B05	116	35.395	23	34	116.590	-23.568	289	458151	7393550	50
CP2B06	116	36.944	23	36	116.616	-23.604	297	460795	7389613	50
CP2B07	116	37.434	23	39	116.624	-23.645	314	461642	7384985	50
CP2B08	116	39.695	23	40	116.662	-23.670	323	465491	7382305	50
CP2B09	116	40.363	23	42	116.673	-23.707	338	466638	7378199	50
CP2B10	116	38.914	23	45	116.649	-23.750	354	464187	7373370	50
CP2B11	116	39.315	23	46	116.655	-23.773	374	464873	7370912	50
CP2B12	116	37.919	23	49	116.632	-23.813	398	462513	7366478	50
CP2B13	116	36.503	23	51	116.608	-23.847	444	460122	7362635	50
CP2B14	116	34.564	23	52	116.576	-23.874	410	456841	7359652	50
CP2B15	116	33.967	23	55	116.566	-23.915	400	455839	7355153	50
CP2B16	116	30.959	23	56	116.516	-23.927	382	450744	7353774	50
CP2B17	116	28.824	23	57	116.480	-23.953	372	447132	7350924	50
CP2B18	116	28.353	23	60	116.473	-23.997	364	446351	7343008	50
CP2B19	116	27.891	24	2	116.465	-24.034	354	445583	7341935	50
CP2B20	116	27.178	24	4	116.453	-24.074	350	444392	7337426	50
CP2B21	116	27.191	24	7	116.453	-24.118	344	444434	7332633	50
CP2B22	116	26.585	24	10	116.443	-24.169	390	443429	7326961	50
CP2B23	116	26.768	24	12	116.446	-24.205	400	443753	7322997	50
CP2B24	116	24.611	24	14	116.410	-24.234	394	440118	7319768	50
CP2B25	116	22.863	24	16	116.381	-24.261	377	437172	7316713	50
CP2B26	116	20.219	24	17	116.337	-24.279	377	432710	7314683	50
CP2B27	116	17.625	24	18	116.294	-24.304	391	428337	7311930	50
CP2B28	116	17.765	24	20	116.296	-24.341	370	428593	7307809	50
CP2B29	116	18.072	24	23	116.301	-24.384	347	429135	7303087	50
CP2B30	116	17.632	24	26	116.294	-24.429	328	428418	7298136	50
CP2B31	116	17.101	24	28	116.285	-24.472	315	427544	7293277	50
CP2B32	116	15.212	24	30	116.254	-24.508	321	424376	7289380	50
CP2B33	116	13.415	24	33	116.224	-24.545	302	421365	7285233	50
CP2B34	116	12.730	24	35	116.212	-24.579	301	420230	7281415	50
CP2B35	116	11.135	24	37	116.186	-24.615	286	417560	7277481	50
CP2B36	116	10.084	24	40	116.168	-24.666	280	415823	7271817	50
CP2B37	116	9.261	24	42	116.154	-24.703	300	414458	7267721	50
CP2B38	116	6.822	24	43	116.114	-24.725	315	410362	7265261	50
CP2B39	116	4.255	24	44	116.071	-24.739	299	406046	7263665	50
CP2B40	116	1.873	24	45	116.031	-24.756	280	402045	7261680	50
CP2B41	116	0.550	24	43	116.009	-24.787	274	399850	7257169	50
CP2B42	115	58.392	24	49	115.973	-24.824	251	396233	7254161	50
CP2B43	115	56.743	24	52	115.946	-24.861	240	393490	7250047	50
CP2B44	115	56.920	24	54	115.949	-24.904	240	393825	7245283	50

Station	Long		Lat		Decimal Coordinates					
Station	(°)	(')	(°)	(')	Long (°) Longitude_dd	Lat (°) Latitude_dd	Elevation	Easting	Northing	Zone
CP2B45	115	58.432	24	56	115.974	-24.939	247	396400	7241451	50
CP2B46	115	57.892	24	59	115.965	-24.978	253	395523	7237074	50
CP2B47	115	57.906	25	1	115.965	-25.024	238	395586	7231981	50
CP2B48	115	57.682	25	3	115.961	-25.056	244	395237	7228474	50
CP2B49	115	58.311	25	6	115.972	-25.098	249	396327	7223804	50
CP2B50	115	8.302	25	8	115.961	-25.138	271	395273	7219328	50
CP2B51	115	55.587	25	10	115.926	-25.170	239	391814	7215808	50
CP2B52	115	54.061	25	13	115.901	-25.209	238	389285	7211494	50
CP2B53	115	54.467	25	15	115.908	-25.249	247	390003	7207033	50
CP2B54	115	51.152	25	18	115.853	-25.293	243	384482	7202100	50
CP2B55	115	52.135	25	16	115.869	-25.273	244	386111	7204333	50
CP3B01	116	40.103	25	16.017	116.668	-25.267	358	466611	7205450	50
CP3B02	116	39.547	25	18.340	116.659	-25.306	367	465688	7201160	50
CP3B03	116	39.666	25	20.663	116.661	-25.344	370	465894	7196874	50
CP3B04	116	39.195	25	23.391	116.653	-25.390	377	465121	7191838	50
CP3B05	116	38.324	25	25.292	116.639	-25.422	387	463698	7188327	50
CP3B06	116	39.184	25	27.589	116.653	-25.460	397	465123	7184087	50
CP3B07	116	38.785	25	30.140	116.646	-25.502	426	464465	7179380	50
CP3B08	116	41.081	25	31.767	116.685	-25.529	414	468318	7176387	50
CP3B09	116	40.716	25	34.005	116.679	-25.567	396	467718	7172255	50
CP3B10 part 1	116	40.045	25	36.481	116.667	-25.608	390	466605	7167682	50
CP3B10 part 2	116	40.045	25	36.481	116.667	-25.608	390	466605	7167682	50
CP3B11	116	39.224	25	38.445	116.654	-25.641	379	465241	7164053	50
CP3B12	116	38.344	25	40.503	116.639	-25.675	376	463782	7160251	50
CP3B13	116	37.438	25	42.791	116.624	-25.713	363	462277	7156024	50
CP3B14	116	37.948	25	45.500	116.632	-25.758	361	463144	7151028	50
CP3B15	116	37.755	25	48.154	116.629	-25.803	352	462833	7146129	50
CP3B16	116	38.963	25	50.612	116.649	-25.844	364	464863	7141598	50
CP3B17	116	40.382	25	52.882	116.673	-25.881	365	467244	7137414	50
CP3B18	116	40.987	25	54.635	116.683	-25.911	350	468263	7134180	50
CP3B19	116	39.272	25	57.009	116.655	-25.950	345	465411	7129791	50
CP3B20	116	37.488	25	59.357	116.625	-25.989	342	462448	7125453	50
CP3B21	116	36.328	26	1.936	116.605	-26.032	334	460527	7120683	50
CP3B22	116	36.107	26	4.644	116.602	-26.077	331	460174	7115684	50

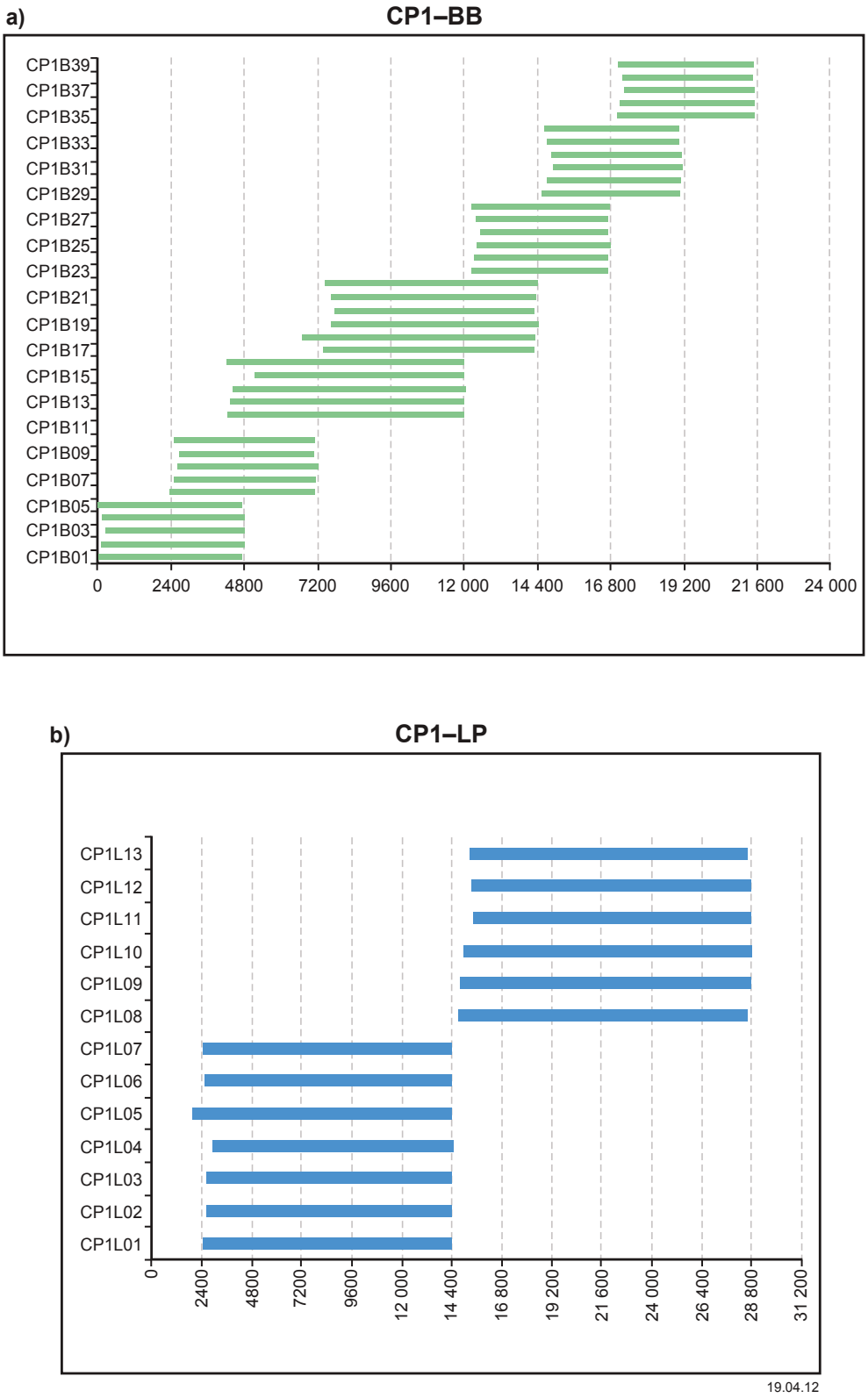

Figure A1. Duration of deployment for line 10GA–CPI

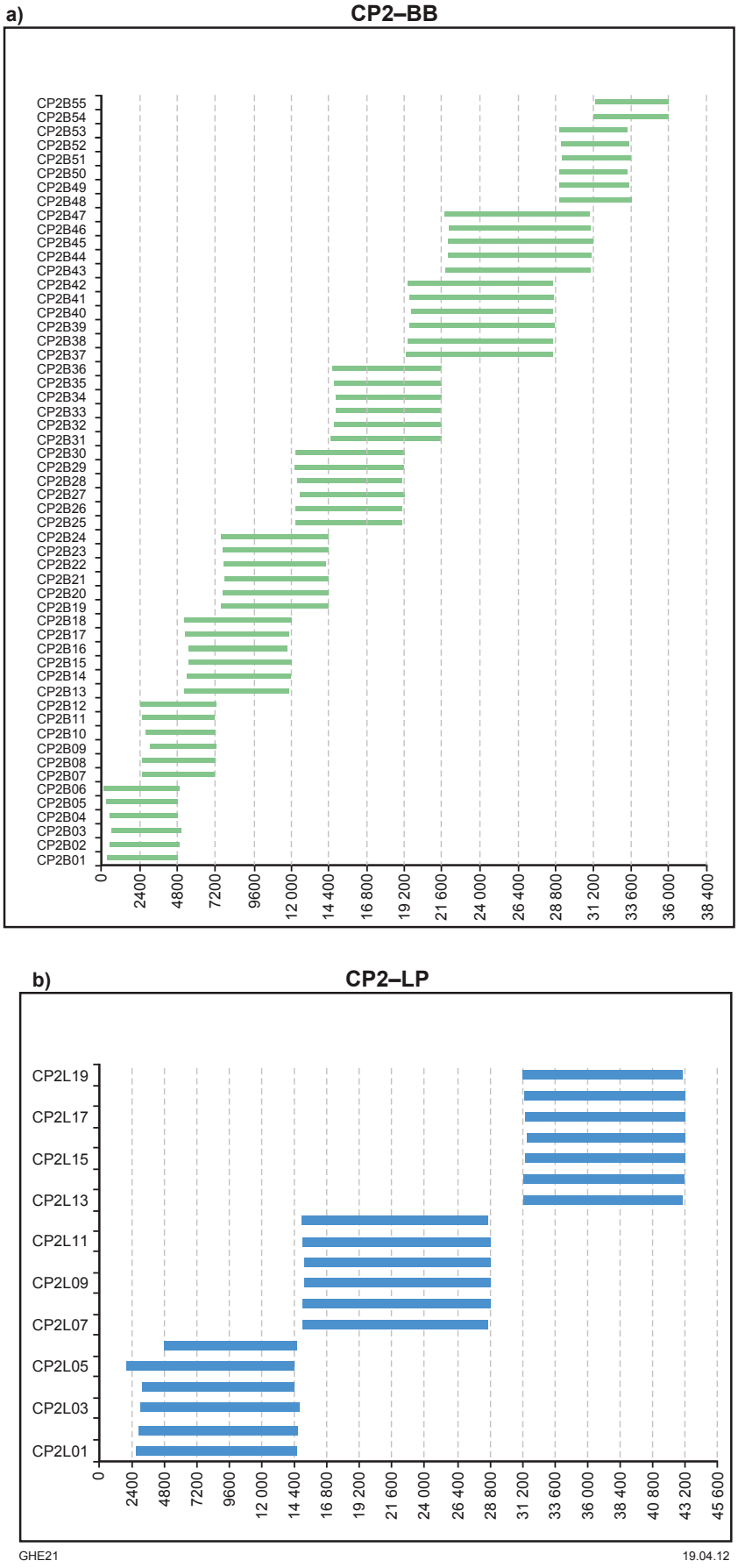

Figure A2. Duration of deployments for line 10GA–CP2

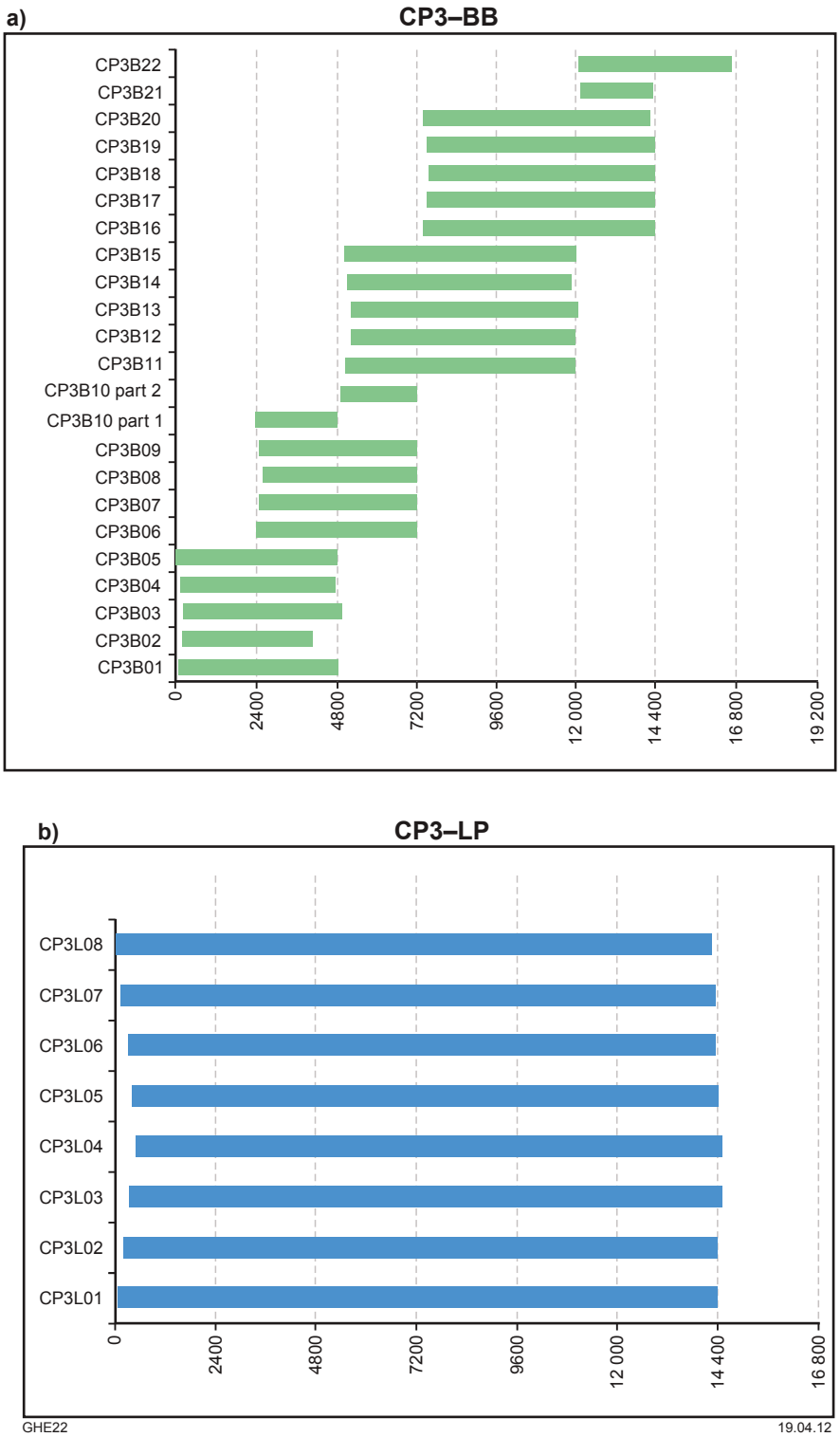

Figure A3. Duration of deployments for line 10GA–CP3

Understanding the lithosphere in the vicinity of the Capricorn seismic lines from passive seismic studies

by

BLN Kennett[1]

Introduction

The Australian National University has carried out deployments of portable broadband seismic recorders across Australia since 1992. These instruments provide high-fidelity recordings of ground motion, and record both regional and distant earthquakes. The seismograms can then be analysed to generate information on the lithospheric structure beneath the Australian region, using a variety of analysis styles; an early example is provided by van der Hilst et al. (1998). An overview is provided by Kennett (2003).

The principal information obtained from regional earthquakes comes from the analysis of the large-amplitude surface waves late in the seismograms. These surface waves travel almost horizontally through the lithosphere and, with a sufficient density of crossing paths, can be used in a tomographic inversion to determine 3D structure in the lithospheric mantle. Receiver-based studies at individual stations exploit the conversions and reverberations following the onset of the P-wave energy. From distant earthquakes, information can be extracted about the structure in the crust and uppermost mantle.

In recent years, additional information has begun to be extracted from the seismic noise field through the stacked cross-correlation of signals at pairs of stations, which provide an approximation of the signal expected for a source at one station recorded at the other location. This ambient noise tomography approach was pioneered in Australia by Saygin (2007), who used the continuous data recordings at the portable stations in association with data from permanent seismic stations to link different experiments. The main signal comes from high-frequency surface waves that provide imaging of upper crustal structure, and which are particularly sensitive to the presence of sediments (Saygin and Kennett, 2010).

[1] Research School of Earth Sciences, The Australian National University, Canberra ACT 2000.

Surface wave tomography

The earthquake belts north of Australia, along the Indonesian arc into New Guinea, and those to the east in the Tonga–Fiji zone, provide frequent seismic events of suitable magnitude that are well recorded in Australia. There are less common events to the south along the mid-oceanic ridge between Australia and Antarctica, but these are important in providing additional directional control. A number of different techniques have been used to analyse the large-amplitude surface waves that arrive late in the seismogram, and from the combination of these results from many paths, to extract 3D models of the seismic shear wavespeed distribution (e.g. van der Hilst et al., 1998; Debayle and Kennett, 2000, 2003; Kennett et al., 2004a,b; Yoshizawa and Kennett, 2004; Fishwick et al., 2005, 2008; Fichtner et al., 2009, 2010). Most of these methods rely on some approximations to wave propagation in three dimensions, although the work of Fitchner et al. (2009, 2010) uses full seismogram calculations in a 3D model. In consequence, the frequency range used is restricted to prevent excessive computational requirements. Fortunately, the results from this sophisticated analysis indicate that the longer wavelength features obtained with the approximate methods are confirmed.

We can now have considerable confidence in the main lithospheric structures at a horizontal scale of about 200 km and a vertical resolution around 30 km. Figure 1 illustrates the shear wave structure in Western Australia, using a new model developed through collaboration between the authors of different studies (Yoshizawa and Kennett, 2004, Fishwick et al., 2008; Fichtner et al., 2010). This new model benefits from the incorporation of more paths than any individual study, and includes the use of techniques that provide improved resolution at depth. The variations in seismic S-wave velocity are displayed in terms of the absolute shear wavespeed, with a neutral colour chosen to represent typical continental values.

Regions with faster S wavespeeds than the continental reference are indicated by bluish tones, and zones with slower S wavespeeds are shown in brown tones in

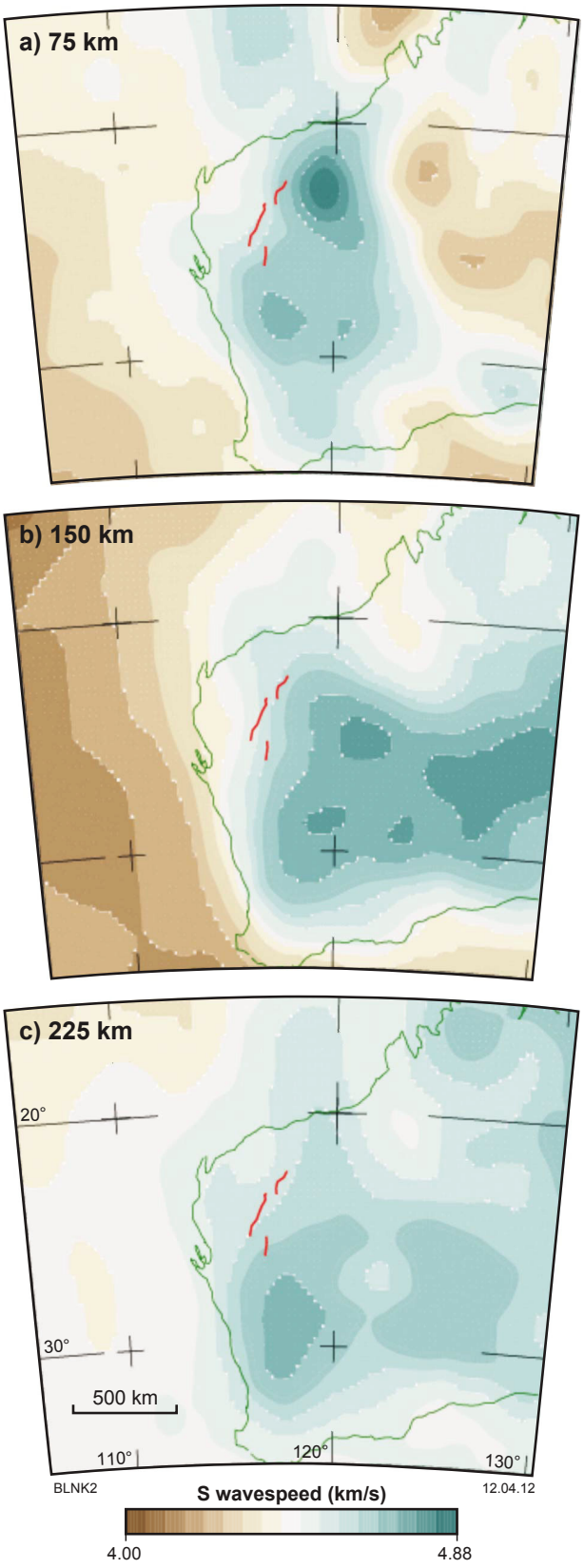

Figure 1. Seismic shear-wavespeed structure in Western Australia, determined from surface wave tomography. Continental scale measurements of seismic wavespeed variation at (a) 75 km; (b) 150 km; and (c) 225 km depth, inferred from the analysis of surface waves. The Capricorn lines are indicated in red in each panel.

Figure 1. Reductions in seismic wavespeed are expected from the influence of temperature, or the presence of volatiles. Faster wavespeeds are produced by cooler temperatures; however, the very fast wavespeeds seen in Figure 1 are very difficult to produce by temperature alone, and suggest the presence of chemical heterogeneity.

The mantle lithosphere below 100 km is marked by distinctly fast seismic wavespeeds, but at about 75 km, there is an indication of somewhat reduced wavespeeds (Fig. 1a) in the east of WA, which may be linked in part to the presence of thickened crust. This feature is not associated with enhanced seismic attenuation, as might be expected if the cause was a concentration of radioactivity in the uppermost mantle.

At 75 km, the Paterson Province is marked by very high seismic wavespeeds, and there is also a distinct, rather fast patch in the northern Yilgarn Craton. There is no distinctive mantle feature associated with the Capricorn Orogen, although we noted that at 225 km the Capicorn Orogen and Pilbara Craton show somewhat lower shear-wavespeeds than in the Yilgarn Craton. The surface wave tomography results are consistent with a situation in which the Capricorn Orogen is more strongly coupled to the Pilbara Craton than the Yilgarn Craton.

Receiver function studies

A powerful method to extract information on crustal structure is to analyse the conversions and reverberations immediately following the onset of the P wave for distant earthquakes using the receiver function technique. The two horizontal components of motion are then combined to produce records with polarization along, (radial) and perpendicular (tangential) to, the great circle back to the source. The rotated components are then deconvolved using the vertical component of motion that represents dominantly P waves. In this way, the influence of the source is largely eliminated, and attention is focused on wave propagation processes close to the receiver. When there is little energy on the tangential receiver function, 3D structural variation is weak and an inversion may then be made using a radial receiver function for an effective 1D structure in the neighbourhood of the receiver (e.g. Shibutani et al., 1996; Sambridge, 1999). Alternative approaches use stacking of receiver functions to emphasise features such as the conversion from the crust–mantle boundary, and hence constrain the depth of the Mohorovičić discontinuity (‘the Moho’). The moveout pattern of conversions and multiples from different source distances can be used to constrain the depth of seismic boundaries and Vp/Vs ratios (Zhu and Kanamori, 2000). It can also be advantageous to make a partial allowance for the influence of the free-surface on the seismograms by a rotation of components in the vertical plane, or a transformation (e.g. Reading et al., 2003a).

The first systematic treatment of receiver function results across Australia was made by Clitheroe et al. (2000a,b), with an emphasis on the thickness of the crust and the base of sediments; a few of these stations lie in the zone near the Capricorn profile.

A particular focus of portable broadband deployments since 2000 has been on Western Australia, with a number of deployments that now provide good coverage of the Archean cratons, and the Proterozoic Capricorn Orogen. Receiver function studies have provided clear evidence for segmentation of the Yilgarn Craton, with characteristic crustal structures for the individual terranes (Reading et al., 2003b, 2007).

In 2005, stations were deployed in association with the University of Western Australia, mostly along the coastal zone of northwestern Australia to monitor seismicity. Subsequently, in 2006–2007, a major deployment of 20 instruments was made throughout the Capricorn Orogen, and along the Telfer Road into the Paterson Province. The locations of many of the stations in this CAPRA project lie close to the reflection profile, and so provide very useful comparisons as to the nature of crustal structure. Reading et al. (2012) presents a detailed analysis of the receiver function responses at these CAPRA stations.

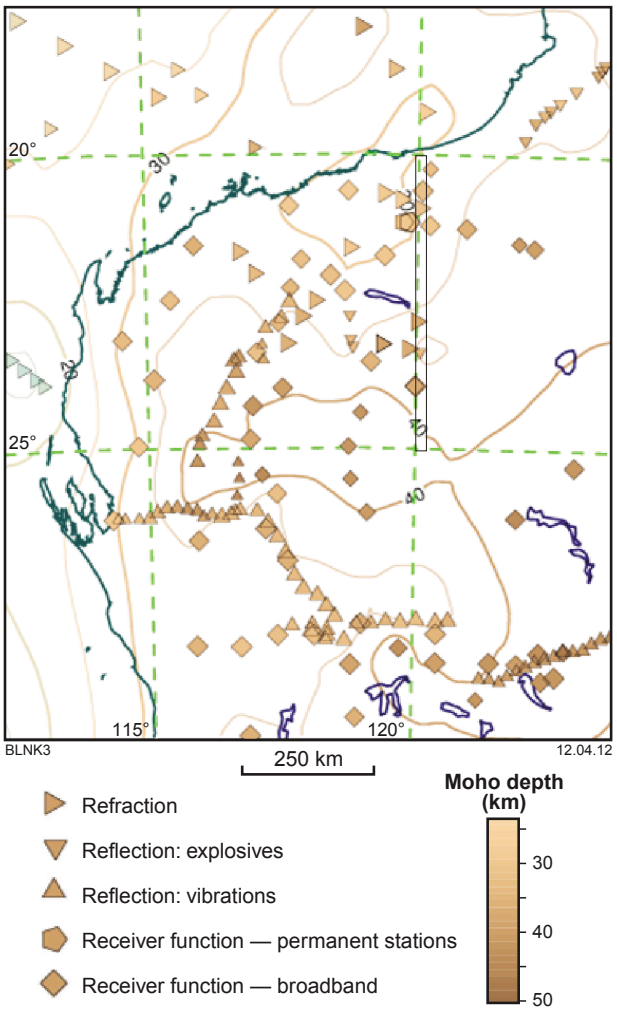

Figure 2. Estimates of crustal thickness derived from refraction experiments (triangles) and receiver function studies (diamonds — broadband stations; squares — short-period stations; less reliable results indicated by smaller symbols). Estimates of the Mohorovičić discontinuity ('the Moho') from reflection work are indicated by the dense lines of triangles. The contours of Moho depth are derived from a continent-wide synthesis (Kennett et al., 2011)

The estimates of crustal thickness derived from the receiver function analysis are summarized in Figure 2, and are plotted alongside results derived from refraction and reflection experiments. In each case, the crust–mantle boundary is taken at the base of the transition to mantle seismic velocities (P wavespeeds above 7.9 km/s, or shear wavespeeds above 4.4 km/s). In addition estimates of the depth to the Moho, derived from the Capricorn line and other reflection lines in the vicinity are included. There is a close correspondence between the estimates obtained from the different techniques and station deployments, even though the methods of analysis differ somewhat. Fortunately, most of the portable seismic stations appear to lie in zones without any dramatic steps in the Moho. The profile of crust thickness along the zone sampled by the recent CAPRA experiment has a similar configuration to that seen on the reflection profile, and in consequence, the receiver function results provide a check on the calibration of the time–depth conversion for these reflection results.

The background contour plot of the Moho in Figure 2 is derived from a continent-wide synthesis of results, using all receiver functions and the refraction data from the compilation of Collins et al. (2003), with additional control from reflection experiments (Kennett et al., 2011).

Discussion and conclusions

Passive seismic methods exploiting natural events provide valuable information on 3D variations in lithospheric structure, which can be helpful in the interpretation of other classes of information, such as reflection seismic profiles. Surface wave tomography provides information on mantle structure, with the most reliable results available below 75 km depth. At shallower depths, there is a strong influence from the crustal structure along the various paths, and the crustal structure can be mapped into the uppermost mantle — especially where the crust is thick. The body-wave portion of the seismograms from distant earthquakes yields additional information on structure in the crust and uppermost mantle from the analysis of receiver functions.

Body wave tomography exploiting the times of arrival of seismic phases from regional and teleseismic events, can provide constraints on crustal structure when stations are sufficiently close together. Abdulah (2007; Fig. 3) shows the results of tomography exploiting all available P-wave readings, from both local events and refraction experiments, and distant earthquakes. The contrasts in P wavespeed show a very high correlation with outcrop of the Pilbara Craton.

The results for the area around the Capricorn Orogen line show a strong distinction in the crust between the Pilbara Craton, with a relative thin crust at 30–33 km, and the Capricorn Orogen, where the crust thickens significantly. There is again a sharp change in crustal thickness into the

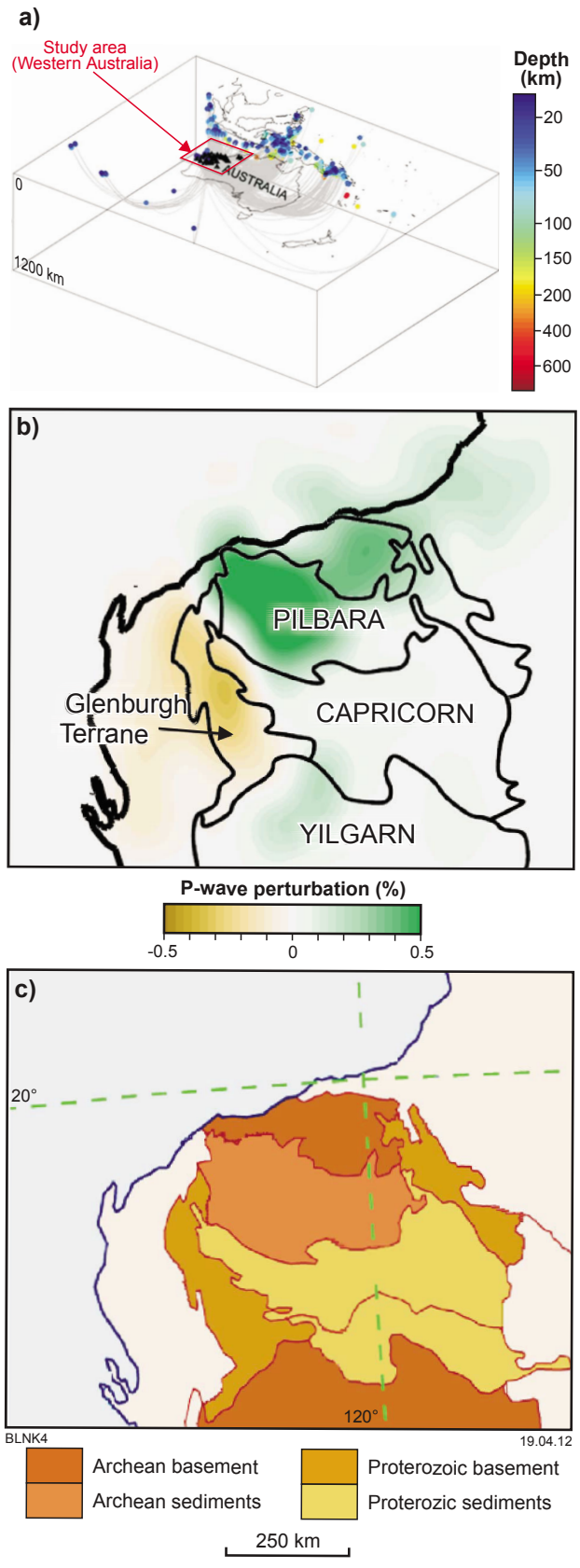

northern Yilgarn Craton. However, the mantle beneath the Capricorn Orogen appears to have greater affinities with the Pilbara Craton, and does not share the rather high-shear wavespeeds seen beneath the Yilgarn Craton.

Acknowledgements

The deployment of portable broadband stations across Australia has depended on the efforts of many people, often working in trying circumstances. Particular thanks are due to John Grant, Steve Sirotjuk, and Qi Li for their major roles in maintaining equipment and logistics, and to Armando Arciadiaco for field support and his critical role in data handling and organization. The CAPRA experiment was led by Dr Anya Reading. Receiver function results draw on the work of Drs Geoff Clitheroe, Anya Reading, Steve Revets, Erdinc Saygin, Michelle Salmon, and Elizabeth Vanacore.

References

Abdulah, A 2007, Seismic body wave attenuation tomography beneath the Australasian region: Australian National University, Canberra, Australian Capital Territory, PhD thesis (unpublished), 163p.

Clitheroe, G, Gudmundsson, O and Kennett, BLN 2000a, The crustal thickness of Australia: Journal of Geophysical Research, v. 105, p. 13697–13713.

Clitheroe, G, Gudmundsson, O and Kennett, BLN 2000b, Sedimentary and upper-crustal structure of Australia from receiver functions: Australian Journal of Earth Sciences, v. 47, p. 209–216.

Collins, CDN, Drummond, BJ and Nicoll, MG 2003, Crustal thickness patterns in the Australian continent, *in* The Evolution and Dynamics of the Australian Plate *edited by* D Müller and R Hillis: Geological Society of Australia, Special Publication 22, and Geological Society of America, Special Paper 372, p. 121–128.

Debayle, E and Kennett, BLN 2000, The Australian continental upper mantle — structure and deformation inferred from surface waves: Journal of Geophysical Research, v. 105, p. 25443–25540.

Debayle, E and Kennett, BLN 2003, Surface wave studies of the Australian region, *in* The Evolution and Dynamics of the Australian Plate *edited by* D Müller and R Hillis: Geological Society of Australia, Special Publication 22, and Geological Society of America, Special Paper 372, p. 25–40.

Fichtner, A, Kennett, BLN, Igel, H and Bunge, H-P 2009, Full seismic waveform tomography for upper-mantle structure in the Australasian region using adjoint methods: Geophysical Journal International, v. 179, p. 1703–1725.

Fichtner, A, Kennett, BLN, Igel, H and Bunge, H-P 2010, Full seismic waveform tomography for radially anisotropic structure: new insights into the past and present states of the Australasian upper mantle: Earth and Planetary Science Letters, v. 290, p. 270–280.

Figure 3. P-wave tomography for northwestern Australia (Abdulah, 2007) for the crustal depth range of 0–35 km; a) configuration of earthquake sources and ray paths, supplemented by local observations from 1977 refraction experiments; b and c) a number of inversions have been undertaken with slightly offset grids, with the results averaged to give a composite image with improved resolution than any individual grid. The zones of fast wavespeed (green) coincide with the elements of the Pilbara and Yilgarn Cratons. Most of the Capricorn Orogen is neutral, but the Glenburgh Terrane shows as distinctly slower (gold).

Fishwick, S, Kennett, BLN and Reading, AM 2005, Contrasts in lithospheric structure within the Australian Craton: Earth and Planetary Science Letters, v. 231, p. 163–176.

Fishwick, S, Heintz, M, Kennett, BLN, Reading, AM and Yoshizawa, K 2008, Steps in lithospheric thickness within eastern Australia, evidence from surface wave tomography: Tectonics, v. 27, no. 4, TC0049, doi:10.129/2007TC002116.

Kennett, BLN 2003, Seismic structure in the mantle beneath Australia, *in* The Evolution and Dynamics of the Australian Plate *edited by* D Müller and R Hillis: Geological Society of Australia, Special Publication 22, and Geological Society of America, Special Paper 372, p. 7–23.

Kennett, BLN, Fishwick, S, Reading, AM and Rawlinson, N 2004a, Contrasts in mantle structure beneath Australia — relation to Tasman Lines?: Australian Journal of Earth Sciences, v. 51, p. 563–569.

Kennett, BLN, Fishwick, S and Heintz, M 2004b, Lithospheric structure in the Australian region — a synthesis of surface wave and body wave studies: Exploration Geophysics, v. 35, p. 258–266.

Kennett, BLN, Salmon, M, Saygin, E and AusMoho working group 2011, AusMoho: the variation in Moho depth across Australia: Geophysics Journal International, v. 187, no. 2, p. 946–958, DOI: 10.1111/j.1365-246X.2011.05194.x.

Reading, A, Kennett, B and Sambridge, M 2003a, Improved inversion for seismic structure using transformed S-wavevector receiver functions: removing the effect of the free surface: Geophysics Research Letters, v. 30, no. 19, p. 1981, doi: 10.1029/2003GL018090.

Reading, AM, Kennett, BLN and Dentith, MC 2003b, The seismic structure of the Yilgarn Craton, Western Australia: Australian Journal of Earth Sciences, v. 50, p. 427–438.

Reading, AM, Kennett, BLN and Goleby, B 2007, New constraints on the seismic structure of West Australia: evidence for terrane stabilization prior to the assembly of an ancient continent?: Geology, v. 35, p. 379–379.

Reading, AM, Tkalčić, H, Kennett, BLN, Johnson, SP and Sheppard S 2012, Seismic structure of the crust and uppermost mantle of the Capricorn and Paterson Orogens and adjacent cratons, Western Australia, from passive seismic experiments: Precambrian Research, v. 196–197, p. 295–308.

Sambridge, MS 1999, Geophysical inversion with a neighbourhood algorithm — I. Searching a parameter space: Geophysics Journal International, v. 138, p. 479–494.

Saygin, E 2007, Seismic receiver and noise correlation based studies in Australia: Australian National University, Canberra, Australian Capital Territory, PhD thesis (unpublished), 175p.

Saygin, E and Kennett, BLN 2010, Ambient noise tomography for the Australian Continent: Tectonophysics, v. 481, p. 116–125, doi:10.106/j.tecto.2008.11.013.

Shibutani, T, Sambridge, M and Kennett, BLN 1996, Genetic algorithm inversion for receiver functions with application to crust and uppermost mantle structure beneath Eastern Australia: Geophysics Research Letters, v. 23, p. 1829–1832.

van der Hilst, RD, Kennett, BLN and Shibutani, T 1998, Upper mantle structure beneath Australia from portable array deployments, *in* The Structure and Evolution of the Australian Lithosphere *edited by* J Braun, J Dooley, B Goleby, R van der Hilst and C Klootwijk: American Geophysical Union, Geodynamics Monograph 26, p. 39–58.

Yoshizawa, K and Kennett, BLN 2004, Multi-mode surface wave tomography for the Australian region using a 3-stage approach incorporating finite frequency effects: Journal of Geophysical Research, v. 109, B02310; doi: 10.129/2002JB002254.

Zhu, L and Kanamori, H 2000, Moho depth variation in southern California from teleseismic receiver functions: Journal of Geophysical Research, v. 105, p. 2969–2980.

Geodynamic implications of the Capricorn deep seismic survey: from the Pilbara Craton to the Yilgarn Craton

by

RJ Korsch[1], SP Johnson, IM Tyler, AM Thorne, RS Blewett[1], HN Cutten, A Joly[2], MC Dentith[2], ARA Aitken[2], JA Goodwin[1], and BLN Kennett[3]

Introduction

The Capricorn Orogen in Western Australia records both the punctuated assembly of the Pilbara and Yilgarn Cratons to form the West Australian Craton, and nearly one billion years of subsequent intracratonic reworking and basin formation (Cawood and Tyler, 2004; Sheppard et al., 2010a). The orogen is over 1000 km long, and includes the passive margin deposits of both the Pilbara and Yilgarn Cratons, variably deformed and metamorphosed granitic and metasedimentary rocks of the Gascoyne Province, and the sedimentary and low-grade metasedimentary rocks that overlie these three tectonic units (Frontispiece 1; Cawood and Tyler, 2004; Sheppard et al., 2010a).

In April and May 2010, 581 km of vibroseis-source, deep seismic reflection and gravity data were acquired along three traverses (10GA–CP1, 10GA–CP2, and 10GA–CP3) through the Capricorn Orogen. The lines started in the southern part of the Pilbara Craton, crossed the Gascoyne Province, and ended in the Narryer Terrane of the Yilgarn Craton (Frontispiece 1; Plate 1). This was a collaborative project between the Geological Survey of Western Australia (GSWA), AuScope (a component of NCRIS, the National Collaborative Research Infrastructure Strategy), and Geoscience Australia. The aim of the survey was to image the crustal architecture in the region, and thereby examine the relationships between the three tectonic units (Kennett et al., 2011). Crustal-scale magnetotelluric data were also collected along, or adjacent to, the seismic traverses (Heinson et al., 2011).

1 Minerals and Natural Hazards Division, Geoscience Australia, GPO Box 378, Canberra ACT 2601.

2 Centre for Exploration Targeting, School of Earth and Environment, University of Western Australia, 35 Stirling Highway, Crawley WA 6009.

3 Research School of Earth Sciences, The Australian National University, Canberra ACT 0200.

Companion papers present summaries of the geological evolution of the region, interpretations of the three seismic lines (Thorne et al., 2011a,b; Johnson et al., 2011a,b; Cutten et al., 2011), and discussions of the potential field geophysics (Goodwin, 2011). The approximate north–south orientation of the seismic lines is essentially perpendicular to the major domains and structures in the region (Frontispiece 1–3; Plate 1), and provides crustal-scale geometries that can be compared with existing geological interpretations. Overall, the crust in the vicinity of the seismic section has variable reflectivity, with some parts of the section containing strong reflections, and other areas having very low reflectivity (Figs 1–3).

Here, we discuss some of the geodynamic implications that arise from interpretation of the new deep seismic reflection data obtained during this project. Of greatest interest is whether there is evidence for a suture between the Pilbara Craton and the Glenburgh Terrane, considered by Johnson et al. (2011c) to be located at the Talga Fault; whether there is a suture between the Glenburgh Terrane and the Narryer Terrane of the Yilgarn Craton, considered by Occhipinti et al. (2004) and Sheppard et al. (2004) to be located at the Errabiddy Shear Zone (Frontispiece 1–3; Plate 1); and whether the Fortescue and Hamersley Groups can be shown to continue south in the subsurface beneath the Ashburton Basin.

Moho

In the region of the Capricorn Orogen seismic sections, the Mohorovičić discontinuity (‘the Moho’) is not well imaged, but is commonly interpreted to occur at the base of the weakly reflective packages, the nonreflective material below which is considered to represent the upper mantle (Figs 1–3). The transition from crust to mantle is most likely gradational along a considerable part of the line length. In the vicinity of seismic line 10GA–CP1, the Moho is gently undulating between the depths of 11.5 to 13 seconds two-way travel time (s TWT; 34–39 km) (Fig. 1; see also Thorne et al., 2011b).

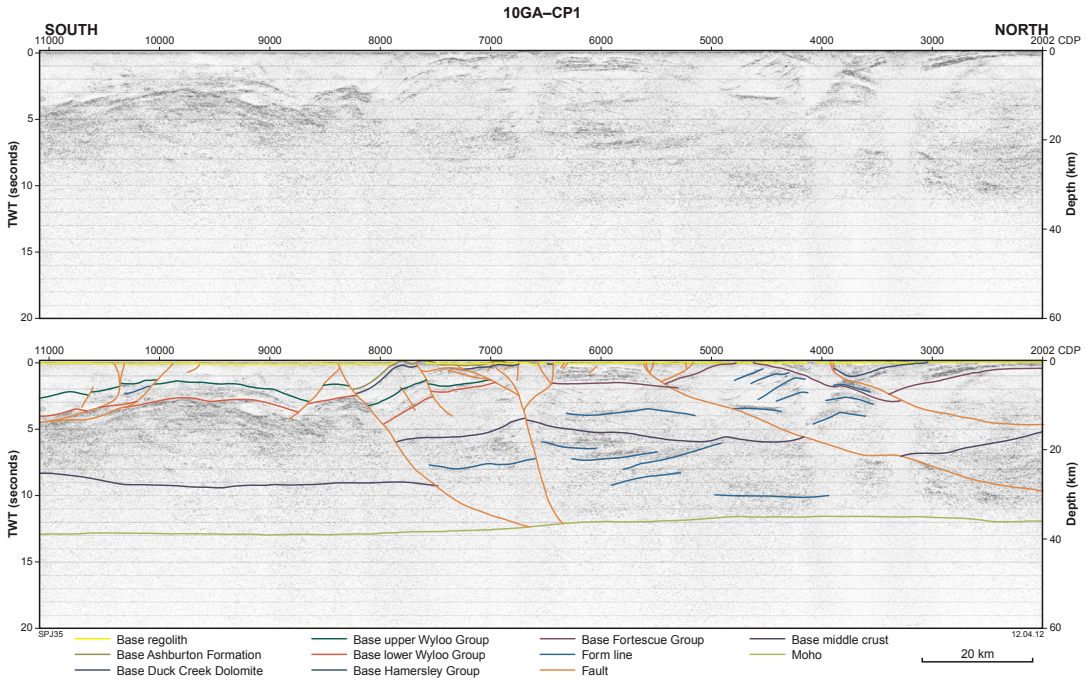

Figure 1. Migrated seismic section for seismic line 10GA–CP1, showing both uninterpreted and interpreted versions. Display is to ~60 km depth, and shows vertical scale equal to horizontal scale, assuming an average crustal velocity of 6000 m/s.

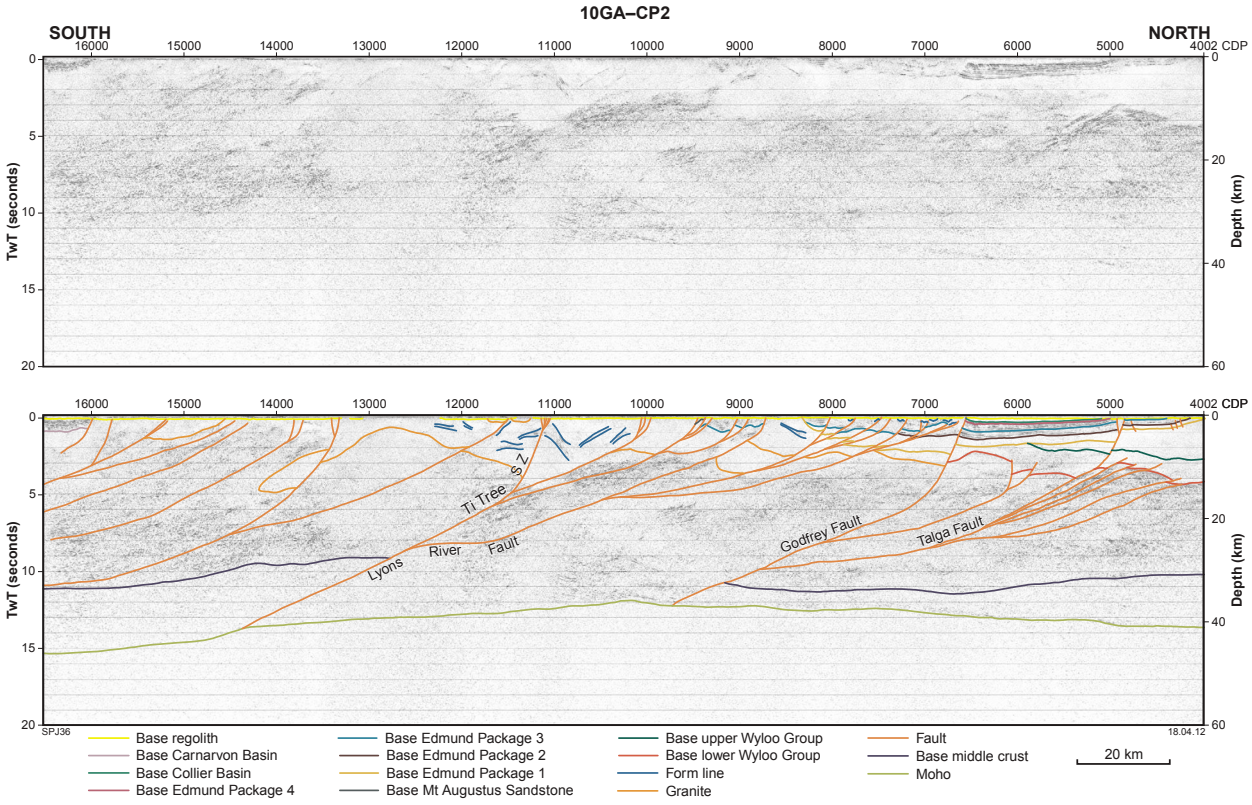

Figure 2. Migrated seismic section for seismic line 10GA–CP2, showing both uninterpreted and interpreted versions. Display is to ~60 km depth, and shows vertical scale equal to horizontal scale, assuming an average crustal velocity of 6000 m/s.

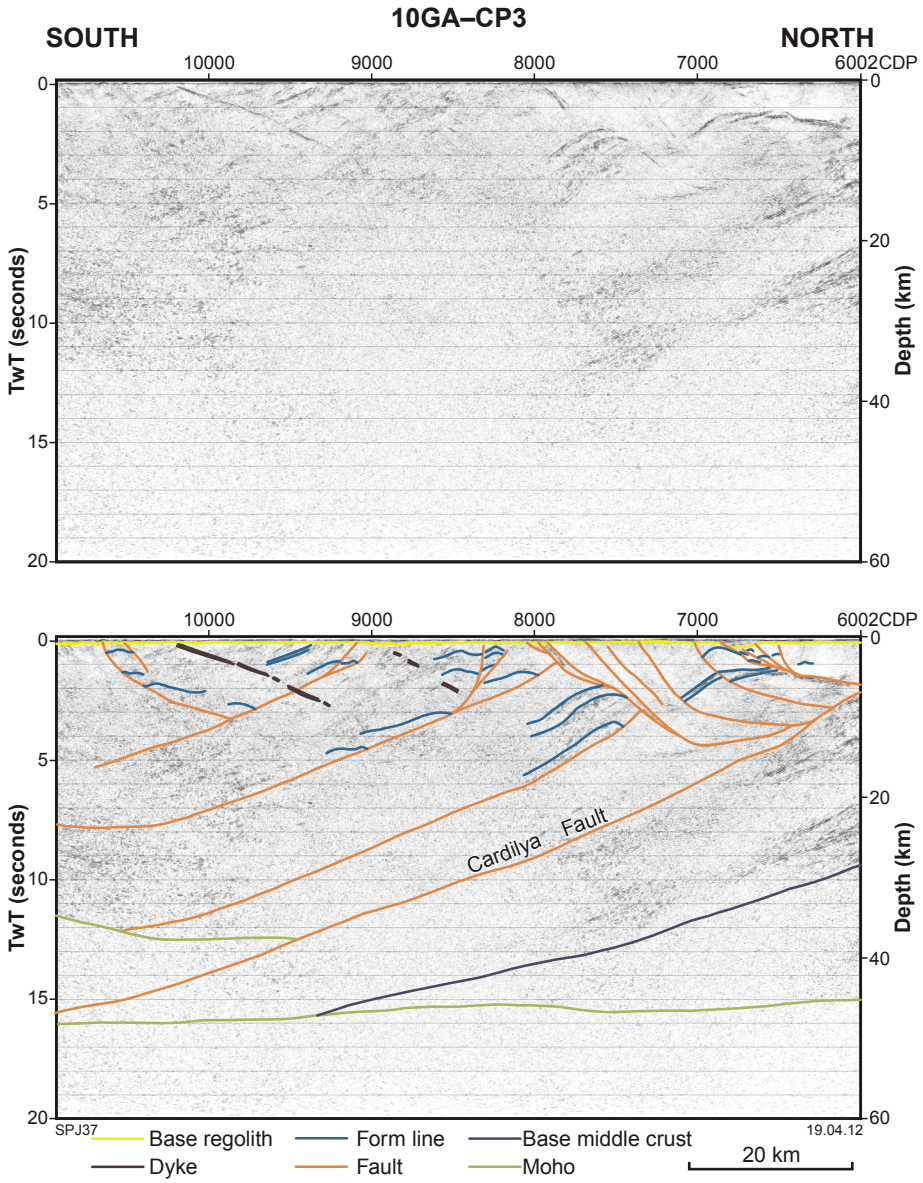

Figure 3. Migrated seismic section for seismic line 10GA–CP3, showing both uninterpreted and interpreted versions. Display is to ~60 km depth, and shows vertical scale equal to horizontal scale, assuming an average crustal velocity of 6000 m/s.

In the vicinity of seismic line 10GA–CP2, the crust is thinnest in the centre of the section, with the Moho at about 12 s TWT (~36 km) depth, and thickest at its southern end, where the Moho is at about 15.3 s TWT (~46 km) depth (Fig. 2; see also Johnson et al., 2011b). This section contains bands of reflections 0.3 – 1.0 s TWT (1–3 km) thick in the lowermost crust, the base of which is interpreted to be the Moho lying above a nonreflective mantle.

On seismic line 10GA–CP3, we have interpreted a complex pattern for the Moho (Figs 3 and 4). At the northern end of the seismic line, the Moho is interpreted to be at about 15 s TWT (~45 km) depth, on the basis of a similar pattern of reflectivity obtained for the lower crust as interpreted on seismic line 10GA–CP2 (Fig. 2). A band of reflections between CDPs 9200 and 10000, at depths of 13–16 s TWT (39–48 km), are interpreted to occur in the lower crust, and thus, the Moho is interpreted to be below these reflections, at about 16 s TWT (~48 km) depth. At the southernmost end of seismic line 10GA–CP3, the Moho is difficult to interpret (Fig. 3); however, this seismic line ties to another, more recently acquired, line across the southern Carnarvon Basin, 11GA–SC1, and ends 40 km to the west of the start of the Youanmi seismic line, 10GA–YU1. In the vicinity of the tie to line 10GA–CP3, the Moho on line 11GA–SC1 is at a depth of about 11 s TWT (~33 km); it is at a similar depth on line 10GA–YU1. This presents a complication in the geometry of the Moho at the southern end of line 10GA–CP3: either the Moho has a very steep ramp from a depth of about

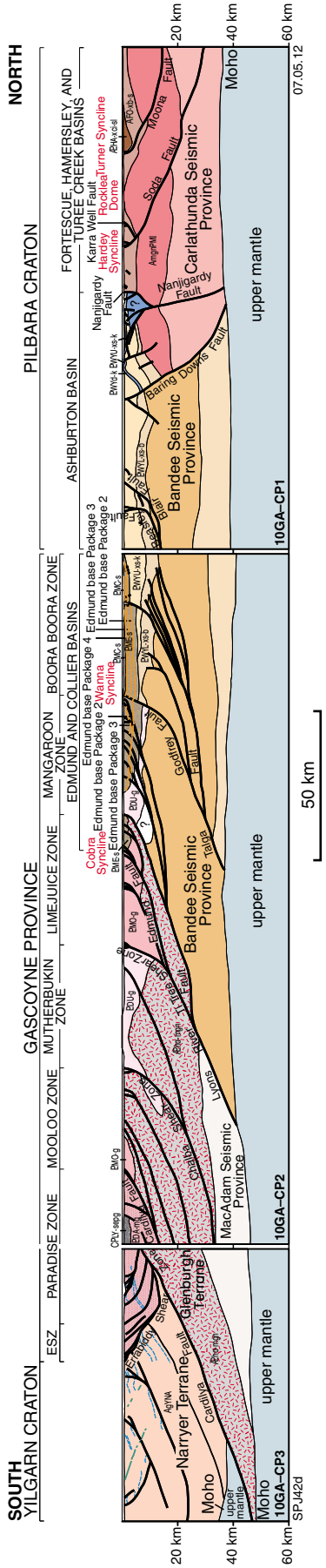

Figure 4. Cross section of the transect across the Capricorn Orogen, combining seismic lines 10GA–CP1, 10GA–CP2, and 10GA–CP3, and showing key faults, terranes, zones, basins, and seismic provinces.

48 km to about 33 km, over a horizontal distance of just over 20 km, or else it has been faulted and duplicated by crustal-scale thrusting. Our preferred interpretation is that the Moho has being faulted (Fig. 3; see also Johnson et al., 2011b) with a substantial localized offset, and that the crust has been duplicated on a crustal-scale thrust fault that also marks the subsurface boundary between the Yilgarn Craton and the Glenburgh Terrane (see below). Therefore, the Glenburgh Terrane may be present below the Narryer Terrane on seismic line 10GA–YU1 at around 15–16 s TWT (45–48 km).

Crustal architecture

In the region of the seismic sections, the upper crust can be subdivided into several provinces, basins, and zones, based principally on surface geological mapping and potential-field data. By comparison, the lower crust appears to consist of at least three discrete seismic provinces. Following Korsch et al. (2010), we use the term 'seismic province' to refer to a discrete volume of middle to lower crust, which cannot be traced to the surface, and whose crustal reflectivity is different to that of laterally or vertically adjoining provinces.

Pilbara Craton

At the northern end of the seismic survey, granite–greenstone rocks of the Pilbara Craton are exposed within the Rocklea Dome, roughly coinciding with CDPs 4620–4780 (line 10GA–CP1; Fig. 1), where they are overlain by sedimentary and igneous rocks of the Fortescue, Hamersley, and Wyloo Groups (Thorne et al., 2011a). The age of the granite–greenstones is constrained to greater than 2775 Ma, which is the age of the overlying lower Fortescue Group. The rocks of the Pilbara Craton sensu stricto are only weakly to moderately reflective, and can be tracked into the middle crust to a depth of about 4–7 s TWT (12–21 km).

Carlathunda Seismic Province

In the subsurface, we have interpreted that the base of the Pilbara granite–greenstone rocks coincides with the top of a highly reflective seismic package in the middle to lower crust (Figs 1 and 4). We term this package the Carlathunda Seismic Province (new name, after Carlathunda Bore), and interpret it to extend to the Moho. As we have not been able to track these rocks to the surface, we have no direct constraints on their lithology or age. Despite this, we consider this seismic province to be a discrete package of rocks that forms the current basement to the granite–greenstones of the Pilbara Craton sensu stricto.

As yet, no study has been undertaken on the age, geochemistry, or isotopic characteristics of the granites in the Rocklea Dome, but such a study is clearly warranted as it could provide information of the composition of the crust in the Carlathunda Seismic Province, below the dome.

The Carlathunda Seismic Province is bounded in the south by the Baring Downs Fault (new name, after Baring

Downs plain). This is a north-dipping fault separating sections of the middle to lower crust with differing seismic reflective characteristics, which we consider to represent different seismic provinces.

Bandee Seismic Province

Between the Baring Downs Fault and the Lyons River Fault, there are sedimentary rocks at the surface that were deposited in the Ashburton, Edmund, and Collier Basins, plus granites of the Durlacher Supersuite (1680–1620 Ma, Sheppard et al., 2010b). Beneath these rocks is a highly reflective middle crust, with a lower crust immediately above the Moho that is only weakly reflective (Figs 1 and 2); we use the term Bandee Seismic Province (new name, after Bandee Bore) to refer to the middle and lower crust in this region (Fig. 4).

Since we cannot track this seismic province to the surface, we do not have direct constraints on its composition or age. Nevertheless, the oldest rocks interpreted above this seismic province are the basal units of the lower Wyloo Group (Fig. 1), which are dated at 2209 ± 15 Ma (Martin et al., 1998), in turn implying that the seismic province is older than about 2210 Ma. The ages of inherited zircons sampled from younger granite intrusions to the south of the Talga Fault suggest the possibility that the Bandee Seismic Province contains material in the age range 2850–2600 Ma (GSWA, unpublished data). In an alternative interpretation, Thorne et al. (2011b) proposed that the Fortescue and Hamersley Groups extend well to the south of the Baring Downs Fault, thereby making the Bandee Seismic Province older than 2775 Ma.

At about CDP 6500 on seismic line 10GA–CP2, the Bandee Seismic Province comes as close to the surface as 2.2 s TWT (~6.5 km) depth, and is up to 11 s TWT (~33 km) thick (Fig. 2). The upper reflective part of the seismic province mostly dips gently to the south, but in places, the fabric is gently folded (Fig. 2). The lower weakly reflective part is up to 4.7 s TWT (~14 km) thick in the north on line 10GA–CP1 (Fig. 1), but thins towards the south, and is eventually truncated by the merged Godfrey and Talga Faults near the Moho (Fig. 2).

Glenburgh Terrane

The Glenburgh Terrane of the Gascoyne Province extends from the Errabiddy Shear Zone in the south, to the Lyons River Fault in the north (Fig. 4). The oldest rocks in this terrane are the granitic protoliths of the Halfway Gneiss in the Mooloo Zone, which have crystallization ages between c. 2555 and c. 2430 Ma (Johnson et al., 2011c). A hafnium isotopic study of these rocks, reported by Johnson et al. (2011d), indicates that the Halfway Gneiss is exotic to both the Pilbara and Yilgarn Cratons (see also Occhipinti et al., 2004). The Glenburgh Terrane also contains the Dalgaringa Supersuite, which was interpreted by Sheppard et al. (2004) to represent an Andean-type, continental-margin magmatic arc active from 2005 Ma to 1975 Ma.

At the present, we have included within the Glenburgh Terrane the reflective packages that extend from close to the surface to the lower crust on seismic line 10GA–CP2 (Fig. 2) and to the Moho on seismic line 10GA–CP3 (Fig. 3). Nevertheless, it is possible that these reflective packages actually represent the basement to this terrane. Thus, for the crust below the Errabiddy Shear Zone, we currently interpret the Glenburgh Terrane as extending from the Lyons River Fault in the north to the Cardilya Fault (new name, after Cardilya Creek) in the south (Fig. 4).

MacAdam Seismic Province

The MacAdam Seismic Province (new name, after MacAdam Plains) is bounded to the north by the Lyons River Fault, and to the south by the Glenburgh Terrane; it is presently confined to the weakly reflective lower crust immediately above the Moho on the southern end of line 10GA–CP2, and the northern end of line 10GA–CP3 (Figs 2–4). It forms the lower crustal basement to the Glenburgh Terrane, and is up to 5.5 s TWT (~16.5 km) thick. As this seismic province is limited to the lower crust, we have no direct constraints on its lithology or age.

Narryer Terrane

At the surface, the Narryer Terrane (as defined by Cassidy et al., 2006) of the northwest Yilgarn Craton occurs to the south of the Errabiddy Shear Zone (Fig. 3), whereas in the subsurface, it is interpreted to extend to the Moho, and is up to 12.5 s TWT (~37.5 km) thick. In seismic line 10GA–CP3, the Errabiddy Shear Zone is interpreted to sole onto the Cardilya Fault, and as a result, this shear zone marks the northern boundary of the Narryer Terrane in the subsurface (Fig. 3).

Crustal sutures

Relationship between Pilbara Craton – Carlathunda Seismic Province and Bandee Seismic Province

There are significant differences in crustal reflectivity across the Baring Downs Fault, which in the north borders the Pilbara Craton in the upper to middle crust and Carlathunda Seismic Province in the middle to lower crust, and in the south edges the Bandee Seismic Province, in turn suggesting that these units are discrete blocks of continental crust (Figs 1 and 4). Thus, we interpret the Baring Downs Fault to mark the site of a fossil suture zone. Given the different seismic character seen in the middle crust on either side of the fault, and considering that the lower Wyloo Group is interpreted to occur on both sides of the fault (Fig. 1), the suture probably formed prior to the deposition of the lower Wyloo Group at c. 2210 Ma, and was later reactivated to displace the sedimentary units. It is also possible that the Fortescue and Hamersley Groups were deposited on both sides of the fault (see Thorne et al., 2011b), which would suggest that the suture is older than the oldest unit in the Fortescue Group (c. 2775 Ma). Furthermore, the northern part of the Bandee Seismic Province may be the same age as the Archean Sylvania Inlier, which is located along-strike about 250 km to the east; this implies that the Baring Downs Fault is a suture that formed prior to 2775 Ma.

Relationship between the Bandee Seismic Province and Glenburgh Terrane

There is a pronounced step in the Moho where the Lyons River Fault soles onto it, rising from 15.5 s TWT (~46.5 km) in the south beneath the MacAdam Seismic Province, to less than 12 s TWT (~36 km) in the north beneath the Bandee Seismic Province (Figs 2 and 4). The fault also separates distinctive blocks of crust, with the Bandee Seismic Province to the north and the Glenburgh Terrane and MacAdam Seismic Province to the south. This raises the question of whether the Lyons River Fault is a fossil suture zone marking the site of a collision between two different continental blocks, and if so, at what time did this collision occur?

Previous tectonic models have inferred subduction followed by collision, either between the Pilbara and Yilgarn Cratons (e.g. Tyler and Thorne, 1990), or between the Pilbara Craton and the Glenburgh Terrane, possibly at the Talga Fault (e.g. Sheppard et al., 2001; Johnson et al., 2011c). Our interpretation suggests that the key structure is the Lyons River Fault, making the location of the suture farther to the south than previously thought.

The collision between the Bandee Seismic Province and the Glenburgh Terrane (Fig. 5) would have occurred sometime after the formation of the oldest rocks in the Glenburgh Terrane, namely the granitic protoliths of the Halfway Gneiss (with crystallization ages between c. 2555 and c. 2430 Ma). The oldest rocks interpreted to occur above the Bandee Seismic Province belong to the lower Wyloo Group, considered by Martin and Morris (2010), and Johnson et al. (2011c), to be foreland-basin deposits associated with the Ophthalmian Orogeny (dated at 2215–2145 Ma by Rasmussen et al., 2005), and which constrains the onset of collision to about 2215 Ma.

Later fault reactivation during one or more subsequent orogenies then allowed the Lyons River Fault to propagate towards the surface, cutting younger rocks in the Edmund Basin.

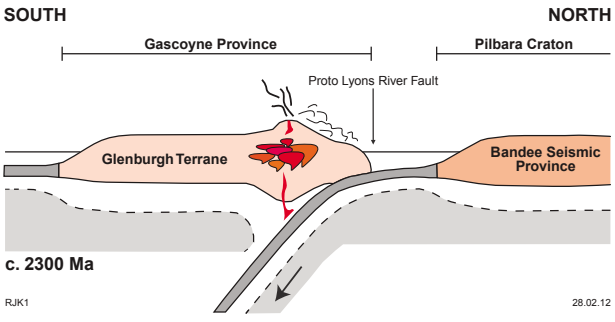

Figure 5. Schematic cross section, showing the evolution of the subduction and magmatic arc leading up to collision between the Glenburgh Terrane and Bandee Seismic Province, and the 2215–2145 Ma Ophthalmian Orogeny. Note that polarity of subduction is poorly constrained.

Relationship between Glenburgh and Narryer Terranes

The Glenburgh Terrane is considered exotic to both the Pilbara and Yilgarn Cratons (Occhipinti et al., 2004; Johnson et al., 2011c,d), and as such, the Narryer and Glenburgh Terranes represent discrete continental blocks sutured by a fossil collision/suture zone. At the surface, the boundary corresponds to the north-dipping Errabiddy Shear Zone, but, as proposed in the models of Sheppard et al. (2003), Hackney (2004), and Johnson et al. (2011c), and as shown in the seismic data, a key structure is another south-dipping, middle- to lower-crustal fault, known as the Cardilya Fault (Fig. 4).

Sheppard et al. (2004) demonstrated that the Dalgaringa Supersuite in the Glenburgh Terrane was an Andean-type, continental-margin magmatic arc that was active from 2005 Ma to 1975 Ma, although Johnson et al. (2011c) instead considered that the initiation of arc magmatism occurred at about 2080 Ma. The magmatic arc developed along the southern margin of the Glenburgh Terrane (Sheppard et al., 2004; Johnson et al., 2011c), constraining the polarity of subduction; that is, dipping northwards under the Glenburgh Terrane (Fig. 6).

There are at least two scenarios that could explain the architecture observed along seismic lines 10GA–CP2 and 10GA–CP3. In the first scenario, both major terrane-bounding structures are related to the Glenburgh Terrane – Yilgarn Craton collision, but their geometric relationship suggests that the Cardilya Fault post-dates the formation of the Errabiddy Shear Zone. The imbrication of the Glenburgh Terrane and Yilgarn Craton lithologies along the Errabiddy Shear Zone suggests that this earlier structure is probably the suture zone. Following the initial collision and interleaving of lithologies along the Errabiddy Shear Zone, this zone was reworked by the Cardilya Fault, which underthrust the southern margin of the Glenburgh Terrane beneath the Narryer Terrane (see Johnson et al., 2011b).

However, the preferred alternative is that during oceanic closure and collision, which occurred at 1965–1950 Ma during the latter part of the Glenburgh Orogeny (Johnson et al., 2011c), the Narryer Terrane was obducted onto the Glenburgh Terrane at the present site of the Cardilya Fault. During the post-collisional phase of the Glenburgh Orogeny, backthrusting at the Errabiddy Shear Zone resulted in a slice of the Glenburgh Terrane being thrust back to the south, over the upper part of the Narryer Terrane, thus producing the present crustal architecture imaged in seismic line 10GA–CP3 (Fig. 4).

Geodynamic implications

Crustal architecture of the Capricorn Orogen

The new deep seismic imaging, extending from the southern Pilbara Craton to the northern Yilgarn Craton, provides, for the first time, a holistic view of the crustal

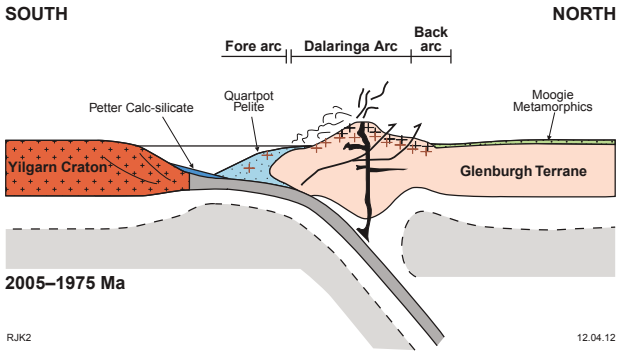

Figure 6. Schematic cross sections, showing the evolution of the Dalgaringa Arc, leading to the collision between the Yilgarn Craton and the Glenburgh Terrane.

architecture of the Capricorn Orogen. Based on the nature of seismic reflectivity, the orogen can be subdivided into several crustal-scale terranes and provinces, with sedimentary basins occupying the upper crust along the northern half of the transect. The region to the north of the Baring Downs Fault is dominated by north-dipping crustal scale structures, whereas to the south of the Baring Downs Fault, the majority of the transect is dominated by south-dipping structures, many of which cut the entire crust through to the Moho. Interestingly, the southern end of the transect is interpreted to have been duplicated by thrust faulting.

Assembly of the West Australian Craton

The new deep seismic lines across the Capricorn Orogen show that the West Australian Craton was built through the progressive accretion of continental slivers onto the southern margin of the Pilbara Craton (and its basement, the Carlathunda Seismic Province). Initially, the Bandee Seismic Province was sutured to the Pilbara Craton, most likely before 2775 Ma. Suturing of the Glenburgh Terrane to the amalgamated Pilbara – Bandee craton most likely occurred at about 2215 Ma during the Ophthalmian Orogeny. The final assembly of the West Australian Craton occurred when the Narryer Terrane of the northern Yilgarn Craton was sutured to the composite Pilbara – Bandee – Glenburgh continental block at about 1950 Ma, during the Glenburgh Orogeny.

Intracontinental reactivation

Following the final assembly of the West Australian Craton, reactivation in an intracontinental setting occurred at several discrete times, with most major faults imaged in the seismic sections showing evidence of post-collisional reactivation during one or more of the later orogenies recognized in the craton (Sheppard et al., 2010a; Johnson et al., 2011a). For example, the Baring Downs Fault significantly displaces units in the Ashburton Basin, including the youngest Ashburton Formation. The Lyons River Fault was reactivated as an extensional fault during deposition of the Edmund Group (Cutten et al., 2011; Johnson et al., 2011b), and was later inverted as a thrust to produce hangingwall anticlines. Splays to the north leading off the Talga Fault show a thrust sense of displacement, but near the surface, the Talga Fault itself appears to have had extensional movement during deposition of the Edmund Group, and later inversion as a positive flower structure. Crustal-scale faults within the Bandee Seismic Province and Glenburgh Terrane, such as the Godfrey Fault and Chalba Shear Zone, also show evidence of late reactivation.

Summary

Interpretation of the Capricorn deep seismic reflection survey has allowed us to examine the geodynamic relationships between the Pilbara Craton, Gascoyne Province, and Yilgarn Craton, which together form the Western Australian Craton. Prior to the seismic survey, suture zones were proposed between the Pilbara Craton and the Glenburgh Terrane at the Talga Fault, and between the Yilgarn Craton and the Glenburgh Terrane at the Errabiddy Shear Zone. Our interpretation of the seismic lines indicates that there is a suture between the Pilbara Craton and the newly recognized Bandee Seismic Province. Our interpretation also suggests that the Gascoyne Province can be subdivided into at least two discrete crustal blocks, with the suture between them interpreted to occur at the Lyons River Fault. Finally, the seismic interpretation has confirmed previous interpretations that the crustal architecture between the Narryer and Glenburgh Terranes consists of a south-dipping structure in the middle to lower crust, indicating where the Glenburgh Terrane has been thrust southward beneath the Narryer Terrane. The Errabiddy Shear Zone therefore represents an upper-crustal thrust system, where the Glenburgh Terrane has been thrust over the Narryer Terrane, possibly as a backthrust.

Acknowledgements

This paper forms part of a collaborative project between GSWA, AuScope, and Geoscience Australia. We thank the following for their contributions to the project: Josef Holzschuh, Ross Costelloe, Tanya Fomin, and Jenny Maher, who were involved in the acquisition and processing of the seismic data; Lindsay Highet and Weiping Zhang, who produced the maps and digital versions of the interpretations of the seismic sections, respectively; and Richard Chopping for input and discussions on the potential field data. We also thank Geoff Fraser and Natalie Kositcin for reviewing this abstract.

References

Cassidy, KF, Champion, DC, Krapež, B, Barley, ME, Brown, SJA, Blewett, RS, Groenewald, PB and Tyler, IM 2006, A revised geological framework for the Yilgarn Craton, Western Australia: Geological Survey of Western Australia, Record 2006/8, 8p.

Cawood, PA and Tyler, IM 2004, Assembling and reactivating the Proterozoic Capricorn Orogen: lithotectonic elements, orogenies, and significance: Precambrian Research, v. 128, p. 201–218.

Cutten, HN, Thorne, AM and Johnson, SP 2011, Geology of the Edmund and Collier Groups, *in* Capricorn Orogen seismic and magnetotelluric (MT) workshop 2011: extended abstracts *edited by* SP Johnson, AM Thorne and IM Tyler: Geological Survey of Western Australia, Record 2011/25, p. 41–48.

Goodwin, JA 2011, Potential-field interpretation of the Capricorn Orogen, Western Australia: worms, forward modeling, and 3D inversion, *in* Capricorn Orogen seismic and magnetotelluric (MT) workshop 2011: extended abstracts *edited by* SP Johnson, AM Thorne and IM Tyler: Geological Survey of Western Australia, Record 2011/25, p. 61–74.

Hackney, R 2004, Gravity anomalies, crustal structure and isostasy associated with the Proterozoic Capricorn Orogen, Western Australia: Precambrian Research, v. 128, p. 219–236.

Heinson, G, Boren, G, Ross, J, Campanya, J, Thiel, S and Selway, K 2011, The Capricorn Orogen magnetotelluric (MT) transect, *in* Capricorn Orogen seismic and magnetotelluric (MT) workshop 2011: extended abstracts *edited by* SP Johnson, AM Thorne and IM Tyler: Geological Survey of Western Australia, Record 2011/25, p. 74–100.

Johnson, SP, Thorne, AM, Cutten, HN, Tyler, IM and Blay, O 2011a, Geology of the Gascoyne Province, *in* Capricorn Orogen seismic and magnetotelluric (MT) workshop 2011: extended abstracts *edited by* SP Johnson, AM Thorne and IM Tyler: Geological Survey of Western Australia, Record 2011/25, p. 27–40.

Johnson, SP, Cutten, HN, Tyler, IM, Korsch, RJ, Thorne, AM, Blay, O, Kennett, BLN, Blewitt, RS, Joly, A, Dentith, MC, Aitkin, ARA, Goodwin, JA, Salmon, M, Reading, A, Boren, G, Ross, J, Costello, RD and Fomin, T 2011b, Preliminary interpretation of deep seismic reflection lines 10GA–CP2 and 10GA–CP3: crustal architecture of the Gascoyne Province, and Edmund and Collier Basins, *in* Capricorn Orogen seismic and magnetotelluric (MT) workshop 2011: extended abstracts *edited by* SP Johnson, AM Thorne and IM Tyler: Geological Survey of Western Australia, Record 2011/25, p. 49–60.

Johnson, SP, Sheppard, S, Rasmussen, B, Wingate, MTD, Kirkland, CL, Muhling, JR, Fletcher, IR and Belousova, EA 2011c, Two collisions, two sutures: punctuated pre-1950 Ma assembly of the West Australian Craton during the Ophthalmian and Glenburgh Orogenies: Precambrian Research, v. 189, p. 239–262.

Johnson, SP, Sheppard, S, Wingate, MTD, Kirkland, CL and Belousova, EA 2011d, Temporal and hafnium isotopic evolution of the Glenburgh Terrane basement: an exotic crustal fragment in the Capricorn Orogen: Geological Survey of Western Australia, Report 110, 27p.

Kennett, BLN, Tyler, IM, Maher, J, Holzschuh, J, Fomin, T and Costelloe, RD 2011, The Capricorn seismic survey: experimental design, acquisition, and processing, *in* Capricorn Orogen seismic and magnetotelluric (MT) workshop 2011: extended abstracts *edited by* SP Johnson, AM Thorne and IM Tyler: Geological Survey of Western Australia, Record 2011/25, p. 1–6.

Korsch, RJ, Preiss, WV, Blewett, RS, Cowley, WM, Neumann, NL, Fabris, AJ, Fraser, GL, Dutch, R, Fomin, T, Holzschuh, J, Fricke, CE, Reid, AJ, Carr, LK and Bendall, BR 2010, Deep seismic reflection transect from the western Eyre Peninsula in South Australia to the Darling Basin in New South Wales: Geodynamic implications, *in* South Australian Seismic and MT Workshop, extended abstracts *edited by* RJ Korsch and N Kositcin: Geoscience Australia, Record 2010/10, p. 105–116.

Martin, DM and Morris, PA 2010, Tectonic setting and regional implications of ca 2.2 Ga mafic magmatism in the southern Hamersley Province, Western Australia: Australian Journal of Earth Sciences, v. 57, p. 911–931.

Martin, DM, Li, ZX, Nemchin, AA and Powell, CM 1998, A pre-2.2 Ga age for giant hematite ores of the Hamersley Province, Australia: Economic Geology, v. 93, p. 1084–1090.

Occhipinti, SA, Sheppard, S, Passchier, C, Tyler, IM and Nelson, DR 2004, Palaeoproterozoic crustal accretion and collision in the southern Capricorn Orogen: the Glenburgh Orogeny: Precambrian Research, v. 128, p. 237–255.

Rasmussen, B, Fletcher, IR and Sheppard, S 2005, Isotopic dating of the migration of a low-grade metamorphic front during orogenesis: Geology, v. 33, p. 773–776.

Sheppard, S, Occhipinti, SA and Tyler, IM 2001, The tectonic setting of granites in the southern Gascoyne Complex, *in* GSWA 2001 extended abstracts: new geological data for WA explorers: Geological Survey of Western Australia, Record 2001/5, p. 3–4.

Sheppard, S, Occhipinti, SA and Tyler, IM 2003, The relationship between tectonism and composition of granitoid magmas, Yalarweelor Gneiss Complex, Western Australia: Lithos, v. 66, p. 133–154.

Sheppard, S, Occhipinti, SA and Tyler, IM 2004, A 2005–1970 Ma Andean-type batholith in the southern Gascoyne Complex, Western Australia: Precambrian Research, v. 128, p. 257–277.

Sheppard, S, Johnson, SP, Wingate, MTD, Kirkland, CL and Pirajno, F 2010a, Explanatory notes for the Gascoyne Province: Geological Survey of Western Australia, 336p.

Sheppard, S, Bodorkos, S, Johnson, SP, Wingate, MTD and Kirkland, CL 2010b, The Paleoproterozoic Capricorn Orogeny: intracontinental reworking not continent–continent collision: Geological Survey of Western Australia, Report 108, 33p.

Thorne, AM, Johnson, SP, Tyler, IM, Cutten, HN and Blay, O 2011a, Geology of the northern Capricorn Orogen, *in* Capricorn Orogen seismic and magnetotelluric (MT) workshop 2011: extended abstracts *edited by* SP Johnson, AM Thorne and IM Tyler: Geological Survey of Western Australia, Record 2011/25, p. 7–18.

Thorne, AM, Tyler, IM, Korsch, RJ, Johnson, SP, Brett, JW, Cutten, HN, Blay, O, Kennett, BLN, Blewitt, RS, Joly, A, Dentith, MC, Aitken, ARA, Holzschuh, J, Goodwin, JA, Salmon, M, Reading, A and Boren, G 2011b, Preliminary interpretation of deep seismic reflection line 10GA–CP1: crustal architecture of the northern Capricorn Orogen, *in* Capricorn Orogen seismic and magnetotelluric (MT) workshop 2011: extended abstracts *edited by* SP Johnson, AM Thorne and IM Tyler: Geological Survey of Western Australia, Record 2011/25, p. 19–26.

Tyler, IM and Thorne, AM 1990, The northern margin of the Capricorn Orogen Western Australia — an example of an early Proterozoic collision zone: Journal of Structural Geology, v. 12, p. 685–701.

Implications of the Capricorn deep seismic survey for mineral systems

by

IM Tyler, SP Johnson, AM Thorne, and HN Cutten

Introduction

The acquisition of the Capricorn deep seismic survey in 2010 was carried out as a collaborative project between the Geological Survey of Western Australia (GSWA), AuScope, and Geoscience Australia, with GSWA's funding provided by the Western Australian Government's Exploration Incentive Scheme (EIS) (Kennett et al., 2011). The survey has provided new insights into the architecture of the Capricorn Orogen, and into its geodynamic setting and tectonic history (Plate 2; Thorne et al., 2011; Johnson et al., 2011a; Korsch et al., 2011). This improved understanding of Capricorn Orogen development can be used to re-evaluate the mineral systems within the orogen, and the resultant implications for regional-scale mineral prospectivity.

One of the aims of the survey was to identify structures that cut through the crust to the mantle and form pathways for fluid flow to mineral systems (Kennett et al., 2011). Known significant mineralization in the Capricorn Orogen is restricted to the reworked orogenic forelands formed along the Pilbara and Yilgarn Craton margins. The hinterland of the Capricorn Orogen has not had a prominent history of major mineral deposit discovery, and currently lacks major resource projects or operating mines (Frontispiece 1; Fig. 1). Central to a reassessment of the orogen's prospectivity is the growing understanding that most giant orebodies are generated by lithosphere-scale deep plumbing systems that concentrate fluids, energy, and metals into specific sites in the crust. These are often related to sites of fossil subduction zones or to old cratonic margins; both settings have been interpreted from the new Capricorn deep seismic survey data (Thorne et al., 2011; Johnson et al., 2011a; Korsch et al., 2011).

Mineral systems in the Capricorn Orogen

Several mineral systems have been recognized in the Capricorn Orogen (Frontispiece 1; Plate 1). These include the world-class hematite iron-ore deposits of the Hamersley Basin, which occur within structural settings in the Ophthalmia Fold Belt; volcanic-hosted metal sulfide (VHMS) copper–gold deposits in the Bryah Basin on the Yilgarn Craton margin; orogenic lode-gold mineralization, such as that at Peak Hill in the southern Capricorn Orogen margin, Glenburgh and the Star of Mangaroon in the Gascoyne Province, and at Paulsens and Mount Olympus in the northern Capricorn Orogen margin; various intrusion- and shear zone related base metal, tungsten, rare earth element (REE), uranium, and rare-metal deposits in the Gascoyne Province; and lead–copper–zinc sediment-hosted mineralization at Abra within the Edmund Basin (Frontispiece 1; Plate 1).

Ophthalmia Fold Belt

The world-class iron deposits of Western Australia's Pilbara region are currently a major driver of Australia's economy. The enriched iron-ore deposits of the Hamersley Basin currently have an estimated resource of over 40 billion tonnes, mainly consisting of banded iron-formation (BIF) hosted bedded iron deposits and channel iron deposits.

The genesis of the Hamersley Basin BIF-hosted iron ores has recently been the subject of a major review by Morris and Kneeshaw (2011). Two major ore types are recognized: the dominant martite–goethite ores, which developed in the Mesozoic to Paleocene, and the premium Paleoproterozoic martite – microplaty hematite ores.

Models for the development of the martite – microplaty hematite ores have been controversial. Initial models, developed in the 1980s (e.g. Morris, 1985), envisaged Paleoproterozoic supergene martite–goethite ores that were upgraded to martite – microplaty hematite ores by regional metamorphism or diagenesis and hydrothermal activity at 80–100ºC, during burial by the Proterozoic lower Wyloo Group (c. 2200 Ma). An alternative hypogene–supergene model for the martite – microplaty hematite ores has been proposed following the identification of hydrothermal fluid-flow related to the c. 2200 Ma Ophthalmian Orogeny (e.g. Powell et al.,

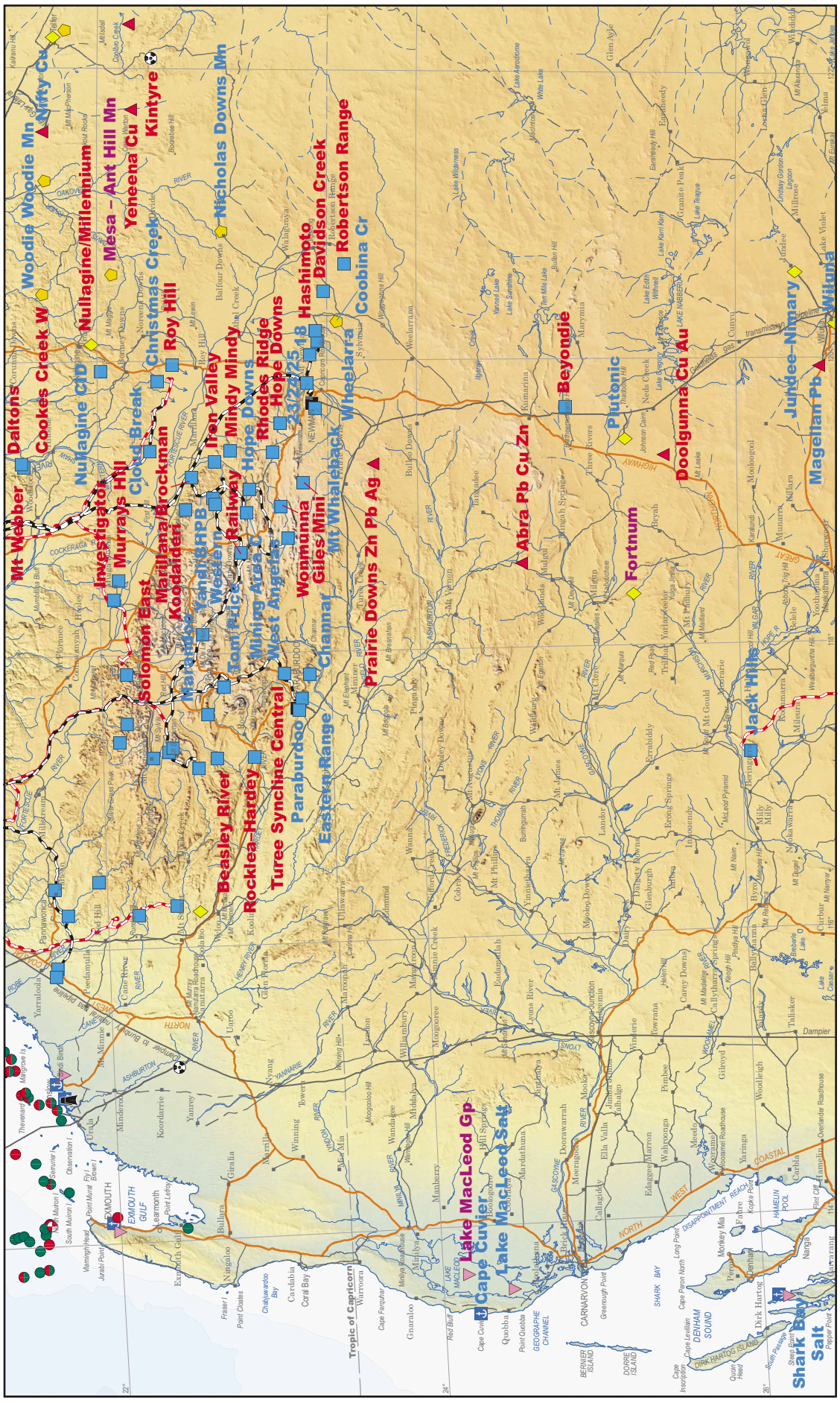

Figure 1. Major resource projects and operating mines of the Capricorn Orogen, Western Australia

1999; Taylor et al., 2001; Brown et al., 2004). The timing of the martite – microplaty hematite ore formation, relative to the history of deposition, deformation, and metamorphism in the Hamersley Basin, and adjacent Turee Creek and Ashburton Basins, is critical to the assessment of these competing models (see Martin and Morris, 2010).

It is clear from Plates 1 and 2 that the major deposits at Tom Price in the Turner Syncline, above the Moona Fault and Paraburdoo on the Nanjilgardy Fault, are spatially associated with large crustal-scale faults, interpreted as being active during the Ophthalmian Orogeny (Martin and Morris, 2010; Thorne et al., 2011; Johnson et al., 2011a; Korsch et al., 2011). This appears to provide support for the hypogene–supergene model, in that there is an expectation of large-scale fluid flow through the faults at the time of orebody formation. It is also unclear how the hydrothermal upgrading of supergene ores could operate as a closed system in such a setting. This may have implications for the exploration for blind premium martite – microplaty hematite orebodies, particularly beneath the Turee Creek and Wyloo Groups south of the Nanjilgardy Fault and along the Soda Fault (Frontispiece 1–3; Plate 1).

Northern Capricorn Orogen: orogenic gold

Evidence of vein-related, orogenic gold mineralization is widespread in the northern Capricorn Orogen (Plate 1; Frontispiece 1); however, most of the historical workings are small and relatively shallow. The largest gold deposits occur within Fortescue Group rocks at Paulsens in the Wyloo Dome, and in Ashburton Basin rocks at Mount Olympus southeast of Paraburdoo. Although host-rock geology is different for each of these deposits, both occur in close proximity to a major mantle-tapping structure, the Nanjilgardy Fault (Thorne et al., 2011).

Paulsens Mine commenced production in 2005, and since that time has consistently produced 70 000 to 80 000 ounces of gold per annum (Northern Star Resources Limited, 2011). It currently has an Indicated and Inferred Mineral Resource estimate of 1 268 000 t @ 5.3g/t for 226 000 oz of gold. Mineralization occurs within a structurally controlled quartz vein, hosted by a folded metasedimentary sequence within the Fortescue Group. Gold is associated with quartz, carbonate, and pyrite, and the high-grade gold is commonly associated with zones of massive sulfides (Northern Star Resources Limited, 2011).

The Mount Olympus mine is not currently operating, but produced about 350 000 oz of gold between 1999 and 2004 (Sipa Resources Limited, 2011). The deposit is hosted by low-grade metasedimentary rocks of the Mount McGrath Formation (upper Wyloo Group), and mineralization consists of submicrometre-sized or solid solution gold in disseminated arsenian pyrite (Young et al., 2003). Mineralization has been dated at c. 1738 Ma, and is associated with quartz–sericite alteration that post-dates the regional metamorphism (Young et al., 2003; Sener et al., 2005).

Southern Capricorn Orogen

In the southern Capricorn Orogen, the Errabiddy Shear Zone has been recognized as a suture between the Narryer Terrane (of the Yilgarn Craton) and the Glenburgh Terrane (Johnson et al., 2011a); however, it shows little evidence of major mineralization, despite being the target of diamond exploration (e.g. Flint et al., 2000). Based on the interpretation of 10GA–CP3, the shear is north-dipping, and is cut off at about 10 km depth by the south-dipping Cardilya Fault, giving it no direct link to the underlying lithospheric mantle (Johnson et al., 2011a).

The Cardilya Fault is recognized as a major crustal-scale fault that offsets the Mohorovičić discontinuity ('the Moho') and separates the Archean Yilgarn Craton from the Paleoproterozoic Gascoyne Province at depth (Johnson et al., 2011a), but as yet shows little evidence of mineralization at the surface.

To the east of the seismic survey, the Bryah Basin, which overlies Yilgarn Craton basement, has recently seen the discovery of the high-grade DeGrussa copper–gold deposit within Sandfire Resources NL Doolgunna tenement package. The deposit has been interpreted as a VHMS, and has Indicated and Inferred Resource of 10.67 Mt @ 5.6% copper, 1.9g/t gold, and 15g/t silver, containing 600 000 t of copper, 660 000 oz of gold, and 5.1 Moz of silver (Sandfire Resources NL, 2011).

There is also renewed interest in gold exploration in the Peak Hill Schist, which forms the contact between the Bryah Basin and the underlying Marymia Inlier, and contains vein-related, orogenic gold mineralization both at the historic Peak Hill Gold Mine and at a recent discovery by Alchemy Resources at Central Bore (Flint et al., 2000, Pirajno et al., 2000; Alchemy Resources Limited, 2011)

Gascoyne Province

The Gascoyne Province is a major Proterozoic tectonic zone that separates the Yilgarn and Pilbara Cratons (Johnson et al., 2011a,b). The oldest part of the province, the Neoarchean to Paleoproterozoic Glenburgh Terrane, has been interpreted as exotic to both the bounding cratons, and is thus separated from the Yilgarn and Pilbara Cratons by two suture zones (Johnson et al., 2011a–c). The province hosts a variety of mineralization styles (Frontispiece 1; Plate 1), including intrusion and shear zone hosted deposits such as:

- molybdenum–copper–tungsten–lead within the Minnie Creek batholith
- carbonatite-related REE, including uranium, within the Gifford Creek Carbonatite Complex
- scheelite skarns within the Chalba Shear Zone and at Nardoo Well
- rare metal (tantalum, bismuth, beryllium) pegmatites at Morrissey Hill

- copper–lead–zinc(–gold) base metal deposits at Mount James, Glenburgh, and the Star of Mangaroon.

Two of the more significant deposits, the carbonatite-related REE mineralization at Gifford Creek and the base metal – gold deposits at Glenburgh, appear to be associated with major crustal sutures along the former margins of the Glenburgh Terrane.

The Gifford Creek Carbonatite Complex comprises sills, dykes, and veins of ferroan carbonatite, ironstone, and hydrothermally altered rocks (fenites), which intrude porphyritic granites (the Pimbyana Granite and Yangibana Granite) of the 1680–1620 Ma Durlacher Supersuite in the central part of the Mangaroon Zone (Frontispiece 1; Plate 1). These rocks, especially the ironstones, contain significant REE and uranium mineralization, with an estimated total resource of ~2.7 Mt, averaging 1.52% REE oxides (Flint and Abeysinghe, 2000). The ferroan carbonatite sills and dykes have been emplaced along a northwest-trending belt, close to and parallel to the Lyons River Fault, whereas the veins of iron-oxide minerals and quartz are mostly perpendicular to that of the carbonatite sills (Frontispiece 1; Plate 1; Pearson et al., 1996). The complex shares the characteristics of igneous systems related to alkaline magmatism in extensional settings, and may be the upper crustal response to a presently unexposed alkaline intrusion (Pirajno et al., 2008). The age of the carbonatite complex is not precisely known, but is younger than c. 1660 Ma — the age of the granites that it intrudes — and older than c. 955 Ma, as some of the ironstones have been folded and deformed during the 1030–955 Ma Edmundian Orogeny. Emplacement of the sills appears to have been controlled by the Lyons River Fault, a major crustal suture that separates the Glenburgh Terrane from the Bandee Seismic Province of the Pilbara Craton (Johnson et al., 2011a). Although this structure is primarily related to the 2215–2145 Ma Ophthalmian Orogeny collision, it has been reactivated numerous times throughout the Proterozoic (Johnson et al., 2011b).

At Glenburgh, in the southern part of the province (Frontispiece 1; Plate 1), base metal and gold mineralization is hosted within high-grade pelitic gneisses that form decametre-scale rafts within granitic gneisses of the 2005–1970 Ma Dalgaringa Supersuite. These granitic rocks formed in a continental-margin arc on the southern margin of the Glenburgh Terrane, prior to the collision of the combined Pilbara Craton – Glenburgh Terrane with the Yilgarn Craton during the 2005–1950 Ma Glenburgh Orogeny (Sheppard et al., 2004; Occhipinti et al., 2004; Johnson et al., 2011d). Subsequent greenschist-facies alteration has upgraded the primary deposit into higher-grade shear zones. Currently, the deposit has an estimated total resource of ~7.2 Mt @ 1.6 g/t gold for 360 000 oz of contained gold, at a 0.8 g/t gold cutoff (Gascoyne Resources Limited, 2011). The age of the secondary upgrading is not known.

Edmund Basin

The Edmund and Collier Basins have a history of minor gold, base metal, and phosphate production; however, only one major orebody, the Abra polymetallic deposit, has been discovered in these rocks to date. This deposit occurs within the eastern part of the Edmund Basin, in a fault-bounded structural corridor that links up with the Lyons River Fault system (Frontispiece 1–3; Plate 1), a major mantle-tapping structure interpreted to be the principal crustal suture between the Bandee Seismic Province of the Pilbara Craton and the Glenburgh Terrane (Johnson et al., 2011a, Korsch et al., 2011).

The Abra deposit has a total Indicated and Inferred resource estimate of 93 Mt at 4% lead and 10 g/t silver, and 14 Mt at 0.6% copper and 0.5 g/t gold (Rasmussen et al., 2010). There is only a weak surface expression of the mineral system, most of which has been delineated using geophysical techniques and drilling. The Abra deposit remains open in most directions, supporting its status as the most significant mineral discovery in the central Capricorn Orogen at the present time.

The Abra mineralization occurs in the upper part of the Irregully Formation and the lower part of the overlying Kiangi Creek Formation. Mineralization is centred on a funnel-shaped brecciated zone, interpreted as a breccia feeder pipe, overlain by stratabound mineralization (Vogt, 1995; Pirajno et al., 2009; Rasmussen et al., 2010) divided into a lower Black Zone and upper Red Zone. The Black Zone comprises veins and rhythmically banded galena, sphalerite, and pyrite, with minor tetrahedrite, chalcopyrite, and scheelite. These ore minerals are associated with laminated and/or brecciated hematite, magnetite, iron-rich carbonate, barite, and scheelite. The Red Zone is dominated by barite, banded jaspilite, hematite, galena, pyrite, quartz, abundant barite, and siderite (Pirajno et al., 2009; Rasmussen et al., 2010). Abra mineralization is considered the product of a dynamic, multiphase hydrothermal system (Pirajno et al., 2009).

The age of mineralization is currently poorly constrained. Direct dating of pyrite from the Black Zone using the Re–Os technique has provided a date of c. 1280 Ma (GSWA, unpublished data). Hydrothermal monazite extracted from sedimentary rocks of the Irregully and lower Kiangi Creek Formations yield a range of ages, with the youngest population at 1385 ± 20 Ma (Rasmussen et al., 2010). However, these dates are at odds with the stratigraphic relationships, which suggest that mineralization is a syndepositional feature (Collins and McDonald, 1994; Thorne et al., 2009). Primary mineralization may have occurred during the deposition of the Irregully and lower Kiangi Creek Formations, with secondary upgrading by intense hydrothermal alteration during the 1385–1200 Ma Mutherbukin Tectonic Event. These hydrothermal fluids may be linked to similar-aged magmatic and hydrothermal activity along the Lyons River Fault system that produced the Gifford Creek Carbonatite Complex.

Future work

The Capricorn seismic survey has identified a series of structures cutting through the crust to the mantle, representing either the ancient margins of the Archean Yilgarn and Pilbara Cratons, or the sites of Paleoproterozoic collision zones reactivated periodically

throughout the Proterozoic. Economic mineralization has yet to be discovered along several of these structures, including the Cardilya and Lyons River Faults; however, the survey has highlighted a spatial relationship between crustal-scale faults and premium martite – microplaty hematite ores in the northern Capricorn Orogen margin.

Future work by GSWA, using EIS funding and conducted in partnership with the Centre for Exploration Targeting at The University of Western Australia, will include an integrated geological and geophysical study of the Capricorn Orogen and its mineral prospectivity. The aim of this study will be to obtain a '4D' understanding of the whole orogen that incorporates both the results presented here, and the other new geophysical, geochronological, and isotopic data that is currently being generated, including a recently acquired magnetotelluric traverse that crossed the orogen from the Marymia Inlier to the Sylvania Inlier. A challenge is to project the structures observed in the seismic survey to the east, where the Gascoyne Province may wedge out, and where the Yilgarn and Pilbara Cratons may be in direct contact (e.g. Cawood and Tyler, 2004, fig. 3).

References

Alchemy Resources Limited 2011, Projects: Alchemy Resources Limited, Perth, Western Australia, viewed 11 November 2011, <http://www.alchemyresources.com.au/projects>.

Brown, MC, Oliver, NHS and Dickens, GR 2004, Veins and hydrothermal fluid flow in the Mt Whaleback Iron Ore District, eastern Hamersley Province, Western Australia: Precambrian Research, v. 128, p. 441–474.

Cawood, PA and Tyler, IM 2004, Assembling and reactivating the Proterozoic Capricorn Orogen: lithotectonic elements, orogenies and significance: Precambrian Research, v. 128, p. 201–218.

Collins, PLF and McDonald, IR 1994, A Proterozoic sediment-hosted polymetallic epithermal deposit at Abra in the Jillawarra sub-basin of the central Bangemall Basin, Western Australia: Geological Society of Australia; 12th Australian Geological Convention, Perth, Western Australia, 1994, Proceedings; Abstract Series, no. 37, p. 68–69.

Flint, D and Abeysinghe, PB 2000, Geology and mineral resources of the Gascoyne Region: Geological Survey of Western Australia, Record 2000/7, 29p.

Flint, DJ, Abeysinghe, PB, Mai, G, Pagel, J, Townsend, DB, Vanderhor, F and Jockel, F 2000, Geology and Mineral resources of the mid west region: Geological Survey of Western Australia, Record 2000/14, 142p.

Gascoyne Resources Limited 2011, Gascoyne Resources Limited, Perth, Western Australia, viewed 10 November 2011, <http://www.gascoyneresources.com.au/projects/>.

Johnson, SP, Cutten, HN, Tyler, IM, Korsch, RJ, Thorne, AM, Blay, O, Kennett, BLN, Blewitt, RS, Joly, A, Dentith, MC, Aitken, ARA, Goodwin, JA, Salmon, M, Reading, A, Boren, G, Ross, J, Costelloe, RD and Formin, T 2011a, Preliminary interpretation of deep seismic reflection lines 10GA–CP2 and 10GA–CP3: crustal architecture of the Gascoyne Province, and Edmund and Collier Basins, *in* Capricorn Orogen seismic and magnetotelluric (MT) workshop 2011: extended abstracts *edited by* SP Johnson, AM Thorne and IM Tyler: Geological Survey of Western Australia, Record 2011/25, p. 49–60.

Johnson, SP, Thorne, AM, Cutten, HN, Tyler, IM and Blay, O 2011b, Geology of the Gascoyne Province, *in* Capricorn Orogen seismic and magnetotelluric (MT) workshop 2011: extended abstracts *edited by* SP Johnson, AM Thorne and IM Tyler: Geological Survey of Western Australia, Record 2011/25, p. 27–40.

Johnson, SP, Sheppard, S, Wingate, MTD, Kirkland, CL and Belousova, EA 2011c, Temporal and hafnium isotopic evolution of the Glenburgh Terrane basement: an exotic crustal fragment in the Capricorn Orogen: Geological Survey of Western Australia, Report 110, 27p.

Johnson, SP, Sheppard, S, Rasmussen, B, Wingate, MTD, Kirkland, CL, Muhling, JR, Fletcher, IR and Belousova, EA 2011d, Two collisions, two sutures: punctuated pre-1950 Ma assembly of the West Australian Craton during the Ophthalmian and Glenburgh Orogenies: Precambrian Research, v. 189, no. 3–4, p. 239–262, doi: 10.1016/j.precamres.2011.07.011.

Kennett, BLN, Tyler, IM, Maher, J, Holzschuh, J, Formin, T and Costelloe, RD 2011, The Capricorn seismic survey: experimental design, acquisition, and processing, *in* Capricorn Orogen seismic and magnetotelluric (MT) workshop 2011: extended abstracts *edited by* SP Johnson, AM Thorne and IM Tyler: Geological Survey of Western Australia, Record 2011/25, p. 1–6.

Korsch, RJ, Johnson, SP, Tyler, IM, Thorne, AM, Blewett, RS, Cutten, HN, Joly, A, Dentith, MC, Aitken, ARA, Goodwin, JA and Kennett, BLN 2011, Geodynamic implications of the Capricorn Orogen deep seismic survey: from the Pilbara Craton to the Yilgarn Craton, *in* Capricorn Orogen seismic and magnetotelluric (MT) workshop 2011: extended abstracts *edited by* SP Johnson, AM Thorne and IM Tyler: Geological Survey of Western Australia, Record 2011/25, p. 107–114.

Martin, DMcB and Morris, PA 2010, Tectonic setting and regional implications of ca 2.2 Ga mafic magmatism in the southern Hamersley Province, Western Australia: Australian Journal of Earth Sciences, v. 57, p. 911–931.

Morris, RC 1985, Genesis of iron ore in banded iron formation by supergene and supergene-metamorphic processes — a conceptual model, *in* Handbook of strata-bound and stratiform ore deposits, v. 13, *edited by* KH Wolf: Elsevier, Amsterdam, The Netherlands, p. 73–235.

Morris, RC and Kneeshaw, M 2011, Genesis modelling for the Hamersley BIF-hosted iron ores of Western Australia: a critical review: Australian Journal of Earth Sciences, v. 58, p. 417–451.

Northern Star Resources Limited 2011, Northern Star Resources Limited, Perth, Western Australia, viewed 10 November 2011, <http://www.nsrltd.com/http-staging-northernstar-indepth-com-au-paulsens/>.

Occhipinti, SA, Sheppard, S, Passchier, C, Tyler, IM and Nelson, DR 2004, Palaeoproterozoic crustal accretion and collision in the southern Capricorn Orogen: the Glenburgh Orogeny: Precambrian Research, v. 128, p. 237–255.

Pearson, JM, Taylor, WR and Barley, ME 1996, Geology of the alkaline Gifford Creek Complex, Gascoyne Complex, Western Australia: Australian Journal of Earth Sciences, v. 43, p. 299–309.

Pirajno, F, Occhipinti, SA and Swager, CP 2000, Geology and mineralization of the Paleoproterozoic Bryah and Padbury Basins, Western Australia: Geological Survey of Western Australia, Report 59, 52p.

Pirajno, F, Sheppard, S, Groenewald, PB and Johnson, SP 2008, Mineral systems in the Gascoyne Complex, Western Australia, *in* GSWA 2008 extended abstracts: promoting the prospectivity of Western Australia: Geological Survey of Western Australia, Record 2008/2, p. 4–7.

Pirajno, F, Hell, A, Thorne, AM and Cutten, HN 2009, The Abra deposit: a breccia-pipe polymetallic mineral system in the Edmund Basin, Capricorn Orogen: implications for mineral exploration, *in* GSWA 2009 extended abstracts: promoting the prospectivity of Western Australia: Geological Survey of Western Australia, Record 2009/2, p. 31–33.

Powell, CMcA, Oliver, NHS, Li, Z-X, Martin, D and Ronaszeki, J 1999, Synorogenic hydrothermal origin for giant Hamersley iron oxide ore bodies: Geology, v. 27, p. 175–178.

Rasmussen, B, Fletcher, IR, Muhling, JR, Gregory, C, Thorne, AM, Cutten, HN, Pirajno, F and Hell, A 2010, In situ U–Pb monazite and xenotime geochronology of the Abra polymetallic deposit and associated sedimentary and volcanic rocks, Bangemall Supergroup, Western Australia: Geological Survey of Western Australia, Record 2010/12, 31p.

Sandfire Resources NL 2011, Doolgunna Project — overview: Sandfire Resources NL, Perth, Western Australia, viewed 11 November 2011, <http://www.sandfire.com.au/doolgunna-project/overview>.

Sener, AK, Young, C, Groves, DI, Krapež, B and Fletcher, I 2005, Major orogenic episode associated with Cordilleran-style tectonics related to the assembly of Paleoproterozoic Australia?: Geology, v. 33, no. 3, p. 225–228.

Sheppard, S, Occhipinti, SA and Tyler, IM 2004, A 2005–1970 Ma Andean-type batholith in the southern Gascoyne Complex, Western Australia: Precambrian Research, v. 128 (Assembling the Palaeoproterozoic Capricorn Orogen), p. 257–277.

Sipa Resources Limited 2011, Sipa Resources Limited, Perth, Western Australia, viewed 10 November 2011, <http://www.sipa.com.au/>.

Taylor, D, Dalstra, HJ, Harding, AE, Broadbent, GC and Barley, ME 2001, Genesis of high-grade orebodies of the Hamersley Province, Western Australia: Economic Geology, v. 96, p. 837–873.

Thorne, AM, Cutten, HN, Hell, A and Pirajno, F 2009, Kiangi Creek Formation paleogeography and the geological setting of the Abra polymetallic deposit, *in* GSWA 2009 extended abstracts: promoting the prospectivity of Western Australia: Geological Survey of Western Australia, Record 2009/2, p. 29–30.

Thorne, AM, Tyler, IM, Korsch, RJ, Johnson, SP, Brett, JW, Cutten, HN, Blay, O, Kennett, BLN, Blewitt, RS, Joly, A, Dentith, MC, Aitken, ARA, Holzschuh, J, Goodwin, JA, Salmon, M, Reading, A and Boren, G 2011, Preliminary interpretation of deep seismic reflection line 10GA–CP1: crustal architecture of the northern Capricorn Orogen, *in* Capricorn Orogen seismic and magnetotelluric (MT) workshop 2011: extended abstracts *edited by* SP Johnson, AM Thorne and IM Tyler: Geological Survey of Western Australia, Record 2011/25, p. 19–26.

Young, C, Groves, DI and Morant, P 2003, Sediment-hosted disseminated gold mineralisation in the Palaeoproterozoic Ashburton Province, Western Australia: a new epizonal orogenic gold province related to Capricorn Orogeny?, *in* Mineral exploration and sustainable development *edited by* D Elinopoulos: Balkema, Rotterdam, The Netherlands, p. 835–838.

Vogt, JH 1995, Geology of the Jillawarra area, Bangemall Basin, Western Australia: Geological Survey of Western Australia, Report 40, 107p.

RECORD
2011/25

CAPRICORN OROGEN SEISMIC AND MAGNETOTELLURIC (MT) WORKSHOP 2011: EXTENDED ABSTRACTS

This Record is published in digital format (PDF) and is available as a free download from the DMP website at <http://www.dmp.wa.gov.au/GSWApublications>.

Further details of geological products produced by the Geological Survey of Western Australia can be obtained by contacting:

Information Centre
Department of Mines and Petroleum
100 Plain Street
EAST PERTH WESTERN AUSTRALIA 6004
Phone: (08) 9222 3459 Fax: (08) 9222 3444
http://www.dmp.wa.gov.au/GSWApublications

Johnson
et al.

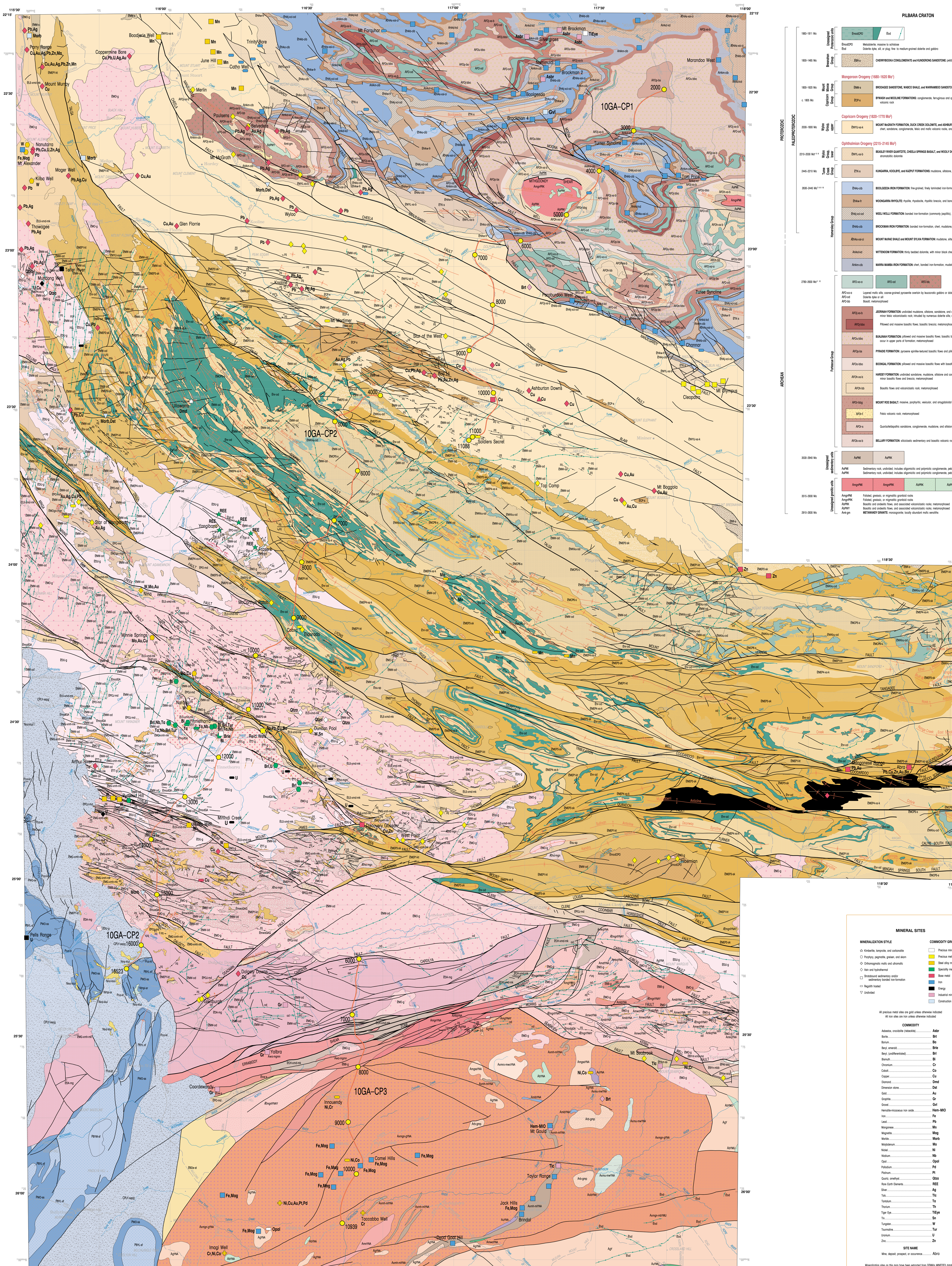

PILBARA CRATON

PROTEROZOIC — PALEOPROTEROZOIC

Unassigned Proterozoic units (1983–1811 Ma)
- ᵽmodCPO — Metadolerite; massive to schistose
- ᵽod — Dolerite dyke, sill, or plug; fine- to medium-grained dolerite and gabbro

Bresnahan Group (1800–1465 Ma)
- ᵽBR-s — **CHERRYBOOKA CONGLOMERATE and KUNDERONG SANDSTONE:** pebble- to boulder-conglomerate, pebbly sandstone, sandstone, siltstone, and mudstone (BRESNAHAN BASIN)

Mangaroon Orogeny (1680–1620 Ma[1])

Mount Minnie Group (1800–1620 Ma)
- ᵽMM-s — **BRODAGEE SANDSTONE, WABCO SHALE, and WARRAMBOO SANDSTONE:** quartz sandstone, conglomerate, siltstone, and mudstone

Capricorn Group (c. 1805 Ma)
- ᵽCP-s — **BYWASH and MOOLINE FORMATIONS:** conglomerate, ferruginous and quartzitic sandstone, ferruginous siltstone and mudstone, dolostone, and felsic volcanic rock

Capricorn Orogeny (1820–1770 Ma[2])

Wyloo Group, upper (2030–1800 Ma)
- ᵽWYU-xs-k — **MOUNT McGRATH FORMATION, DUCK CREEK DOLOMITE, and ASHBURTON FORMATION:** wacke, mudstone, ferruginous mudstone, banded iron-formation, chert, sandstone, conglomerate, felsic and mafic volcanic rocks, and locally stromatolitic dolomite

Ophthalmian Orogeny (2215–2145 Ma[3])

Wyloo Group, lower (2210–2030 Ma[4 5 6])
- ᵽWYL-xs-b — **BEASLEY RIVER QUARTZITE, CHEELA SPRINGS BASALT, and WOOLY DOLOMITE:** conglomerate, sandstone, mudstone, basalt, chert, and locally stromatolitic dolomite

(ASHBURTON and BLAIR BASINS)

Turee Creek Group (2445–2210 Ma)
- ᵽTK-s — **KUNGARRA, KOOLBYE, and KAZPUT FORMATIONS:** mudstone, siltstone, sandstone, conglomerate, local stromatolitic dolomite, and basalt; metamorphosed (TUREE CREEK BASIN)

Hamersley Group (2630–2445 Ma[7 8 9 10])
- ᵽHAo-cib — **BOOLGEEDA IRON FORMATION:** fine-grained, finely laminated iron-formation, mudstone, siltstone, and chert; metamorphosed
- ᵽHAw-fr — **WOONGARRA RHYOLITE:** rhyolite, rhyodacite, rhyolitic breccia, and banded iron-formation; metamorphosed
- ᵽHAj-xci-od — **WEELI WOLLI FORMATION:** banded iron-formation (commonly jaspilitic), mudstone, siltstone, and numerous dolerite sills; metamorphosed
- ᵽHAb-cib — **BROCKMAN IRON FORMATION:** banded iron-formation, chert, mudstone, and siltstone; metamorphosed
- ÆHAs-xsi-ci — **MOUNT McRAE SHALE and MOUNT SYLVIA FORMATION:** mudstone, siltstone, chert, banded iron-formation, and dolomite; metamorphosed
- AHAd-kd — **WITTENOOM FORMATION:** thinly bedded dolomite, with minor black chert, shale, and sandstone; metamorphosed
- AHAm-cib — **MARRA MAMBA IRON FORMATION:** chert, banded iron-formation, mudstone, and siltstone; metamorphosed

(HAMERSLEY BASIN)

ARCHEAN

Fortescue Group (2780–2630 Ma[11 12])
- AFO-xo-a — Layered mafic sills; coarse-grained pyroxenite overlain by leucocratic gabbro or dolerite; local basal serpentinite; metamorphosed
- AFO-od — Dolerite dyke or sill
- AFO-bb — Basalt; metamorphosed
- AFOj-xs-b — **JEERINAH FORMATION:** undivided mudstone, siltstone, sandstone, and chert; massive basaltic flows, basaltic pillow lava, basaltic breccia; minor felsic volcaniclastic rock; intruded by numerous dolerite sills; metamorphosed
- AFOj-bbo — Pillowed and massive basaltic flows; basaltic breccia; metamorphosed
- AFOu-bbo — **BUNJINAH FORMATION:** pillowed and massive basaltic flows; basaltic breccia and basaltic volcanic sandstone; minor chert; amygdaloidal basalt flows occur in upper parts of formation; metamorphosed
- AFOp-bs — **PYRADIE FORMATION:** pyroxene spinifex-textured basaltic flows and pillow lava with mafic volcaniclastic rock; minor chert and local komatiite; metamorphosed
- AFOo-bbo — **BOONGAL FORMATION:** pillowed and massive basaltic flows with basaltic breccia, siltstone, and mudstone; minor chert; metamorphosed
- AFOh-xs-b — **HARDEY FORMATION:** undivided sandstone, mudstone, siltstone and conglomerate; felsic and mafic volcanic sandstone and conglomerate; minor basaltic flows and breccia; metamorphosed
- AFOh-bb — Basaltic flows and volcaniclastic rock; metamorphosed
- AFOr-bbg — **MOUNT ROE BASALT:** massive, porphyritic, vesicular, and amygdaloidal basalt; some pillow basalt; metamorphosed
- AFOr-f — Felsic volcanic rock; metamorphosed
- AFOr-s — Quartzofeldspathic sandstone, conglomerate, mudstone, and siltstone; metamorphosed
- AFOb-xs-b — **BELLARY FORMATION:** siliciclastic sedimentary and basaltic volcanic rocks; metamorphosed

(FORTESCUE BASIN)

Unassigned sedimentary units (3530–2940 Ma)
- AsPMI — Sedimentary rock, undivided; includes oligomictic and polymictic conglomerate, pebbly sandstone, sandstone, mudstone, siltstone, and chert; metamorphosed
- AsPRK — Sedimentary rock, undivided; includes oligomictic and polymictic conglomerate, pebbly sandstone, sandstone, mudstone, siltstone, and chert; metamorphosed

Unassigned granitic units (3515–2930 Ma; 2910–2830 Ma)
- AmgnPMI — Foliated, gneissic, or migmatitic granitoid rocks
- AmgnPRK — Foliated, gneissic, or migmatitic granitoid rocks
- AbPRK — Basaltic and andesitic flows, and associated volcaniclastic rocks; metamorphosed
- AbPWY — Basaltic and andesitic flows, and associated volcaniclastic rocks; metamorphosed
- Amt-gm — **METAWANDY GRANITE:** monzogranite; locally abundant mafic xenoliths

(PILBARA CRATON)

SOUTHERN CARNARVON BASIN

CENOZOIC
- PLEISTOCENE — Nna-klul — **NADARRA FORMATION:** silty micritic limestone; includes minor calcrete; muddy, commonly silicified; lacustrine
- MIOCENE — Nmpi-sr — **PINDILYA FORMATION:** poorly sorted sandstone, commonly lithic, and granule to pebble conglomerate; generally very silicified

PALEOZOIC — PERMIAN

Byro Group
- PBYM-sf — **BULGADOO SHALE, CUNDLEGO FORMATION, QUINNANIE SHALE, and WANDAGEE FORMATION:** interbedded black mudstone, siltstone, and fine-grained sandstone
- PBYL-sf — **COYRIE FORMATION and MALLENS SANDSTONE:** fine-grained bioturbated sandstone overlying interbedded sandstone, siltstone, and mudstone

Wooramel Group
- PWO-ss — Fine- to coarse-grained sandstone, siltstone, minor granule- to pebble-conglomerate
- Pca-kt — **CALLYTHARRA FORMATION:** fossiliferous, calcareous siltstone to calcisiltite; interbedded, hard fossiliferous calcarenite

CARBONIFEROUS–PERMIAN

Lyons Group
- CPLY-sepg — Diamictite, sandstone and siltstone (locally calcareous), shale, and boulder beds and lags; glacigene

(SOUTHERN CARNARVON BASIN)

GASCOYNE PROVINCE

Unassigned units
- od — Dolerite dykes, sills, or plugs; fine- to medium-grained dolerite; age uncertain
- zq — Quartz vein or pod; massive, crystalline, or brecciated; age uncertain

PROTEROZOIC — NEOPROTEROZOIC

Mulka Tectonic Event (c. 570 Ma)

c. 755 Ma[13]
- ᵽMW-od — **Mundine Well Dolerite Suite:** dolerite dykes, sills, and small intrusions with locally abundant xenoliths and potassic alteration of wallrocks; includes minor quartz diorite, syenite, tonalite, and biotite monzogranite

Edmundian Orogeny (1030–955 Ma[14])

Thirty Three Supersuite (995–955 Ma)
- ᵽTT-g — Leucocratic granite and metagranite, and pegmatite

MESOPROTEROZOIC

c. 1055 Ma
- ᵽBDe-st — **ERRABIDDY SANDSTONE:** feldspathic sandstone; minor pebble conglomerate lenses (BADGERADDA BASIN)

Gifford Creek Carbonatite Complex (1620–1030 Ma)
- ᵽgc-rf — Ferroan carbonatite; sills and dykes of Fe-carbonate, phlogopite, and sodic amphibole and variable amounts of quartz
- ᵽgc-zi — Hematite–magnetite, in places altered to massive goethite; fenitic alteration comprises variable amounts of K-feldspar, albite, sodic amphibole, cancrinite, pyrochlore, phlogopite, and lamprophyllite

c. 1070 Ma
- ᵽWKku-od — **KULKATHARRA DOLERITE:** dolerite and gabbro sills intruded into **Edmund Group** and **Collier Group**

Collier Group (1200–1075 Ma)
- ᵽMCP6-s — **ILGARARI FORMATION:** siltstone, mudstone, and fine-grained sandstone
- ᵽMCP5-s — **BACKDOOR FORMATION and CALYIE FORMATION:** siltstone, mudstone, and sandstone; minor dolostone, chert, and conglomerate

(COLLIER BASIN)

Mutherbukin Tectonic Event (1385–1200 Ma)

c. 1465 Ma
- ᵽnr-od — **NARIMBUNNA DOLERITE:** dolerite and gabbro sills intruded into **Edmund Group**

MESO–NEOPROTEROZOIC

Edmund Group (1620–1465 Ma)
- ᵽMEP4-xs-k — **DISCOVERY, DEVIL CREEK, ULLAWARRA, and CODDARDOO FORMATIONS:** siltstone and mudstone; sandstone, dolostone, dolomitic mudstone, chert, and minor conglomerate
- ᵽMEP3-sk — **KIANGI CREEK FORMATION and MUNTHARRA FORMATION:** siltstone and mudstone, sandstone, and dolostone; minor conglomerate
- ᵽMEP2-sk — **GOORAGOORA FORMATION, BLUE BILLY FORMATION, and CHEYNE SPRINGS FORMATION:** siltstone and mudstone, sandstone, and dolostone; locally sulfidic
- ᵽMEP1-kt — **YILGATHERRA FORMATION and IRREGULLY FORMATION:** stromatolitic and non-stromatolitic dolostone, dolomitic siltstone, sandstone, siltstone, and conglomerate

(EDMUND BASIN)

1620–1465 Ma
- ᵽau-sp — **MOUNT AUGUSTUS SANDSTONE:** sandstone, pebbly sandstone, and conglomerate; minor siltstone (MOUNT AUGUSTUS BASIN)

PALEOPROTEROZOIC

Mangaroon Orogeny (1680–1620 Ma[1])

Unassigned units (1667–1280 Ma)
- ᵽmodGA — Massive metadolerite and foliated amphibolite; fine and medium grained
- ᵽmodgGA — Metadolerite, locally with garnet coronas around pyroxene

Durlacher Supersuite
- ᵽDU-g — Granite and minor gabbro, and metamorphosed equivalents

Pooranoo Metamorphics (1760–1680 Ma)
- ᵽPO-md — Pelitic and psammitic schist, quartz metasandstone, feldspathic metasandstone and metaconglomerate, and phyllite
- ᵽPOJ-md — **MOUNT JAMES SUBGROUP:** pelitic and psammitic schist, metamorphosed quartz sandstone, feldspathic metasandstone, and metaconglomerate
- ᵽcw-s — **COOR-DE-WANDY FORMATION:** siliciclastic sedimentary rock; metamorphosed

Capricorn Orogeny (1820–1770 Ma[2])

Moorarie Supersuite (1820–1775 Ma)
- ᵽMO-g — Undivided; granite and minor gabbro, and metamorphosed equivalents
- ᵽMOgo-mgn — **GOOCHE GNEISS:** strongly foliated, porphyritic metagranodiorite and metamonzogranite, and augen gneiss
- ᵽMO-mog — Massive, subophitic metagabbro; medium grained; amphibolite; minor hornblende schist

Leake Spring Metamorphics (1840–1810 Ma)
- ᵽLS-xmd-mk — Pelitic and psammitic schist; calc-silicate rock; minor amphibolite

Bertibubba Supersuite (1965–1945 Ma)
- ᵽBB-g — Granite and metagranitic rocks

Glenburgh Orogeny (2005–1950 Ma[15])

Unassigned units (2430–1965 Ma)
- ᵽmwaGAG — Amphibolite
- ᵽmogGAG — Plagioclase–actinolite–tremolite gneiss; after gabbro
- ᵽmusGAG — Fine- to medium-grained actinolite(–clinozoisite–albite–titanite) and tremolite(–serpentine–talc–calcite) schist

Camel Hills Metamorphics (2000–1955 Ma)
- ᵽCH-xmd-mk — Pelite, calc-silicate rock, quartzite, metamorphosed banded iron-formation and amphibolite

Dalgaringa Supersuite (2005–1985 Ma)
- ᵽDA-mg — Metagranite and granitic gneiss

Moogie Metamorphics (2240–2125 Ma)
- ᵽMG-xmh-mk — Psammitic and pelitic schist; calc-silicate rock; minor quartzite, marble, amphibolite, and ultramafic schist

ARCHEAN–PROTEROZOIC (2555–2430 Ma)
- Æha-mgn — **HALFWAY GNEISS:** interlayered leucocratic and mesocratic granitic gneiss, pale-grey granitic gneiss and foliated metagranite, and gneissic to foliated porphyritic metagranodiorite

(Glenburgh Terrane; GASCOYNE PROVINCE)

YILGARN CRATON

PROTEROZOIC — PALEOPROTEROZOIC

Padbury Group (1983–1811 Ma)
- ᵽPA-s — Undivided; sandstone, siltstone, mudstone, banded iron-formation, granular iron-formation, conglomerate, and dolostone
- ᵽPAm-ss — **MILLIDIE CREEK FORMATION:** sandstone and shale; minor granular iron-formation
- ᵽPAw-scq — **WILTHORPE FORMATION:** pebble to boulder conglomerate; clasts include vein quartz, minor chert, quartz wacke, and granitoid; quartz wacke and finely bedded siltstone; locally chloritic; graded beds
- ᵽPAl-ssq — **LABOUCHERE FORMATION:** quartz wacke and siltstone with local quartz-pebble conglomerate; metamorphosed; includes quartz schist, quartz–muscovite schist, and minor biotite–muscovite schist, locally with chloritoid, staurolite, and andalusite

(PADBURY BASIN)

Glenburgh Orogeny (2005–1950 Ma[15])

Bryah Group (c. 2000 Ma)
- ᵽBYn-mbb — **NARRACOOTA FORMATION:** metabasalt and mafic–ultramafic schist; locally pillowed and plagioclase-phyric; interbedded with volcaniclastic and sedimentary rock (coeval and interbedded with RAVELSTONE FORMATION)
- ᵽBYnt-xmo-ma — **Trillbar Member:** interleaved foliated metagabbro, metamicrogabbro, metabasalt, metapyroxenite, and serpentinized metaperidotite; local magmatic layering well preserved

(BRYAH BASIN)

ARCHEAN

Unassigned meta-igneous units (Narryer Terrane)
- ÆmgnYNAY — Leucocratic granitic gneiss; derived from 3300–2660 Ma biotite granite and granitic gneiss, and sheets and veins of coarse-grained granite and pegmatite (ᵽMO-g); deformed and metamorphosed at c.1810 Ma
- ÆmgnYNAY — Granite gneiss; reworked during the Paleoproterozoic

Unassigned granitic units (3010–2610 Ma; Youanmi Terrane)
- AgY — Granitic rocks, undivided; metamorphosed
- Axmgn-mbYMU — Granitic gneiss with greenstone enclaves

Unassigned greenstone units (3010–2700 Ma)
- AmwaYMU — Amphibolite; may include meta banded iron-formation
- AuYMU — Ultramafic rock, undivided; metamorphosed
- AfYMU — Felsic volcanic rock, undivided; metamorphosed
- AbYMU — Mafic volcanic rocks with minor mafic and ultramafic intrusive rocks; subordinate felsic rocks; metamorphosed

Unassigned meta-sedimentary units (3100–2630 Ma; Narryer Terrane)
- AmkqYNA — Calc-silicate gneiss; fine- to coarse-grained plagioclase–quartz–diopside–tremolite(–microcline) and diopside–tremolite–titanite rock
- AcibYNA — Banded iron-formation and ferruginous banded chert; metamorphosed
- AmibYNA — Meta banded iron-formation; quartz–magnetite(–hematite) rocks; grunerite abundant locally
- Axmh-mlYNA — Quartzite, quartz–mica schist, pelite, amphibolite, meta-ultramafic rocks; may include minor metamorphosed banded iron-formation and metachert
- AmtqYNA — Foliated quartzite; minor quartz–diopside gneiss

Unassigned igneous units (3731–2608 Ma)
- AmgYNAY — Foliated metagranitic rocks
- AbYNA — Mafic rock, undivided; metamorphosed
- AgYNA — Granitic rocks, undivided; metamorphosed
- AmatYNA — Fine- to medium-grained serpentine–talc–magnetite–calcite(–tremolite–titanite) rock after peridotite
- AmnYNA — Gneiss, undivided
- AmwaYNA — Amphibolite; fine- to medium-grained, aphyric hornblende–plagioclase rock and medium-grained porphyritic hornblende–plagioclase rock; locally includes metagabbro and metaleucogabbro
- AuYNA — Ultramafic rock, undivided; metamorphosed
- Axmgn-gYNA — Granitic gneiss and granitic rocks; minor granodiorite, muscovite granite, amphibolite, and ultramafic rocks
- Axmro-mwoYNA — Felsic and mafic granulite, undivided
- Axmu-mwYNA — Interlayered meta-ultramafic and metamafic rocks
- AmgnYNA — Granitic gneiss; locally migmatitic
- AmgssYNA — Foliated biotite metamonzogranite; even textured to porphyritic; medium grained

c. 2615 Ma; 2758–2585 Ma
- Arb-gmp — **ROCKY BORE GRANITE:** porphyritic monzogranite with tabular feldspar phenocrysts; medium grained
- Awa-mgmn — **WARRIGAL GNEISS:** foliated to gneissic, even-textured to sparsely porphyritic metamonzogranite; locally contains sheets and pods of amphibolite; cut by c. 1800 Ma pegmatite dykes; deformation is Paleoproterozoic

(YILGARN CRATON)

MINERAL SITES

MINERALIZATION STYLE
- Kimberlite, lamproite, and carbonatite
- Porphyry, pegmatite, greisen, and skarn
- Orthomagmatic mafic and ultramafic
- Vein and hydrothermal
- Stratabound sedimentary and/or sedimentary banded iron-formation
- Regolith hosted
- Undivided

COMMODITY GROUP
- Precious mineral
- Precious metal
- Steel alloy metal
- Speciality metal
- Base metal
- Iron
- Energy
- Industrial mineral
- Construction material

All precious metal sites are gold unless otherwise indicated
All iron sites are iron unless otherwise indicated

COMMODITY

Commodity	Code
Asbestos, crocidolite (riebeckite)	Asbr
Barite	Brt
Barium	Ba
Beryl, emerald	Brle
Beryl, (undifferentiated)	Brl
Bismuth	Bi
Chromium	Cr
Cobalt	Co
Copper	Cu
Diamond	Dmd
Dimension stone	Dst
Gold	Au
Graphite	Gr
Gravel	Gvl
Hematite–micaceous iron oxide	Hem–MIO
Iron	Fe
Lead	Pb
Manganese	Mn
Magnetite	Mag
Marble	Marb
Molybdenum	Mo
Nickel	Ni
Niobium	Nb
Opal	Opal
Palladium	Pd
Platinum	Pt
Quartz, amethyst	Qtza
Rare Earth Elements	REE
Silver	Ag
Talc	Tlc
Tantalum	Ta
Thorium	Th
Tiger Eye	TiEye
Tin	Sn
Tungsten	W
Tourmaline	Tur
Uranium	U
Zinc	Zn

SITE NAME

Mine, deposit, prospect, or occurrence .... Abra

Mineralization sites on this map have been extracted from GSWA's MINEDEX database. For clarity, names have been shown only for selected sites. Full details of site numbers, site locations, site status, mineralization, and commodities can be obtained from the MINEDEX database, accessed at <http://www.dmp.wa.gov.au/minedex>.

TOTAL MAGNETIC INTENSITY

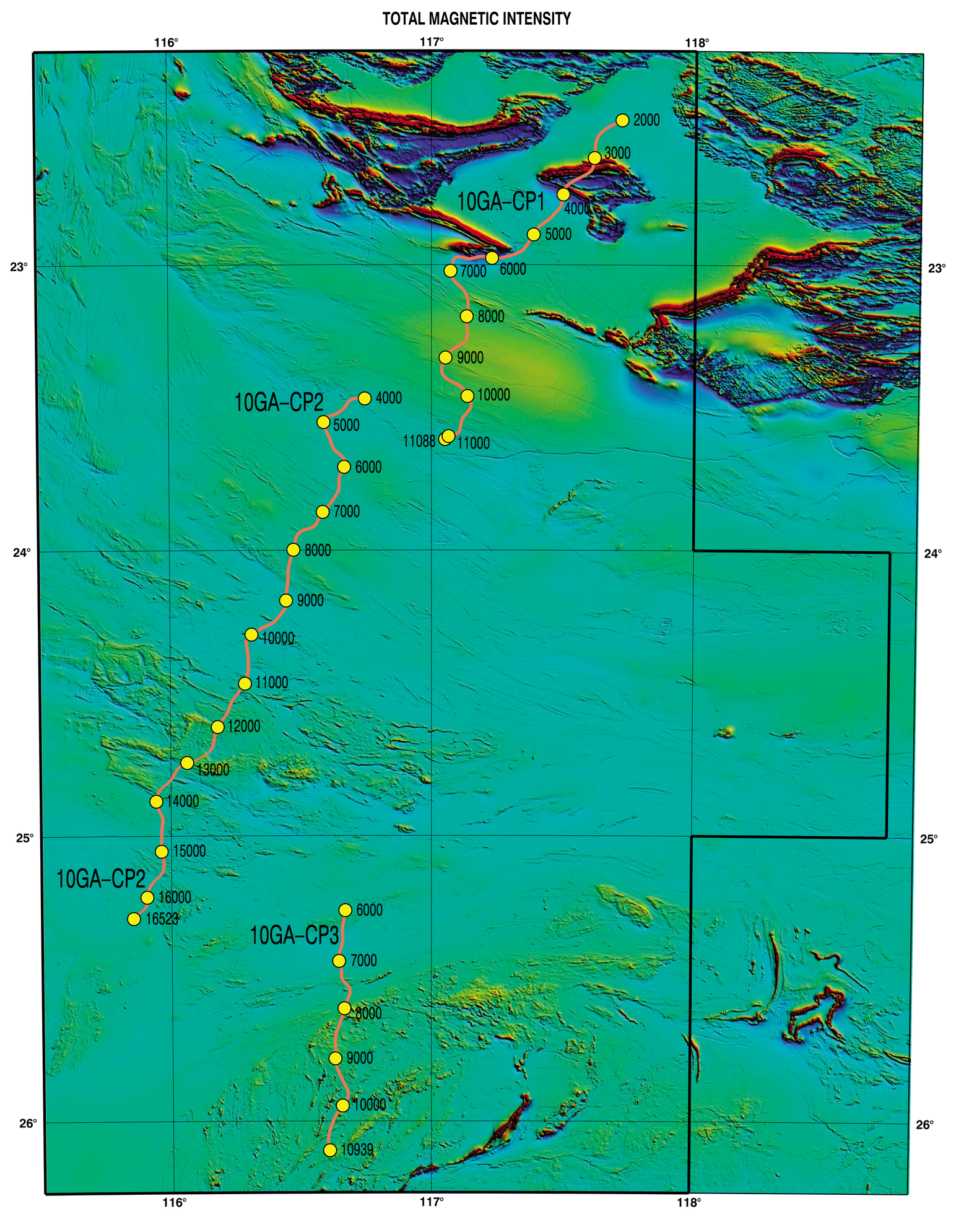

SCALE 1:2 000 000
0 — 100 Kilometres

GRAVITY

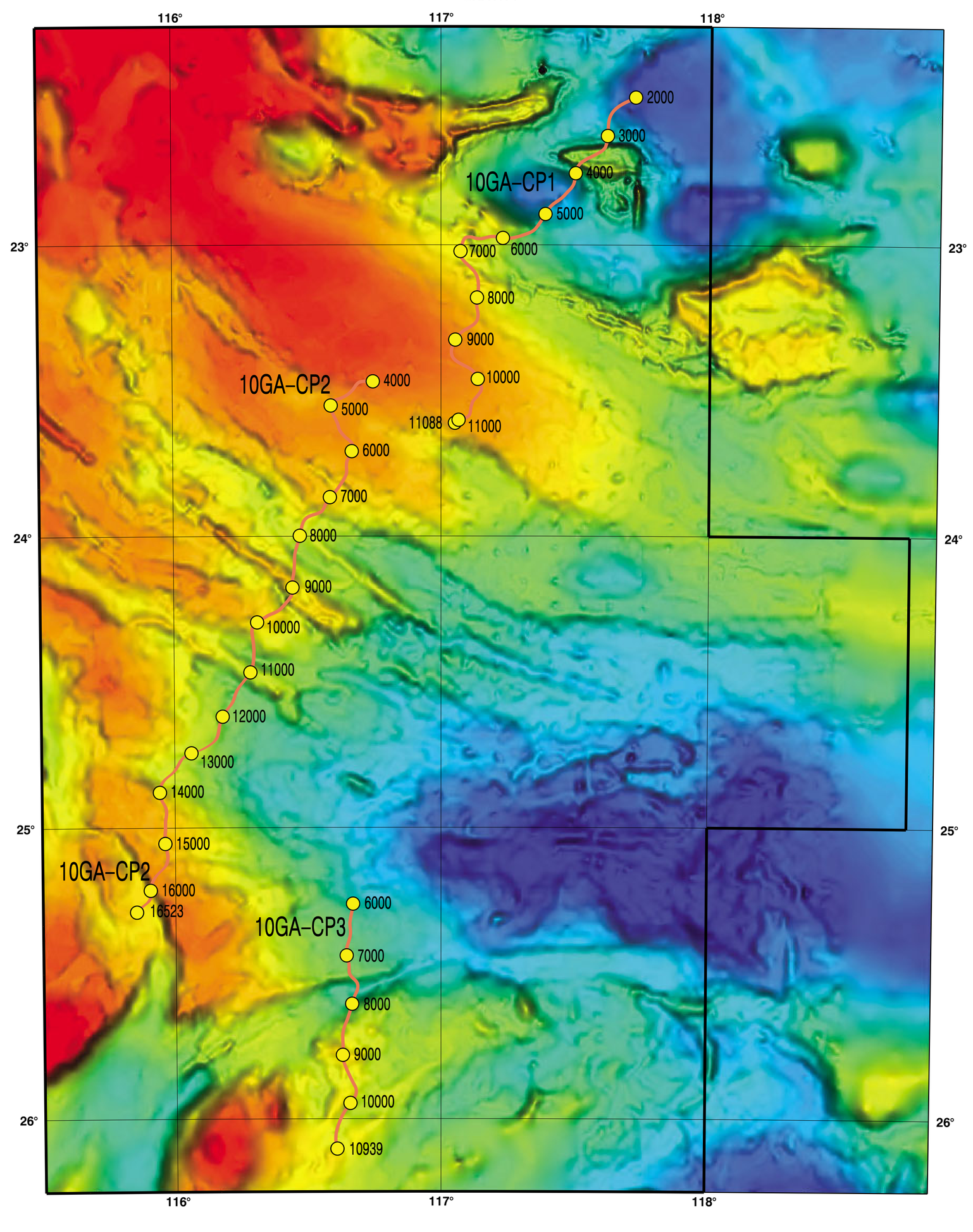

DATA DIRECTORY

Theme	Data Currency	Organization†
Geology*	2011	Geological Survey of Western Australia, Department of Mines and Petroleum
Mineral sites*	OCT 2011	Geological Survey of Western Australia, Department of Mines and Petroleum
Structural data	OCT 2011	Geological Survey of Western Australia, Department of Mines and Petroleum
Horizontal control	OCT 2011	Landgate
Topographic nomenclature	2011	Landgate
Topography	2011	Landgate

* DMP data can be viewed interactively via GeoVIEW.WA <http://www.dmp.wa.gov.au/geoview>, and related datasets can be downloaded from the GSWA Data and Software Centre <http://www.dmp.wa.gov.au/datacentre>.
† WA State Government unless otherwise indicated

Fault
- major
- minor

Fold, showing axial trace
- anticline, exposed
- syncline, exposed
- overturned syncline, exposed
- antiform, exposed
- synform, exposed

Bedding
- trend of bedding

Foliation
- trend of foliation

Seismic line, with CDP point — 9000

Highway
Sealed road
Unsealed road
Railway
Airport
Homestead — Landor
Townsite — TOM PRICE
Watercourse

Compiled by SP Johnson, AM Thorne, HN Cutten, and O Blay

Geology by — refer to individual 1:100 000 map sheets

Geochronology by:

(1) Sheppard, S et al. 2005, Australian Journal of Earth Sciences, v.52, p.443–460.
(2) Evans, DAD et al. 2003, Australian Journal of Earth Sciences, v.50, p.853–864.
(3) Rasmussen, B et al. 2005, Geology, v. 33, p. 773–776.
(4) Müller, SG et al. 2005, Geology, v. 33, p. 577–580.
(5) Martin, DM et al. 1998, Economic Geology, v. 93, p. 1084–1090.
(6) Martin, DM and Morris, PA 2010, Australian Journal of Earth Sciences, v. 57, p.911–931.
(7) Barley, ME et al. 1997, Nature, v. 385, p. 55–58.
(8) Pickard, AL 2002, Australian Journal of Earth Sciences, v. 49, p. 491–507.
(9) Rasmussen, B et al. 2005, Geology, v. 33, p. 725–728.
(10) Trendall, AF et al. 1998, Australian Journal of Earth Sciences, v. 45, p. 137–142.
(11) Rasmussen, B and Fletcher, IR 2010, Geology, v. 38, p. 299–302.
(12) Arndt, NT et al. 1991, Australian Journal of Earth Sciences, v. 38, p. 261–281.
(13) Wingate, MTD and Giddings, JW 2000, Precambrian Research, v. 100, p. 335–337.
(14) Sheppard, S et al. 2007, Journal of Metamorphic Geology, v. 25, p. 477–494.
(15) Johnson, S et al. 2011, Precambrian Research, v. 189, p. 239–262.

Cartography by D Ladbrook
Edited by S Martin, S White, and S Coldicutt
Published by the Geological Survey of Western Australia
This map is published in digital format (PDF) and is available online at <http://www.dmp.wa.gov.au/GSWApublications>.
Copies of this map are available from the Information Centre, Department of Mines and Petroleum,
100 Plain Street, East Perth, WA 6004.
Phone (08) 9222 3459 Fax (08) 9222 3444
Website <http://www.dmp.wa.gov.au/gswa> Email geological.survey@dmp.wa.gov.au
The recommended reference for this map is:
Johnson, SP, Thorne, AM, Cutten, HN and Blay, O (compilers) 2012, Geological interpretation of the western Capricorn Orogen, *in* Capricorn Orogen seismic and magnetotelluric (MT) workshop 2011: extended abstracts *edited by* SP Johnson, AM Thorne, and IM Tyler: Geological Survey of Western Australia, Record 2011/25, Plate 1.

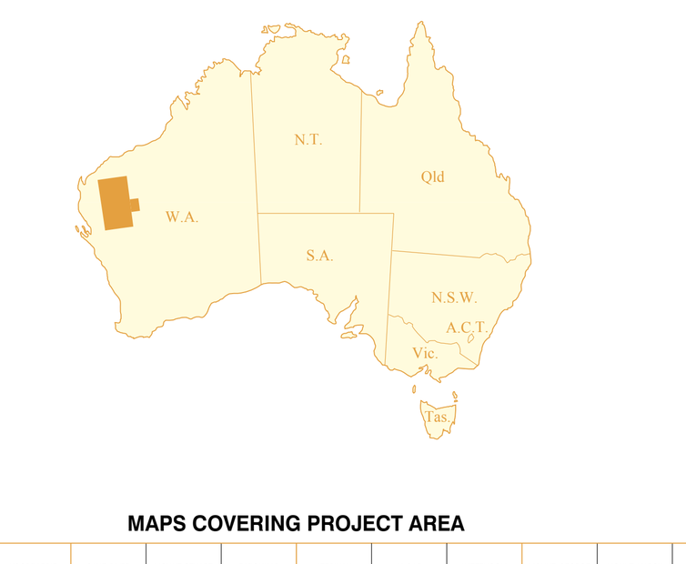

MAPS COVERING PROJECT AREA

1:100 000 maps shown in black
1:250 000 maps shown in brown
Search for current GSWA map products online at <http://www.dmp.wa.gov.au/GSWApublications>

Government of Western Australia
Department of Mines and Petroleum
HON. NORMAN MOORE, M.L.C.
MINISTER FOR MINES AND PETROLEUM

Geological Survey of Western Australia
RICK ROGERSON
EXECUTIVE DIRECTOR

ROYALTIES FOR REGIONS
EXPLORATION INCENTIVE SCHEME

SCALE 1:500 000
5000 Metres 0 5 10 15 20 25 30 35 40 45 50 Kilometres

UNIVERSAL TRANSVERSE MERCATOR PROJECTION
HORIZONTAL DATUM: GEOCENTRIC DATUM OF AUSTRALIA 1994
VERTICAL DATUM: AUSTRALIAN HEIGHT DATUM
Grid lines indicate 25 000 metre interval of the Map Grid Australia Zone 50

GDA
The Map Grid Australia (MGA) is based on the Geocentric Datum of Australia 1994 (GDA94)
GDA94 positions are compatible within one metre of the datum WGS84 positions

GEOLOGICAL SURVEY OF WESTERN AUSTRALIA

RECORD 2011/25 PLATE 1

GEOLOGICAL INTERPRETATION OF THE WESTERN CAPRICORN OROGEN

February 2012

INTERPRETED MIGRATED SEISMIC SECTIONS

INTERPRETED MAGNETOTELLURIC SECTIONS

INTERPRETED GEOLOGICAL CROSS SECTIONS

PRINCIPAL TECTONIC ELEMENTS

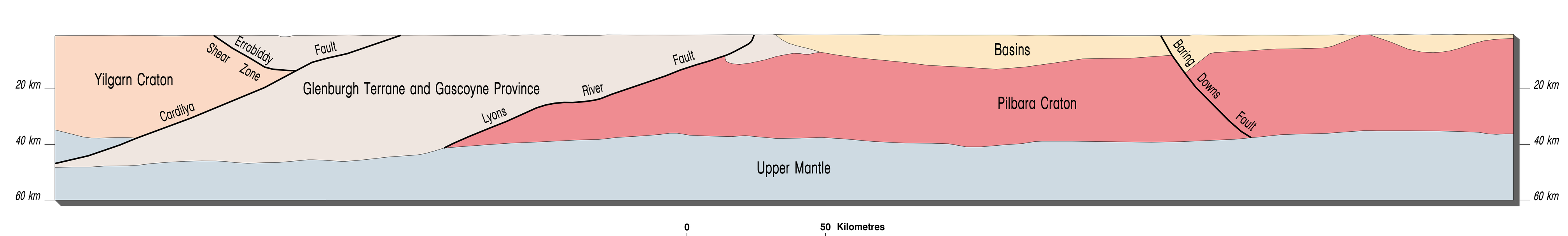

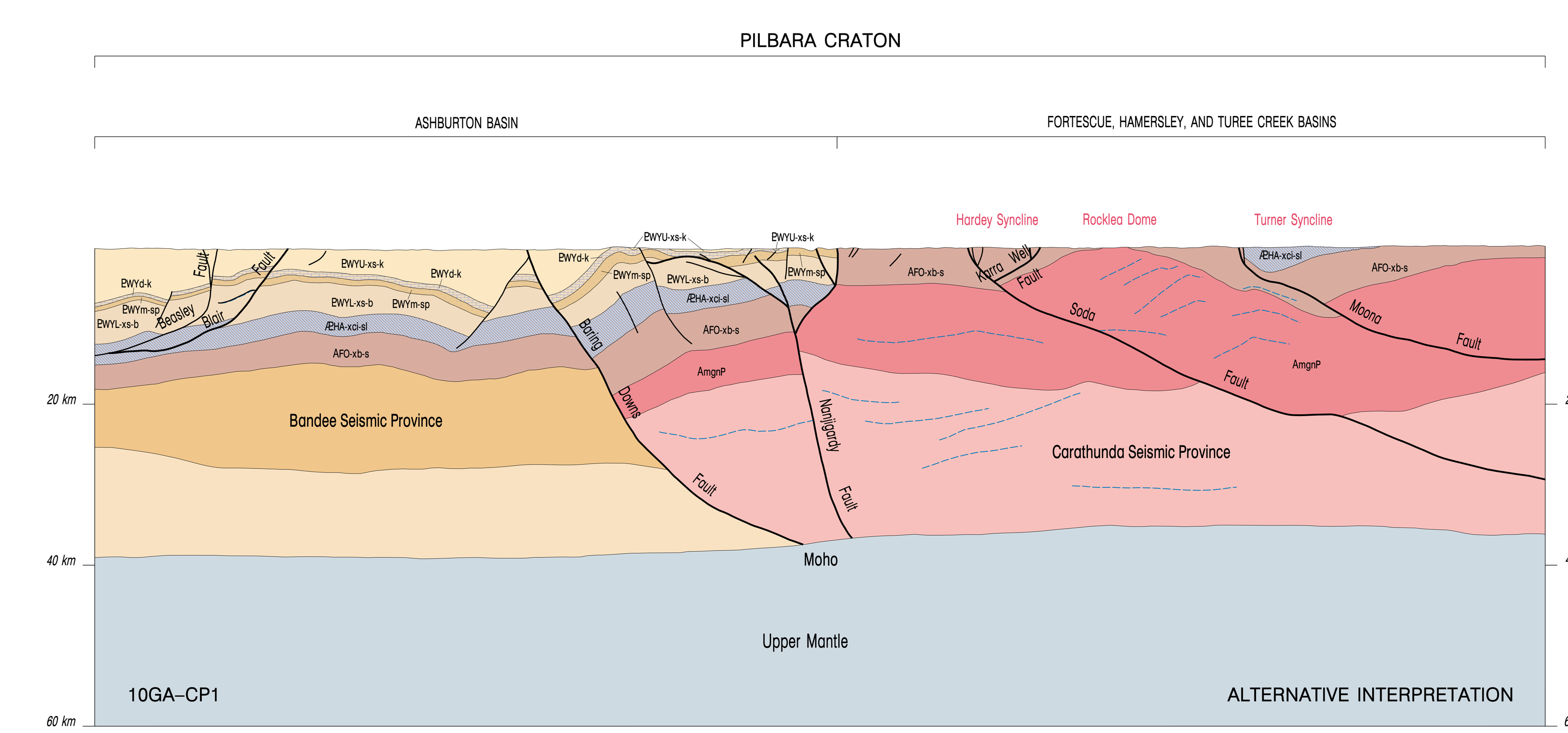

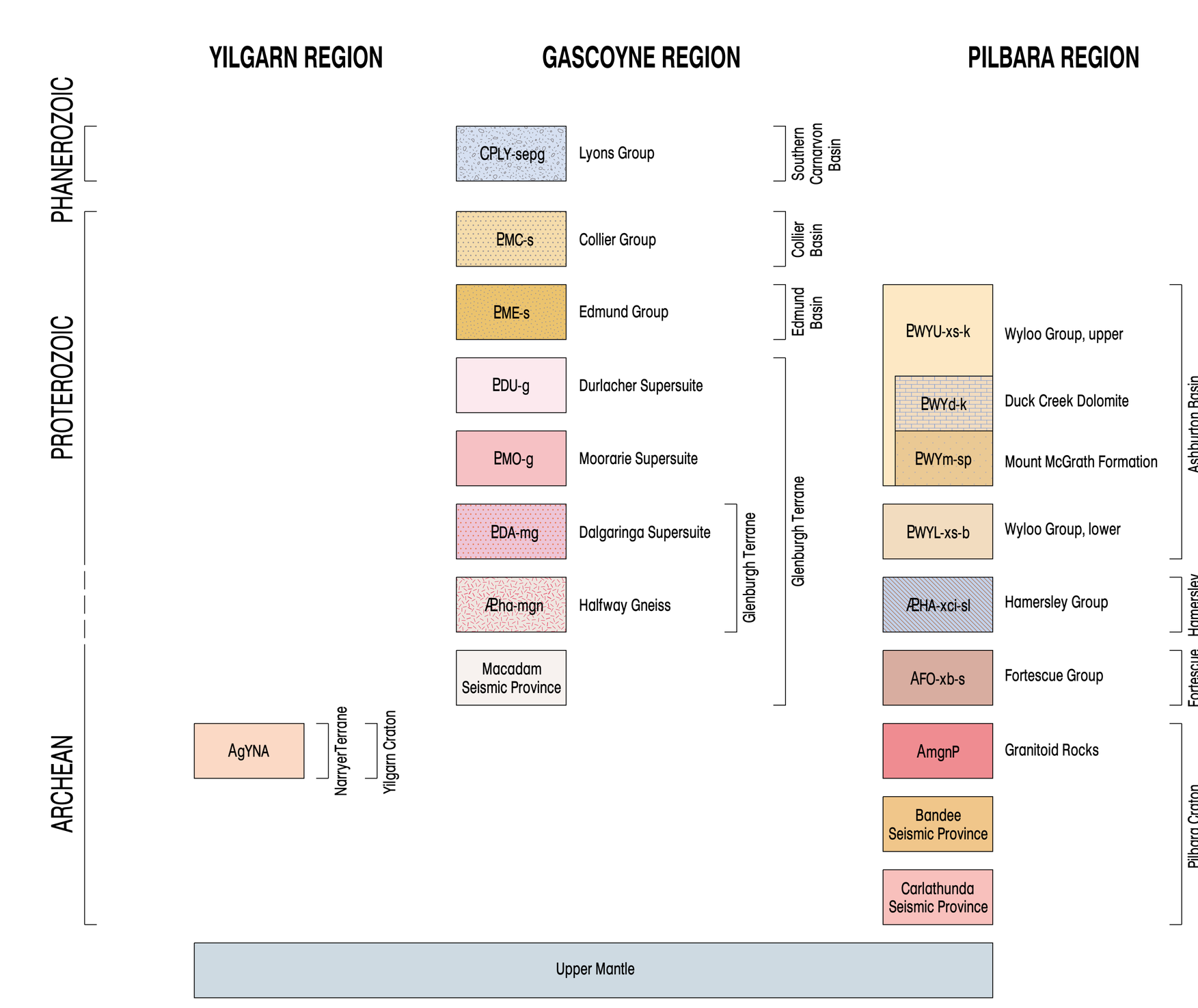

Government of Western Australia
Department of Mines and Petroleum

HON. NORMAN MOORE, M.L.C.
MINISTER FOR MINES AND PETROLEUM

Geological Survey of Western Australia

RICK ROGERSON
EXECUTIVE DIRECTOR

SCALE 1:500 000

5000 Metres 0 10 20 30 40 50 Kilometres

GEOLOGICAL SURVEY OF WESTERN AUSTRALIA

RECORD 2011/25 PLATE 2

GEOLOGICAL INTERPRETATION OF THE CAPRICORN OROGEN SEISMIC AND MAGNETOTELLURIC LINES 10GA–CP1, 10GA–CP2, and 10GA–CP3

February 2012

Compiled by SP Johnson and AM Thorne

Interpretation by SP Johnson, AM Thorne, IM Tyler, RJ Korsch, BLN Kennett, HN Cutten, A Joly, MC Dentith, RS Blewett, ARA Aitken, J Goodwin, G Heinson, G Boren, J Ross, J Campanya, S Thiel, K Selway, RD Costelloe, M Salmon, A Reading, J Holzschuh and T Fomin

Cartography by P Taylor

Edited by S Martin and S White

Published by the Geological Survey of Western Australia

This plate is published in digital format (PDF) and is available online at <http://www.dmp.wa.gov.au/GSWApublications>.

The recommended reference for this plate is:
Johnson, SP and Thorne, AM (compilers) 2012, Geological interpretation of the Capricorn Orogen seismic and magnetotelluric lines 10GA–CP1, 10GA–CP2, and 10GA–CP3, *in* Capricorn Orogen seismic and magnetotelluric (MT) workshop 2011: extended abstracts *edited by* SP Johnson, AM Thorne, and IM Tyler: Geological Survey of Western Australia, Record 2011/25, Plate 2.

ROYALTIES FOR REGIONS
EXPLORATION INCENTIVE SCHEME

Australian Government
Geoscience Australia

AuScope

ANSIR NATIONAL RESEARCH FACILITY FOR EARTH SOUNDING

THE UNIVERSITY of ADELAIDE

MAPS COVERING PROJECT AREA